CEMI Publications Series #PS09-01

CEMI
Centre for Excellence in Mining Innovation

Keynote lectures by Peter K. Kaiser
2000 - 2009

1. Kaiser, P. K., S. Maloney, P. Vasak and G. Wang, 2009. Seismic excavation hazard evaluation in underground construction. *7th RaSiM6*, Dalian, China, 1-26.

2. Kaiser, P. K. and B-H. Kim, 2008. Rock mechanics advances of underground construction and mining.
Korea Rock Mech. Symposium, Seoul, 1-16.

3. Kaiser, P. K. and B-H. Kim, 2008. Rock mechanics challenges in underground construction and mining.
1st Southern Hemisphere International Rock Mech. Symposium, **1**: 3-38;
Summary in ACG News, Vol.31, Dec 2008.

4. Kaiser, P. K., 2007. Rock mechanics challenges and opportunities in underground construction and mining.
1st Canada-U.S. Rock Mech. Symposium, Vancouver, ppt on CD 47p.

5. Kaiser, P. K., 2006. Rock mechanics consideration for construction of deep tunnel in brittle ground.
Asian Rock Mechanics Symposium, Singapore, 12 p. on CD.

6. Kaiser, P. K., 2005. Tunnel stability in highly stressed, brittle ground - Rock mechanics considerations for Alpine tunnelling.
Geological AlpTransit Symposium GEAT'05, Zürich, Switzerland, 183-201.

7. Kaiser, P.K., Vasak, P. and Suorineni, F.T. and Thibodeau, D., 2005. New dimensions in seismic data interpretation with 3-D virtual reality visualization in burst-prone grounds. *RaSiM6*, Perth, Australia, 33-47.

8. Kaiser, PK., M.S. Diederichs, C.D. Martin, J. Sharp, and W. Steiner, 2000. Underground works in hard rock tunnelling and mining.
GeoEng2000, Melbourne, Australia, Technomic Publishing Co., **1**: 841-926.

mirarco MINING INNOVATION

grc GEOMECHANICS RESEARCH CENTRE

Laurentian University
Université Laurentienne

SEISMIC HAZARD EVALUATION IN UNDERGROUND CONSTRUCTION

PETER K. KAISER
Centre for Excellence in Mining Innovation, Sudbury, Ontario, Canada; pkaiser@miningexcellence.ca

With contributions by

SEAN MALONEY, PAVEL VASAK, GREG WANG
Geomechanics Research Centre, MIRARCO, Laurentian University, Sudbury, Ontario Canada;
www.mirarco.org

ABSTRACT - This keynote highlights recent developments in mining-induced seismicity research and the development of procedures and tools for mine operators based on experience in the Sudbury Basin, Ontario, Canada. The basin hosts major copper-nickel sulphide deposits that have been mined since the early 1900's. The 25th anniversary of the deaths of four miners in a seismic event at Falconbridge Mine serves as a reminder that much needs to be completed to improve our understanding of mining-induced seismicity and to develop control mechanisms for low risk mining at depth. With over a century of mining, most operations are producing at greater depth where seismicity is a concern and seismic monitoring is now standard practice.

Many mines and deep tunnels are plagued with strainbursts that are either triggered by seismic events or self-initiated due to stress concentrations near excavations. This topic is covered first with both a civil and mining focus. The rest of the paper deals with structurally-induced seismicity and the procedures and tools developed to aid mine operators in dealing with seismic hazards by use of Seismic Excavation Hazard Maps, and with integrated modeling approaches for mine-wide seismicity assessment.

1 Background

1.1 Safety First

"The most important thing to come out of a mine is the miner."
Frederic LePlay (1806-82), French Inspector General of mines in France.

June 22, 2009: "Under a teardrop-laden sky, mourners marked the 25th anniversary of the deaths of four miners in a seismic event 4,000 feet below surface at Falconbridge Mine. The event, which took place on June 20, 1984, was a seismic event that measured 3.5 on the Richter scale. While an initial rescue attempt was underway, a second seismic event occurred. That resulted in the rescue effort being halted while the mine was evacuated. When it resumed, for the first 27 hours, rescuers were in constant voice contact with one of the trapped miners; but just as they were within minutes of rescuing him, he died.

The Mine, Mill and Smelter Workers' Union annually remembers the miners during a Workers' Memorial Day service. Today, the event honours the memory of not only those four men, but all 86 miners who have died in workplace accidents since 1929 at what is now Xstrata Nickel.

What happened 25 years ago is one of those events where you remember exactly where you were and what you were doing when you heard the news."
(*modified based on a recent article in THE SUDBURY STAR by Bob Vaillancourt.)*

Eventually, the mine was closed and 400 workers were laid off (Bray and Thompson 1992), and in response to this and other rockbursts in Northern Ontario, the Ontario Government engaged the Stevenson Commission to advise the government on emergency preparedness and ground control.

After 17 months, 46 public hearings, 16 mine visits, consultations with mining companies, local and international unions, and many related stakeholders, the report contained nearly one hundred

recommendations, amongst others, recommendations about communication, training and education, mine design and planning, mine lighting, and emergency preparedness. It also urged the government to take action to enhance applied research in direct collaboration between industry and universities. One year later, on the third anniversary in 1987, I was on the way to Sudbury to assume a Research Chair in Rock Mechanics and Ground Control at Laurentian University with the mandate to establish a Geomechanics Research Centre (GRC; now part of MIRARCO) with the mandate to coordinate and undertake research to enhance workplace safety.

In a recent panel discussion of the International Association of Labour Inspection (IALI-AIIT) (*www.iali-aiit.org/iali/event_docs/Conference_Proceedings.pdf*; 2007), Pakalnis (Government), Gerard (Labour) and Hodgson (OMA) provided an overview of factors contributing to health and safety improvements in Ontario. Lost time injuries dropped from about 11 in 1976 to 4 in 1986 to 1 in 2006 and the mining/aggregate industry today has amassed outstanding performance records (Figure 1). Total mining industry fatalities dropped from about 19 in 1976 to 10 in 1986 to 2 in 2006.

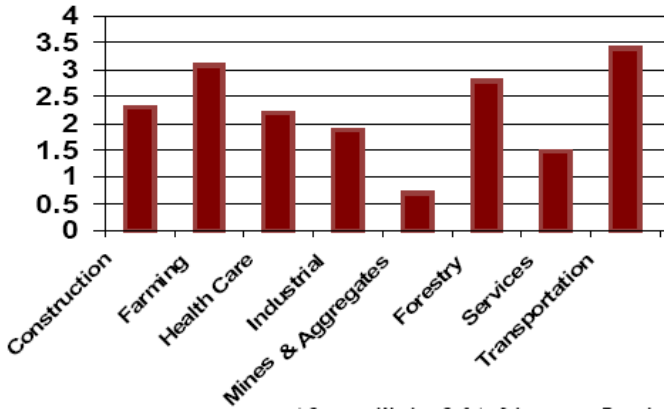

Figure 1 Ontario lost time injuries by industry sector 2005 (Worker Safety & Insurance Board; per 100 employees).

While we can be proud of these huge improvements, much remains to be done to achieve a highly desired zero tolerance limit.

In 1985, under CANMET's and industry's leadership extensive monitoring systems (MP250's at the time) were deployed to better measure the "pulse" of deep, burst-prone mines. In 1990, the Canadian Rockburst Research Program was initiated under the leadership of CAMIRO, with the author and his colleagues delivering the Canadian Rockburst Support Handbook (Kaiser et al., 1996). During this period, major advances to seismic monitoring (full-waveform) and data interpretation technology were made. Many new developments were presented during the 3rd International Symposium on Rockbursts and Seismicity in Mines in Kingston, Ontario, Canada (Young, 1993).

Seismically active mines are now all monitored by real- or near-real-time monitoring systems and policies are in place on how to utilize this data as part of daily risk management procedures (e.g., re-entry policies, etc.).

Clearly, no one would claim that the stress and fault slip problems in deep mines have been solved but the rockburst problem is today sufficiently understood so that it can be tackled from several fronts to lessen the chances for further tragedies. Today, as then, the RaSiM symposium is all about making workplaces even safer; for a humane society, even a single fatality is one too many.

Of course, there are also economic motivators to better understand and manage seismicity and micro seismicity in mines. While also important, this keynote focuses largely on means to improve safety and to reduce the risk when mining at depth.

1.2 Managing Uncertainty in Burst-Prone Mines and Deep tunnels

Ideally, we would like to predict where, when and how large a seismic event will be triggered, and where and how severe the related damage to an excavation could be. In other words, we all would like to predict rockbursts. As we proceed to greater depth, the state of stress is in a fragile state of equilibrium and it takes little to disturb it. Hence, with certainty, we can say that mining will cause seismicity and trigger rockbursts. However, for the foreseeable future, it will not be possible to predict the time of bursting with any degree of certainty. At best, we may be able to anticipate the location (spatial distribution) of rockbursts and the anticipated severity of damage to excavations.

We are also making good progress in controlling energy release by systematic mine designs and operational procedures; we are able to reduce the potential for bursting and the severity of damage to excavations. However, there will always be a finite risk of bursting, e.g., due to the complex nature of rock. Hence, we must accept that rockbursts are inevitable and unpredictable; consequently, constructive ground control techniques must be adopted to maximize worker safety, minimize the risk for production interruptions, ore sterilization, etc.

With respect to worker safety, uncertainty in burst-prone ground is best managed by a combination of at least the following three elements that represent the focus of this keynote: (1) exposure minimization, (2) worker protection, and (3) understanding seismic migration patterns.

By selecting mining methods that expose the least number of workers, and by adopting semi-empirical re-entry policies and other operational procedures, worker exposure can be minimized. By providing the best possible support systems and, for economic reasons, installing them at the most critical locations (areas of highest risk of damage), workers can be provided with protection although with limited capacity. By better understanding seismic migration patterns, it is possible to reduce uncertainty and better deploy workers to safer work places.

This keynote focuses on three aspects of a wide spectrum of risk management for worker safety in burst-prone mines and underground excavations:

- Strainbursting, a well understood but unpredictable burst process. Since we do not have reliable means to predict the location or energy release from strainbursts, this section focuses on control measures and damage mitigation matters.
- Hazard characterization, a means to identify where the demand on ground support may reach or exceed the capacity of the reinforced rock mass. The concept of hazard maps was introduced during the last RaSiM symposium in Perth, Australia, and recent advances will be highlighted. This approach is based on understanding where the rock mass is damaged by micro-seismicity, stability compromised by seismically active structures, and where shake-down by major seismic events may occur.
- Mine-wide seismicity, a yet poorly understood phenomenon whereby seismicity is travelling far beyond the influence of mining-induced stress changes. In this section, we introduce and report some progress on one of many yet unresolved issues. It is hoped that this will stimulate and focus future research efforts.

2 Stress-induced Seismicity – Strainbursts

Depending on the cause, rockbursts are classified as fault slip, pillar, or strainbursts. This section deals specifically with strainburst.

A strainburst is a rockburst occurring when the stresses near the boundary of an excavation exceed the (unsupported or reinforced) strength and failure proceeds in an unstable, violent manner. The tangential stress, and thus the stress deviator, near an excavation increases as an excavation (tunnel) is advanced (see Figure 6.a) and eventually, particularly in brittle rock, fails with various degrees of energy release. During mining, the stress state is often disturbed and may lead to a further increase in stress deviator (either by stress increases or confinement reduction), and thus an increase in strainburst potential. Finally, remote seismic events (e.g., fault slip events) or major blasts may add a dynamic stress component and thus trigger strainbursts (Kaiser et al.

1996). During violent failure, the stored energy in the rock is suddenly released, largely by stressed-induced spalling and often assisted by structural weaknesses (joints), and failure propagates to a limited depth (d_f).

In addition, the strength may degrade with time leading to delayed failures. In either case, the strength-to-stress ratio reaches unity and the rock fails. The failure process is sudden and violent if the stored strain energy in the is not dissipated by friction in the supported rock near the excavation boundary. The strainburst potential is particularly high when the stiffness of the loading system, i.e., the mine stiffness, is lower (softer) than the unloading stiffness of the volume of failing rock.

Strainbursts and the released energy potential are difficult to predict. Hence, it is necessary to use constructive techniques to minimize the potential for and the severity of damage to excavations.

2.1 Rock Failure and Strainburst Processes during Tunnel (drift) Advance

Spalling

Spalling is a progressive, brittle rock failure process that is predominantly observed near excavation walls. It involves extension or tensile failure (fracture propagation; Figure 2.a) and shear failure processes (predominantly along pre-existing weaknesses; Figure 2.b). Spalling may occur progressively or violently in the form of a strainburst.

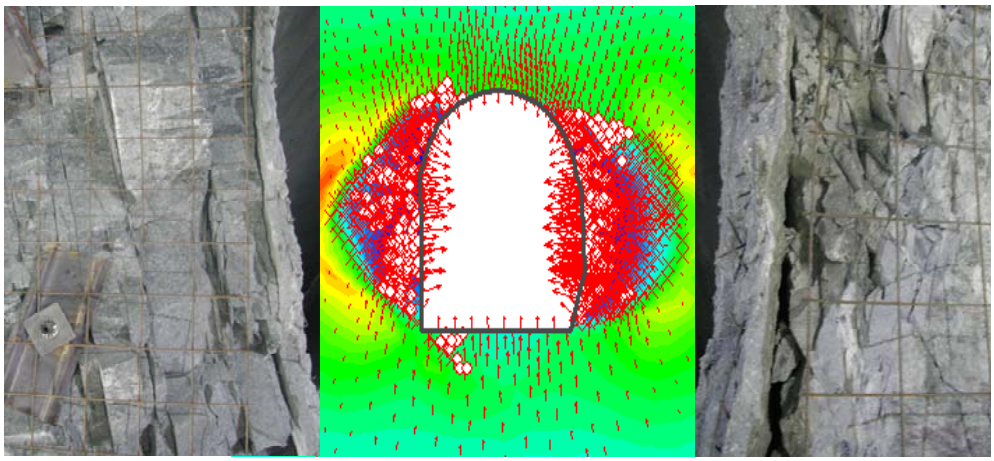

(a) (b) (c)

Figure 2 Stress- induced failure in Gneiss: (a) surface-parallel extensional spalling, and (b) predominantly shear failure along weaknesses together with some spalling; centre: model showing tensile (circles) and shear (crosses) failure zones on each side of the drift.

Depth of Failure

Failure in massive to moderately jointed, brittle rocks generally starts when the maximum, tangential stress at the excavation boundary (defined for a circular excavation as $\sigma_{max} = 3\,\sigma_1 - \sigma_3$) exceeds about 40% of the UCS or σ_c determined from undamaged core. The depth of failure (d_f) is proportional to the stress level defined as the ratio of this maximum stress to the unconfined rock strength as illustrated in Figure 3 (after Martin et al., 1999).

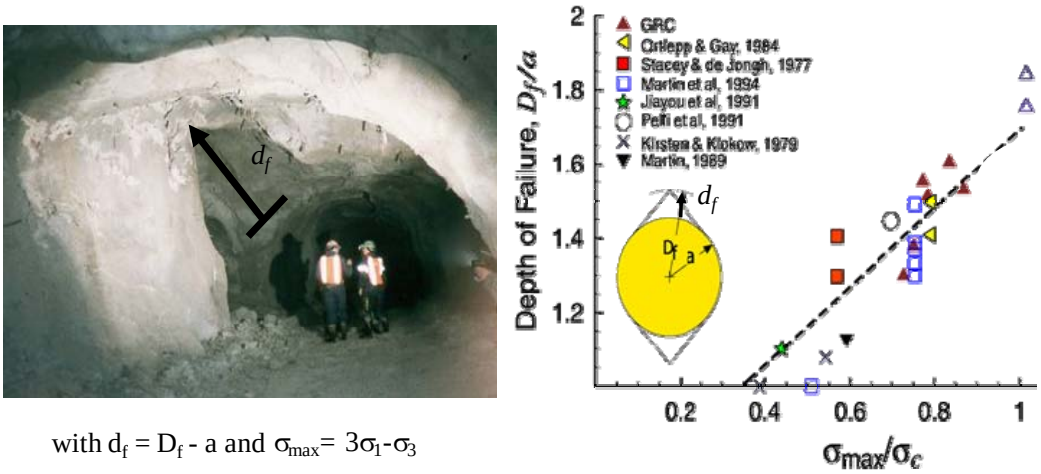

with $d_f = D_f - a$ and $\sigma_{max} = 3\sigma_1 - \sigma_3$

Figure 3 Observed depths of failure as a function of stress level σ_{max}/σ_c.

Severity of Damage

Damage can vary in intensity or severity from minor rock spalling to severe unravelling of the fractured rock. The dynamic nature of rockburst damage means that there is the potential for energy release during the failure that may lead to extensive damage to or complete destruction of supported and unsupported underground excavations.

Kaiser et al. (1996) define the severity of rockburst damage by the depth of failure and the lateral extent along the circumference of the tunnel (Figure 4).

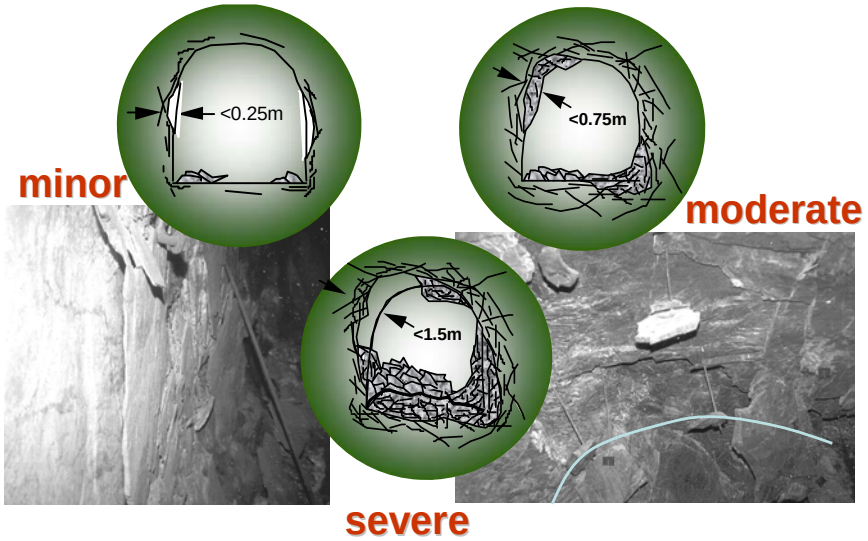

Figure 4 Severity of rockburst damage as a function of depth of failure.

From a support perspective, it is important to note that high capacity burst-resistant support with yielding bolts are required for severe bursts with depth of failure exceeding 0.75 to 1m.

Rock Mass Bulking

Rock mass bulking is a process of volume increase due to the fracturing of massive to moderately jointed rock. Figure 5 shows a massive rock mass damaged during a rockburst. As a result of lateral convergence, the rock disintegrated into “blocky” ground that tends to radially dilate and thus move into the excavation. In this case, it deforms excessively and the support fails because it has inadequate deformation capacity.

If unsupported, the bulking factor can be as high as 35%, but bulking can be reduced to 5 to 10% with appropriate support systems that control the dilation of the broken rock (Kaiser et al. 1996).

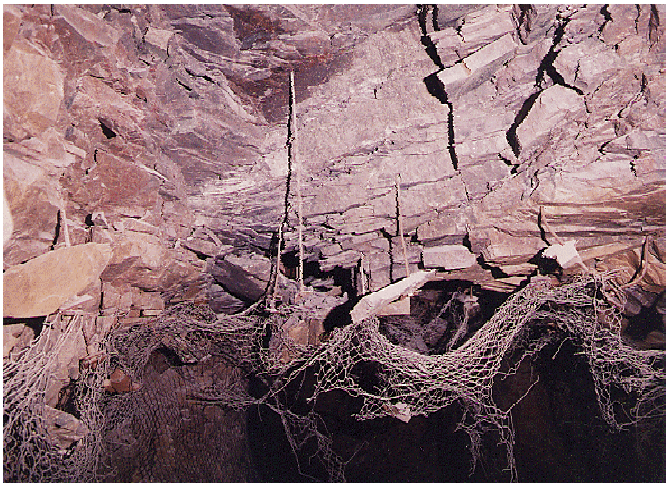

Figure 5 Stainburst creates "blocky" ground that causes large, radial tunnel convergence due to rock mass bulking. It also tends to unravel, leading to short stand-up times when insufficiently supported.

Spalling processes and related bulking can be observed in many deep tunnels. Most pictures of rockburst damage, like the one shown in Figure 5, suggest that bulking is a predominant process during failure. Consequently, ground support must be designed to reduce bulking and to deform with the bulking rock.

2.2 Location Prediction of Strainbursts

The question whether rockbursts can be predicted must be subdivided into two components: (1) Can the location of a strainburst, and more specifically, the location where the damage will be encountered be predicted?, and (2) Can the timing of a strainburst be predicted?

In the authors' opinion, it is next to impossible to predict the time or location of a rockburst along a tunnel to such a degree of accuracy that it could be used to place burst-resistant support selectively. However, it is often possible to establish rules for the timing of a strainburst within the advance cycle (see below). The location with respect to the tunnel face can also be estimated by considering the tangential stress development near the tunnel face. This is schematically illustrated by Figure 6.a, where the tangential stress is seen to peak at the face (leading to bursting at the face or in the shield) and, then gradually increases to the maximum stress at about 1 to 3-times the tunnel diameter (D) from the face. In elastic ground, strainbursts should be anticipated at or before the maximum stress is reached; i.e., between the face and about 2 to 3 diameters from the face.

Also shown in Figure 6, is the time delay between the face and 1, 2 and 3D from the face for a TBM driven tunnel. This illustrates when respective stress levels are reached (85% at 1D to 99% at 3D). Bursting occurs when the rocks capacity is exceeded by the induced tangential stress σ_θ. This can occur between the face and when the maximum tangential stress is reached at about 2 to 3D. Hence, for rock satisfying the underlying assumption of elastic rock behaviour and time-independent rock strength, Figure 6.b, provides an estimate of the maximum time to bursting for a tunnel advancing at a steady advance rate (AR).

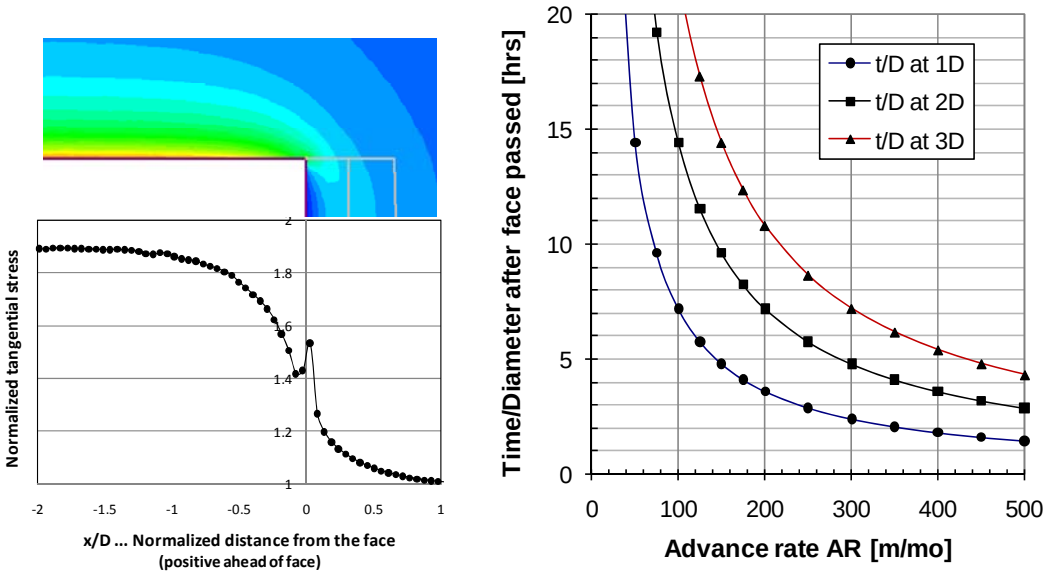

(a) (b)

Figure 6 (a) Development of tangential stress near the face of a circular tunnel in elastic ground (K_o = 1), and (b) estimated normalized times (t/D) for locations at 1, 2 and 3D from face as a function of average tunnel advance rate.

Figure 6.b shows that for high advance rates (>500m/mo), delays of bursting could be 4 to 5t/D or up to 50 hrs for a 10m wide tunnel, for intermediate advance rates (~300m/mo) up to 7t/D or 70 hrs for a 10 m tunnel, and for low advance rates (~150m/mo), delays of bursting could exceed 15t/D or 150 hrs for D = 10m.

This analysis suggests that the advance rate can be used to estimate the maximum time to bursting. In tunnels with large numbers of strainbursts, this hypothesis can be verified and then semi-empirically revised to take account of other factors such as time-dependent behaviour of various rock types. Where data is lacking, the graph in Figure 6.b can be used to estimate re-entry times for worker access restrictions when signs of imminent bursting (spitting rock) is encountered.

2.3 Damage Location for TBM versus Drill and Blast (D&B) Advance

Figure 7 shows σ_3-contours together with the type of yielding (tensile or shear) and iso-lines for deviatoric stress for a D&B advance with a round length of approximately D/2. For the selected stress and ground conditions (elastic-brittle plastic), deep-seated failure of the face (Kaiser 1999) and relatively shallow failure of the wall rock is encountered. Tensile spalling is predicted in the face and at the wall within half a diameter from the face. The iso-lines of the deviatoric stress (axial-radial) show rabbit-ear-like shapes staring at the face and reaching back over about one round length. During D&B advance, illustrated by Figure 7, this deviatoric stress lobes and the related tensile spalling is pushed ahead by each round. However, during TBM advance, it is moved ahead incrementally. As a consequence, the damage location is quite different for the two excavation methods: continuous damage for TBM and stepped damage for D&B. Furthermore, the damaged zone is typically excavated during a blast, while it sits on the shield of a TBM. This difference can lead to construction difficulties (Kaiser and Kim, 2008) and increases the uncertainty about timing of strainbursting in TBM tunnels.

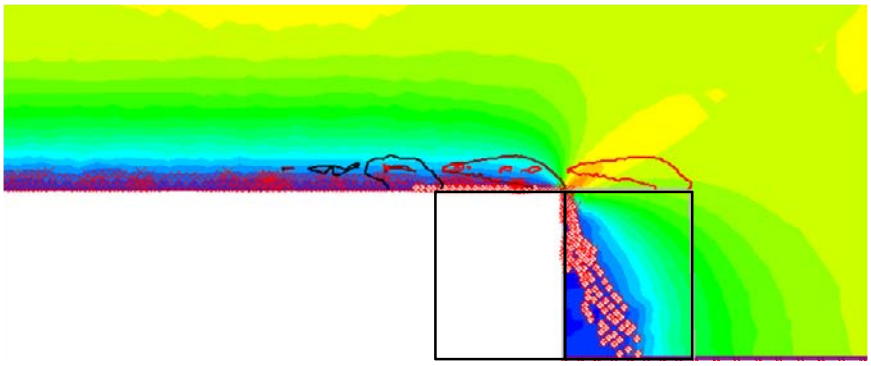

Figure 7 Axi-symmetric model of a tunnel in yielding ground: shown are shaded σ_3-contours during second of three excavations stages of round lengths (D/2); x = shear failure; o = tensile failure; iso-lines of deviator (axial- radial) at 35MPa are shown for all three excavation stages; each lobe belongs to the respective face location.

It must be noted that the burst potential generally is higher in TBM-driven tunnels as more energy can be stored in the less damaged rock near a TBM. However, the kinetic energy release in TBMs should be lower due to the incremental excavation damage process as illustrated above.

2.4 Support Selection in Strainbursting Tunnels

Support Demand

Support design is a matter of providing sufficient capacity to cover the demand. In this case, the demand will come from: (a) deformations due to bulking; (b) gravity loading by broken rock; and (c) energy release during rock fracture.

(a) Wall deformations due to rock mass bulking, e.g., for anticipated depths of failure of 1, 2 and 3m, respectively, and bulking factors of 5 to 10% depending on support effectiveness (Kaiser et al. 1996), could range from 50 to 300 mm.
(b) The load equivalent to the weight of 1 to 3m of broken rock is to be carried by bolts extending beyond the respective depth of failure.
(c) In rockbursts of minor to moderate severity, much of this energy will be dissipated through friction between broken rock pieces. Thus, design for deformation and load demands is considered sufficient (Kaiser et al. 1996) for bursts of minor to moderate severity. For severe bursts, however, support elements with significant energy dissipation capacity need to be considered.

Role of Support in Burst-prone Ground

An effective burst-resistant support system consists of compatible support components and connections that are superior to the (deformation and load) capacity of the individual components. The system should consist of three components with differing ground control roles (Figure 8) to help:

- Reinforce the rock, e.g., grouted rebar, to hold broken rock together and to minimize the bulking of the broken rock;
- Retain the broken rock, e.g., mesh supported by rock bolts, to prevent ravelling of broken rock between bolts; and
- Hold the package of retained, reinforced rock by tying it back to stable ground (outside the depth of failure).

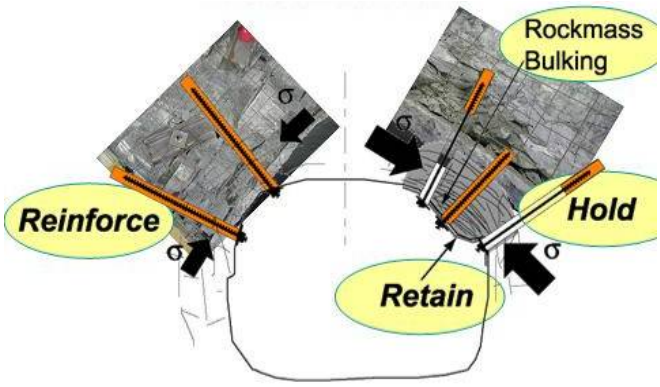

Figure 8 Role of support system components: Reinforce - to hold broken rock together; Retain – to prevent raveling of broken rock; Hold – to tie support system consisting of retaining and reinforcement components back to stable ground.

Reinforcement, Holding and Energy Dissipation Function of Rock Bolts

Stiff bolts, like grouted rebar, are rapidly loaded and thus are best suited to reinforce the rock, but they may fail when strained excessively. Thus, in burst-prone ground they need to be combined with a ductile or yielding bolt such as a Splitset™, Swellex™, or Superswellex™ bolt. For severe bursting conditions, high load capacity yielding bolts must be applied (e.g., the Modified Cone Bolt).

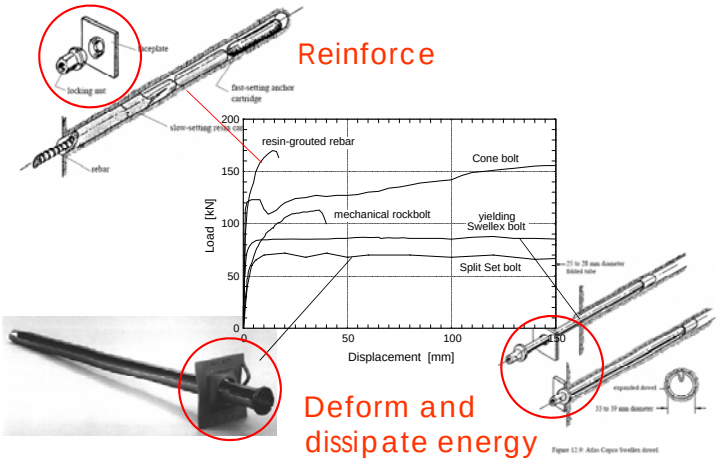

Figure 9 Bolt types with typical load - displacement characteristics (Hoek et al. 1995; Kaiser et al. 1996).

These bolts must be plated and well connected to the retaining system (through mesh or shotcrete) as illustrated by Figure 10.a.

Retaining System Components

Mesh, fiber-reinforced shotcrete or mesh-reinforced shotcrete provide suitable retaining systems with increasing capacity in the order listed. Straps or U-profiled steel ribs, or properly bolted I-ribs may be used to reduce the effective span and thus to further increase the load capacity of these retaining components.

Mesh must overlap and bolts must hold the mesh such that, when loaded by broken rock, the overlaps do not open up as illustrated by Figure 10.b.

Fiber-reinforced shotcrete is superior only if small deformations (about <50mm central deflection between bolts) are expected in minor and possibly in moderate burst conditions.

(a) (b)

Figure 10 (a) Example of good quality, plated bolting and mesh-overlap practice; also shown is stack of mesh (2.5x1.5m); (b) mesh damaged by a minor rockburst due to insufficient overlap and inadequate plate size.

System Integration

A support system is only as good as its weakest component; i.e., the weakest link. Hence, it is of utmost importance that all connections are of superior quality. This includes:

- *Bolts* must be plated: with sufficient plate size to prevent shearing of mesh wires, hole to match bolt and nut size, straight loading of bolts (use of domed nut and plate);
- *Grout* quality (w/c ratio) must be such that high strength is reached rapidly; pre-tensioning is not recommended for support in burst-prone ground;
- *Mesh* must overlap and straps should possibly be used to enhance the load bearing capacity of the retaining system (if no steel ribs are installed);
- *Shotcrete* should be of optimal mix to achieve little rebound and penetrate between mesh strands, particularly at overlaps; and in severe rockburst situations
- *Mesh over shotcrete* may have to be considered (as ejected shotcrete is as dangerous to workers as ejected rock).

Location of Support Installation

According to the Swiss standard, for example, it is generally recommended to install 1/3 of the ground support (bolts) in each of L1, L2 and L3[1], respectively. In burst-prone ground, this is not sufficient as burst-resistant support is needed at the face and sufficient burst-resistant support must be installed in L1. At least 2/3 of the required bolting should be installed in L1 together with a strong retaining system; possibly a first layer of shotcrete.

In TBM tunnels, the shotcrete may be delayed to L2, if the mesh is of sufficient (system) capacity, well bolted and combined with straps or U-profiles.

In D&B tunnels, fibre-reinforced shotcrete may replace mesh in areas where minor to moderate bursting is expected (not in severe bursting conditions).

From a worker safety perspective it is not acceptable to work under unsupported ground in burst-prone ground.

[1] L1 refers to the immediate face area behind the face, typically within 0 to 1 D where overhead protection is to be installed; L2 refers to tunnel section where the ground needs to be safely secured, typically within 2 to 3 D; and L3 refers to zone beyond where the final support can be installed with significant delay.

2.5 Risk Mitigation Concept for Burst-prone Ground

Hoek (1992) illustrated by Figure 11.a how good engineering practice is used to gradually reduce the factor of safety, not by moving the mean value of capacity and demand apart, but by reducing the variability in the design from wide distributions, during feasibility studies, to narrow distributions, once a detailed design can be verified by back-analyses.

In burst-prone ground, it is often difficult to reduce the width of the distributions due to many uncertainties introduced by stiffness, strength and energy storage parameters. Hence, good engineering practice involves separating the demand and capacity distributions. The energy dissipation capacity of support can be either increased by increasing the load capacity or by increasing the deformation capacity.

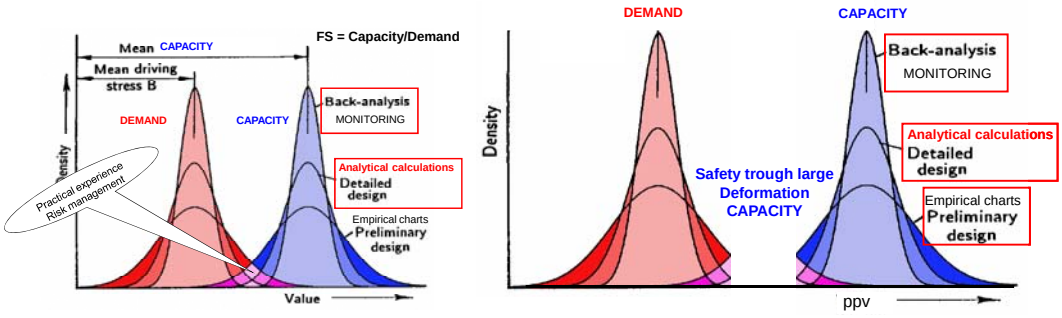

(a) .(b)

Figure 11 Demand and capacity distributions: (a) for conventional design, and (b) for burst-resistant support (modified from Hoek (1992)).

As illustrated by Figure 9, burst resistant support must be able to deform such that energy (the area under the load-displacement curve) is high. Hence, it follows, as shown by Figure 11.b, that it is most effective to add deformation capacity in an effort to improve the safety (capacity) of burst resistant support systems.

3 Excavation Hazard Assessment

3.1 Seismic Excavation Hazard Maps

MIRARCO has pioneered the use of virtual reality (VR) technology for solving complex problems in underground mining. The technology, first introduced for earth modelling in the oil and gas sector, is well suited for multidisciplinary evaluation of information at all stages of the mining cycle. VR has proven to be beneficial in developing 3D geology models, planning exploration drilling and resource models. Furthermore, these developments have demonstrated that VR technology can be extended to handle spatiotemporal data used for planning mine infrastructure, optimizing stope sequences and using mine monitoring data to understand how production practices impact the safety of the operation. The latter is particularly relevant to deep mining where rockbursts can have an adverse effect on both safety and the economic viability of an operation. VR and visual interpretation is quickly shifting the data analysis paradigm for highly complex engineering problems. While we have been applying the technology to other fields such as stope stability assessments, in this section, we focus on the development and application of the Seismic Excavation Hazard Maps (SEH Maps) for deep mines (Figure 12). The technology has matured to the point where it now can be used on real-time data and it is thus fitting to integrate virtual reality and scientific visualizations methods, with large screen, immersive, stereoscopic visualization capability at mine sites. MIRARCO has established such facilities at mines of Goldcorp (Red Lake, Canada), Vale Inco (Creighton Mine, Sudbury, Canada), Kennecott (Rio Tinto, Northern Hemisphere Interpretation Centre, Salt Lake City, USA), and recently at the Xuzhou Coal Mining Company (Xuzhou, China) as well as in the Timmins Library (Ontario, Canada) and North-eastern University (Shenyang, China).

Vale Inco's Creighton Mine Virtual Reality facility is the first purposely built for seismic hazard evaluation and is used to assess location, severity and occurrence (timing) of seismic hazard for mine safety by tracking how the rock mass responds to mining, using direct monitoring of the damage processes (seismicity)

in the rock mass. The SEH Maps are also used for planning of future infrastructure (deepening of ramp system, raises, etc.) and planning infrastructure rehabilitation, particularly the strategic placement of dynamic support, during mine maintenance shutdown periods. The SEH Maps are the direct implementation of the concepts and principles introduced in the previous RaSiM6 symposium (Kaiser et al., 2005). Since then, it has been applied, tested and validated at four of Vale Inco's seismically active mines in the Sudbury Basin.

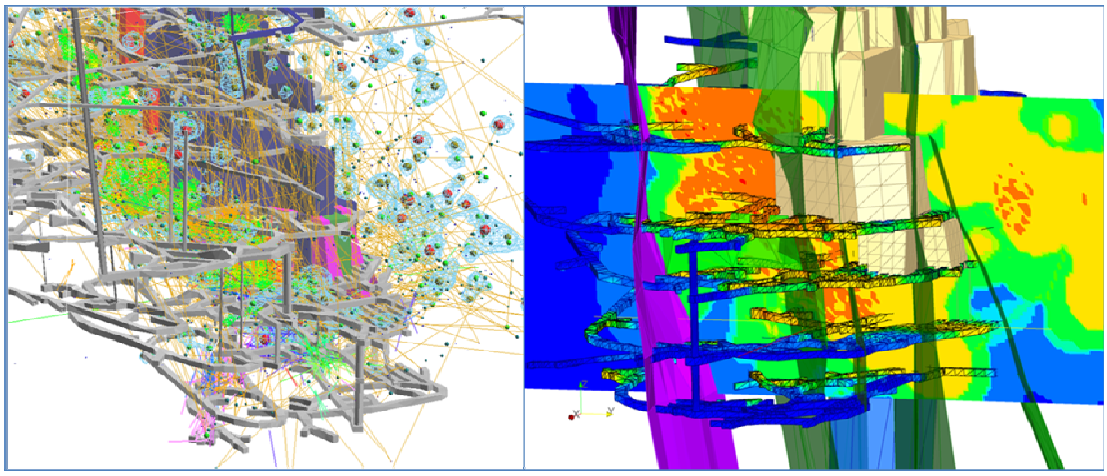

(a) (b)

Figure 12 Seismic data processed to create Seismic Excavation Hazard Maps: (a) Seismic and micro-seismic data with density contours and time links (lines connecting events); (b) SEH map with drifts colored by hazard level (also shown is a vertical plane of enquiry).

3.2 Seismic Excavation Hazard Maps

The objective of monitoring seismicity at mines is to enhance worker safety and to reduce risk in general, e.g., to minimize production interruptions. These goals can be achieved by various means, all involving some form of data analysis to produce practically useful outputs (e.g., re-entry policies, stoping sequence guidelines, etc.). Here we focus on means to identify hazards related to infrastructure, i.e., the development of excavation hazard maps.

These maps provide an overall picture of the stability (or potential instability) conditions in a mine for planning and operational control purposes. They show hazardous areas in the mine by identifying zones of degraded rock, seismically active structures such as faults and shear zones, and areas of high impact by seismic waves (dynamic stressing). Degraded zones of rock, if close to excavations and infrastructure crossing seismically active planes or active fault zones will require higher support levels and mining sequences must be properly managed to minimize impact on hazardous areas. For planning new mine infrastructure, avoiding the high hazard zones should be a primary consideration, where this is economically acceptable.

Principles of Hazard Maps

Vasak et al. (2004) and Kaiser et al. (2005), introduced the concept of hazard maps and illustrated that there are three fundamental excavation hazards to be considered: (1) degradation manifested as microseismic events due to stress-induced damage close to mined excavations, (2) loosening (tension) or shear-slip on existing small-scale geological structures (e.g. joint sets) within the mining-induced stress envelope and manifested as oriented microseismic clusters, and (3) dynamic loading or shakedown due to seismic wave propagation as a result of shear-slip on large-scale geological structures.

Rock Mass Degradation

This hazard results from the degradation by fracturing of relatively intact to moderately jointed rock in regions of high stress concentration. As fracturing continues, the rock mass loses its capacity to support itself and gravity-induced ground falls may occur in the backs of excavations. The MS (or crack) density is used to identify areas of elevated rock mass degradation and the cumulative damage is tracked over time. Each

microseismic event implies a new crack or extension of an existing crack. A microseismic density number is assigned to each event and is defined as the number of MS counts in a search sphere. Discrete regions of high MS density are used to identify areas of significant degradation in the rock mass and particularly near excavations.

Seismically Active Planes

Whereas the previous hazard tracks the fragmentation of the rock, this hazard tracks the deformation of large scale weaknesses in the rock mass. Natural rock contains various scales of flaws ranging from micro-fractures to regional fault zones. The right combination of tensile or shear loading will cause deformation along these pre-existing flaws and new weakness zones may be created and propagated. The planarity of related microseismic records is used to identify structures that may transmit deformations over long distances. In the approach adopted here, Seismically Active Plane (SAP) hazards are used to identify the current (during the most recent predefined time interval) micro-seismically active planes. This is to account for the fact that the SAP hazard is driven where mining is active and eventually disappears when mining moves to a new location or structures become aseismic when the residual strength is reached. The identification of such SAP hazards over time is important to establish a discontinuum model of a mine as illustrated by the two SAP representations for a slice of ground at one level of Creighton Mine (Figure 13). It can be observed that there is a direct correlation with some of the visually identified geological structure (e.g., Figure 13 (iii)) and newly identified geological structure; e.g., Structure (i) is interpreted as a vertical structure that is responsible for the largest magnitude seismic event recorded at the mine and it has an active area of about 1800 feet in diameter (Vasak, 1999); Structure (ii) can be indentified when it is activated by local stress perturbations caused by mining of stopes.

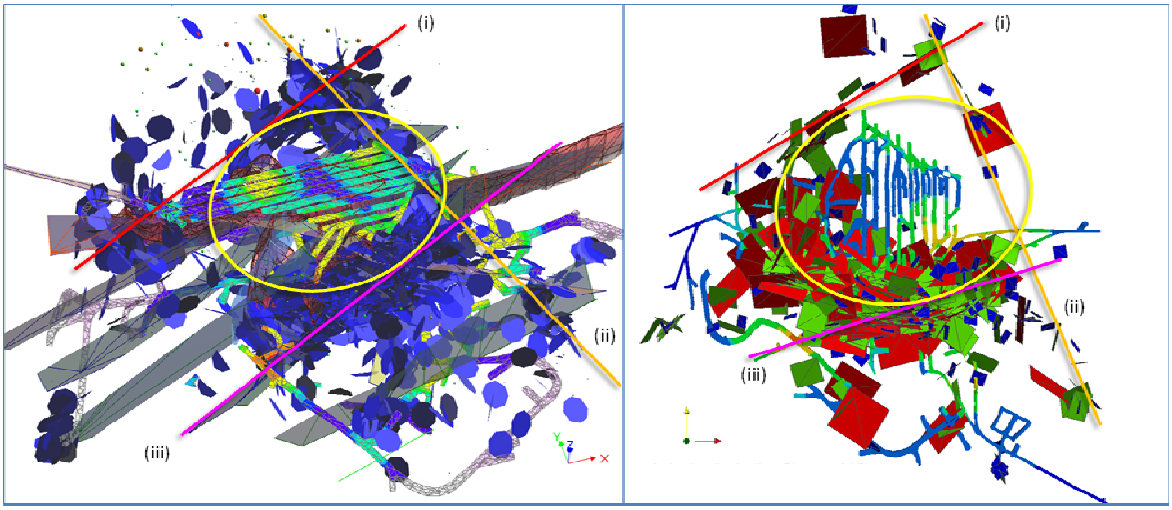

Figure 13. Accumulation of SAP hazards indicating the larger scale discontinum model and the effect of the mining-induced stress zone. Both interpreted (i and ii) and known (iii) geological structures are shown in context with the inferred mining-induced stress halo around the ore zone: (a) Oblique view showing SAPs as oriented circles, mapped mine structures as surfaces and the dynamic (seismic) hazard ranking painted on the drifts; (b) Plan view showing SAPs as oriented planes sized and coloured by Es/Ep ratio (low = small to high = large planes). The total seismic hazard is painted on the drifts, but the SAPs obscure the high hazard areas.

Seismic Loading Hazard

When a rockburst occurs additional loading in the form of dynamic stress waves are imposed on the walls of mine infrastructure and ground support. Marginally stable rock masses may be induced to fall by dynamic acceleration. Mine structures that were already close to failure (factors of safety close to one) could be triggered to fail by strainbursting or by seismically induced falls of ground as a consequence of this additional, dynamic loading. If the dynamic loading does not lead to instabilities, it may still cause additional rock mass damage and reduce the long-term factor of safety such that subsequent rockburst may trigger failure.

The consequences of dynamic loading are fracturing and bulking, as well as shakedown in blocky rock masses. In the following, we only deal with the effect of dynamic stress (Kaiser et al., 1996; for seismically induced falls of ground refer to same publication). The dynamic far-field stress change modifies the stress near an excavation (by $\Delta\sigma^d$) causing rotating stress concentrations. The maximum dynamic stress increase at the excavation is estimated for the shear wave case as follows:

$$\Delta\sigma^d_{\max} = \pm 4\, c_s \rho\ \ ppv_s$$

Using rock mass parameters determined for Creighton Mine by Kaiser et al. (1996) and calibrating the scaled distance (rockburst to the damage locations) to the source event magnitude, the dynamic stress loading hazard impact rating at a mine site can be determined as shown in Table 1. These values take into account the effect of the currently installed support. Improving the support at the mine site can improve the dynamic impact rating; conversely, deteriorating conditions over time will result in a reduction of the dynamic impact rating. Seismic hazard is a dynamic property that continually changes as mining progresses.

Table 1. Seismic loading hazard impact rating for Creighton Mine based on equivalent dynamic stress change.

Hazard factor	Parameter	Parameter impact rating			
		Negligible	Low	Moderate	High
Seismicity	ppv (m/s)	<0.28	0.28 – 0.56	0.56 – 1.12	≥1.12
Dynamic stress equivalent (MPa)	$\Delta\sigma^d$	< 10	10 - 21	21 - 43	≥ 43

Case Example - Creighton Mine

Seismic hazards are calculated for the rock mass volume, but can be represented as iso-surface contours, or more traditionally as plans and sections (e.g. Figure 12). Alternatively, the data can be projected onto any other geometric object such as geological structures (e.g. faults), mine stopes or drifts (as shown in Figure 13). A simple colour scale (blue, cool, low hazard to red, hot, high hazard) represents the hazard level. Two practical applications of the SEH Maps recently used at Creighton Mine are provided.

The first application of the SEH Map is to identify areas of high degradation and target these areas for support review. Based on underground observations, decisions to rehabilitate and/or enhance the support for worker safety were carried out during the annual maintenance shutdown period (per. com, A. Punkkinen, Rock Mechanics Specialist, Creighton Mine). Figure 14(a) shows the identified high priority zones that encompass critical ore handling (high exposure) infrastructure in the footwall.

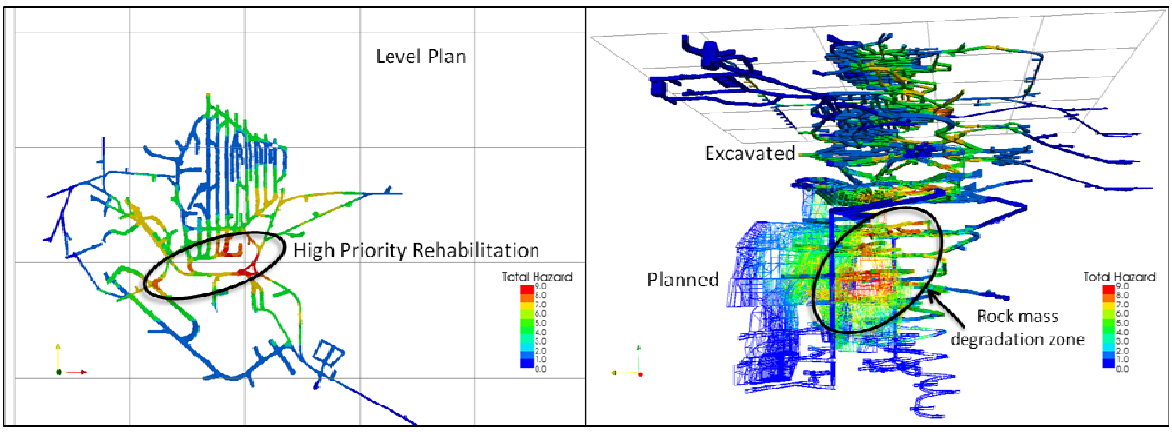

(a) (b)

Figure 14. Practical applications Seismic Excavation Hazard Maps: (a) targeting support rehabilitation and enhancement in critical traffic areas; (b) identifying zones of rock mass degradation from the seismic record and projecting it on planned infrastructure.

The second application was identified in the Creighton Mine Virtual Reality facility where the seismic hazard was projected onto planned infrastructure (wire frame portion in Figure 14 (b)). It became evident that mining of a critical stope at the deepest level of the mine is impacting the surrounding rock mass much more than is typically encountered. This example illustrates the power of peering into the rock mass, using real data and virtual reality visualization means. Potential problems may be avoided by tracking the progress and extent of the rock mass deterioration and adjusting the mine plan where warranted.

Application to other Sudbury Basin Mines

Implementation of the SEH Map logic to three shallower, less seismically active mines was achieved in less than 48 hours for each mine site. This included a data integration model from data provided by the mine; SEH Map calibration based on seismic sensor array size and the quantity and frequency of mining-induced seismicity collected by the system; and the production of SEH Maps. In all cases the models were validated by the Ground Control Specialist at each site by use of VR technology. At Garson Mine. the mine SEH Maps were presented to the OSEH (Operations Safety, Health and Environment) committee with most favourable feedback: "The mine will continue using ParaViewGeo and the Hazard Map software as part of its regular operation" (per. com, L. Moreau-Verlaan, Senior Ground Control Specialist, Garson Mine).

3.3 Case study using GeoHazard Approach for Fall of Ground Forecasting

In an effort to improve our ability to forecast the relative hazard of ground fall ("FOG") due to fault-slip rockburst events, the Centre for Excellence in Mining Innovation (CEMI) recently commissioned Mira Geoscience of Montreal, Canada, to produce a methodology and a tool to better anticipate locations of FOGs. At this stage the methodology has been tested on one case study.

Work flow

A disciplined workflow for hazard identification was devised which allows the user to select:

- a knowledge-driven framework in which expert knowledge is used to manually classify, score, and weight individual criteria;
- a data-driven framework in which training data of known valid fall of ground occurrences in the model are used to classify and weight the input criteria.

Furthermore, this methodology was developed in a manner that allows the GeoHazard assessment team to utilize their knowledge and to derive information for decision-making:

- Inject information based on team understanding of geotechnical model and processes;
- Produce explicit, repeatable, auditable chain of reasoning from conceptual model to data to spatial hazard forecast;
- Apply approach to all geotechnical hazards; and
- Arrive at hazards ranked and prioritized on quantitative geotechnical criteria.

As illustrated by Figure 15.a, an earth model forms the core of the approach where geology, structure, geometry, stress, seismicity and other factors can be integrated. Furthermore, Figure 15.b shows that two practical aspects dictated an effective work flow: rapid data and model development for rapid, evidence-based hazard forecasting.

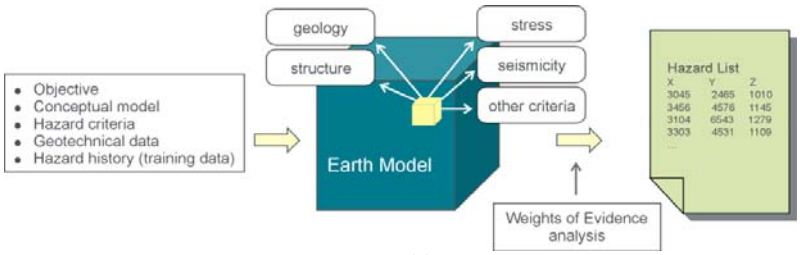

(a)

(b)

Figure 15 Workflow summaries for (a) modelling approach, and (b) hazard identification approach.

Verification of approach

A mine in a geologically complex environment experienced a series of rockburst related falls of ground and thus provided an opportunity to develop, calibrate and verify the adopted approach for GeoHazard assessment. A data-driven approach was adopted to identify and weight the most critical hazard criteria based on spatial and temporal correlations between each of the hazard data layers and the locations of known FOGs. This weights of-evidence analysis produced the following most influential factors for the given case study:

- For the orebody: microseismic density; age of mine development; proximity to fault segments with a high slip tendency (ratio of shear to normal stress); mining method; and E_s/E_p ratio of local microseismic events.
- for the host rock: proximity to ore; disking and core breaks; rock quality; and microseismic density.

These preliminary results indicate that the orebody FOGs are primarily correlated to hazard variables related to mining activity whereas the host rock FOGs are primarily correlated to hazard variables related to local rock quality. This highlights the importance of defining a comprehensive conceptual model prior to modelling and geotechnical hazard forecasting.

Weighted hazard criteria were combined using the binary weights-of-evidence algorithm resulting in a 4D GeoHazard model. Drifts and stopes were coloured by increasing GeoHazard (cold to hot), computed for each date at which a FOG occurred, and compared with observed fall of ground locations. As illustrated by Figure 15, while not all hot zones experienced rock falls, rock falls did occur in areas of anticipated elevated GeoHazard. Further studies will be required to refine the approach and to ensure that all critical factors are considered.

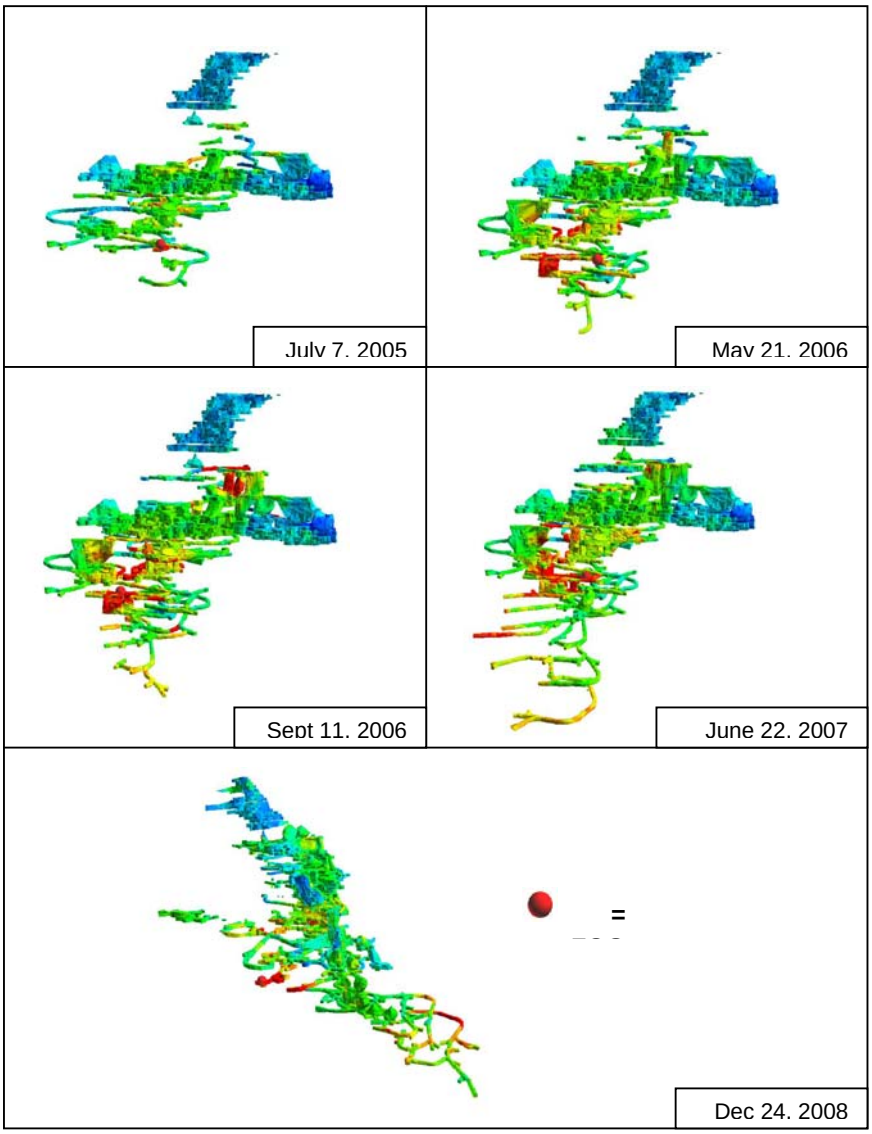

Figure 16 Verification of hazard map: cold to hot colours indicating increasing GeoHazard and dot showing location of observed falls of ground (FoG).

A beta-version of this tool has been deployed to the sponsoring companies and further testing is in progress.

4 Mine-Wide Seismic Migration

Mining-induced seismicity is typically caused by stress changes near an excavation or on geological structures that may become critically stressed and eventually fail violently causing fault slip rockbursts. Clearly, if stress change was the trigger, such events would have to be in the zone of influence of mining, i.e., some stress change would have to trigger the event as is evidenced in the footwall activity in Figure 13. However, there is ample evidence that seismic events may migrate far beyond the direct influence of stress as determined by continuum stress models. This is typically observed in the deep hangingwall at Creighton mine.

4.1 Time-links - Evidence of Mine-wide Seismicity

Time-links is a term introduced to describe “time linked” seismic events, i.e., events that occur, after filtering of blast data, sequentially with time. Time-links connect events with immediate pre-cursor and “aftershock” to visualize seismic migration patterns.

The lines in Figure 12.a and Figure 17.a, connecting seismic events, show such time-links for a relatively long time period (15 years in Figure 17.a and several highly active months in Figure 17.b). From the patterns of sub-parallel time links, it is evident that distinct migration patterns between mining blocks exist (for scale refer to Figure 17.b). Some seismicity travels in excess of 500m, e.g., from a mining block A to a mining block B that is clearly not connected to the stress disturbance or redistribution zone caused by mining in zone A. In other words, seismic events not only occur near the excavation boundaries or on critically stressed geological structures directly affected by mining but may migrate far from a triggering event, i.e. at a mine-wide scale. This type of seismicity is problematic as it cannot be anticipated from stress models alone and may be highly disruptive to mining production due to its apparent unpredictability. Similar migration patterns are often observed for several days following large seismic tremors.

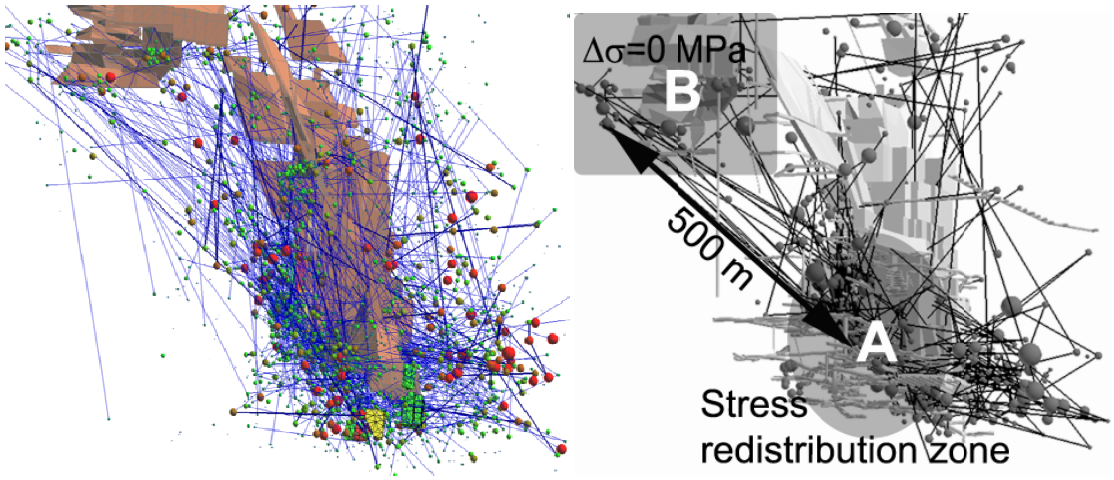

(a) (b)

Figure 17 Time-links illustrating seismic aftershock sequence links as lines; scale shows related activity in mining blocks at >500m from each other.

The same type of mine-wide interaction with distinct time-link patterns is illustrated for a different mine in Figure 18. In this case, seismic events migrate between geological structures, such as dykes and fault zones. Again, seismicity is travelling far beyond the influence of mining-induced stress changes. At this mine, seismicity travels between mining blocks (c and d) and interaction points of geological structures (a, b e and f). The reader is referred to Bewick et al. (2009) and Castro et al. (2009) for a detailed interpretation of this data.

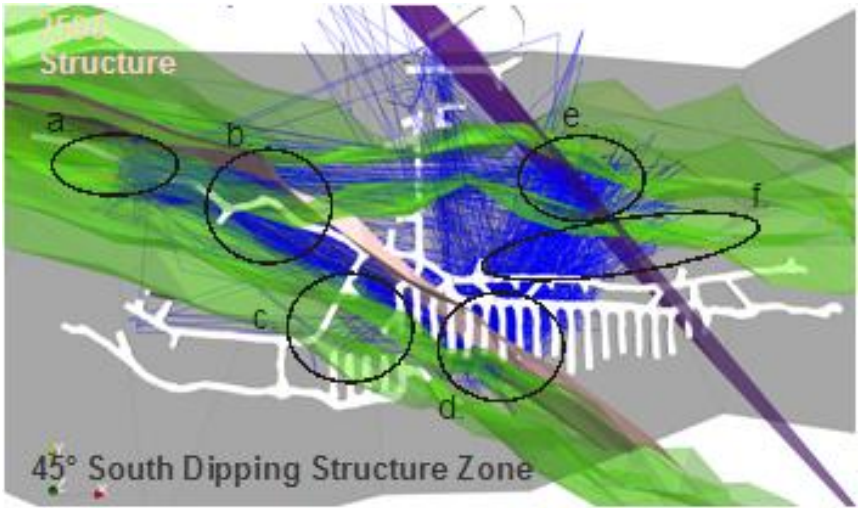

Figure 18 Time-links illustrating linkages between several seismic activity centres (labelled a to f) in mining blocks and along geological structures; at distances exceeding hundreds of meters.

4.2 Gravity-driven and Displacement-Controlled Seismicity Migration

For a study, funded by a strategic research grant of NSERC (Natural Sciences and Engineering Research Council), it was hypothesized that, in deep mines, gravitational forces combined with displacement controlled boundary condition changes lead to mine-wide stress migrations and thus seismic events remote from active mining zones. The concept of gravity-driven and thus displacement dependent mine-wide seismicity migration is briefly introduced here by two analogues: a train and a simple slope stability analogue.

Introduction to Hypothesis and Concept

The concept can best be understood by considering a train analogue where the behaviour of the last car depends on the characteristics of the engine, the couplings between the cars, and the length of the train (the number of cars). The characteristics of the train drastically changes whether running on a flat or inclined surface. In this train analogue, the time between actions at the front of the train, at the engine, and at the last car depends, amongst other factors, on the displacement and acceleration of the engine, the gaps at the couplings (that changes with the inclination of the track), the number of couplings, etc. The force acting on the last car, or the energy transmitted to it, depends on the speed of the engine at the time of the engagement of the car, the grade, etc. In other words, a train is a model of mine-wide seismicity where the energy transmission is largely a gravity-driven process that depends on the displacement characteristics of the connecting elements and the actions of the engine. In mining, the engine is the rate of mining, causing deformations as a function of extraction ratio. The "train" is a complex assembly of geological structures with a largely unknown distribution of weakness planes that are gradually mobilized as the extraction ratio increases.

The relevance of gravity in this concept is best understood by a simple slope stability analogue (Figure 19). If a slope is flat (a), and all blocks are stable, the gravitational forces are insufficient to cause slip and thus only elastic deformations with related stress redistribution are encountered. The effect of removing a block causes little deformation and certainly no stress change in a block remote from mining (block #3 in the analogue). On the other hand, if the blocks are inherently unstable (b), on a steep slope, such that equilibrium can only be retained by introducing a stabilizing force at the lowest block, removal of a block will cause deformations and stress changes on either side of the removed block (#3). This migration will propagate to the uppermost block unless the strength of the interface of any block is sufficient to hold the blocks at higher elevations.

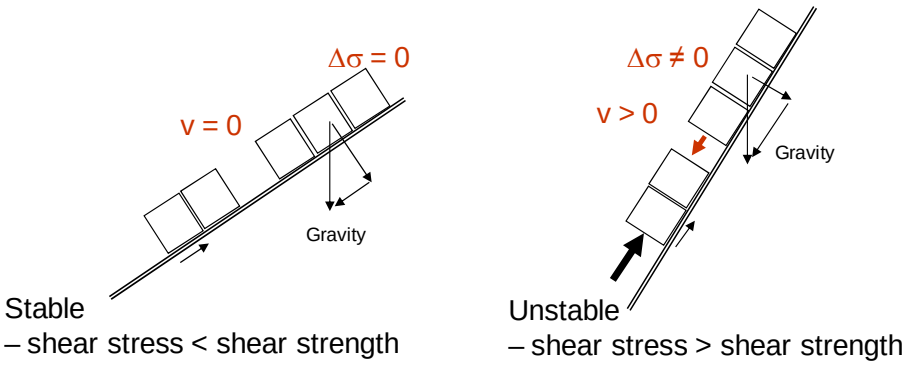

Figure 19 Slope analogue for the demonstration of "mine-wide" deformation and stress migration.

3D Equivalent of Gravity-driven and Displacement Controlled Migration Concept

In 3D, blocks are not free to move downward as they tend to get wedged if ground is removed at depth by mining. This is conceptually illustrated by a stacked disk analogue in Figure 20.a. Mining–induced deformations at the extraction point cause gravity-driven downward displacements of the stacked disks. The downward movement pattern depends on the inclination of the lateral, zero-displacement boundary (black line) and the inter-disk properties (called gap elements).

As the disks get wedged, gravity and extraction-driven stress changes occur at shallower depths (indicated by arrows in top disk). In turn, if openings or pillars exist at the location where the stresses change, these stress changes may be magnified near excavations or in pillars, and thus may lead to rockbursting far from the extraction point.

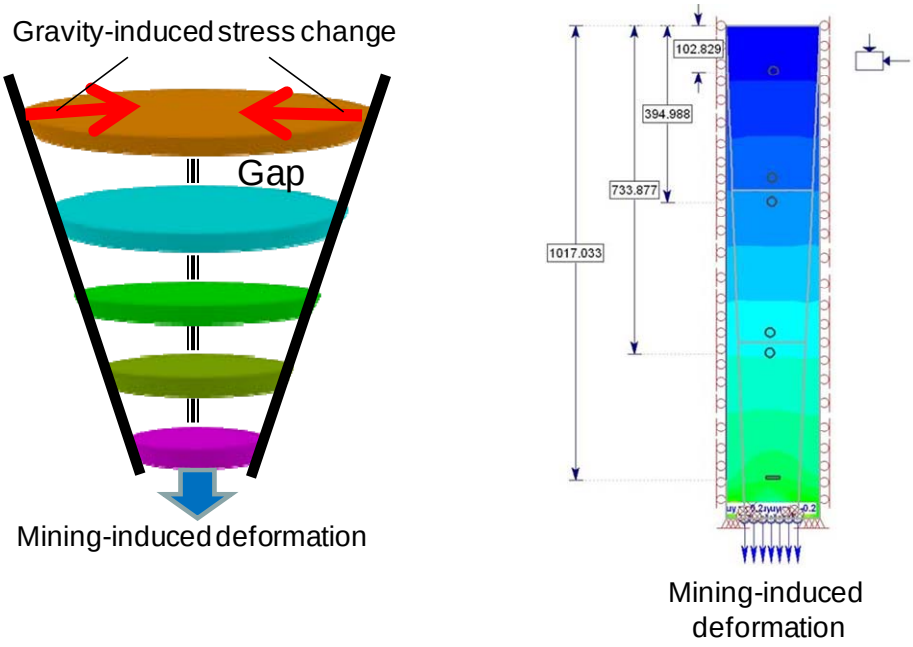

(a) (b)

Figure 20 (a) Stacked disk model with inclined displacement boundaries; (b) equivalent 2D model for 1000m deep extraction level model with two simulated gaps (joint elements).

The effect of deformation-induced stress migration is illustrated by a 2D elasto-plastic model presented in Figure 20.b. Mining is simulated by gradually displacing part of the lower boundary at 1000m depth. The upward migration of the displacement depends on the properties of the inclined displacement boundary elements, the gap models (2 each in this model), and the rock mass strength. This is illustrated for two extreme assumptions of stiff and very soft element properties and three excavation stages in Figure 21.a. The

total (mostly vertical) displacement profiles for the two cases are distinctly different, with the stiff model showing a gradual decrease in deformation toward the ground surface, and the soft model showing step-like displacement patterns with a more or less full transfer of extraction related deformations to the surface. Most importantly, the displacement gradient (strain) differs for the two displacement profiles. As a consequence, the mining-induced straining of excavations at higher elevations will depend on the mining-induced displacement or strain profile, and, most importantly, the stresses and stress changes near these excavations at higher elevations will change. This is illustrated by Figure 21.b where it was assumed that a circular opening was excavated in a hydrostatic stress field (K_o = 1) and then strained by a slightly inclined mining-induced strain of 1%. As a result, the local stress and stress ratio changes causing failure propagation and related stress redistribution near the tunnel. In this case, the major principal stress increases by about 20% and the depth of failure propagates in a differential manner. If this tunnel was excavated in burstprone ground, bursting would be triggered by the mining at a location remote from this tunnel.

This example, while rather simplistic compared to real mining conditions, clearly illustrates the process of gravity-driven, displacement-controlled stress redistribution and mine-wide rockburst and seismicity migration.

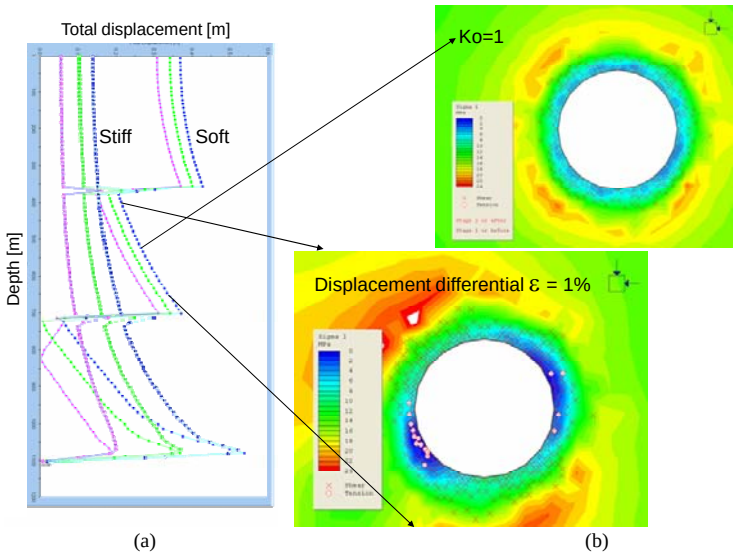

Figure 21 (a) Total displacement distribution for three mining steps and two gap model assumptions: stiff and soft; (b) induced stress field around tunnel in the centre block: top with uniformly displaced boundary (K_o = 1) and bottom with 1% displacement differential due to displacement gradient (see (a)).

As indicated above, the actual transfer function of mining-related displacements, and thus strain and stress change, depends on various factors such as geometric and rock mass properties. Since it is, in general, not possible to model, a priori, a geologically complex rock mass with all geological structures that control the displacement distribution and thus the seismicity migration, it is necessary to revert to methods introduced in the early stages of salt mechanics whereby the behaviour was simulated by phenomenological analogues such as Kelvin and other time-dependent models.

As illustrated by the time-links, mining blocks are often linked and each link can be described within a given time window by a phenomenological model that represents the transfer function. This is illustrated by the trellis-like model connecting various mining blocks. Each link consists of different, serial elements as shown in Figure 22. These links have different characteristics and may be uni-directional or bi-directional. They also change with time as the underlying failure process or displacement transfer functions change.

Research by Vasak and Wang (e.g., Wang at al. 2009) is in progress to develop models to capture the transfer functions by a systematic, statistical analysis of seismic data (e.g., Kaiser et al, 2005) and by use of time-dependent displacement migration or channelled flow models. Once the transfer functions are

established, it is possible to use conventional numerical models to estimate the mining-related remote straining and thus the anticipated related stress changes and induced failures, including rockbursts.

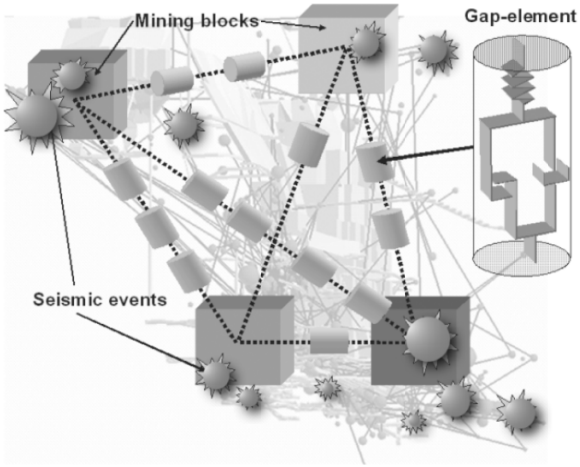

Figure 22 Trellis model illustrating interaction between directly related mining blocks; each connection consists of complex chains of gap-elements that have time-independent and time-dependent characteristics.

4.3 Channel Element Model

Tectonic plate movements have created shear zones that are often critically stressed in deep mines and thus form channels of preferred displacement transmission. These shear zones constitute a spatial network, in which a disturbance can travel uni-directionally, triggering seismic events in connected mining blocks, or bi-directionally, such that the induced disturbance may also travel back and lead to further seismicity in the source block.

To translate this concept of displacement and gravity-driven seismicity migration into an analytical approach, a Channel Element Model (CEM), based on mine networks and phenomenological transition models is under development (Wang et al. 2009). A channel element has equivalent shear zone characteristics that will change as a mine matures. The CEM is a mathematical model that describes the time-dependent migration and remote interactions from source disturbances. In contrast to mechanical contact interactions, simulated, for example, by the Discrete Element Method (DEM), or continuum, constitutive relations in the Finite Element Method (FEM), the CEM describes the phenomenon of gravity-driven displacement and thus stress, seismicity and rockburst migration.

As indicated earlier, time links patterns define which mining blocks are connected and what migration channels exist at a mine. Thus, a mine is divided into discrete mining blocks to form the nodes (centroids of each block) of the CEM path network geometry. Figure 23.a and b show how a trellis-like model of connecting changes is developed. This channel network extends about 1 km in the longest dimension. The linkage characteristics consisting of time-dependent and deformation-dependent elements (Figure 22) can be obtained from observed migration patterns, i.e., seismic data, and basic information such as distance, delay time and expected magnitudes. These characteristics are then converted to rheological constants for each phenomenological element. The links are equivalent to unstable shear zones at a mine and the nodes represent the intersection area of the linkages. As disturbances travel along the links between nodes and displacements accumulate at nodes where they arrive. Once a threshold is exceeded, a seismic event is triggered, introducing a new disturbance into the channel network. In this example, the disturbance starts at node A, triggers an (aftershock) event at B one hour later. The two disturbances interact and migrate in the channel network to generate a third aftershock at node C two hours after the initial disturbance was introduced. Work is currently in progress to calibrate and validate the CEM model against two major seismic events (3.9 M_n (1998) and 4.1 M_n (2006) at Creighton Mine). This example of a mine wide seismic migration simulation (Figure 23.c) shows how displacements change in a mine over a two hour period and how such displacements can potentially trigger seismicity in remote locations.

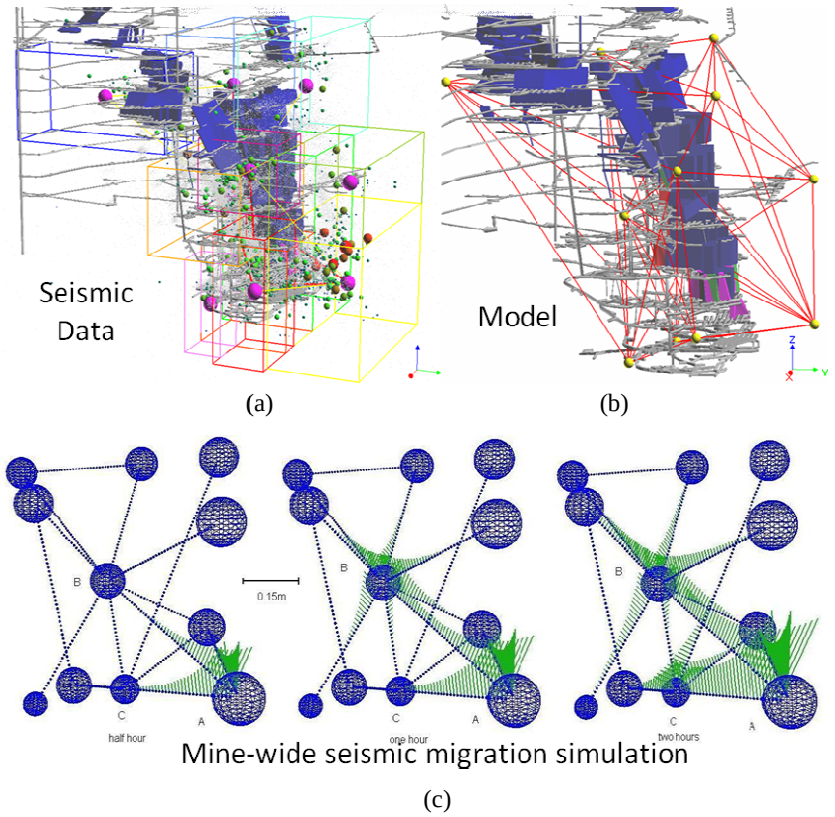

Figure 23 (a) sSeismic activity clusters, called mining blocks, are connected to form a seismic migration network (b); (c) results of a seismic migration model showing cumulative effects at nodes (size of balls) and displacement-migration pattern (bar graph showing influence function along migration legs).

5 Concluding remarks – Need for Integrated Mine-wide Design Approach

Recent experience in structurally complex mining environments, such as in the Sudbury Basin, shows that sudden shear deformation along large scale structural features (fault or shear zones) can occur in unexpected areas and at long distances (>200 m) away from active mining areas. As mines move deeper the risk for unexpected major seismic events (>2.0 M_n; Nuttli magnitude) to occur increases. The mechanics of sudden seismic energy release in structurally complex environments requires the implementation of a holistic understanding of the structures, their characteristics, and interactions. Only then can the complex dynamic behaviour of a mine involving geological structures, mining induced perturbation and occurrence of seismic events be captured. Based on such holistic models it is then possible to mitigate risks by implementing strategic geomechanical management practices in order to minimize hazardous ground exposure to mine personnel and to ensure that stakeholder value is maintained (Bewick et al. 2009). This approach was recently presented by Bewick et al. (2009) and Castro et al. (2009) and the reader is encouraged to explore the potential benefits of this integrated approach using engineering geology models based on complex geologic, seismic and numerical modeling data.

When mining at depth, activities in one part of the mine can significantly affect other parts and this needs to be considered during the design process. At depth, geological structures are often critically stressed and thus are sensitive to mining-induced stress changes and, most importantly, to mining-induced displacement boundary changes that can lead to mine-wide seismicity migrations and remote rockbursts. These processes can, to some extent, be captured by the hazard map approach presented here but further work is required to better understand the impact of mine-wide seismicity migration. This migration causes mine-wide stress changes that are not captured by conventional modelling techniques. Finally, this effect needs to be considered

when assessing the strainburst potential in mines and when selecting respective support and ground control measures.

6 Acknowledgements

The authors wish to acknowledge the contributions of the Canadian mining industry, particularly Vale Inco, for their continuous support of our research. Without valuable data and continuous interaction between mine staff and our researchers, progress would be severely limited. We also acknowledge the financial support from NSERC (Natural Sciences and Engineering Research Council) in the form of discovery, strategic and collaborative research grants. The list of collaborators is too long to mention all, but we wish to thankfully acknowledge the contributions of Mira Geosciences, particularly John McGaughey, and the contributions of Golder Associates Ltd., particularly Rob Bewick (Sudbury) and Luiz Castro (Mississauga).

7 References

Bewick, R.P., Valley, B., Runnalls, S., Whitney, J., Krynicki, Y. 2009. Global Approach to Managing Deep Mining Hazards. RockEng09: Proceedings of the 3rd CANUS Rock Mechanics Symposium, Toronto, May 2009 (e.d: M. Diederichs and G. Grasselli).

Bray, M. and A. Thompson, 1992. At the End of the Shift – Mines and Single Industry Towns. 144p. Dundrun Press, ISBN 1-55002-150-8.

Castro, L.A.M., Carter, T.G., & Lightfoot, N. 2009. Investigating Factors Influencing Fault-Slip in Seismically Active Structures. RockEng09: Proceedings of the 3rd CANUS Rock Mechanics Symposium, Toronto, May 2009 (e.d: M. Diederichs and G. Grasselli).

Hoek, E., P.K. Kaiser and W.F. Bawden, 1995. Rock Support for Underground Excavations in Hard Rock. A.A. Balkema, Rotterdam, 215 p. (www.mirarco.org)

Hoek, E. 1992. When is a design in rock engineering acceptable? - 1991 Müller lecture. Proc. 7th Congress Int. Soc. Rock Mech., Aachen. Rotterdam : A.A. Balkema. 3: 25p.

Kaiser, P. K. and B-H. Kim, 2008. Rock mechanics challenges in underground construction and mining. Keynote lecture, *1st Southern Hemisphere International Rock Mech. Symposium*, **1**:23-38. (download from www.miningexcellence.ca)

Kaiser, P.K., Vasak, P., Suorineni, F.T., & Thibodeau, D. 2005. New dimensions in seismic data interpretation with 3-D virtual reality visualization in burst-prone grounds. Keynote Address to 6th RaSiM6, Perth, Australia, 33-47.

Kaiser, P. K., 2005. Tunnel stability in highly stressed, brittle ground - Rock mechanics considerations for Alpine tunnelling. Keynote lecture, Geological AlpTransit Symposium GEAT'05, Zürich, Switzerland, 183-201. (download from www.miningexcellence.ca)

Kaiser, P. K., Diederichs, M. S., Martin, C. D., Sharp, J. and Steiner, W. (2000) Underground Works in Hard Rock Tunnelling and Mining. In: Keynote lecture at GeoEng2000, Melbourne, Australia. 1: 841-926. (download from www.miningexcellence.ca)

Kaiser, P.K., D.R. McCreath, and D.D. Tannant, 1996. Canadian Rockburst Support Handbook, Mining Research Directorate, Sudbury, Canada, 314 p. (In Report of Canadian Rockburst Research Program 1990-95. Vol.2, 324 p; published by CAMIRO, Sudbury).

Martin, C.D., P.K. Kaiser, and D.R. McCreath, 1999. Hoek-Brown parameters for predicting the depth of brittle failure around tunnels. *Canadian Geotechnical Journal*, **36**(1):136-151.

Vasak, P., Suorineni, F.T., Kaiser, P.K. & Thibodeau, D. 2004. Hazard Map Approach Using space-time clustering analysis of Mine-induced Microseismicity. CIM conference 2004. Edmonton. Canada.

Wang G., Kaiser, P.K. & Pavel V. 2009. Modeling of mining-induced seismicity migration. *ROCKENG09: Proceedings of the 3rd CANUS Rock Mechanics Symposium, Toronto (Ed: M.Diederichs and G. Grasselli)*

Keynote lecture, Korea Rock Mechanics Symposium, 2008, Seoul, p.1-16.

Rock Mechanics Advances for Underground Construction in Civil Engineering and Mining

Peter K. Kaiser (Centre for Excellence in Mining Innovation, Canada)
Bo-Hyun Kim (Geomechanics Research Centre at MIRARCO, Canada)

Abstract

The underground construction and mining are facing many geomechanics challenges stemming from, geological complexities and stress-driven rock mass degradation processes. Brittle failing rock at depth poses unique problems as stress-driven failure processes often dominate the tunnel behaviour. Such failure processes can lead to shallow unravelling or strainbursting modes of instability that cause difficult conditions for tunnel contractors. This keynote address focuses on the challenge of anticipating the actual behaviour of brittle rocks in laboratory testing, for empirical rock mass strength estimation, and by back-analysis of field observations. This paper summarizes lessons learned during the construction of deep Alpine tunnels and highlights implications that are of practical importance with respect to constructability. It builds on a recent presentation made at the 1st Southern Hemisphere International Rock Mechanics Symposium held in Perth, Australia, in September this year, and includes results from recent developments.

1. Introduction

This paper draws on experiences from major, mostly deep, mining projects and from large, deep tunnelling operations. The author's experience with brittle failing rock in deep mining, underground construction, and Alpine tunnelling was previously presented in keynote lectures: at GeoEng 2000 (Kaiser et al., 2000), summarizing a decade of collaborative research work on brittle rock failure; at the Rockburst and Seismicity in Mines Symposium (Kaiser et al., 2005), introducing new means of complex data interpretation in seismically active mines; at GEAT'05 (Kaiser, 2006), focusing on experiences from deep Alpine tunnelling; at the Asian Rock Mechanics Symposium, highlighting the impact on constructability (Kaiser, 2006); and expands on aspects covered at the Canada–U.S. Rock Mechanics Symposium (Kaiser, 2007) and the 1st Southern Hemisphere International Rock Mechanics Symposium (Kaiser and Kim, 2008). Recent developments and implications of practical importance are highlighted, particularly with respect to the selection of strength parameters for the design of underground excavations in highly stressed rock.

When building in highly stressed rock, instability is imminent and careful engineering with a sound understanding of the rock behaviour is of critical importance for risk management and sound engineering.

In the following, some lessons learned in recent years are reviewed from a geomechanics perspective to facilitate future problem solving and to identify opportunities for improved rock excavation techniques, support design and other ground control measures. By interpreting observed rock failure processes, by explaining factors affecting constructability, and by questioning some well established principles (e.g. commonly used failure criteria), deficiencies in our current state of knowledge can be identified and overcome.

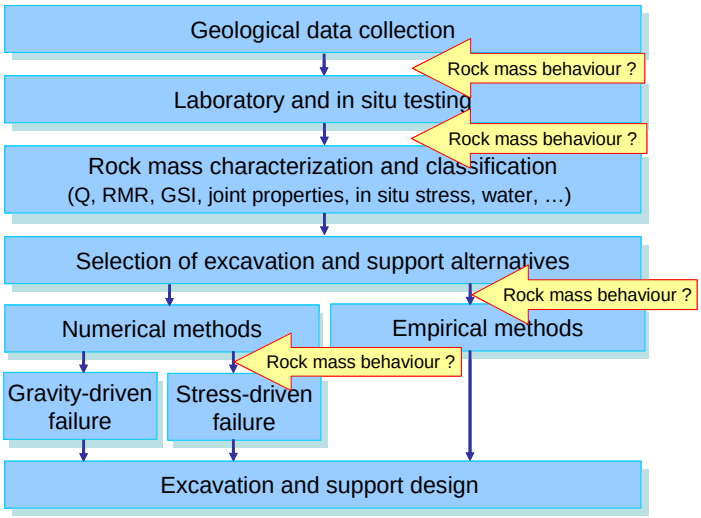

Figure 1 Site characterization approach for standard geo-engineering projects; highlighted are where a sound understanding of rock mass behaviour is needed

2. Anticipating the rock behaviour

The first principle in understanding rock behaviour is to carefully observe and then interpret field evidence. In this manner, it was found that spalling often dominates over shear failure and that this process is highly dependent on rock confinement (Kaiser and Kim, 2008). It should therefore be anticipated that the strength and bulking behaviour near excavation surfaces (open pit or underground) should differ from those encountered at some distance from an excavation. It also follows that

fractured rock loses its self-supporting capacity and thus must be more difficult to control during construction (Kaiser, 2006 & 2007; Kaiser and Kim, 2008). This paper build on the previous keynote lectures and expands the concept of s-shaped failure criteria from intact rock to rock mass behaviour.

If brittle rock failure behaviour is not anticipated, e.g., when going deeper or when entering highly stressed ground, rock may behave in an unexpected manner, good "old" ground may become bad ground, and proven technologies may fail to perform well. The geotechnical engineer is thus challenged to anticipate changing rock behaviour modes and to design control measures in such a manner as to facilitate ease of construction. For this reason, three main elements of underground construction are discussed here: (1) the relevance and consequences of brittle failure processes in underground engineering and construction; (2) challenges in anticipating the rock or rock mass strength when brittle failure processes affect or dominate the failure modes of underground excavations, and (3) the consequences for stability assessment on underground constructions.

2.1 Rock behaviour characterization

Site or rock characterization generally follows a well established path (Figure 1) from Geological model to Rock Mass model development, whereby the spatial distributions of rock types as well as rock and rock mass properties and characteristics are characterized and classified. It is however not sufficient to just provide a geological and a rock mass model; it is necessary to translate the knowledge gained from Geological to Rock Mass and then to Rock Behaviour models. Most tender documents elaborate much on the geological and rock mass model but fall short of providing proper descriptions of the rock mass behaviour models. In Figure 1, the arrows indicate where it is necessary to consider anticipated rock behaviour models during the site characterization process.

In underground construction, commonly recognized behaviour modes include wedge failure, squeezing, swelling, etc., and these are reflected in respective modelling tools (UDEC, 3DEC, Unwedge, FLAC, Phases, etc.). Almost exclusively, the most commonly recognized behaviour modes are related to shear failure, either along block boundaries or through the rock mass (elements 1,1 to 1,3 and 3,3 in the tunnel behaviour matrix presented in Figure 2). The effects of tensile failure or spalling are rarely anticipated and correctly modelled, even though they often dominate the degradation process near

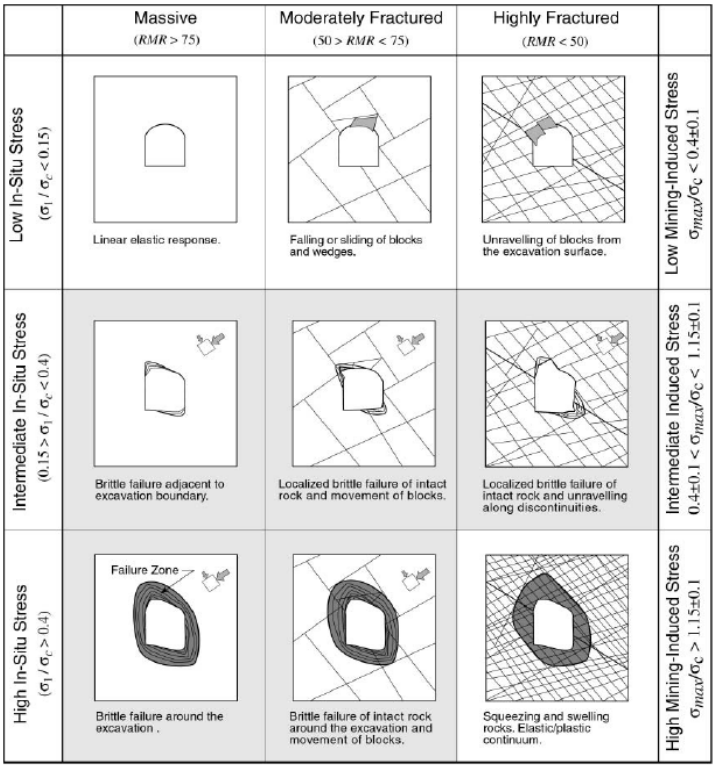

Figure 2 Tunnel failure modes (Kaiser *et al.*, 2000)

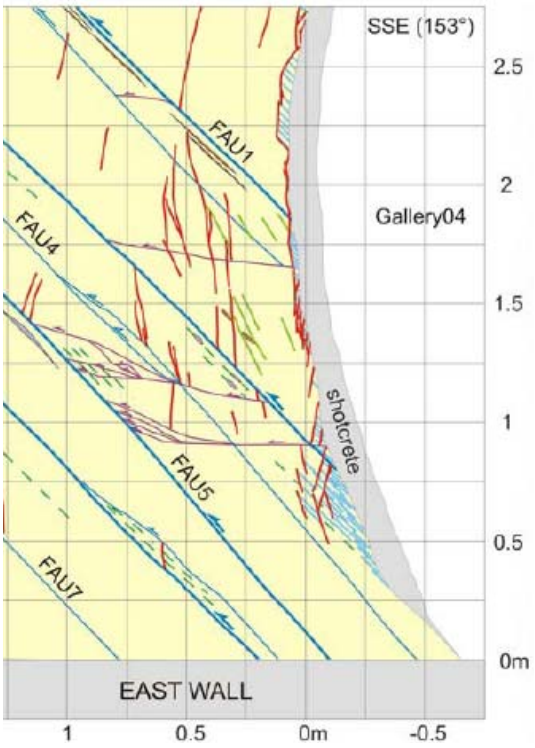

Figure 3 Brittle fracturing near tunnel in Opalinus Clay (Yong *et al.*, 2008)

excavations and negatively affects constructability issues such as stand-up time.

Brittle, tensile rather than shear, failure modes play a role at intermediate to high stress levels and in massive to moderately jointed rock masses (elements 2,1 to 2,3 and 3,1 to 3,2 in tunnel behaviour matrix of Figure 2). Brittle rock behaviour near excavations is more wide spread than commonly anticipated. For example, over-consolidated clays like the Opalinus Clay at Mt. Terri (Yong et al., 2007) show clear signs of tensile failure (Figure 3). Many weaker rock types such as lightly cemented sandstones, Kimberlite, clay shale, etc., do often fail in a brittle manner when lightly confined.

2.2 Brittle failure characteristics

Difficulties in designing underground excavations are often experienced because constitutive laws in numerical models do not necessarily reflect the actual behaviour of the rock. This is particularly true when the fundamental paradigm of the Coulomb yield criteria $\tau = c + \sigma_n \tan \phi$, relating the shear strength τ to a strain-independent cohesion c and a simultaneously acting frictional resistance $(\sigma_n \tan \phi)$, is not valid (Martin, 1997; Martin *et al.*, 1999; Kaiser *et al.*, 2000). As intact rock is strained, cohesive bonds fail first and damage accumulates (Diederichs, 2003). The propagation of tensile fractures depends on the level of confinement (Hoek (1968); used to explain brittle failure by collaborating researchers in Kaiser *et al.* (2000)). Figure 4(a) illustrates that an s-shaped criteria is required to properly describe the entire failure envelope from low confinement with spalling to high confinement shear failure. The existence of this s-shaped failure envelope for many rock types is further examined and verified in this paper.

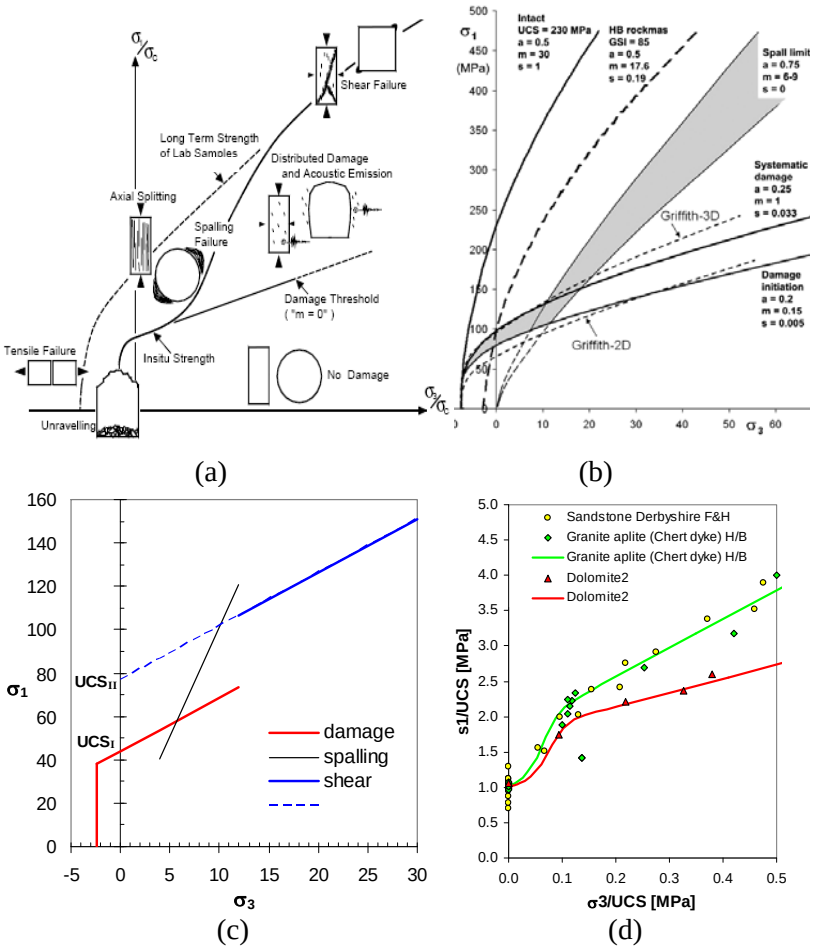

Figure 4 (a) S-shaped failure criteria showing damage threshold, spalling limit and rock mass strength envelope (Kaiser et al. (2000); Diederichs (2003)); (b) bi-nonlinear approximation by Diederichs et al. (2007) for damage threshold and spalling limit; (c) tri-linear failure envelope used for examples presented here; (d) s-shaped failure criteria fitted to data from Sandstone, Granite and Dolomite

A bi-linear or bi-nonlinear criterion is required to capture this dependence on confinement in the low confinement range (near excavations) for rock that is prone to spalling (Figure 4(b)). However, when the confinement is sufficient to prevent spalling, shear failure processes take over and a flatter "shear failure" envelop is reached (Figure 4(c)). For intact rocks (Figure 4(d)) as well as for rock masses (Figure 4(a)), the failure envelop therefore is s-shaped. In the following, the practical relevance of an s-shaped envelope, reaching into the high confinement range, is discussed first by use of a tri-linear failure envelope approximation (Figure 4(c)) with a tension cut-off. This envelope consists of a damage limit through the rock's unconfined compressive strength USC_I (lab test), a spalling limit with slope k_s, and a shear limit with an intercept or apparent unconfined compressive strength UCS_{II}.

For the tri-linear envelope of Figure 4(c), the spalling limit is reached at about 5 MPa (in the middle of the contour range shown in Figure 5) and the shear failure envelope is reached at about 10 MPa (at the outer range of the contours shown in the same figure). In other words, as indicated on Figure 5, there is an "inner shell" where spalling dominates (in this case for $\sigma_3 < 5$ to 8 MPa or < 0.1 to 0.15 UCS_I) and an "outer shell" (at > 0.1 to 0.15 UCS_I) where shear failure dominates.

This separation of behaviour mode has long been recognized in deep South African mines where shear failure is detected far ahead of the advancing face and spalling-type failure near a stope (Spottiswoode et al. (2008) and pers.com.; Ortlepp (1997)).

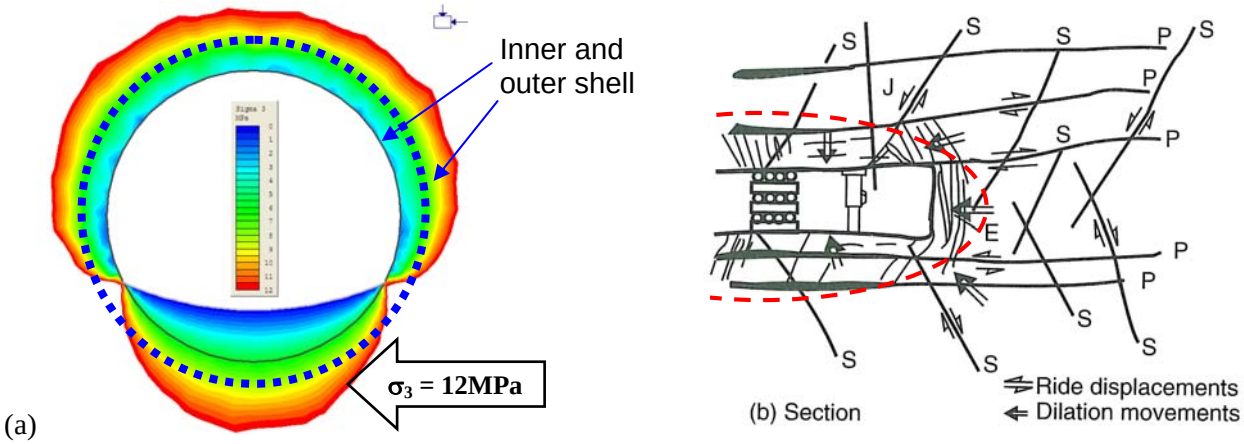

Figure 5 (a) Minor principal stress contours (range 0 - 12 MPa) around excavation in elastic rock for K_o = 0.75; (b) inner shell with spalling and outer shell with shear failure (pers. com. Spottiswoode et al. 2008)

3. Consequences of brittle failure of excavations and pillars

3.1 Strength development near excavations

Contrary to the tangential or major principal stress near an underground excavation, the radial or confinement stress zone (σ_3) is nearly parallel to the excavation geometry as illustrated by Figure 5.

The rapid development of σ_3 in the wall results in a rapid strength development as illustrated by Figure 6 for the wall of the tunnel. Since the σ_3-contours are essentially parallel to the tunnel boundary, nearly identical strength developments occur in the roof as in the walls.

Due to the tri-linear or s-shape of the failure envelope, the rock strength is relatively low near the excavation and increases rapidly to about double strength at a depth of about 1.3m for this case. The tangential stress σ_1 for K_o = 1.33 is also shown in Figure 6 for the roof and walls. Due to the flat, reduced strength near the wall, the tangential stress exceeds the strength not just in the roof (where it would be anticipated for K_o = 1.33) but also in the walls. Field evidence supports this finding (Kaiser 2007).

For support design and support selection, to manage brittle rock failure, it is therefore necessary to identify the rock strength near the excavation (in the inner shell) and this can be approximated by a bi-linear or bi-nonlinear envelope (Diederichs, 2003; Diederichs *et al.*, 2007). For pillar stability assessment, an outer shell problem as discussed below, however, it is necessary to consider all three parts of the s-shaped curve, including the shear failure branch.

In the floor of excavations, the strength increases less rapidly, promoting deeper tensile fracturing and spalling than near curved walls and roof. This has several practical consequences. Some of them are described next.

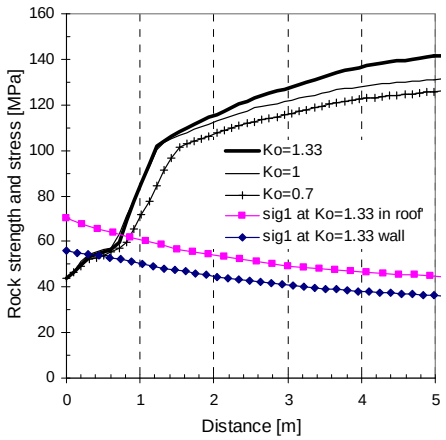

Figure 6 Rock strength development for three stress rations K_0 near excavation wall for tri-linear criteria of Figure 4(c)

3.2 Swelling and slaking potential enhancement by brittle failure

Once the damage and spalling thresholds are exceeded, the volumetric deformation characteristic of brittle failing rock changes drastically as tensile fractures tend to open fractures, and geometric incompatibilities between rock fragments lead to high radial dilation (bulking; Kaiser, 2006). As a consequence, water access to the rock is facilitated through stress

fractures. This supply of water to rock fragments enhances the swell or slaking potential (Kaiser and Kim, 2008).

Brittle failure processes during tunnel advance may therefore play a significant role in rocks where rock degradation processes are facilitated by water ingress. For example, brittle fracturing may enhance the swelling potential and swelling rates in preconditioned or stress damaged zones, e.g., below flat floors (Einstein, 1996) or below insufficiently curved inverts.

In rocks that are prone to slaking (softening and weakening due to water ingress), brittle failure processes can lead to preferential water access paths and thus to non-uniform slaking. In Kimberlites, for example, it is often observed that initially stable tunnels start to squeeze after some time. Tensile fracturing again can provide preferred access paths for water and thus locally enhanced slaking potential.

Recent advances in modelling techniques involving fracture propagation (e.g., ELFEN™) and models permitting combined failure modes involving discontinuities and intact rock (e.g., SRM, synthetic rock mass model) will eventually facilitate the proper simulation of combined shear and tensile failure processes. For the time being however, much can be achieved by recognizing the impact of the s-shaped failure envelope on excavation behaviour and by approximating it by a bi-(non)linear envelope for support design (in the inner shell) and by a tri-linear envelope for aspects involving confined rock (in the outer shell: pillars, etc.).

3.3 Strength development in brittle failing pillars

As indicated above, for pillar stability assessment, it is necessary to consider all three parts of the s-shaped curve (Figure 4) if the confinement inside the pillar exceeds the threshold σ_3 –value at the intersection of the spalling limit with the shear failure envelope (about σ_3 = 10 MPa or σ_3/UCS = 0.1 for case shown in Figure 4(c and d)). Martin and Maybee (2000) used brittle Hoek and Brown parameters (Martin *et al.* 1999) to demonstrate that the pillar strength, contrary to the "best"-fit curves presented by many Figure 7, should non-linearly increases (with an upward rather than a downward curvature) as the pillar width to height ratio (W/H) increases. The authors justified this by the fact that spalling or hour-glassing weakens narrow pillars more than wide pillars. Their interpretation also makes intuitive sense as wide pillars should approach the strength of the confined rock mass, which should be much higher than suggested by the horizontal asymptotic value of about 0.7 to 0.8 UCS_I (Figure 7).

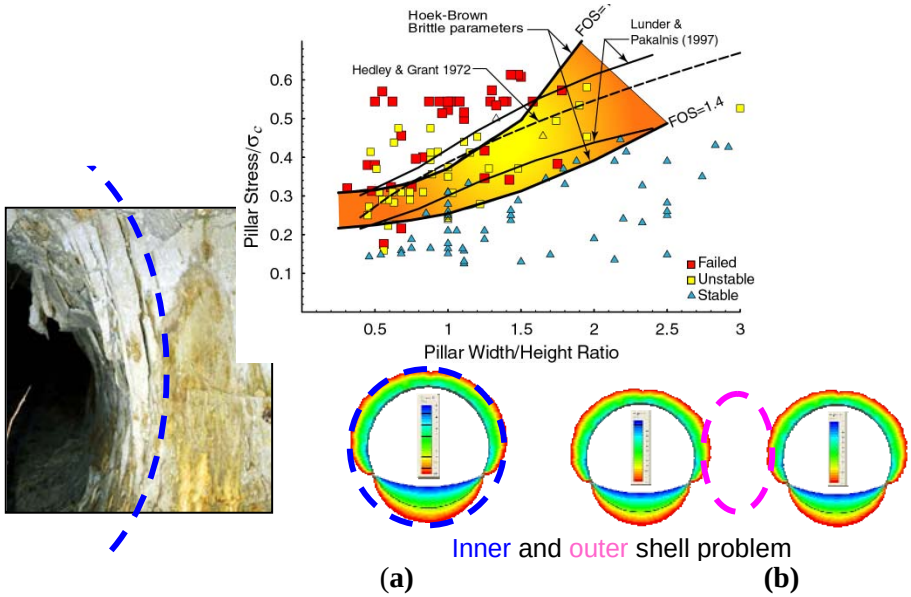

Figure 7 Pillar stability – an inner/outer shell problem: (a) Narrow pillars fail if inner shells join or overlap; and (b) wide pillars (W/H > 1.5 to 1.8) tend to be stable with stable core (inserted chart: Martin and Maybee (2000))

It follows that the strength of wide pillars is strongly influenced by the confined strength of the rock mass and thus by the third leg (the shear strength) of the s-shaped envelope. As illustrated by Figure 7, narrow pillars (W/H< about 1.5) are dominated by inner shell behaviour (leading to hour-glassing; indicated as "failed" by red squares and as illustrated by the photo), while wider pillars are significantly stronger due to the rapid increase in strength in the core (in the outer shell).

3.4 Rock support considerations for brittle failing rock

As illustrated by Figure 5, a low confinement zone of more or less constant depth exists near an unsupported excavation. Even if the tunnel was supported with a liner providing a radial support pressure (typically between 0 and 1 MPa), a low

confinement zone still would exists. Hence, the damage threshold defines the rock strength near the excavation as shown in Figure 6. However, the strength rapidly increases as soon as the confinement is sufficient to reach the spalling limit (at about 0.7 m depth or ~5 MPa for case shown in Figure 6). For a deep tunnel, tensile fracturing is therefore largely confined to the inner shell and, most importantly, tensile failure induced spalling should be expected all around the tunnel independent of K_o.

Kaiser (2007) illustrated how the rock mass bulks in the stress fractured zone and that bulking is highly dependent on confinement. For typical support pressures of $\leq$ 1 MPa, bulking ranges from 7 to 10% (Kaiser *et al.*, 1996). As a consequence, the radial strains in the inner shell are much larger than predicted by standard constitutive models, and the cumulative displacements or convergence with bulking is also much larger (Kaiser and Kim, 2008).

It follows for support design that the wall strength is defined by the low-confinement strength of the rock mass, i.e, by the first and second leg of the tri-linear failure envelope (the damage and spalling strength), that support needs to be designed to control the bulking and manage the resulting elevated convergences.

Stress-driven rock "fragmentation" in the inner shell creates broken rock with varying fragment size and shape distributions (Kaiser, 2007). This stress-driven degradation transforms a rather stable rock mass (if massive to moderately jointed) to a fractured rock mass with a much reduced stand-up time. From a constructability perspective this implies that it is difficult to retain stability of the inner shell when stress-driven fracturing causes rock degradation. Such rock behaviour has slowed the rate of progress at various tunnelling projects utilizing open TBMs (Kaiser, 2007).

4. Laboratory test data revisited

Based on the above presented consequences of brittle rock failure, it is evident that it is necessary to re-evaluate the shape of constitutive models for use in rock mechanics modelling and design.

Both the Coulomb and the Hoek-Brown criterion assume a steady increase in strength with increasing confinement. More importantly, for both criteria it is implied that cohesive and frictional strength components are simultaneously mobilized. Furthermore, rock mass degradation, e.g., using GSI, does not change the form of the failure envelope, and

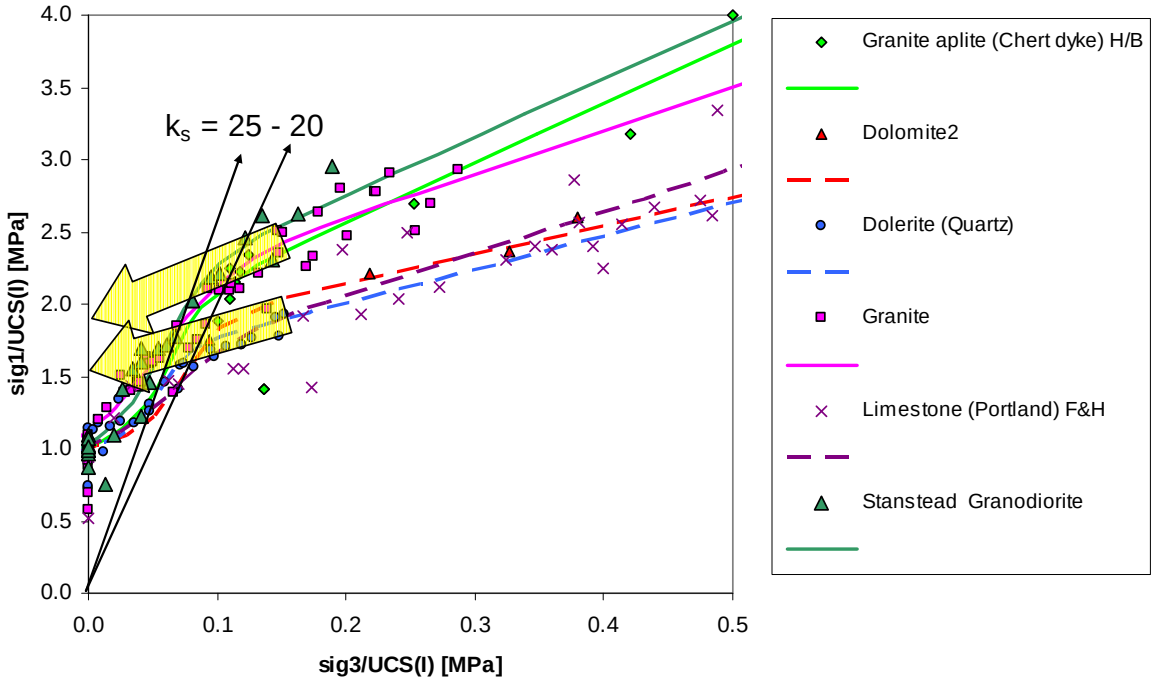

Figure 8 Laboratory test data of two groups with similar behaviour are fitted with s-shaped failure criteria: (a) Granite Aplite, Granite, Granodiorite (apparent UCS_{II} = 1.8 UCS_I; ϕ = 35-37°; k_s = 25; and (b) Dolomite, Dolerite and Limestone (apparent UCS_{II} = 1.55 UCS_I; ϕ = 23-25°; k_s = 20) (data courtesy: E. Hoek and J. Archibault; arrows point at apparent UCS_{II} for two rock types)

various means for residual strength determination (e.g., Cai et al., 2006) do also not alter the shape of the strength envelope.

Ample evidence has been presented in the recent literature by colleagues (primarily Diederichs and Martin) and other researchers that support the bi-linear or bi-nonlinear shape of the failure envelope of rock in the low confinement zone (Figure 4(a & b)). This is now well established based on field observations and extensive back-analyses of cases involving spalling failure.

However, if this process is a fundamental characteristic of brittle failing rock, it should also be observed in laboratory tests. Indeed, when testing hard rocks, it is often observed that samples fail, particularly in unconfined or low confinement tests, by axial splitting, shattering or by progressive spalling. Only at high confinement levels or when a sample contains distinct foliation or weakness planes are shear failure processes observed. Hence, it should be anticipated that brittle rocks might show a similarly tri-linear or s- shaped failure envelop when tested under laboratory conditions.

Kaiser and Kim (2008) revisited Dr. Hoek's data base and showed that the rock strength was typically reduced to the left of a spalling limit of about $\sigma_1/\sigma_3 = 25$ to 20 or typically for $\sigma_3 \leq UCS_I/10$. This is evident from the data and fitted s-shaped failure envelopes shown in Figure 8 for five distinctly different rock types. The strength in the shear failure zone can be described with an apparent unconfined strength, UCS_{II}, of 1.5 to 2- times the standard unconfined compression test strength (UCS_I).

4.1 s-shaped failure criteria for brittle failing intact rock

The s-shaped failure criterion shown in Figure 8 can be described by the following equation:

$$\sigma_1' = k_2\sigma_3' + UCS_{II} + [\frac{(UCS_I - UCS_{II})}{1 + e^{(\sigma_3' - \sigma_3^0)/\delta\sigma_3}}] \qquad \text{Eqn (1)}$$

where k_2 is gradient at zero confinement (assumed to be the same as in the high confinement range), k_s is the spalling limit (varying with rock type), σ^0_3 and $\delta\sigma_3$ are shape parameters, and UCS_I and UCS_{II} are intercepts at zero confinement (actual and apparent UCS, respectively).

Since most numerical modeling programs do not yet allow for the use of an s-shaped failure criterion, the strength envelope can be approximated by a tri-linear criteria as illustrated in Figure 4(c) or as superimposed on Figure 9(b) for the Quartzite (UCS_I = 140 ±30 MPa; UCS_{II} = 300 ±15 MPa; k_s = 35 to 15 to 10 for intact to structurally controlled breaks).

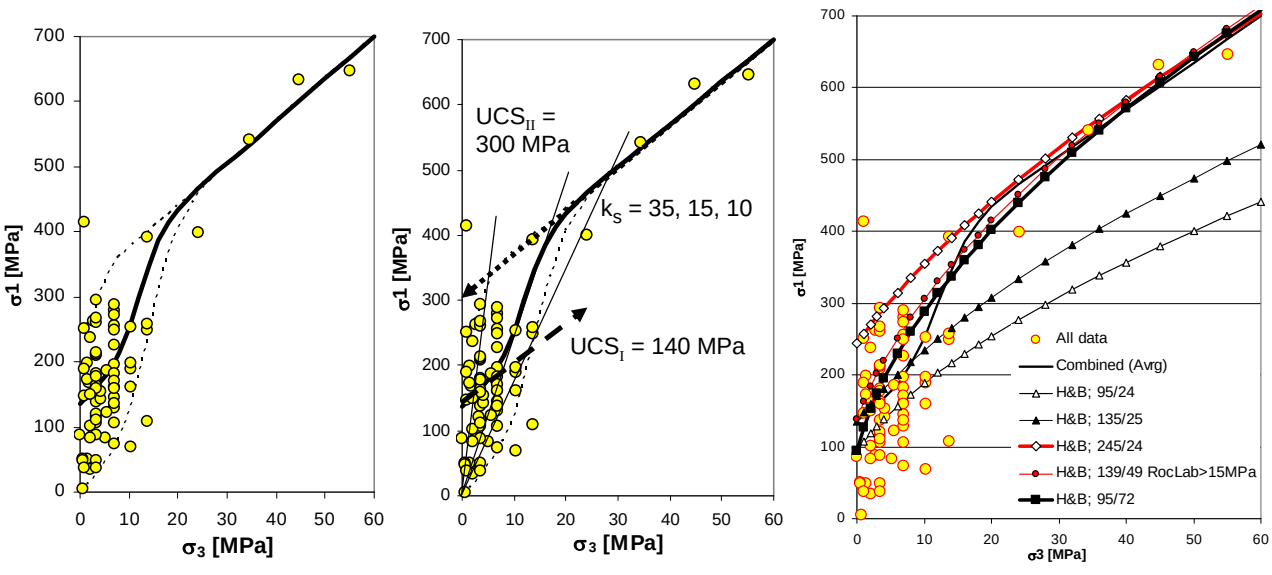

Figure 9 Data from friable Quartzite: (a) fitted s-curve for all data and upper and lower limit; (b) respective linearized approximations; (c) Hoek and Brown envelopes obtained by various fitting approaches with parameters listed in Table 1 (UCS and m_i values are shown in legend as UCS/ m_i)

From a brief review of published data from igneous, metamorphic and sedimentary rocks, it is found that the UCS ratio (UCS_{II}/UCS_{I}) typically ranges between 1.5 and 2 with a range of 1.3 to >3. This indicates that most rocks have a brittle failure component.

4.2 Guidelines for design parameter selection for brittle intact rock

It is evident from the above that design parameters for brittle failing rocks must be selected with care and with the design problem in mind. Until an s-shaped failure criterion has been finalized, tested and is ready for use in numerical modelling, constitutive model and failure envelope adopted for support design may have to differ from those used for pillar design (see above). This is illustrated here for the data set shown in Figure 9(a). The average UCS for this rock (data not shown) is 95 MPa for all data and 125 MPa for intact breaks only. Parameters for four approaches to obtain the rock strength are listed in Table 1 and the corresponding non-linear envelopes are shown in Figure 9(c).

The obvious question arises: how to select the most appropriate intact rock strength envelope for this Quartzite? A detailed discussion of parameter selection was presented by Kaiser and Kim (2008) and is reproduced in the following since it is most important that rock strength parameters are selected following an appropriate process.

The m_i -values for approach B and D are clearly out of range based on commonly recommended values and thus would be rejected. However, based on the above presented discussion, an unusually high m_i-value of 72 would clearly overall represent the results from the laboratory testing program best (Figure 9(c))

Table 1 Parameters for Hoek and Brown criteria shown in Figure 9(c)

	Approach	UCS [MPa]	m_i
A	Average from UCS tests and m_i from published rock type tables: $m_i = 23\pm3$ for Quartzite	95 (average)	24 (assumed)
B	RocLab™ (Rocscience) applied to all data	139	50
C	RocLab™ applied to data from samples failing through intact rock	245	24
D	Best fit to all data without RocLab constraint of $m_i \leq 50$ and average UCS	95	72

Approach A and C: Approximation using UCS data from laboratory tests and published mi-values

In mining, modelling is often based on UCS data only and m_i is estimated from recommended property tables (e.g., Hoek, 2007). The resulting failure envelope (Approach A) clearly underestimates the intact rock strength of the Quartzite in the high confinement range (> 10 MPa; Figure 9(c)) if the average UCS were used. On the other hand, if the UCS of only those tests with intact breaks were used (Approach C), then the resulting failure envelope clearly over-estimates the strength of the Quartzite in the low confinement range (<10 MPa; Figure 9(c)).

Approach B and C: Use of RocLab™

When using any fitting procedure to obtain Hoek and Brown parameters, data must cover the confinement range of σ_3 = 0 to UCS/2 (see frequently asked question about determination of m_i on homepage of RocLab™ http://www.rocscience.com). Because of test cell constraints, triaxial test are commonly conducted with confining pressures up to 60 MPa. Consequently, as for the Quartzite shown above, fitting approaches to obtain Hoek and Brown parameters are strictly only applicable for rocks with UCS < 120 MPa and parameters can thus, strictly speaking, not be obtained for hard brittle rocks. Furthermore, RocLab™ limits m_i to 50 and thus cannot be used for rocks with distinct s-shaped failure behaviour.

Obtaining representative Hoek and Brown parameters for rocks with s-shaped failure behaviour

For rocks with distinct s-shaped failure behaviour, a best-fit Hoek and Brown parameter set can be obtained by linear regression in the $(\sigma_1 - \sigma_3)^2/UCS^2$ versus σ_3/UCSspace (Approach D; forcing A linear regression line through (σ_1 –

$\sigma_3)^2/UCS^2 = 1$). However, it must be noted that the corresponding m_i-value ($m_i = 72$ for the Quartzite) are unusually high and that standard approaches to obtain the rock mass strength (e.g., by GSI-based degradation) may not be applicable. Nevertheless, such a fitting approach will lead to a parameter set for the intact rock that is on average representative for the entire confinement range (with high uncertainty in the low confinement range).

Sectional fitting for limited confinement ranges

For rocks with distinct s-shaped failure behaviour, it is therefore more appropriate to consider the confinement range relevant for a given engineering problem before fitting and selecting design parameters. For the Quartzite of Figure 9(c) reproduced Figure 10, the inner zone extends to about $\sigma_3 < 0.1\ UCS_I$ and the outer zone beyond.

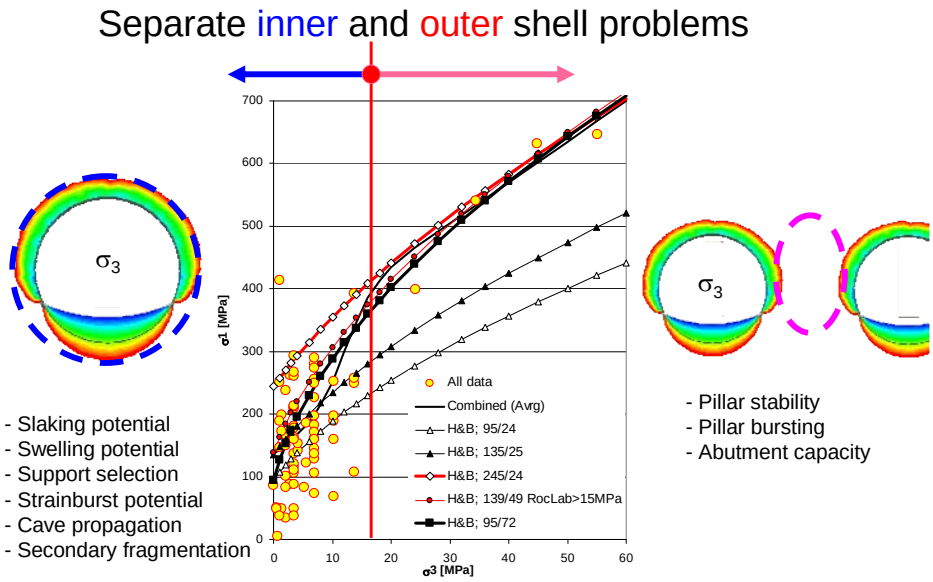

(a) (b) (c)

Figure 10 (a) Illustration and listing of "inner shell" problems; (b) (c) Hoek and Brown envelopes as presented in Figure 9; and (c) illustration and listing of "outer shell" problems

For support design, the rock behaviour near the excavation, in a confinement range of 0 to typically 5 MPa, is most relevant. From Figure 9(c), it follows that the parameter sets (between 95/24 to 139/24, or 120/24 on average with a standard deviation of about 40 MPa on UCS) would be appropriate for the low confinement zone (inner shell). However, a cut-off as recommended by Diederichs *et al.* (2008), or with $k_s = 15$ to 10, would have to be applied to prevent excessive depths of failure predictions.

For pillar design, the rock behaviour in the pillar core, in a typical confinement range of > 5 MPa for mining at depth, is most relevant. From Figure 9(c), it is evident that the parameter sets (245/24) with a standard deviation of about 15 MPa on UCS, would be appropriate for the highly confined zone (outer shell). However, the effect of spalling and hour-glassing is to be predicted by using the parameter set for the inner shell.

This is further highlighted by the division of the stress space into an inner and outer shell (Figure 10). The type of problems that are inner shell problems are listed on the left side (Figure 10(a)) and those that are outer shell problems on the right side (Figure 10(c)).

5. s-shaped failure criteria for brittle failing rock masses

From the previous discussion, it follows that Figure 4(a) needs to be modified to take into account that the intact rock strength is also s-shaped. This is illustrated by the data superimposed on Figure 11.

Procedures to obtain s-shaped failure envelopes for the rock mass corresponding to the s-shaped intact rock strength, following the GSI approach (Figure 12), are under development. If it is assumed that the currently adopted degradation approach to obtain the Hoek and Brown parameters s and m_b for the rock mass is applicable, then it can be applied for each section of the s-curve (the low and the high confinement range) to obtain an s-shaped rock mass envelope. This aspect remains an outstanding challenge for rock engineering in brittle rock masses and will require further research and calibration.

Nevertheless, rock and rock mass strength parameters for brittle failing rock should be established separately for the low and high confinement zones and then applied to zones where spalling or shear failure modes are dominating the rock behaviour (e.g., for inner and outer shell modeling).

The most general form of the Hoek-Brown criterion is given by:

$$\sigma_1 = \sigma_3 + \sigma_c \left(m_b \frac{\sigma_3}{\sigma_c} + s \right)^a \qquad \text{Eqn (2)}$$

where, m_b and a are constants for the rock masss; σ_c is the uniaxial compressive strength of the intact rock; and σ_1 and σ_3 are the axial and confining effective principal stresses, respectively.

This criterion works well for most rocks of good to fair quality, when the rock mass strength is controlled by tightly interlocking angular rock pieces. The failure of such rock masses can be defined by setting a = 0.5 in Equation 2:

$$\sigma_1 = \sigma_3 + \sigma_c \left(m_b \frac{\sigma_3}{\sigma_c} + s \right)^{0.5} \qquad \text{Eqn (3)}$$

For poor quality rock masses in which the tight interlocking has been partially destroyed by shearing or weathering, the rock mass has no tensile strength or cohesion and specimens will fall apart without confinement. For such rock masses s = 0 and a may be a function of rock mass quality (Hoek et al. 1995). When highly confined, the rock mass may though have an apparent cohesion with s > 0 for $\sigma_3 > 0.1\ UCS_I$.

It is practically impossible to carry out triaxial or shear tests on rock masses at a scale appropriate for surface or underground engineering. Numerous attempts have been made to overcome this problem by testing small scale models, made up from assemblages of blocks or elements of rock or of carefully designed model materials. However, our ability to predict the strength of jointed

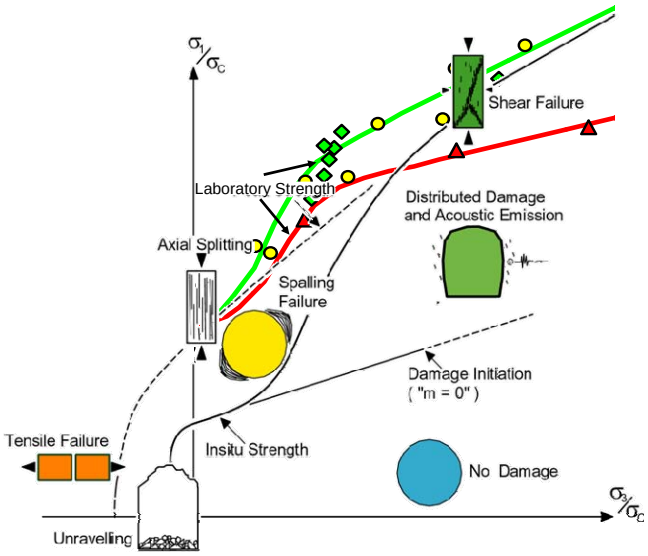

Figure 11 S-shaped failure criteria concept showing modified intact rock strength s-curves (modified after Kaiser *et al.* (2000) or Diederichs (2003))

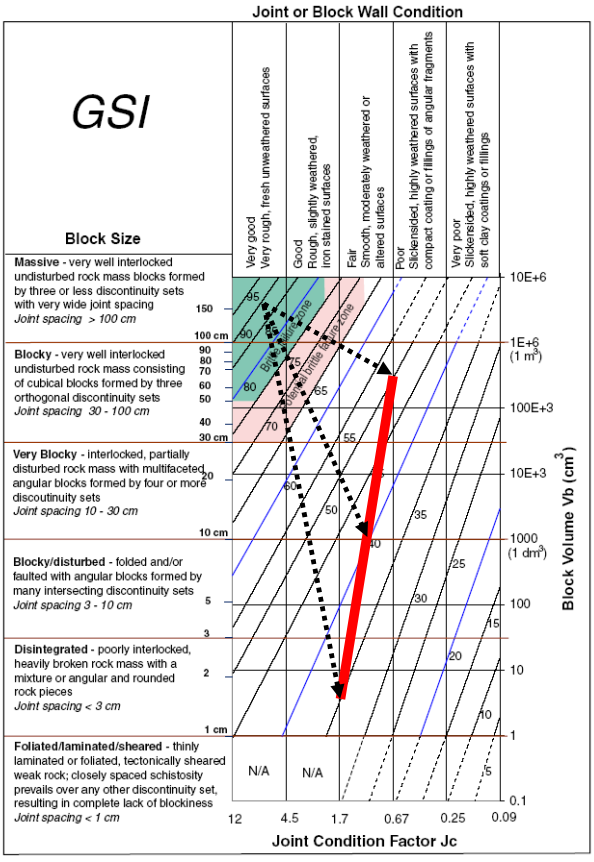

Figure 12 GSI-chart showing degradation paths for various rock types from massive gneiss, to friable quartzite, to massive granite (Kaiser, 2007)

rock masses on the basis of direct tests or of model studies is still severely limited.

For this reason, Equations 2 and 3 are of little practical value unless the values of the material constants m_b and s can be estimated in some manner. Hoek and Brown (1988) suggested that these constants could be estimated from the 1979 version of Bieniawski's Rock Mass Rating (RMR), assuming completely dry conditions and a very favorable joint orientation. While this process is acceptable for rock masses with RMR values of more than about 25, it does not work for very poor rock masses since the minimum value which RMR can assume is 18. In order to overcome this limitation, a new index called the Geological Strength Index (GSI) was introduced (Hoek et al. 1995; Figure 12). The value of GSI ranges from about 10, for extremely poor rock masses, to 100 for massive rock.

The relationships between m_b/m_i and s for a = 0.5 and the Geological Strength Index (GSI) according to Hoek et al. (1995) are as follows for 70 > GSI > 25 (and undisturbed rock masses):

$$\frac{m_b}{m_i} = \exp\left(\frac{GSI - 100}{C_m}\right)$$ with C_m = 28 recommended by Hoek et al. (1995) Eqn (4)

$$s = \exp\left(\frac{GSI - 100}{C_s}\right)$$ with C_s = 9 recommended by Hoek et al. (1995) Eqn (5)

The constants C_m and C_s characterize the rate of strength loss as a function of rock quality degradation and Hoek et al. (1995) assumed that these parameters are constant over the entire confinement range, i.e., they are assumed to be the same for the inner and outer shell. For brittle rocks, however, it is now understood that the degradation by spalling processes is much more rapid and more significant in the low confinement range (in the inner shell) than at high confinement when shear failure dominates (in the outer shell). Hence, these constants should be a function of confinement $C_s = f(\sigma_3)$ and $C_m = g(\sigma_3)$ or at least should differ for the inner and outer shell. The constants should be higher in the outer shell where spalling and dilation is constrained and some failure though intact rock (rock bridges and asperities) must occur.

The change in degradation rate for s is illustrated by Figure 12; illustrating that the brittle limit of $\sqrt{s}$ = 0.4 (Martin et al. 1999) is reached for GSI = 84 with Cs = 9. Cai et al. (2004) found that brittle behaviour may be encountered in rocks with GSI as low as 65. Thus, C_s = 5 to 15 (on average C_s = 9 as originally proposed) should be applicable for brittle rocks in the inner shell.

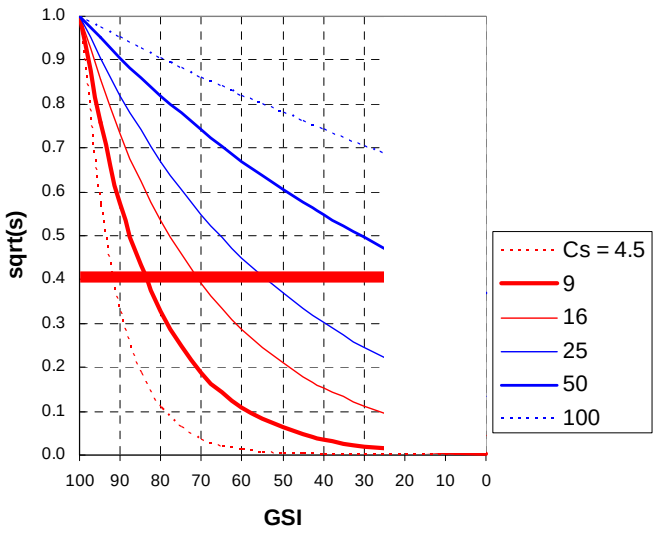

Figure 13 Rate of rock mass degradation $\sqrt{s}$ as a function of GSI for various C_s- constant

Furthermore, it is hypothesized that the rate of degradation in the outer shell is less rapid for several reasons. First, when highly confined rough joints are prevented from dilating, an apparent cohesion is mobilized as shear through asperities must occur. Second, rock bridges, when confined, are stronger (less prone to tensile failure) and thus add an additional apparent cohesion. Consequently, C_s must be higher in the outer shell than in the inner shell or C_s >> 9 for highly confined (>0.1 UCS) and very tight rock.

At this stage, it is not yet know how to determine C_s for the outer shell and further research is required. The impact on the failure envelope though is illustrated by the three cases shown in Figure 14 of the Quartzite presented in Figure 9.

In Figure 14 (a), only the inner shell properties are degraded with C_s = 9 and the outer shell in not degraded at all ($C_s = \infty$). The scatter in data due to the effect of flaws and weaknesses in the Quartzite in the low confinement zone can be nicely fitted by this GSI-dependent degradation.

In Figure 14 (b), the inner shell properties are degraded with C_s = 9 and the outer shell is degraded at a lesser rate with C_s = 50. A GSI of 100 to 70 covers the entire range of laboratory test on small samples with flaws and weaknesses (Figure 14

(b)). If the rock mass would degrade at this rate, the rock mass failure envelop would be s-shaped for the entire applicable GSI range (100 to 25).

In Figure 14 (c), the inner shell and outer shell properties are degraded equally at $C_s = 9$. A GSI of 100 to 95 covers the range of laboratory test on small samples with flaws and weaknesses. In this case the s-shaped failure envelope is rapidly lost at about GSI < 80.

As indicated above, further studies and back-analyses of pillars or micro-seismicity near caves will be required to establish guidelines for C_s in the shear failure range. From qualitative observations it is anticipated that C_s may range from 15 to 50 for the outer shell in hard, competent (non-altered) rock masses.

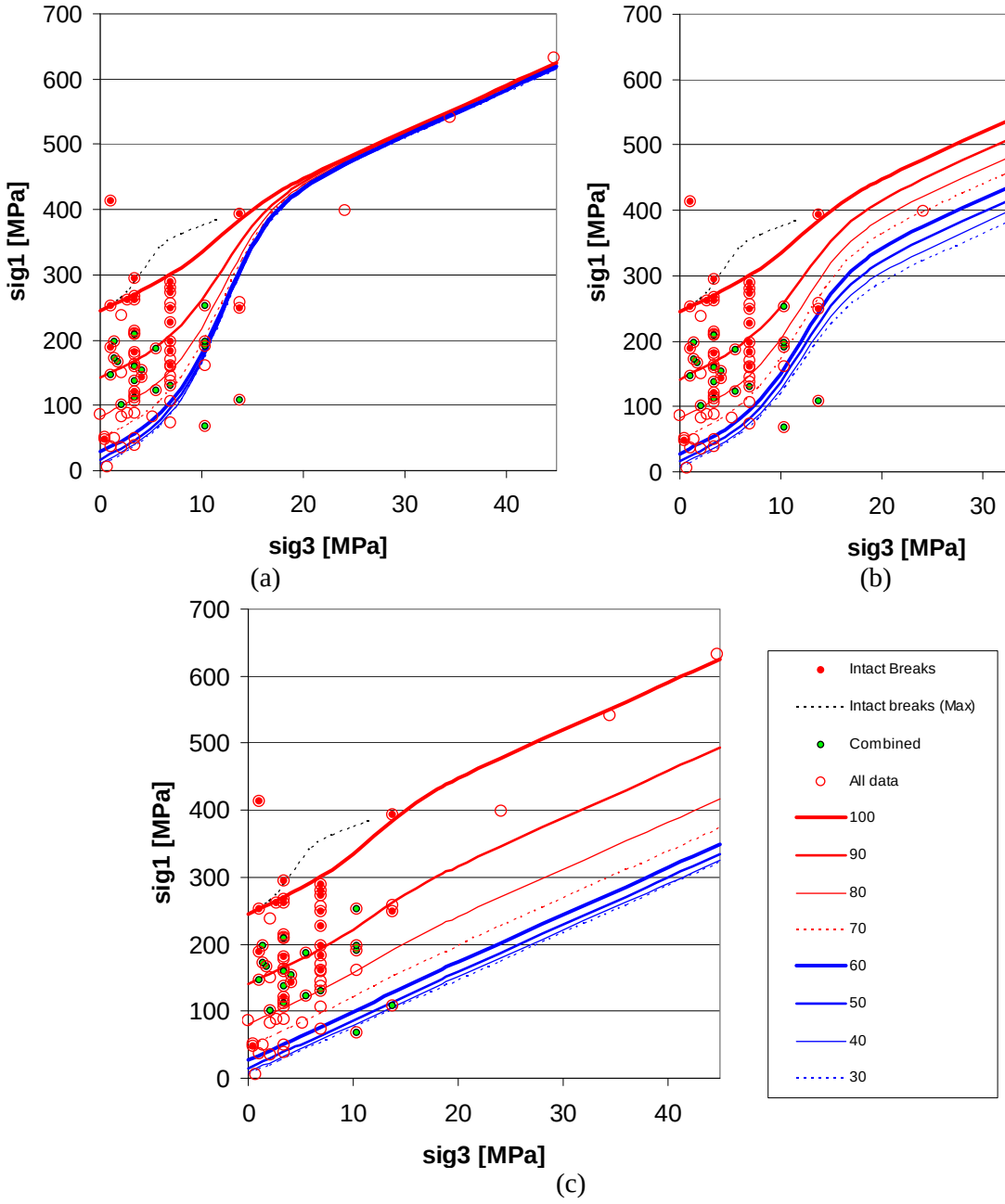

Figure 14 Rate of rock mass degradation $\sqrt{s}$ as a function of GSI for various C_s- constant Figure 15 Three cases of increasing rock mass degradation in the shear failure zone (outer shell): (a) $C_s = 9/\infty$; (b) $C_s = 9/50$; and (c) $C_s = 9/9$

6. Conclusion - Lessons learned

When mining in brittle ground, the rock behaviour can change drastically when progressing to greater depth where the rock mass may be highly confined.

By observing and interpreting brittle rock behaviour, it is now possible to understand and anticipate the rock behaviour such that design and construction procedures can be matched to the ground. At depth, rock becomes brittle and fails at least in part, i.e., near the excavation, by tensile failure processes. This degradation cannot be prevented but must be managed by appropriate rock reinforcement and retention techniques.

Design based on convention failure criteria (Coulomb or Hoek-Brown) may mislead the designers. This is of particular concern when numerical codes with conventional constitutive models and inappropriate strength parameters are adopted. As a consequence, failure may both be over- or under-predicted depending on which part of the s-shaped curve is used to select rock strength parameters.

Due to the distinctly different behaviour in the inner shell, extreme care must be taken when using measurements from the low confinement zone to determine confined rock parameters for the outer shell (e.g., for pillar design). There is a distinct possibility that back-analyses of measurements in the inner shell will significantly underestimate the confined rock mass strength and thus lead, for example, to conservative pillar designs.

With respect to anticipating underground construction difficulties, it is most important to recognize that the rock and rock mass strength near the excavation may be significantly reduced for brittle failing rock (in the inner shell). Hence, spalling, stain-bursting, limited stand-up time of the inner shell, and high potential for overbreak should be anticipated. Equipment (e.g., type of TBM) is to be selected to properly manage these unfavourable rock behaviour modes.

Such processes cannot only occur at the excavation walls or tunnel backs but in the floor and at the tunnel face. The latter may lead to tunnel face instability issues (Kaiser, 2006 and 2007) with related implications for the utilization of TBMs. The former may lead to floor heave or degradation (including slaking and swelling) potential.

In summary, spalling processes must be understood when selecting excavation and support techniques or classes; they must be appropriate to manage broken ground.

Acknowledgements

Some of the studies presented in this article were partially funded by the Natural Sciences and Engineering Research Council of Canada and contributions of former graduate students and long-term research collaborators listed in the quoted references below are thankfully acknowledged. Much practical experience reflected in this paper stems from valuable collaborations with representatives of underground contractors (MATRANS and TAT consortia, Switzerland), TBM manufacturer (Herrenknecht AG, Germany), mining companies (Vale Inco, Goldcorp, Rio Tinto, etc.), and many others. Their contributions and support are thankfully acknowledged.

References

1. Cai, M., Kaiser, P.K., Tasaka, Y., and Minami, M. (2006). Determination of residual strength parameters of jointed rock masses using GSI system. Int. J. of Rock Mech., 44(2): 247-265.
2. Cai, M., P.K. Kaiser, H. Uno, Y.Tasaka, M. Minami and Y. Hibino, 2004.Estimation of rock mass strength and deformation modulus using GSI system – a quantitative approach. International Journal of Rock Mechanics and Mining Sciences, 41(1): 3-19.
3. Diederichs, M.S., Carvalho, J.L. and Carter, T.G. and (2007). A modified approach for prediction of strength and post yield behaviour for high GSI rock masses in strong, brittle ground. , 1st Canada-U.S. Rock Mech. Symp., pp. 249-257.
4. Diederichs, M.S., Kaiser, P.K. and Eberhard, K.E. (2004). Damage initiation and propagation in hard rock and influence of tunnelling induced stress rotation. Int. J. Rock Mech. Min. Sci., 41: 785-812.
5. Diederichs, M.S. (2003). Rock fracture and collapse under low confinement conditions, Rocha Medal Recipient, Rock Mech. Rock Engr., 36(5):339-381.
6. Einstein, H.H. (1996). Tunnelling in difficult Rock – swelling behaviour and identification of swelling rocks. Rock Mechanics and Rock Engineering. 29(3):113-124; see also: Einstein, HH.; Bischoff,, N. und Hofmann E., 1972. Das Verhalten von Stollensohlen in quellendem Mergel. Proc. Symposium Untertagbau, Luzern, pp. 296 – 312.
7. Hoek, E., 2007. Practical rock engineering, 2nd ed. Rocscience Inc.

8. Hoek, E., P.K. Kaiser and W.F. Bawden, 1995. Rock Support for Underground Excavations in Hard Rock. A.A. Balkema, Rotterdam, 215 p.
9. Hoek, E. (1968). Brittle Failure of Rock. In Rock Mechanics and Engineering Practice, John Wiley & Sons Ltd. London, 99-124.
10. Martin, C.D. and Maybee, W.G. (2000). The strength of hard-rock pillars. Int J Rock Mech. and Min. Sc. 37(8):1239-1246.
11. Martin, C.D.. McCreath, D.R. and Maybee W.G. (2000). Design approaches for hard-rock pillars. Proc. 53rd Can. Geot. Conf., Bitech Publishers Ltd., Richmond, (ed. LeBoeuf), 1:291-298.
12. Martin, C.D., Kaiser, P.K. and McCreath, D.R. (1999). Hoek-Brown parameters for predicting the depth of brittle failure around tunnels. Canadian Geotechnical Journal, 36(1):136-151.
13. Kaiser, P.K. and B-H. Kim, 2008. Rock mechanics challenges in underground construction and mining, Keynote lecture, 1st Southern Hemisphere International Rock Mechanics Symposium, Perth, Australia, 1:23-38.
14. Kaiser, P. K. (2007). Rock mechanics challenges and opportunities in underground construction and mining. . Keynote lecture, 1st Canada-U.S. Rock Mechanics Symposium, on CD, 47p.
15. Kaiser, P. K. (2006). Rock mechanics consideration for construction of deep tunnel in brittle ground. Keynote lecture, Asia Rock Mechanics Symposium, Singapore, 12 p, on CD.
16. Kaiser, P.K. (2005). Tunnel stability in highly stressed, brittle ground - Rock mechanics considerations for Alpine tunnelling. Geologie und Geotechnik der Basistunnels, Keynote lecture at GEAT'05 Symposium, Zürich, Switzerland, pp. 183-201 (2006).
17. Kaiser, P.K., Diederichs, M.S., Martin, C.D., Sharp, J. and Steiner, W. (2000). Underground works in hard rock tunnelling and mining. GeoEng2000, Technomic Publ. Co., pp. 841-926.
18. Kaiser, P.K., McCreath, D.R. and Tannant, D.D. (1996). Canadian Rockburst Support Handbook, Mining Re-search Directorate, Sudbury, Canada, 314 p.; also Drift support in burst-prone ground. CIM Bulletin, 89(998): 131-138.
19. Ortlepp, W.D. (1997). Rock Fracture and Rockbursts: an illustrative study. Monograph series M9. South African Inst. Min. Metall. 220p.
20. Spottiswoode, S.M., L.M. Linzer and Majiet, S. (2008). Energy and stiffness of mine models and seismicity. 1st Southern Hemisphere International Rock Mechanics Symposium, Perth, Australia, 1:693-707.
21. Yong, S., Kaiser, P.K., Löw, S. and Corrado, F. (2008). The Role of heterogeneity on the development of excavation-induced fractures in the Opalinus Clay, Canadian Geotechnical Conference, Edmonton, 8p (in press).

Rock Mechanics Challenges in Underground Construction and Mining

P.K. Kaiser *Centre for Excellence in Mining Innovation, Canada*

B-H. Kim *Geomechanics Research Centre at MIRARCO – Mining Innovation, Laurentian University, Canada*

Abstract

The underground construction and mining industry are facing many geomechanics challenges. This keynote address presents an overview of some practical challenges, recent developments and some new technical opportunities. In mining, going deeper, increasing safety standards, and aiming for high productivity demands engineering to maximise value. In underground construction, geological complexities and mechanisation demand better integration of engineering to ensure ease of construction.

Lack of engineering for constructability when tunnelling in weak or brittle rock at depth often leads to unnecessary delays and extra costs. Furthermore, brittle failing rock at depth poses unique problems as stress-driven failure processes often dominate the tunnel behaviour. Such failure processes can lead to shallow unravelling or to strainbursting modes of instability that cause difficult conditions for tunnel constructors.

This paper summarises lessons learned during the construction of deep Alpine tunnels and highlights implications that are of practical importance with respect to constructability. Special attention is given to issues of rock behaviour identification and to the selection of appropriate rock properties for underground construction in brittle failing ground.

1 Introduction

This paper draws on experiences from major, mostly deep, mining projects and from large, deep tunnelling operations. The author's experience with brittle failing rock in deep mining, underground construction, and Alpine tunnelling was previously presented in keynote lectures: at GeoEng 2000 (Kaiser et al., 2000), summarising a decade of collaborative research work on brittle rock failure; at the Rockburst and Seismicity in Mines Symposium (Kaiser et al., 2005), introducing new means of complex data interpretation in seismically active mines; at GEAT'05 (Kaiser, 2006), focusing on experiences from deep Alpine tunnelling; and at the Asian Rock Mechanics Symposium, highlighting the impact on constructability (Kaiser, 2006). This paper also summarises some aspects of the presentation made at the Canada–U.S. Rock Mechanics Symposium (Kaiser, 2007). After a brief review of findings from these studies, recent developments and implications of practical importance are highlighted, particularly with respect to the proper design for constructability of underground excavation in brittle rock.

The two most important lessons learned from these projects are: (1) at depth, the rock is much less forgiving, and (2) costly mistakes can be made. Hence, we have to learn from them and design smarter.

Furthermore, as Leopold Müller already stated in the 1960s: "*We don't know the rock mass strength. That is why we need an International Society*". Almost fifty years later, rock mass strength determination is still a challenge for rock engineers. Hence, recent developments related to rock and rock mass strength determination for brittle failing rock are discussed in some detail.

1.1 Challenges and opportunities

Current opportunities and challenges arise from: (a) our desire to answer some questions of 21st century science (Deep Underground Science and Engineering Laboratory (DUSEL) and URLs), and (b) unprecedented growth in mining and underground construction. This growth and globalisation drives innovation in many sectors, including rock mechanics and rock engineering.

The unique image, created for deep science to reflect *"As the miner's headlamp casts light on subterranean darkness, research in deep underground laboratories illuminates many of the most compelling questions in 21st century science"* (www.deepscience.org), also indicates that the DUSEL project, as all major underground excavation projects, offers fantastic opportunities to cast light on strategic rock mechanics and rock engineering questions. Of the many challenges we face, this paper addresses the need to improve our ability to better understand rock mass behaviour. It would be a mistake if we would not take these opportunities to advance our knowledge and rock engineering state-of-the-art.

Of the many technical challenges in geo-engineering, to build on and in rock, this paper focuses on these aspects:

- Going underground – mining in weak ground.
- Going deeper – mining in stressed ground.
- Going faster – safe, rapid development.

Innovative solutions to overcome related challenges offer opportunities for huge economic gains. For example, to go underground, one major mining company alone has to sink four to five shafts per year and advance on average between 50 and 80 km of tunnels per year. Progress in the previously listed topics would be highly beneficial.

The value of these opportunities lies primarily in the speed of construction, reduced risks during construction, and enhanced long-term quality of the related infrastructure, i.e. less or little rehabilitation as mining affects the infrastructure. In civil engineering tunnelling, many projects suffer from costly delays; often as a result of engineering that does not facilitate optimal construction (Kaiser, 2006). It can be easily demonstrated that an increase in development rate can reduce the cost of large construction or mining projects by hundreds of millions of dollars. This economic opportunity and the related technical challenges are the driver for innovation and must guide our path of discovery in rock mechanics.

In the following, some lessons learned in recent years are reviewed from a geomechanics perspective to facilitate future problem solving and to identify opportunities for improved rock excavation techniques, support design and other ground control measures. By interpreting observed rock failure processes, by explaining factors affecting constructability, and by questioning some well established principles (e.g. commonly used failure criteria), some deficiencies in our current state of knowledge and thus opportunities for improvements are identified

2 Anticipating the "true" rock behaviour – a primary geomechanics challenge

The first principle in understanding rock behaviour is to carefully observe and then interpret field evidence. In this manner, it was found that spalling (or brittle failure) often dominates over shear failure and that this process is highly dependent on rock confinement (both from a strength as well as a rock dilation (bulking) perspective). It should therefore be anticipated that the strength and bulking behaviour near excavation surfaces (open pit or underground) should differ from those encountered at some distance from an excavation. It also follows that fractured rock loses its self-supporting capability (reduced stand-up time) and thus must be more difficult to control during construction (Kaiser, 2006; 2007).

If brittle rock failure behaviour is not anticipated, e.g. when going deeper or when entering highly stressed ground, rock may behave in an unexpected manner, good "old" ground may become bad ground, and proven technologies may fail to perform well. The geotechnical engineer is thus challenged to anticipate changing rock behaviour modes and to design control measures in such a manner as to facilitate ease of construction.

In tender documents, descriptions of the geology and the rock characteristics are often overemphasised while descriptions of the anticipated rock and rock mass behaviour are underemphasised, or, in many cases, the "true" rock mass behaviour is not anticipated. When the actual rock behaviour is not correctly anticipated or even worse misunderstood, inappropriate constitutive models may be used for numerical simulations and resulting stability assessments and support designs may be deficient or impractical causing construction difficulties.

For this reason, three main elements of underground construction are discussed in more detail: (1) the relevance and consequences of brittle failure processes in underground engineering and construction; (2) challenges in anticipating the rock or rock mass strength when brittle failure processes affect or dominate the failure modes of underground excavations, and (3) the consequences for stability assessment and underground constructions.

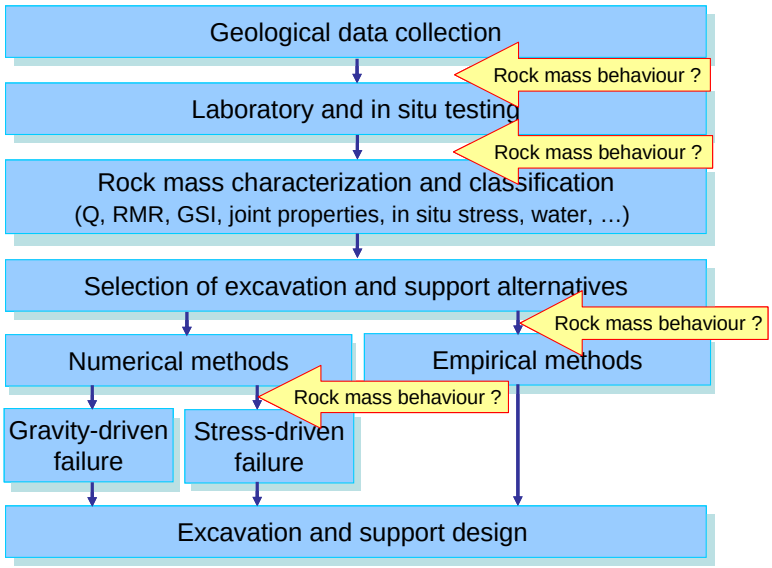

Figure 1 Site characterisation approach for standard geo-engineering projects; the arrows are where a sound understanding of rock mass behaviour is needed

2.1 Rock behaviour characterisation

Site or rock characterisation generally follows a well established path (Figure 1) from geological model to rock mass model development, whereby the spatial distributions of rock types (lithologies) as well as rock and rock mass properties (including in situ stress) and characteristics (including jointing, water, etc.) are characterised and classified. However, when stepping out of the world of experience, e.g. by going from shallow to deep tunnelling, costly mistakes can be made because the rock behaviour may change and the rock may behave in an unexpected manner. Furthermore, rock may behave differently when unconfined (near an excavation) or when confined (in the core of a pillar). Hence, it is not sufficient to just provide a geological and a rock mass model; it is necessary to translate the knowledge gained from geological to rock mass and then to rock behaviour models. Most tender documents elaborate much on the geological and rock mass model but fall short of providing proper descriptions of the rock mass behaviour models. In Figure 1, the arrows indicate that the anticipated rock behaviour model should influence many steps in the site characterisation process.

In slope engineering, it is common practice to classify slope behaviour modes (Figure 2); planar, circular, wedge, multi-block failure, etc.) and to match each class with a respective limit equilibrium model (Bishop, Janbu, Hoek and Bray, Morgenstern and Price, Sharma, etc.). Unfortunately, by the proliferation of numerical modelling, with continuum and somewhat less with discontinuum models, this distinction by failure or behaviour mode is often ignored or even misrepresented by the chosen numerical model.

In underground construction, commonly recognised behaviour modes include wedge failure, squeezing, swelling, etc., and these are reflected in respective modelling tools (UDEC, 3DEC, Unwedge, FLAC, Phases, etc.). Almost exclusively, the most commonly recognised behaviour modes are related to shear failure; either along block boundaries or through the rock mass (elements 11–13 and 33 in the tunnel behaviour matrix presented in Figure 3). The effects of tensile failure or spalling are rarely anticipated and correctly modelled, and thus not properly described in tender documents even though it is often the related near excavation degradation process that negatively affects constructability issues such as stand-up time.

Failure mode	Mechanism	Influence of internal shear	Method of Analysis
Class I 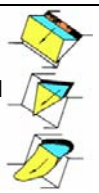	Rigid body motion	None	Hoek and Bray (1974)
Class II 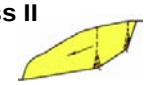	Local yielding to allow basal movement	Minor	Morgenstern and Price (1965)
Class III 	Internal shears and block dilation to allow basal shear	Major	Sarma (1979)

Figure 2 Slope failure mode classification (after Corkum and Martin, 2004)

Brittle, tensile rather than shear, failure modes play a role at intermediate to high stress levels and in massive to moderately jointed rock masses (elements 21–23 and 31–32 in tunnel behaviour matrix of Figure 3). In general, brittle rock behaviour near excavations is more wide spread than commonly anticipated. For example, over-consolidated clays like the Opalinus Clay at Mount Terri (Yong et al., 2008, show clear signs of brittle failure (Figure 4). Many weaker rock types such as lightly cemented sandstones, Kimberlites, shales, etc., do also fail in a brittle manner when lightly confined.

2.2 Brittle failure characteristics

Difficulties in designing underground excavations are often experienced because constitutive laws in

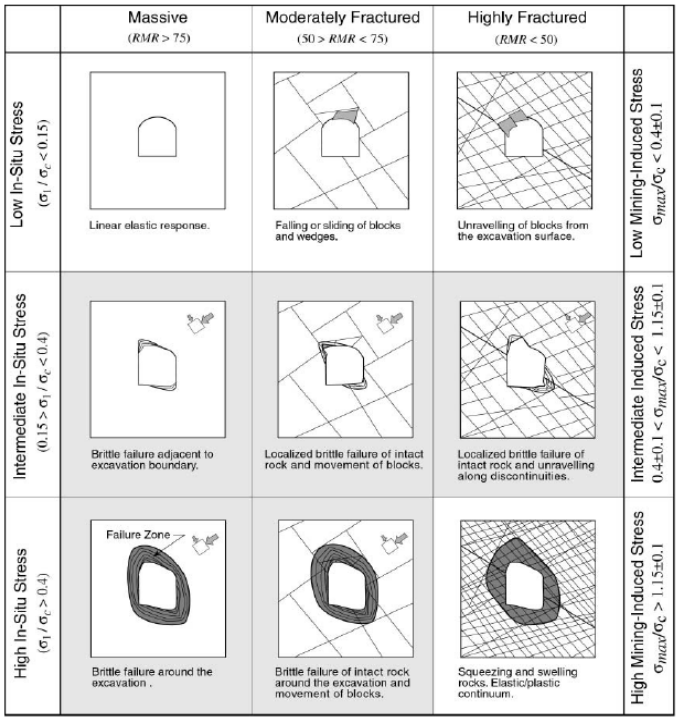

Figure 3 Tunnel failure modes (Kaiser et al., 2000)

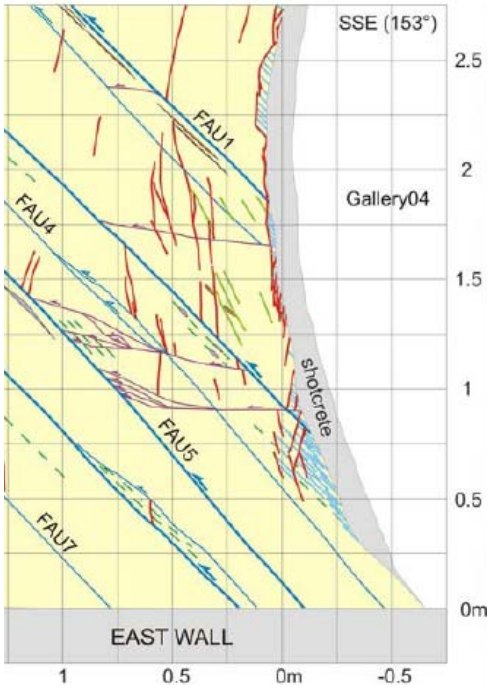

Figure 4 Brittle fracturing near tunnel in Opalinus Clay (Yong et al., 2008)

numerical models do not necessarily reflect the actual behaviour of the rock. This is particularly true when the fundamental paradigm of the Mohr–Coulomb yield criteria $\tau = c + \sigma_n \tan \phi$, relating the shear strength τ to a strain-independent cohesion c and a simultaneously acting frictional resistance $(\sigma_n \tan \phi)$, is not valid (Martin, 1997; Martin et al., 1999; Kaiser et al., 2000). As intact rock is strained, cohesive bonds fail and damage initiation and propagation occurs at different stress thresholds (Diederichs, 2003). The propagation of tensile fractures depends on the level of confinement (as established by tests of Hoek (1968)) and is used to explain brittle failure by collaborating researchers in Kaiser et al. (2000). Figure 5(a) illustrates that an s-shaped criteria is required to properly describe the entire failure envelope from low confinement, spalling failure to high confinement shear failure. The existence of this s-shaped failure envelope for many rock types is further examined and verified in this paper.

A bi-linear or non-linear criterion is required to capture this dependence on confinement in the low confinement range (near excavations) for rock that is prone to spalling (Figure 5(b)). Brittle failure by tensile spalling occurs when the stress path moves above the damage threshold and to the left of the spalling limit. The practical relevance of an s-shaped envelope, reaching into the high confinement range, is discussed by use of a tri-linear failure envelope approximation (Figure 5(c)) with a tension cut-off, a damage limit through USC_I (lab test), a spalling limit with a slope k_s, and a shear limit with an intercept or apparent unconfined strength UCS_{II}.

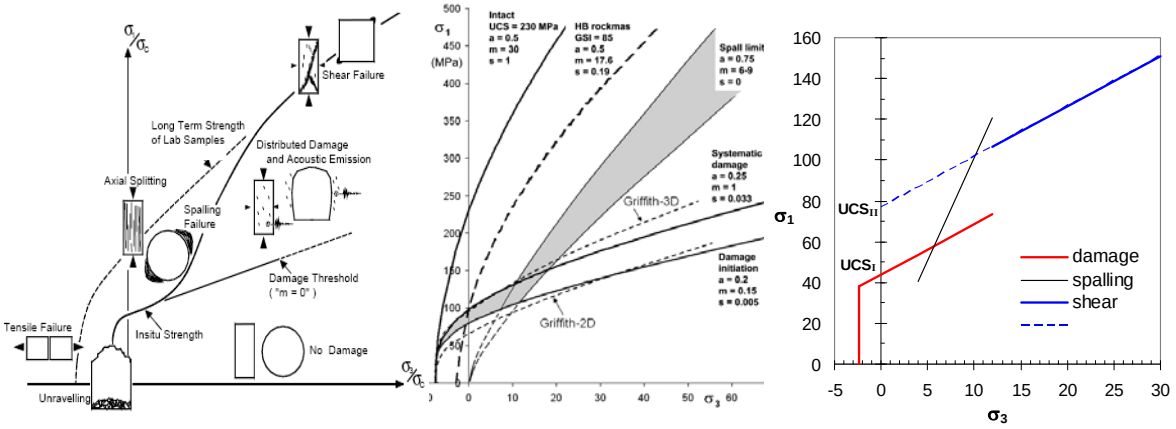

(a) (b) (c)

Figure 5 S-shaped failure criteria concept showing damage threshold, spalling limit and confined rock strength envelope (Kaiser et al., 2000; Diederichs, 2003); (b) bi-nonlinear approximation introduced by Diederichs et al. (2007) for damage threshold and spalling limit; (c) tri-linear failure envelope used for examples presented in Section 2.3

2.3 Consequences of brittle failure on tunnel behaviour

2.3.1 Strength development near excavations

Contrary to the tangential or major principal stress near an underground excavation, the radial or confinement stress zone is nearly parallel to the excavation geometry as illustrated by Figure 6. As a consequence, contours of equal rock strength are essentially parallel to the σ_3-contours and the rock strength distribution in the radial direction, with the exception of the floor, is very similar for all three cases and for the walls as well as for the roof. For the tri-linear envelope of Figure 5(c), the spalling limit is reached at about 5 MPa (in the middle of the contour range shown in Figure 6) and the shear failure envelope is reached at about 10 MPa (at the outer range of the contours shown). The development of σ_3 in the wall for the three cases is shown in Figure 7(a) and the resulting strength development in the radial direction is illustrated by Figure 7(b) for the wall. Since the σ_3-contours are essentially parallel to the tunnel boundary, nearly identical strength developments are applicable for the walls and roof.

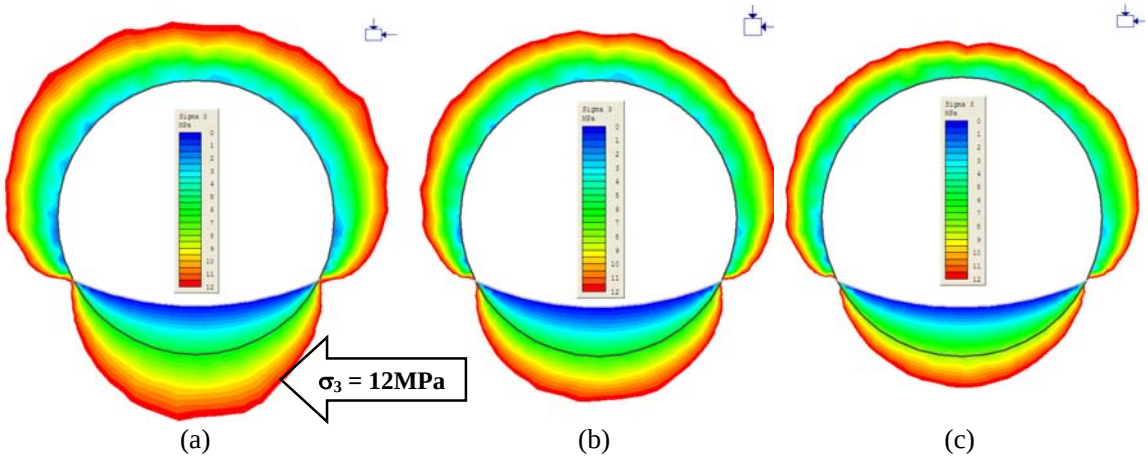

Figure 6 Minor principal stress contours (range 0–12 MPa) around excavation in elastic rock for K_o = 0.75, 1, 1.33

Due to the tri-linear or s-shape of the failure envelope, the rock strength, for all three stress ratios, is relatively low near the excavation (to a depth of about 0.7 m for this case), then rapidly increases to about double strength at a depth of about 1.3 m, and then increases further but at a lower rate. The tangential stress (σ_1) for K_o = 1.33 is also shown in Figure 7(b) for the roof and walls. Due to the flat, reduced strength near the wall, the tangential stress exceeds the strength not just in the roof (where it would be anticipated for K_o = 1.33) but also in the walls. Field evidence supports this as shallow stress-induced overbreaks were more widely distributed in the roof than would be anticipated from conventional breakout models (Figure 7(c); Kaiser, 2007).

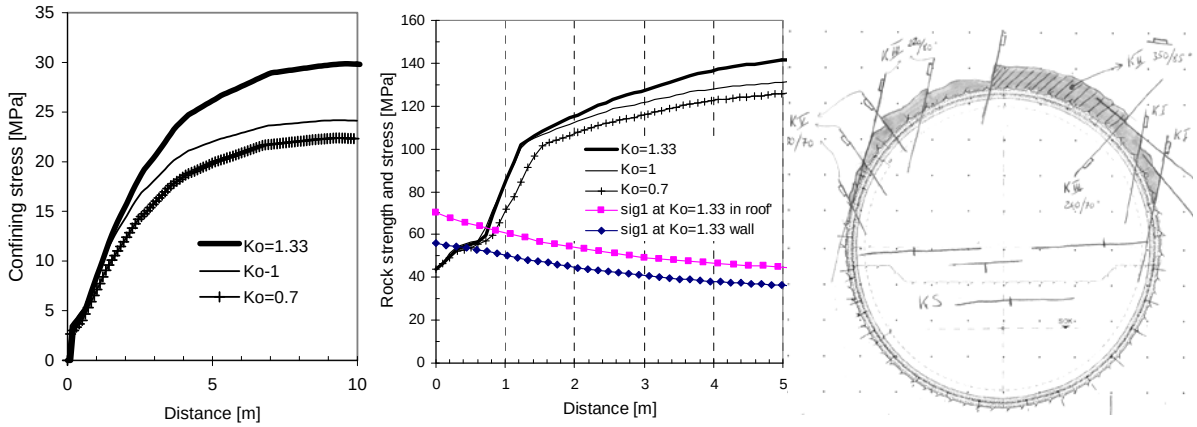

Figure 7 (a) Radial stress distribution for K_o = 0.75, 1, 1.33 (b) rock strength development near excavation for tri-linear criteria (Figure 5) (c) observed shallow stress-induced overbreak in 9 m tunnel excavated in moderately jointed rock

For support design and support selection, to manage brittle rock failure, it is therefore necessary to properly reflect the rock strength near the excavation and this can be properly approximated by a bi-linear or bi-nonlinear envelope (Diederichs, 2003; Diederichs et al., 2007). For pillar stability assessment, however, it is necessary to consider all three parts of the s-shaped curve.

In the floor, the strength increases less rapidly, due to the deeper low confinement zone (Figure 6), thus promoting deeper tensile fracturing and spalling than in the walls and roof. This has several practical consequences.

2.3.2 Swelling potential enhancement by brittle failure

Once the damage and spalling thresholds are exceeded, the volumetric deformation characteristic of brittle failing rock changes drastically as tensile fractures tend to open fractures, and geometric incompatibilities between rock fragments lead to high radial dilation (bulking) (Kaiser, 2006). As a consequence, water access to the rock is facilitated through stress fractures, particularly in the low confinement zone of the floor (Figure 6). This increases the supply of water to rock fragments, and when combined with the reduced confinement, enhances the swell potential.

The author hypothesises that brittle failure processes during tunnel advance may play a significant role in rocks where rock degradation processes are facilitated by water ingress, i.e. in rocks with swelling or slaking potential. For example, brittle fracturing may enhance the swelling potential and swelling rates in preconditioned or stress damaged zones, e.g. below flat floors (Einstein, 1996) or below insufficiently curved inverts, because tensile fracturing provides preferential access paths for water in a zone of low confinement. This is illustrated in Figure 8(a) and (b) for a horseshoe-shaped tunnel; the Belchentunnel and a model with K_o = 1.2.

While the numerical example presented here does not take into account the confining effect of a liner, these figures clearly illustrate that brittle rock tends to preferably spall and fracture in the floor, even when a curved invert is used. As the radius of the invert is reduced and thus deepened, the amount of fractured rock is reduced and it is speculated that this is, at least in part, responsible for lower swelling pressures in tunnels with circular profile or with deep floor arches.

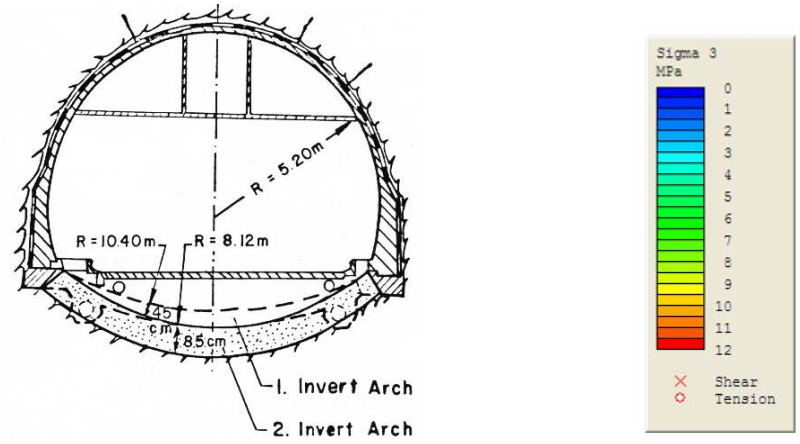

(a)

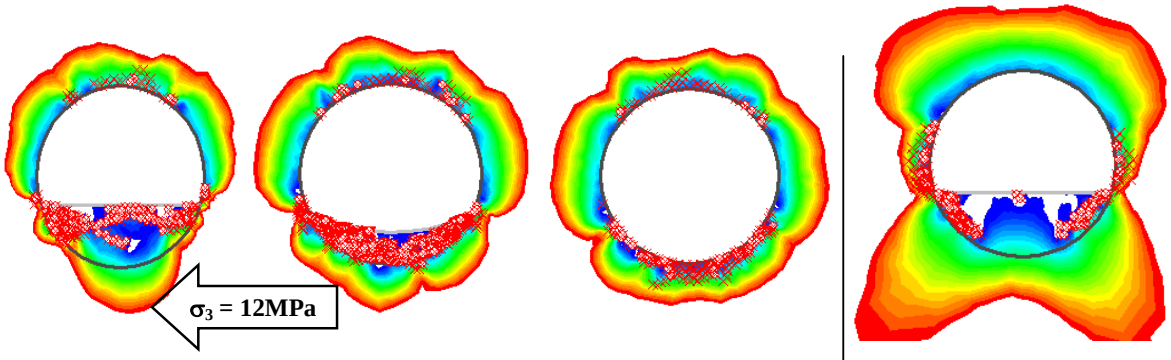

(b) (c)

Figure 8 **(a) Belchentunnel (Grob, 1972) showing pre- and post-reconstruction invert arches; (b) K_o=1.2: flat, curved and circular invert; shown are tensile and shear failure (o and x) and σ_3-contours (0–12 MPa); (c) minor principal stress contours for K_o = 0.5 with tensile and shear failure locations**

2.3.3 Enhanced slaking potential due to brittle failure

In rocks that are prone to slaking (softening and weakening due to water ingress), brittle failure processes can lead to preferential water access paths and thus to non-uniform slaking. In Kimberlites, for example, it is often observed that tunnels are initially stable and may even show signs of fracturing (spalling), but that, after some time, squeezing behaviour starts to dominate the tunnel behaviour. Tensile fracturing again can provide preferred access paths for water and thus regionally enhanced slaking potential.

While the extent and location of spalling will differ in various rock types (properties), Figure 8(c) illustrates for K_o = 0.5 that both the lower walls and floor are most susceptible to tensile fracturing and thus, as a consequence, to slaking. This is in good agreement with frequently observed degradation processes.

Recent advances in modelling techniques involving fracture propagation (e.g. ELFEN, Rockfields, UK) and models permitting combined failure modes involving discontinuities and intact rock (e.g. synthetic rock mass (SRM) model) will eventually facilitate the proper simulation of combined shear and tensile failure processes. For the time being however, much can be achieved by recognising the impact of the s-shaped failure envelope on excavation behaviour and by approximating it by a bi-nonlinear envelope for support design and by a tri-linear envelope for aspects involving unconfined and confined rock (pillars, cave propagation, etc.).

2.3.4 Strength development in brittle failing pillars

As indicated previously, for pillar stability assessment, it is necessary to consider all three parts of the s-shaped curve (Figure 5(a) and (c)) if the confinement inside the pillar exceeds the σ_3–value at the intersection of the spalling limit and the shear failure envelope (about σ_3 = 10 MPa for case shown in Figure 5(c)). Martin and Maybee (2000) used brittle Hoek and Brown parameters (Martin et al., 1999) to demonstrate that the pillar strength, contrary to the best-fit curves presented by many (Figure 9(a)), should non-linearly increase (with an upward rather than a downward curvature) as the pillar width to height ratio (W/H) increases. The authors justified this by the fact that spalling or hour-glassing weakens narrow pillars more than wide pillars. Their interpretation also makes intuitive sense as very wide pillars should approach the strength of the confined rock mass, which should be much higher than suggested by the horizontal asymptotic value of about 0.7 UCS, as indicated in Figure 9(a). The development of stresses and strength for two pillar sizes, W/H = 1 and 2, are shown in Figure 9(b). Near the wall, the damage threshold is reached and the local factor of safety FS = strength / stress = 1 and the major principal stress (sig1) is reduced as a consequence. The confining stress (sig3) reaches about 18 MPa in the centre of both pillars and the shear failure envelope (Figure 5(c)) defines the strength of the pillar core. For the rock properties given in Figure 5(c), the strength in the core far exceeds the pillar stress and the local factors of safety (FS) reach 3 and 4.5 for the two pillars, respectively. The overall factors of safety (average pillar strength / average pillar stress) are 3.5 and 2.2, respectively, indicating that both pillars would spall (hour-glass) but would be overall stable due to a stable core. It follows that the pillar strength is strongly influenced by the confined strength of the rock mass and thus by the third leg (the shear strength) of the s-shaped envelope.

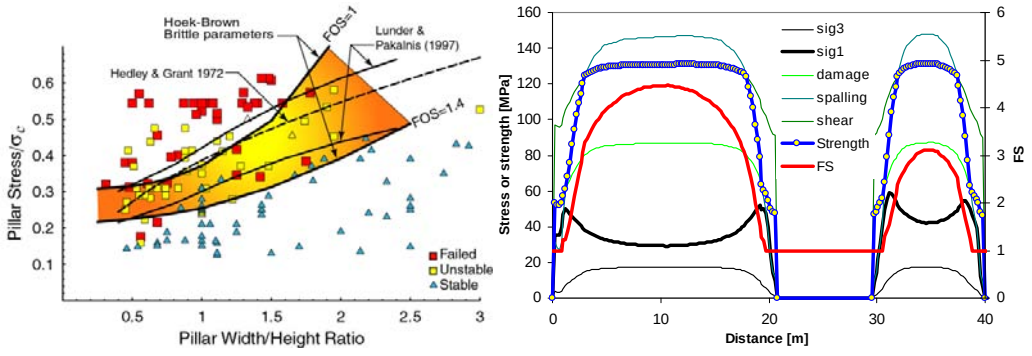

(a) (b)

Figure 9 (a) Pillar strength (Martin and Maybee, 2000); (b) distributions of pillar stress, strength and factor of safety (FS) for two pillars (H = 10 m; W/H = 2 and 1) at 1100 m depth with K_0 = 0.6

2.3.5 Potential impacts on cave propagation

While cave propagation is a complex phenomenon and beyond the scope of this paper, it is worthwhile noting that the strength distribution shown in Figure 7(b) has two potential practical implications: (1) the reduced strength in the shallow, low confinement zone (inner shell) may promote break-up of the rock mass into relatively small size blocks (production of smaller than typically anticipated fragmentation); and (2) the rapid increase of strength in the deeper, high confinement zone (outer shell) may tend to choke the cave propagation process. These aspects deserve further study and thus present an opportunity for technical advancement.

2.3.6 Rock support considerations for brittle failing rock

As illustrated by Figure 6, a low confinement zone of more or less constant depth exists near an unsupported excavation. Even if the tunnel was supported with a liner providing a radial support pressure (typically between 0 and 1 MPa), such a low confinement zone still exists. Hence, the damage threshold defines the rock strength near the excavation as shown in Figure 7(b). However, the strength rapidly increases as soon as the confinement is sufficient to reach the spalling limit (at about 0.7 m depth or ~5 MPa in Figure 7(b)).

2.3.6.1 Rock mass bulking control

As illustrated by Figure 10(a) for a deep tunnel, tensile fracturing (circles) is largely confined to the inner hell of about 1.5 m depth in this case. Most importantly, this figure illustrates that tensile failure induced spalling should be expected all around the tunnel, even for K_o = 0.5. This is consistent with the observed overbreak profile shown in Figure 7(c). Since damage by tensile fracturing is affected by the tensile strength of the rock (tension cut-off), the actual location of stress fracturing can vary in anisotropic rock as the tensile strength perpendicular to foliation is often smaller than parallel to it. Hence, in a horizontally foliated rock (e.g. gneiss), the back would be more prone to stress fracturing than the walls. This was the case at the tunnel illustrated by Figure 7(c).

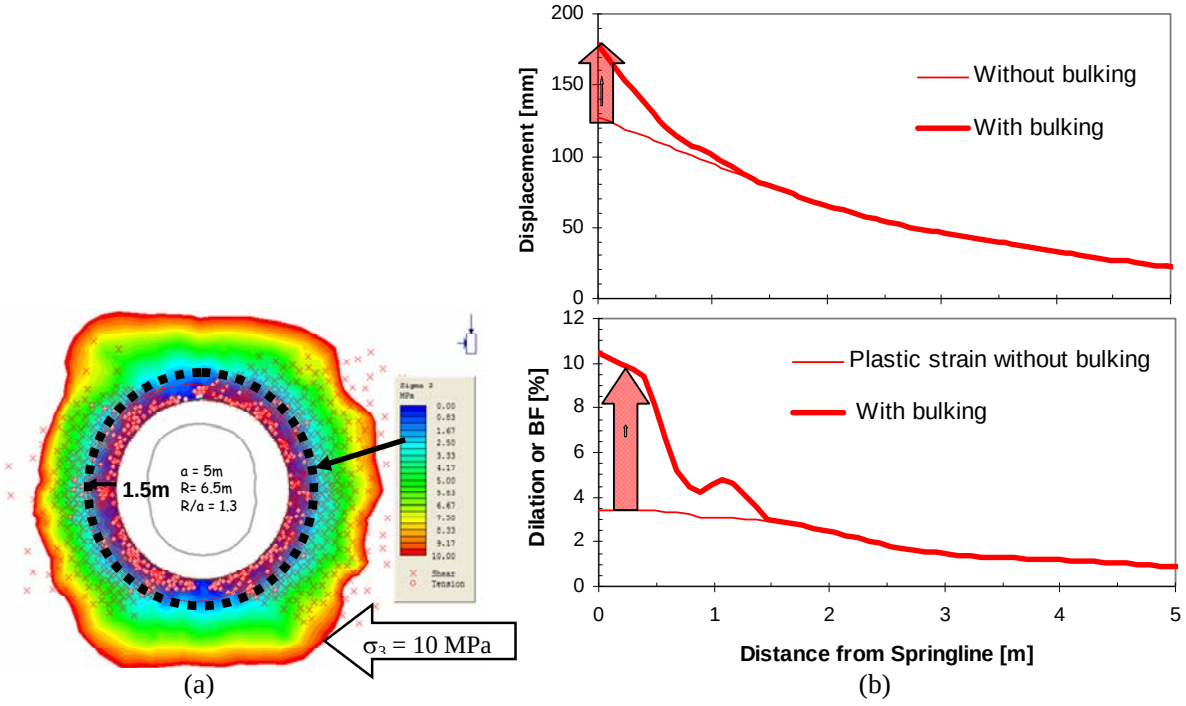

Figure 10 Tunnel at 2000 m depth with K_0 = 0.5; (a) σ_3-contours showing an almost circular (inner) zone of low confinement; (b) corresponding radial dilation or bulking factor (%) and resulting cumulative displacement with 41% more convergence due to bulking

Kaiser (2007) illustrated bulking in the stress fractured zone. It was shown by numerical modelling that bulking is highly dependent on confinement. For typical support pressures of ≤1 MPa, bulking increases rapidly to values in the range of 7–10%. This is consistent with bulking factors derived from field measurements (Kaiser et al., 1996) showing >30% for unconfined floors and 1–10% depending on support type. As a consequence, the radial strains in the inner shell are much larger than predicted by standard constitutive models. For a given parameter set with an elasto-plastic rock mass behaviour model, Figure 10(b) shows how the radial strain increases toward the tunnel (maximum about 3.5% at the tunnel wall for the selected parameter set). Due to the superimposed bulking process, the total or combined strain is much larger to a depth of about 1.5 m, reaching >10% at the wall (Figure 10(b)). The cumulative displacements without and with bulking is shown in the upper diagram of Figure 10(b). The consequence of bulking in the first 1.3 m is a 41% increase in tunnel convergence.

It follows for support design that, contrary to the pillar strength, the wall strength is strongly influenced by the low-confinement strength of the rock mass, i.e. by the first and second leg of the tri-linear failure envelope (the damage and spalling strength). For brittle failing rock, support needs to be designed / selected to control (reduce) the bulking and manage the resulting elevated convergences.

2.3.6.2 Stand-up time management

Stress-driven rock "fragmentation" in the inner, low confinement shell creates broken rock with varying fragment size and shape distributions (Kaiser, 2007). This degradation is plotted on the GSI chart (Cai et al., 2006; Figure 11), showing that stress-driven degradation transforms a rock mass of GSI>65 to a damaged, fractured rock mass of 35<GSI<55 and, most importantly, from a continuum or tight discontinuum, often with non-persistent joints, to a loose discontinuum with often continuous and open fractures.

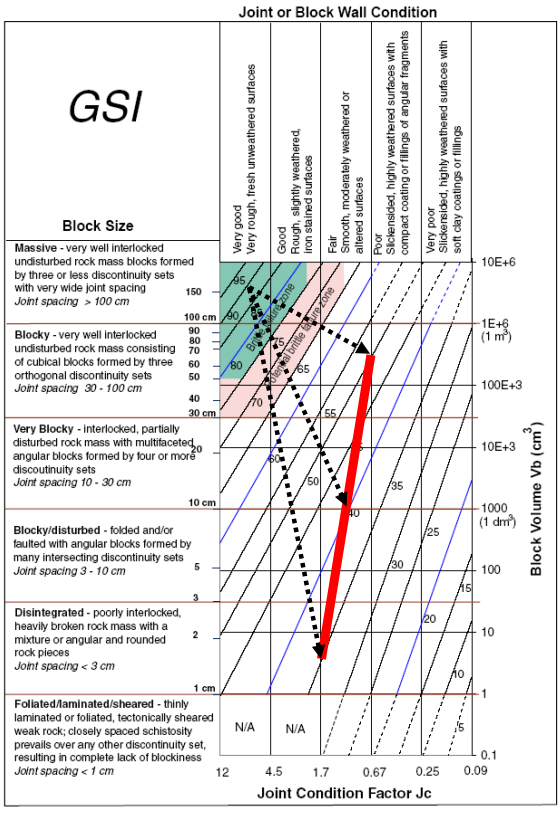

Figure 11 SI-chart showing degradation paths for various rock types from massive gneiss, to friable quartzite, to massive granite (Kaiser, 2007)

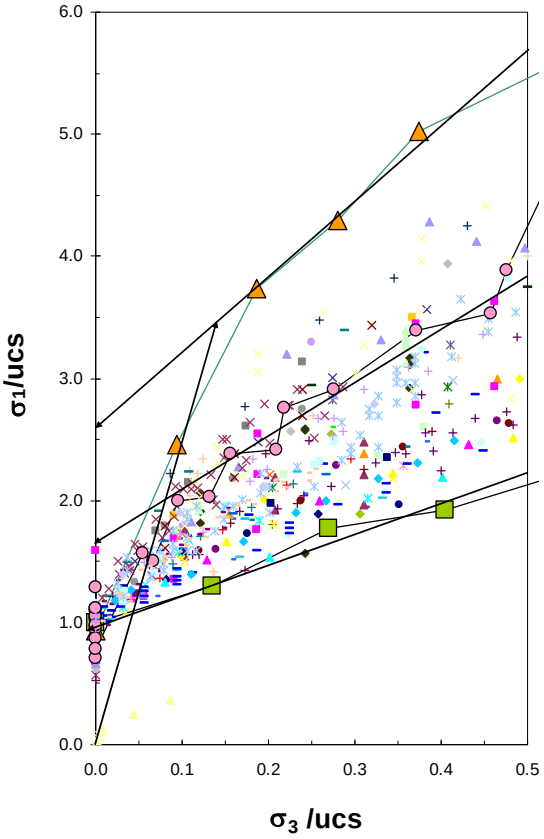

Figure 12 Triaxial test data from tests on 73 rock types (data courtesy E. Hoek (pers. comm., 2008))

When rock is excavated, the stress path eventually ends in a nearly unconfined state (in the spalling zone of Figure 5(a) for brittle rocks). According to the stand-up-time chart (Bieniawski, 1989) essentially permanent stability, with stand-up times of several months to greater one year, can be achieved (for a 5–10 m wide unsupported tunnel) when RMR≥65±5 or GSI≥60±5. However, only very short stand-up times, say 6–24 hours, can be achieved when RMR≤40±5 or GSI≤35±5. From a constructability perspective this implies that it is difficult to retain stability in the inner shell when stress-driven fracturing causes rock degradation in the inner shell. However, while it may be difficult to retain the broken rock, the demand on the support will be often rather limited due to stronger rock in the outer shell.

Stress-driven fracturing and rock mass degradation can bring a stable, self-supporting rock mass to the brink of ravelling with low to zero stand-up times. In other words, brittle failure processes will tend to cause constructability problems as the fractured rock mass near the excavation will not be self-stabilising. Such rock behaviour has slowed the rate of progress at various projects utilising open tunnel boring machines (Kaiser, 2007).

2.4 Laboratory test data revisited

Based on the previously presented consequences of brittle rock failure, it is clearly necessary to re-evaluate and reconsider constitutive models used in rock mechanics.

Both Mohr–Coulomb and Hoek and Brown assume a steady increase in strength with increasing confinement; a linear increase for the former and a non-linear increase for the later. More importantly, for both criteria it is implied that cohesive and frictional strength components are simultaneously mobilised. Furthermore, rock mass degradation, e.g. using GSI, does not change the form of the failure envelope, and various means for residual strength determination (Cai et al., 2006) do also not alter the shape of the peak strength envelope.

Ample evidence has been presented in the recent literature by colleagues (Diederichs and Martin; see list of references) and other researchers that support the bi-linear or bi-nonlinear shape of the failure envelope of rock (Figure 5(a) and (b)). This is now well established based on field observations and extensive back-analyses of cases involving spalling failure.

However, if this process is a fundamental characteristic of brittle failing rock, it should also be observed in the laboratory. Indeed, when testing hard rocks, it is often observed that samples fail, particularly in unconfined or low confinement tests, by axial splitting, shattering or by progressive spalling. Only at high confinement levels or when a sample contains distinct foliation or weakness planes are typical shear failure processes observed. Hence, it should be anticipated that brittle rocks might show a similarly bi-linear or s-confinement levels or when a sample contains distinct foliation or weakness planes are typical shear failure shaped failure envelope as back-analysed from field observations.

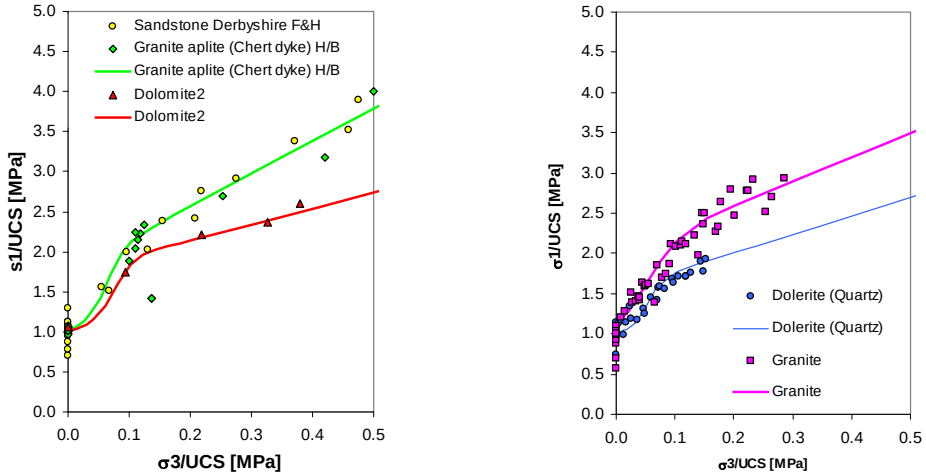

Figure 13 Laboratory test data fitted with s-shaped failure criteria (data courtesy E. Hoek, pers. comm.)

2.4.1 S-shaped failure criteria for brittle failing intact rock

Figure 12 presents data contained in Dr Hoek's database with three of over 70 rock types highlighted (the strongest, the weakest and one intermediate rock type). Also shown is a spalling limit at $\sigma_1/\sigma_3 = 25$ (arrow from origin) and three linear back-projections (arrows pointing to ordinate; Figure 12) intersecting for the three rock types at $\sigma_1/UCS_I = 2.6$, 1.65, and 1.0.

While data maybe missing in the low confinement range for some rock types, this figure suggests that there may indeed be a reduced strength zone for $\sigma_3 \leq UCS_I/10$. This is most evident from the data shown in Figure 13(a) for Sandstone, Granite Aplite and Dolomite. While less pronounced, it is also detectable from the Dolerite and Granite tests shown in Figure 13(b). Fitted s-shaped failure criteria are shown for each rock type. The strength in the shear failure zone can be described with an apparent unconfined strength, UCS_{II}, of 1–2.6 times the UCS obtained from standard unconfined compression tests (UCS_I).

Figure 14(a) presents data from a series of triaxial tests on a Quartzite. The scatter in the low confinement range ($< UCS_I/10$) is large and can be attributed to various degrees of sample disturbance and varying failure modes (breakage of intact rock near upper limit; failure along pre-existing weakness planes near lower limit; and mixed modes of failure near the fitted s-shaped line).

An s-shaped failure criterion for brittle rock is under development by the authors and the fitted lines to all data as well as for the upper and lower limit is shown in Figure 14(a). In the interim, the laboratory strength can be approximated by a tri-linear criteria as illustrated in Figure 5(c), used for the presented examples, or as superimposed on Figure 14(b) for the Quartzite ($UCS_I = 140\pm30$ MPa; $UCS_{II} = 300\pm15$ MPa; $k_s = 35$ to 15 to 10 for intact to structurally controlled breaks).

2.4.2 Guidelines for design parameter selection for brittle intact rock

It is evident that design parameters for brittle failing rocks must be selected with extreme care and with the design problem in mind. Until an s-shaped failure criterion has been formalised, tested and is ready for use in numerical modelling, constitutive model and failure envelope adopted for support design may have to differ from those used for pillar design. This is illustrated here for the data set shown in Figure 14(a). The average UCS for this rock (data not shown) is 95 MPa. Parameters for four approaches are listed in Table 1 and the corresponding non-linear envelopes are shown in Figure 14(c).

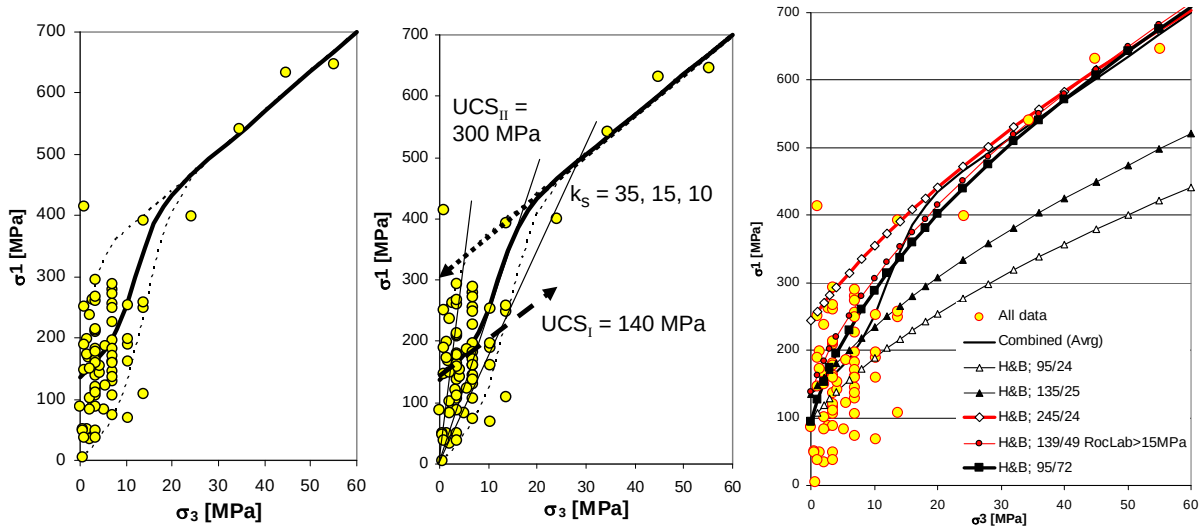

(a) (b) (c)

Figure 14 Data from friable Quartzite (a) fitted s-curve for all data and upper and lower limit; (b) respective linearised approximations; (c) Hoek and Brown envelopes obtained by various fitting approaches with parameters listed in Table 1 (UCS and m_i values shown in legend as UCS/m_i)

Table 1 Parameters for Hoek and Brown criteria shown in Figure 14

	Approach	UCS (MPa)	mi
A	Average from UCS tests and mi from published rock type tables: mi = 23±3 for Quartzite	95 (average)	24 (assumed)
B	RocLab™ (Rocscience) applied to all data	139	50
C	RocLab™ applied to data from samples failing through intact rock	245	24
D	Best fit to all data without RocLab constraint of mi ≤50 and average UCS	95	72

The obvious question arises: how to select the most appropriate intact rock strength envelope for this Quartzite? The m_i-values for approach B and D are clearly out of m_i-range based on commonly recommended values for m_i and thus would be rejected. However, based on the above presented discussion, an unusually high m_i-value of 72 would clearly overall best represent the results from the laboratory testing program (Figure 14(c)).

2.4.2.1 Approach A and C: approximation using UCS data from laboratory tests and published m_i-values

In mining, modelling is often based on UCS data only and m_i is estimated from recommended property tables (Hoek, 2007). The resulting failure envelope (approach A) clearly underestimates the strength of the Quartzite in the high confinement range (>1 MPa; Figure 14(c)) if the average UCS is used. On the other hand, if the UCS of only those tests with intact breaks were used (approach C), then the resulting failure envelope clearly over-estimates the strength of the Quartzite in the low confinement range (<10 MPa; Figure 14(c)).

2.4.2.2 Approach B and C: use of RocLab™

When using any fitting procedure to obtain Hoek and Brown parameters, data must cover the confinement range of σ_3 = 0 to UCS/2. Because of test cell constraints, triaxial tests are commonly conducted with confining pressures up to 60 MPa. Consequently, as for the Quartzite, fitting approaches to obtain Hoek and Brown parameters are strictly only applicable for rocks with UCS<120 MPa thus parameters can, strictly speaking, not be obtained for hard brittle rocks. Furthermore, RocLab™ limits m_i to 50 and thus cannot be used for rocks with distinct s-shaped failure behaviour.

2.4.2.3 Obtaining representative Hoek and Brown parameters for rocks with s-shaped failure behaviour

For rocks with distinct s-shaped failure behaviour, a best-fit Hoek and Brown parameter set can be obtained by linear regression in the $(\sigma_1 - \sigma_3)^2/UCS$ versus σ_3 space (approach D; forcing linear regression line through $(\sigma_1 - \sigma_3)^2/UCS = 1$). However, it must be noted that the corresponding m_i-value (m_i = 72 for the Quartzite) are unusually high and that standard approaches to obtain the rock mass strength (e.g. by GSI-based degradation) may not be applicable. Nevertheless, such a fitting approach will lead to a parameter set for the intact rock that is on average representative for the entire confinement range (with high uncertainty in the low confinement range).

2.4.2.4 Sectional fitting for limited confinement ranges

For rocks with distinct s-shaped failure behaviour, it is therefore more appropriate to consider the confinement range relevant for a given engineering problem before fitting and selecting design parameters.

For support design, the rock behaviour near the excavation, in a confinement range of 0–5 MPa, is most relevant. From Figure 14(c) it follows that the parameter sets, between 95/24 to 139/24, or 120/24 on average with a standard deviation of about 40 MPa on UCS, would be appropriate for the low confinement zone (inner shell). However, a cut-off as recommended by Diederichs et al. (2007), or with k_s = 15–10, would have to be applied to prevent excessive depths of failure predictions.

For pillar design, the rock behaviour in the pillar core, in a typical confinement range of >5 MPa for mining at depth, is most relevant. From Figure 14(c) it is evident that the parameter sets (245/24) with a standard deviation of about 15 MPa on UCS, would be appropriate for the highly confined zone (outer shell).

However, the effect of spalling and hour-glassing is to be predicted by using the parameter set for the inner shell.

2.4.3 S-shaped failure criteria for brittle failing rock masses

Procedures to obtain corresponding s-shaped failure envelopes for the rock mass, following the GSI approach, are under development by the authors. If it is assumed that the currently adopted degradation approach to obtain the Hoek and Brown parameters s and m_b for the rock mass is applicable, then it could be applied for each section of the s-curve (the low and the high confinement range) to obtain an s-shaped rock mass envelope. However, this aspect will require further work and calibration. It remains an outstanding challenge for rock engineering in brittle rock masses.

Nevertheless, rock and rock mass strength parameters for brittle failing rock should be established separately for low and high confinement zones and then applied to zones where each mode is dominating the rock behaviour (e.g. for inner and outer shell modelling).

3 Conclusion — lessons learned

When mining in brittle ground, the rock behaviour can change drastically when progressing to greater depth or when stresses change due to advancing mining fronts.

3.1 Engineering for brittle behaviour

By observing and interpreting brittle rock behaviour, it is now possible to understand and anticipate the rock behaviour such that design and construction procedures can be matched to the ground. As a consequence of brittle failure processes, the ground becomes less forgiving at depth as stress breaks even good ground and disintegrates massive to moderately jointed rock to cohesionless ground (at least in the inner shell). As a consequence, this leads to a quantum shift in construction difficulties, e.g. it affects stand-up times, and thus engineering must address this by providing appropriate ground control measures and excavation tools.

At depth, rock becomes brittle and fails at least in part by tensile failure processes. This degradation cannot be prevented but must be managed by appropriate rock reinforcement and retention techniques.

Design based on convention failure criteria (Mohr–Coulomb or Hoek and Brown) may mislead designers. This is of particular concern when numerical codes with conventional constitutive models and inappropriate strength parameters are adopted. As a consequence, failure may both be over- or under-predicted depending on which part of the s-shaped behaviour dominates the rock strength parameter selection.

Due to the distinctly different behaviour in the inner shell, extreme care must be taken when using measurements from the low confinement zone to determine confined rock parameters (e.g. for pillar design). There is a distinct possibility that back-analyses will significantly underestimate the confined rock mass strength and thus lead, for example, to conservative pillar designs.

3.2 Anticipating construction problems

With respect to anticipating underground construction difficulties, it is most important to recognise that the rock and rock mass strength near the excavation may be significantly reduced for brittle rock near the excavation (in the inner shell). Hence, spalling, strainbursting, limited stand-up time of the inner shell, and high potential for overbreak should be anticipated. Equipment (e.g. type of TBM) is to be selected to properly manage these unfavourable rock behaviour modes.

Such processes cannot only occur at the excavation (pillar) walls or tunnel backs but in the floor and at the tunnel face. The latter may lead to tunnel face instability issues (Kaiser, 2006; 2007) with related implications for the utilisation of TBMs, and the former may lead to floor heave or degradation (including slaking and swelling) potential.

In summary, spalling processes must be understood when selecting excavation and support techniques; they must be appropriate to manage broken ground.

Acknowledgements

Some of the studies presented in this paper were partially funded by the Natural Sciences and Engineering Research Council of Canada and contributions of former graduate students and long-term research collaborators listed in the quoted references are thankfully acknowledged. Much practical experience reflected in this paper stems from valuable collaborations with representatives of underground contractors (MATRANS and TAT consortia, Switzerland), TBM manufacturer (Herrenknecht AG, Germany), mining companies (Vale Inco, Goldcorp, Rio Tinto, etc.), and many others. Their contributions and support are thankfully acknowledged. The authors also would like to thank Dr. E. Hoek for providing access to his extensive triaxial test data base.

References

Bieniawski, Z.T. (1989) Engineering Rock Mass Classification, Wiley, New York.

Cai, M., Kaiser, P.K., Tasaka, Y. and Minami, M. (2006) Determination of residual strength parameters of jointed rock masses using GSI system, International Journal of Rock Mechanics and Mining Sciences, 44(2), pp. 247–265.

Corkum, A.G. and Martin, C.D. (2004) Analysis of a rock slide stabilized with a toe-berm: a case study in British Columbia, Canada, International Journal of Rock Mechanics and Mining Sciences, 41(7), pp. 1109–1121.

Diederichs, M.S., Carvalho, J.L. and Carter, T.G. (2007) A modified approach for prediction of strength and post yield behaviour for high GSI rock masses in strong, brittle ground, 1st Canada–U.S. Rock Mech. Symposium, pp. 249–257.

Diederichs, M.S., Kaiser, P.K. and Eberhard, K.E. (2004) Damage initiation and propagation in hard rock and influence of tunnelling induced stress rotation, International Journal of Rock Mechanics and Mining Sciences. 41, pp. 785–812.

Diederichs, M.S. (2003) Rock fracture and collapse under low confinement conditions, Rocha Medal Recipient, Rock Mechanics and Rock Engineering., 36(5), pp. 339–381.

Einstein, H.H. (1996) Tunnelling in difficult Rock – swelling behaviour and identification of swelling rocks, Rock Mechanics and Rock Engineering, 29(3), pp. 113–124; see also: Einstein, HH.; Bischoff, N. und Hofmann E., 1972. Das Verhalten von Stollensohlen in quellendem Mergel. Untertagbau Symposium, Luzern, pp. 296–312.

Grob, H. (1972) Schwelldruck im Belchentunnel, Internationales Symposium für Untertagbau, Luzern, pp. 99–109.

Hoek, E. (2007) Practical rock engineering, 2nd ed. Rocscience Inc.

Hoek, E. and Bray, J.W. (1981) Rock Slope Engineering, London: Institution of Minerals and Metals.

Hoek, E. (1968) Brittle Failure of Rock, In Rock Mechanics and Engineering Practice, John Wiley and Sons Ltd. London, pp. 99–124.

Martin, C.D. and Maybee, W.G. (2000) The strength of hard-rock pillars. International Journal of Rock Mechanics and Mining Sciences , 37(8), pp. 1239–1246.

Martin, C.D., McCreath, D.R. and Maybee, W.G. (2000) Design approaches for hard-rock pillars, 53rd Canadian Geotechnical Conference, Bitech Publishers Ltd., Richmond 1, pp. 291–298.

Martin, C.D., Kaiser, P.K. and McCreath, D.R. (1999) Hoek–Brown parameters for predicting the depth of brittle failure around tunnels, Canadian Geotechnical Journal, 36(1), pp. 136–151.

Martin, D. (1997) The effect of cohesionloss and stress path on brittle rock strength. Canadian Geotechnical Journal, 34, pp. 698–725.

Morgenstern, N.R. and Price, V.E. (1965) The analysis of the stability of general slip surfaces, Geotechnique 15(1), pp. 79–93.

Kaiser, P.K. (2007) Rock mechanics challenges and opportunities in underground construction and mining, Keynote lecture, 1st Canada–U.S. Rock Mechanics Symposium, on CD, 47 p.

Kaiser, P.K. (2006) Rock mechanics consideration for construction of deep tunnel in brittle ground, Keynote lecture, Asia Rock Mechanics Symposium, Singapore, 12 p., on CD.

Kaiser, P.K., Vasak, P. and Suorineni, F.T. and Thibodeau, D. (2005) New dimensions in seismic data interpretation with 3-D virtual reality visualization in burst-prone grounds. Keynote Address to 6th RaSiM6, Perth, Australia, 33–47.

Kaiser, P.K. (2006) Tunnel stability in highly stressed, brittle ground – Rock mechanics considerations for Alpine tunnelling, Geologie und Geotechnik der Basistunnels, Keynote lecture at GEAT'05 Symposium, Zürich, Switzerland, pp. 183–201.

Kaiser, P.K., Diederichs, M.S., Martin, C.D., Sharp, J. and Steiner, W. (2000) Underground works in hard rock tunnelling and mining, GeoEng 2000, Technomic Publ. Co., pp. 841–926.

Kaiser, P.K., McCreath, D.R. and Tannant, D.D. (1996) Canadian Rockburst Support Handbook, Mining Research Directorate, Sudbury, Canada, 314 p.; see also Drift support in burst-prone ground, CIM Bulletin, 89(998), pp. 131–138.

Sarma, S.K. (1979) Stability analysis of embankments and slopes, ASCE Journal of Geotechnical Engineering Division, 105(GT12), pp. 1511–1524.

Yong, S., Kaiser, P.K., Löw, S. and Corrado, F. (2008) The Role of heterogeneity on the development of excavation-induced fractures in the Opalinus Clay, Canadian Geotechnical Conference, Edmonton, 8 p. (in press).

Rock Mechanics Challenges and Opportunities in Underground Construction and Mining

Peter K. Kaiser
Chair for Rock Mechanics and Ground Control
Laurentian University, Sudbury, Canada

Acknowledgements
Cai, Diederichs, Hajibdolmajid, Martin
Swiss contractors: MATRANS, TAT, Herrenknecht AG, ...
Canadian Mining companies: CVRD INCO, Goldcorp, Rio Tinto, ...
and many more ... Courtesy xyz (200x)

CEMI's Key R&D Programs

- Exploration
- Deep Mining
- Automation and Telerobotics
- Environmental Stewardship
- **Integrated Mining Process Engineering**
  - Planning and optimization
  - Productivity enhancement
  - Risk management

Today ... draw on experiences from major mining and tunnelling operations

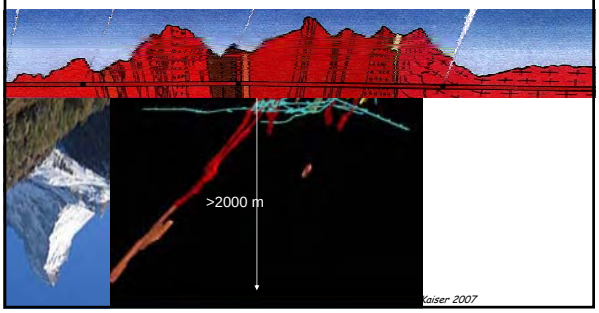

Lessons learned ...

1 - At depth ... rock is less forgiving
2 - must learn from costly mistakes
and ... smarten-up to design properly

Opportunities and Challenges

- Answering some of "the most compelling questions in 21st century science"
  - DUSSEL and URLs ... Opportunities for geo-science
- Unprecedented growth in ...
  - Mining
  - Underground construction

→ new opportunities and challenges

Growth and globalization drives innovation

... including in rock mechanics and rock engineering

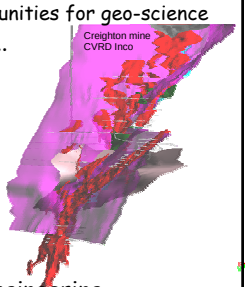

'High Level' Report

Overview of DUSEL
Deep Underground Science and Engineering Laboratory
Goals and Objectives

Download from www.dusel.org

DEEP SCIENCE

As the miner's headlamp casts light on subterranean darkness, research in deep underground laboratories illuminates many of the most compelling questions in 21st century science …

and

offers unique opportunities to cast light on strategic rock mechanics and rock engineering questions

Rock mass behaviour – still a challenge

"We don't know the rock mass strength. That is why we need an International Society." Müller, 24 May 1962

- Müller 1962: we don't know the rock mass strength …

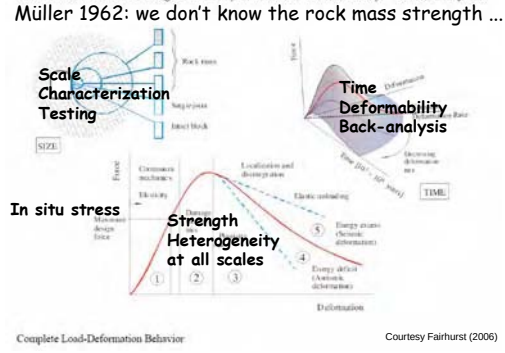

Courtesy Fairhurst (2006)

DUSEL – geo-challenges

- Amongst many others …
  - How do coupled Hydro-Thermal-Mechanical-Chemical-Biological processes in fractured rock masses vary with physical and time scales?
    - Rock fracture and flow at depth
    - Models of fracture initiation and propagation
    - Effects on proximal fluid flow and transport
    - Wellbore interaction
    - Roles of fractures in bacterial colonization
  - Can progress in geophysical sensing methods and computational advances be applied to make the earth "transparent"?
    - Advance geophysical sensing and computational methods to make the earth transparent, to 'see' real-time interaction of processes
    - Relate surface and subsurface deformations/stresses
  - How does the earth crust move?
    - Controls of onset and propagation of seismic slip

and much more … www.dusel.org

Outline

Part I

- Unprecedented growth in mining
  → Valuing opportunities

Part II

- Unprecedented opportunities to learn
  - Alpine tunnels
  - Mining
  - Nuclear waste disposal facilities
- Use case examples to highlight some deficiencies in our knowledge
  → Refocus our path of discovery (research)?
  - Overemphasis of predicting geology
  - Increasing over-reliance on modelling

and where to push the knowledge boundaries

Challenges and Opportunities

- Unprecedented growth in mining …
  - Mining is engine of globalization
  - Mining is leading the way in underground construction
  - Mining challenges the rock mechanics community

Mining – unprecedented growth

- Discovery of large deposit
- Stock market as indicator

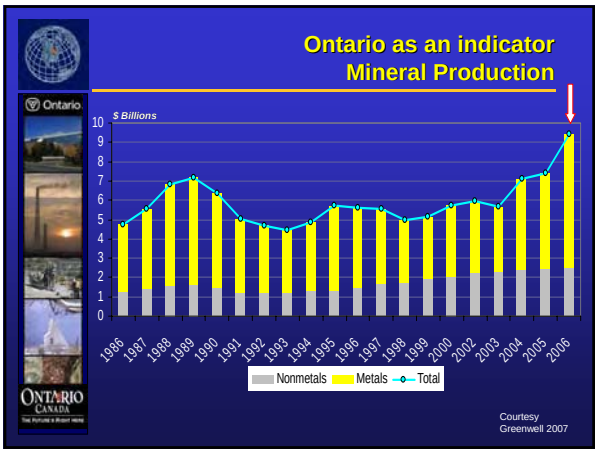
Ontario as an indicator
Mineral Production
Ontario
$ Billions
10
9
8
7
6
5
4
3
2
1
0
1986 1987 1988 1989 1990 1991 1992 1993 1994 1995 1996 1997 1998 1999 2000 2002 2003 2004 2005 2006
Nonmetals
Metals
Total
ONTARIO
CANADA
Courtesy
Greenwell 2007

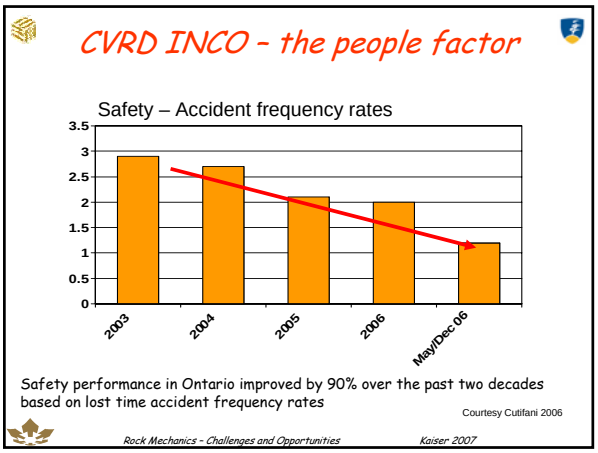
CVRD INCO – the people factor
Safety – Accident frequency rates
3.5
3
2.5
2
1.5
1
0.5
0
2003
2004
2005
2006
May/Dec 06
Safety performance in Ontario improved by 90% over the past two decades based on lost time accident frequency rates
Courtesy Cutifani 2006
Rock Mechanics - Challenges and Opportunities
Kaiser 2007


This growth brings Technical Challenges
Focus on …
• Going deeper near surface – deep open pits
• Going underground – mining in weak ground
• Going deep - mining in stressed
• Going faster – rapid drifting & moving >100kt/d
and many other challenges, e.g., caving, fragmentation, …
… opportunity of huge financial gains by finding solutions to these challenges
Rock Mechanics - Challenges and Opportunities
Kaiser 2007


Going deeper - pits

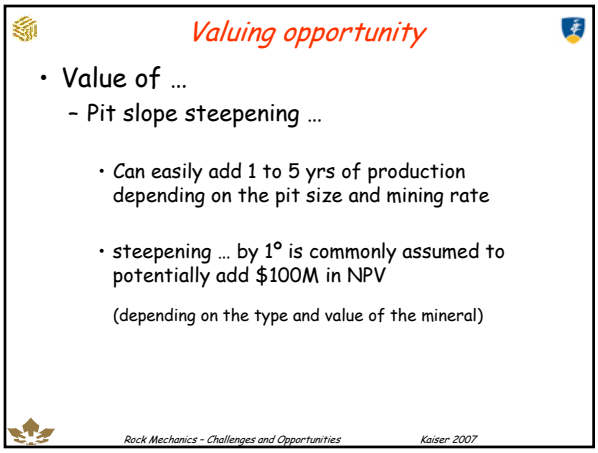
Valuing opportunity
• Value of …
– Pit slope steepening …
• Can easily add 1 to 5 yrs of production depending on the pit size and mining rate
• steepening … by 1° is commonly assumed to potentially add $100M in NPV
(depending on the type and value of the mineral)
Rock Mechanics - Challenges and Opportunities
Kaiser 2007

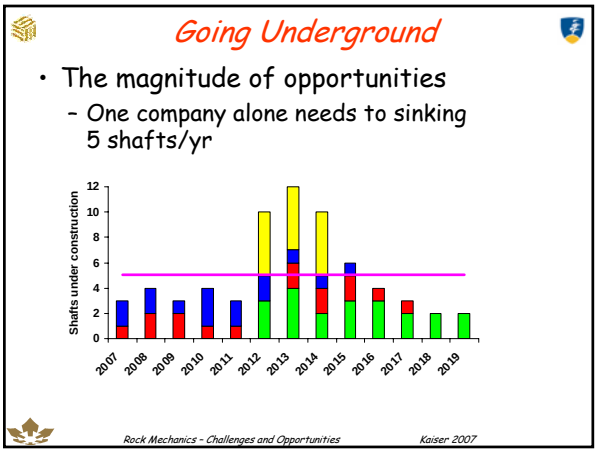
Going Underground
• The magnitude of opportunities
– One company alone needs to sinking 5 shafts/yr
Shafts under construction
12
10
8
6
4
2
0
2007 2008 2009 2010 2011 2012 2013 2014 2015 2016 2017 2018 2019
Rock Mechanics - Challenges and Opportunities
Kaiser 2007

Going fast

- The magnitude of opportunities
  - One company alone needs to develop 80km of tunnels per year

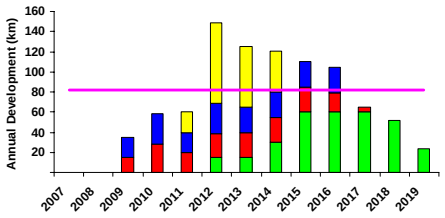

Valuing opportunities

- Value of …
  - Tunnel **advance rate** increase
  - Development **cost saving**

on net present value (NPD)

for a generic cash flow model of a large mine:

- Mine Construction
  - Critical path construction reduced by 1 yr → ΔNPV $73M
    increased by 1 yr → ΔNPV ($91M)
  - Development savings ($1,000/m) → ΔNPV $42M
- Mine Construction
  - Rapid Development
    Rate increased from 4-5m/d by 25% → ΔNPV $65M
    Rate increased by 100% → ΔNPV $195M

Primary rock mechanics challenge

- Anticipating the actual ***rock behaviour***
  - Brittle failure
    - spalling often dominates over shear failure
  - Strain-dependent strength
    - when stress exceeds strength, strain management is critical
  - Confinement dependent strength and "dilation" (bulking)
    - near surface (pit or excavation walls) rock fractures more readily
  - Geo-engineering for constructability
    - fractured rock is difficult to control

Objective of Part II

- Review some lessons learned … from a geomechanics perspective
  - Interpret observed rock failure processes
  - Explain factors affecting constructability
- to facilitate future problem solving
- to identify opportunities for improved
  - support design
  - rock excavation techniques
  - ground control measures

The Challenge – e.g., when going deep

When stepping out of the world of experience

… i.e. from shallow to deep tunnelling

… costly mistakes can be made

… because the rock behaviour may change and the rock may **behave in an unexpected manner**

Key for good UG excavation design

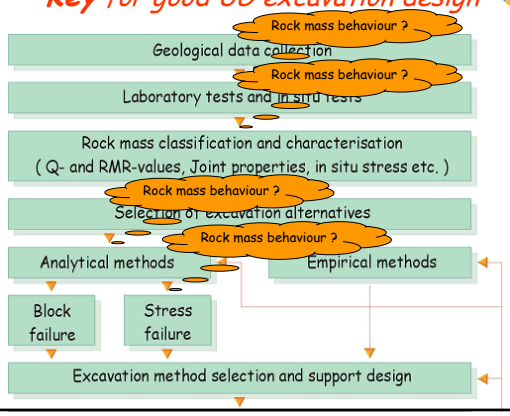

Site characterization

Geological Model !

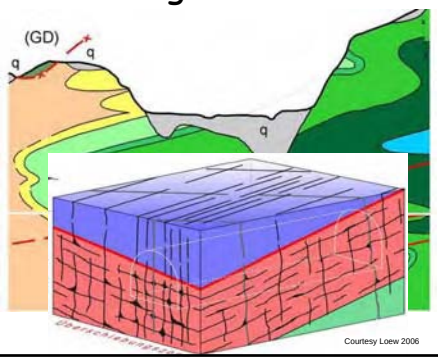

Courtesy Loew 2006

Behaviour Models - Slopes

Type of Failure	Mechanism	Influence of internal shears on: Failure Mechanism	Influence of internal shears on: FOS	Method of Analyses
Class I	Rigid body motion	NONE	NONE	Hoek & Bray (1974)
Class II	Local yielding to allow basal movement	MINOR	NONE	Morgenstern & Price 1965
Class III	Internal block dilation to allow basal movement	MAJOR	MAJOR	Sarma 1979

Courtesy Martin 2004

Tunnel instability modes

Focus on massive to moderately jointed, stressed rock

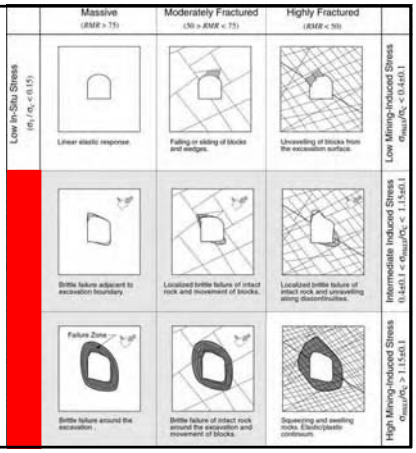

Hoek, Kaiser, Bawden 1995
Kaiser et al 2000

Rock behaviour Modes - Excavations

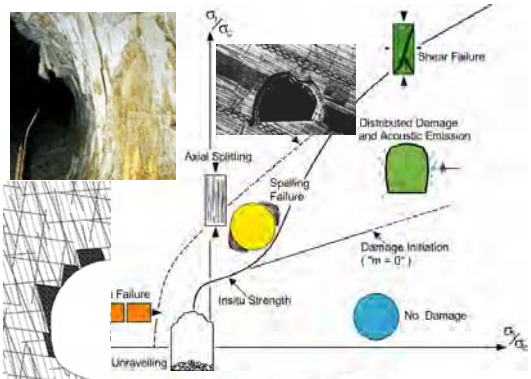

The Challenge – going deep

- When rock behaves in an **unexpected manner**

→ good "old" ground may become bad ground

→ proven **technologies may fail** to perform

→ How to **adapt** old tools to manage "unexpected" behaviour?

→ Challenge … to **anticipate the new behaviour**

At depth …
- same geology behaves differently -

- We tend to …
  - overemphasise description of geology, rock, and rock mass
  - underemphasise description of the anticipated rock **behaviour**

- Getting rock behaviour wrong
  → models are likely wrong
  → often dominate constructability

Challenges

1. **Anticipating the rock behaviour**
   - **Failure mode**
2. Anticipating more than the rock strength
   - Strain and confinement dependence
   - Volume change (bulking)
3. Anticipating the construction problems
   - Wall stability
   - Face stability
   - Stand-up time

So -Why do we get behaviour wrong ?

For example …

- reduction in advance rate [

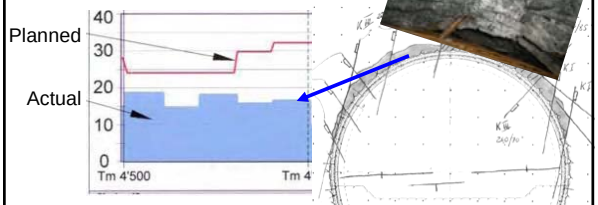

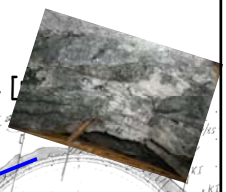

→ **Raveling** rock behind the open TBM "split" the advance and support cycle

Stress-driven rock mass degradation

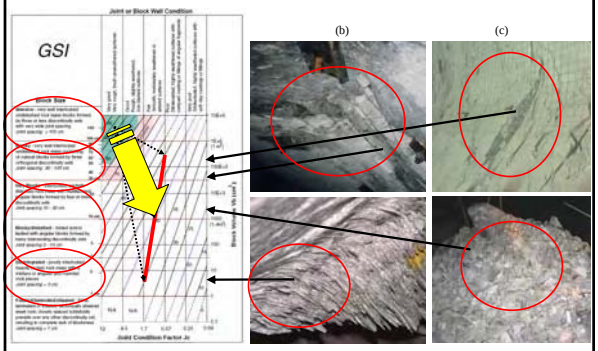

Rock mass degradation in numbers

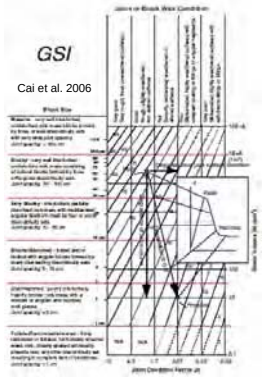

GSI = 70 - 100 → 55,45 or 35

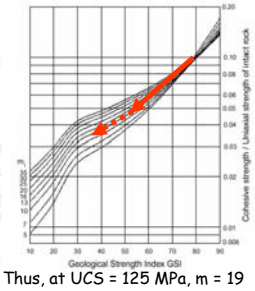

Thus, at UCS = 125 MPa, m = 19

UCS(rm) = 45 → 16, 12 or 9 MPa

or a strength loss of >75%

Stand-up time reduction

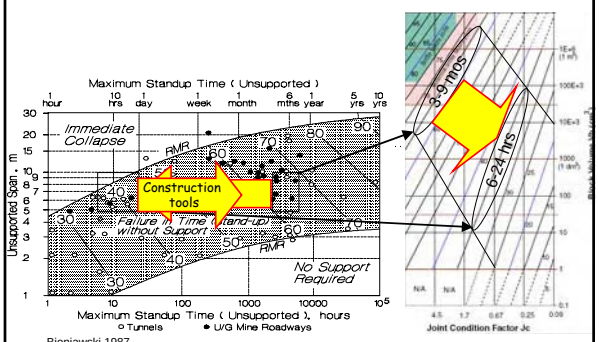

Bieniawski 1987

Challenges

1. Anticipating the rock behaviour
   - Failure mode
2. **Anticipating more than the rock strength**
   - **Strain and confinement dependence**
   - Volume change (bulking)
3. Anticipating the construction problems
   - Wall stability
   - Face stability
   - Stand-up time

Challenge - anticipate the failure mode

- **Observe**
- Interpret
  Understand
- Extrapolate

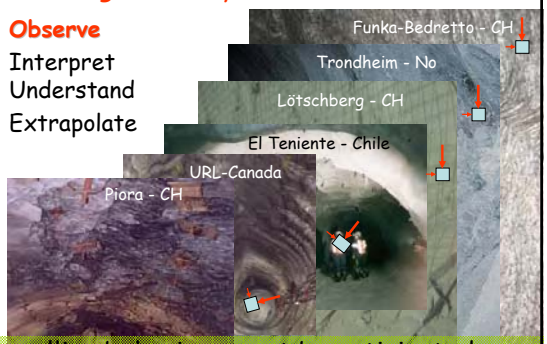

→ spalling behaviour must be anticipated …
so, design for it !

Heterogeneity causes tensile stresses

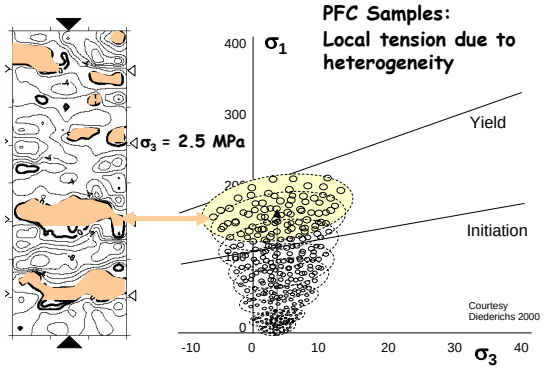

Construction of Deep Tunnel in Brittle Rock Kaiser 2006

Internal tensile stresses causes spalling

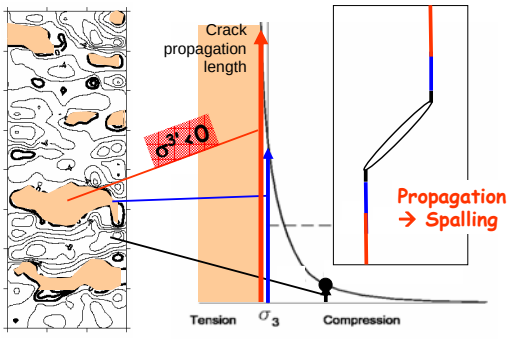

Construction of Deep Tunnel in Brittle Rock Kaiser 2006

% tensile stresses → spalling limit

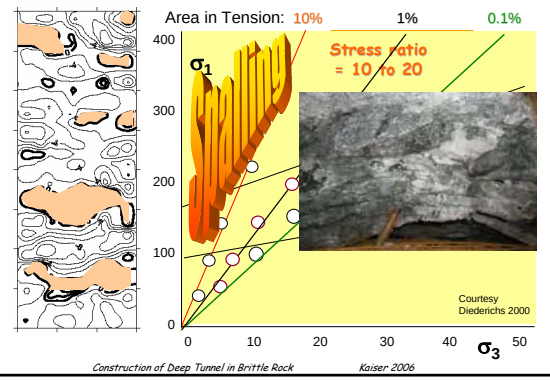

Construction of Deep Tunnel in Brittle Rock Kaiser 2006

New failure criteria to model near-wall behaviour …

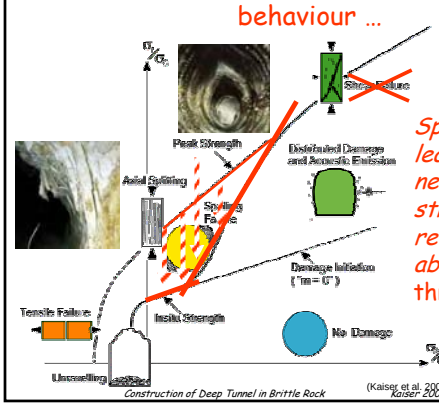

Spalling leads to near-excavation strength reduction above damage threshold

Construction of Deep Tunnel in Brittle Rock (Kaiser et al. 2000) Kaiser 2006

Conventional models for progressive failure consider post-peak strength loss

$\tau = c + \sigma' \tan(\phi + i)$ $\tau = c(\varepsilon) + \sigma' \tan(\phi + i)$

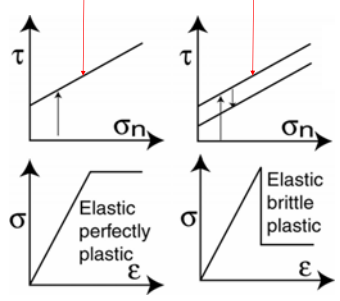

Construction of Deep Tunnel in Brittle Rock Kaiser 2006

Strength mobilization

(a) Terzaghi

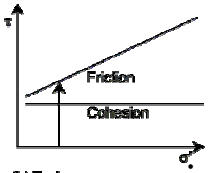

- simultaneous cohesion and frictional strength mobilization

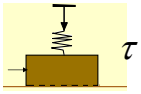

$$\tau = c + \sigma' \tan\phi$$

(b) Taylor

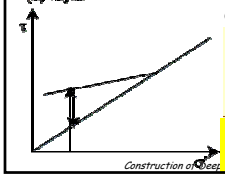

- sequential mobilization of cohesion and frictional strength

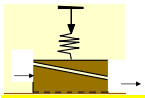

$$\tau = c(\varepsilon) + \sigma'(\varepsilon)\ \tan\phi$$

Mobilization of frictional & cohesional strength components

$$\tau = c(\varepsilon) + \sigma'(\varepsilon)\ \tan(\phi + i)$$

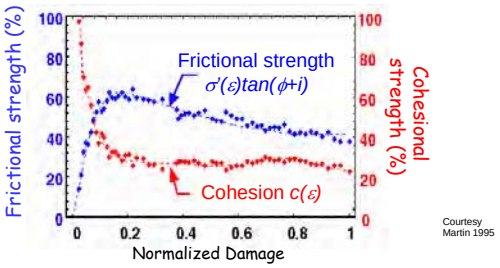

Courtesy Martin 1995

Schmertman and Osterberg 1960

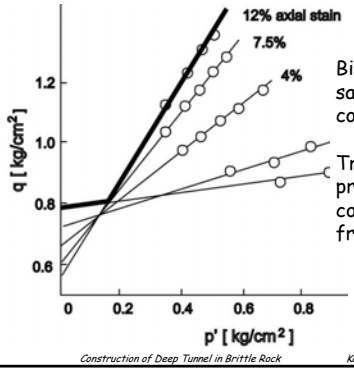

Bilinear envelope for sandy (over-) consolidated" clay

Transition from predominantly cohesive to a frictional yield mode

$$\tau = c(\varepsilon) + \sigma'(\varepsilon)\ \tan(\phi + i)$$

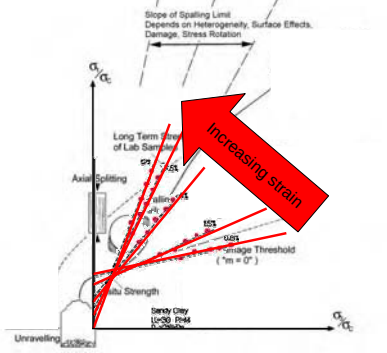

Strength mobilization in brittle rock

(a) Terzaghi

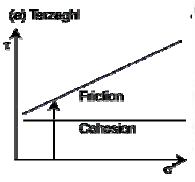

(b) Taylor

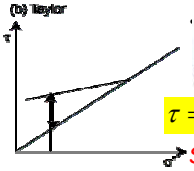

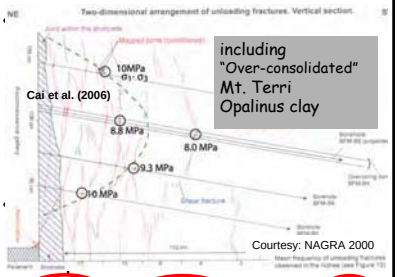

including "Over-consolidated" Mt. Terri Opalinus clay

Courtesy: NAGRA 2000

$$\tau = c(\varepsilon, \sigma_3) + \sigma'(\varepsilon, \sigma_3)\ \tan(\phi + i(\sigma_3))$$

Strain and confinement dependent!

EDZ and fracturing - Ko = 0.5 - ELFEN

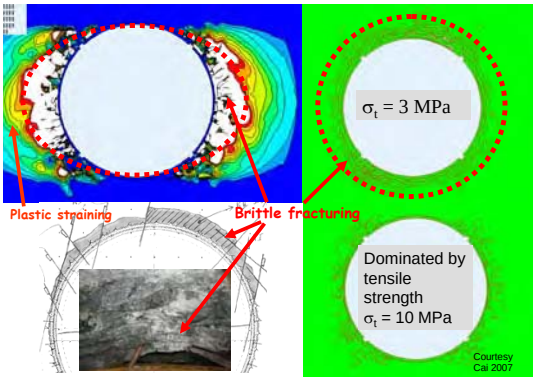

Courtesy Cai 2007

Challenges

1. Anticipating the rock behaviour
   - Failure mode
2. **Anticipating more than the rock strength**
   - Strain and confinement dependence
   - **Volume change (bulking)**
3. Anticipating the construction problems
   - Wall stability
   - Face stability
   - Stand-up time

Progressive failure process produces "blocky", unravelling ground with rock mass bulking

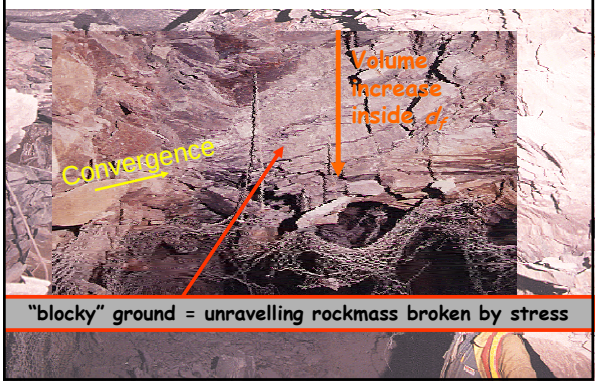

Challenge – anticipate rock mass bulking (geometric volume increase)

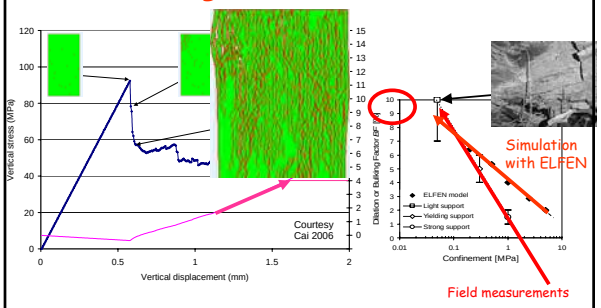

Yield pattern near tunnel

- Circular tunnel at 2000m and K_o=0.5

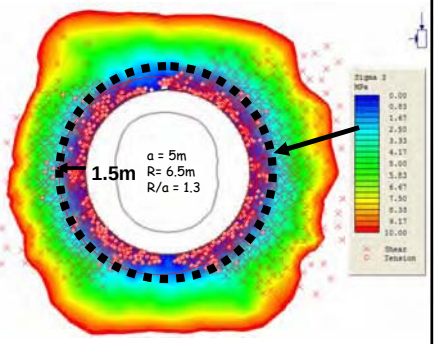

Radial strain (%) control

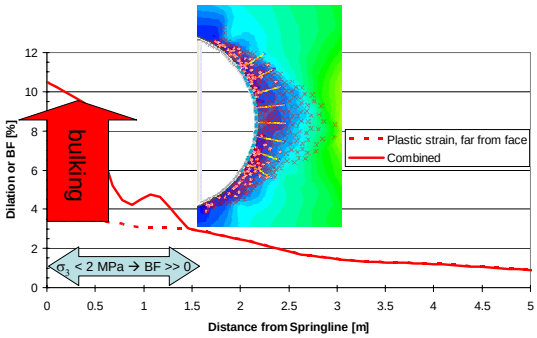

→ with dense bolting and retention (shotcrete)

ELFEN model – influence of rockbolt length

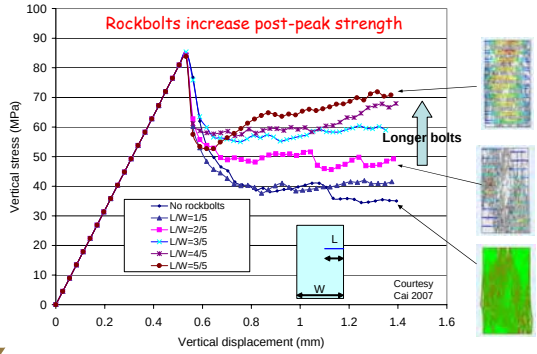

Challenge - anticipate face behaviour

- Observe
- Interpret
- Understand
- **Extrapolate**
  - to depth
  - Effect of weakness zones
  - **Face behaviour**

→ now can also anticipated spalling at tunnel face

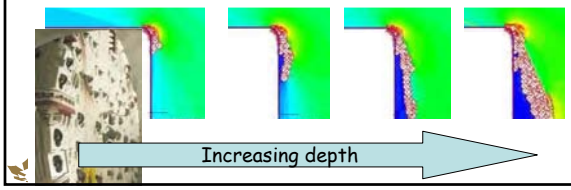

Challenge - anticipate face behaviour

- Observe
- Interpret
- Understand
- **Extrapolate**
  - to depth
  - Effect of weakness zones
  - **Face behaviour**

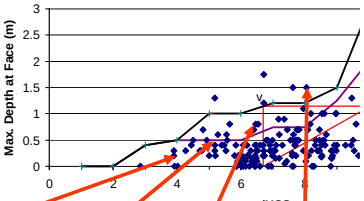

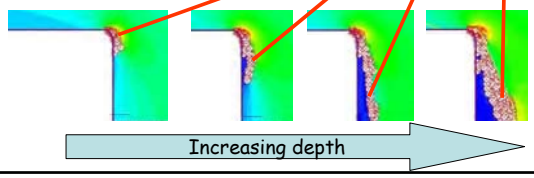

Spalling at tunnel face

- Predictions and observations

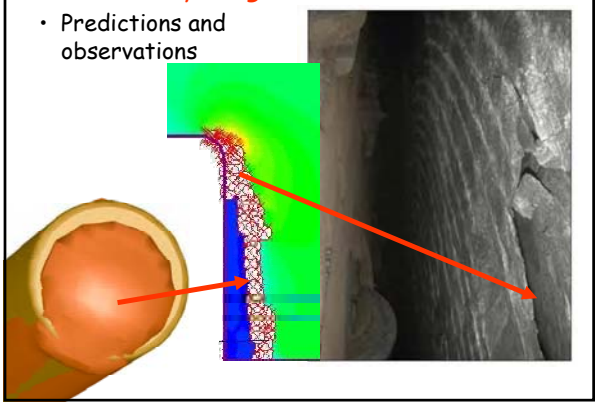

Lessons learned ...

When going from shallow to deep tunnelling ...

→ **observe, interpret, understand, compare to worldwide experiences, extrapolate**

→ **adjust design and construction procedures to match ground behaviour**

- At depth the ground is less forgiving
  - → **stress breaks even good ground**
  - → **good ground becomes poor ground**
  - → **massive, brittle rock disintegrates**
    - → **"cohesionless" ground**

→ **Quantum shift in constructability**

Lessons learned ...

At depth rock becomes brittle fails by spalling

→ **degradation cannot be prevented**

→ **conventional failure criteria mislead designers**

→ **spalling process affects both tunnel walls and face**

→ **select excavation and support techniques appropriate for broken rock**

→ **No ravelling, raining rock and flying arches!**

Similar approach applies to slopes

Rock mass description

→ rating (Q, RMR, or GSI)

→ strength parameters

→ rock mass behaviour

→ modeling

→ decision making

Knowledge gap – strain-dependence

$\tau = c(\varepsilon) + \sigma'(\varepsilon)\ \tan(\phi + i(\sigma_3))$

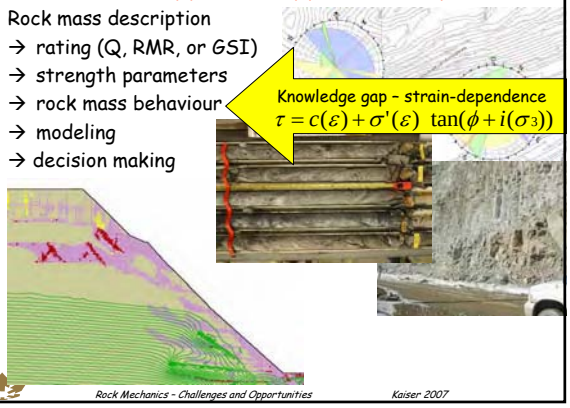

Cohesive and frictional strengths are not simultaneously mobilized

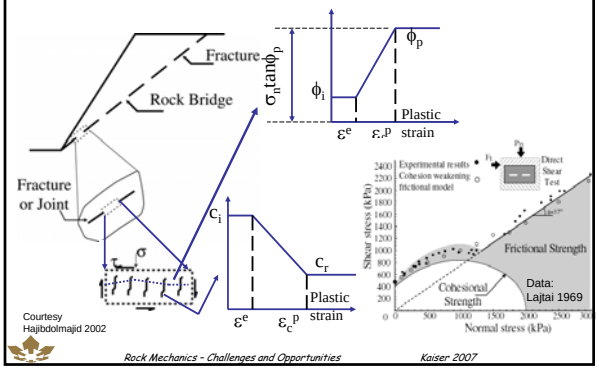

Frank Slide (Alberta, Canada)

Frank Slide Model (FLAC)

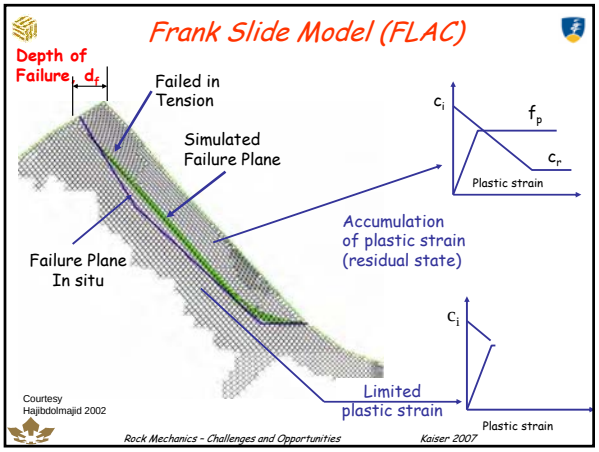

Depth of failure plane vs brittleness I_B

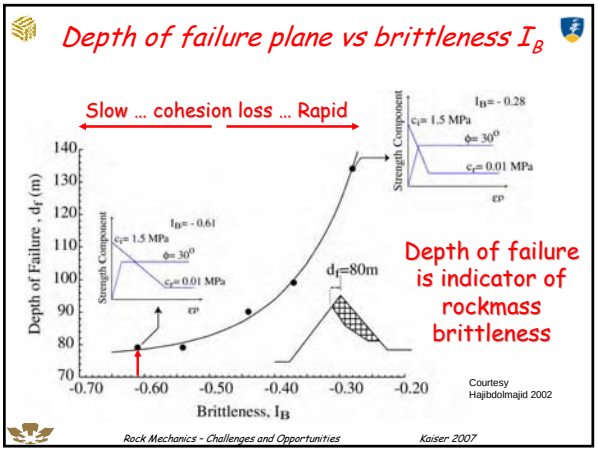

Lessons learned ...

- Rate of strength mobilization

$$\tau = c(\varepsilon, \sigma_3) + \sigma'(\varepsilon)\tan(\phi + i)$$

controls the failure mode
  - depth of failure
  - shape of the failure plane
  - location of internal shears
- Brittleness of rock must be considered for design of high slopes (especially large-scale slope)
  - Monitoring and back-analysis

Hoek et al. 2000

by Davidson and Rees-Mogg (1996)

"Contrary to the general assumption that technology is an offshoot of science, the primacy is really the other way around.
Great advances in science tend to **occur after technological innovation** has given human mind access to a broader range of information."

→ *Directly applicable to mining and tunnelling ...*

→ *Those that make new technologies work for them benefit first!*

→ *Those that communicate and use information properly keep costs down !*

Risk Management

with virtual reality

Spatial & Time Dependencies

Gaining new insight through visualization

Turning data into information

The age of the visual scientist

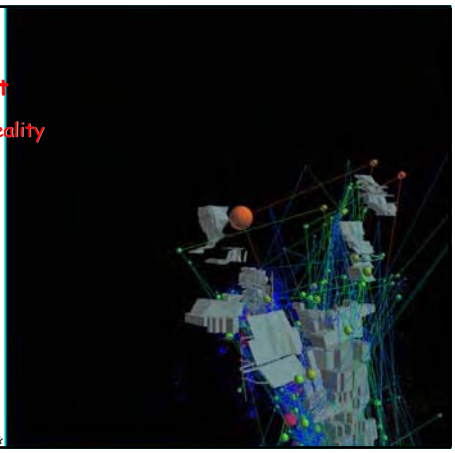

UNIVERSITY of TORONTO LASSONDE INSTITUTE

- **Newest**
  - **Rock F**

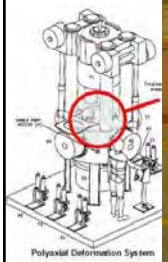

- Polyaxial loading frame with integral geophysical imaging capabilities that are unique in the world
- Innovative geophysical monitoring hardware and software offer new insights into internal deformation mechanisms in rock

*Discovery – **Rock behaviour***

RFDL developed to address critical gaps in science of rock fracture … enable new discoveries about rock behaviour

- Examine the micromechanics of rock **behaviour**
- Formulation of new constitutive models of rock **behaviour**
- Validated numerical codes of rock **behaviour** beyond limitations inherent to conventional data
- Generate large-scale, generalized predictive simulations for
  - earthquake processes
  - coupled process
  - mine and nuclear waste repository design and construction

A Final Word

biggest challenge …

… people, knowledgeable people, people!

ROCK MECHANICS CONSIDERATIONS FOR CONSTRUCTION OF DEEP TUNNELS IN BRITTLE ROCK

Peter K. Kaiser
MIRARCO – Mining Innovation, Laurentian University, Sudbury, Ontario, Canada
(*pkaiser@miningexcellence.ca)*

ABSTRACT: Tunnelling in brittle rock at depth poses unique problems as stress-driven failure processes often dominate the tunnel behaviour. Such failure processes can lead to gradual unravelling or to violent, strainbursting modes of instability that cause difficult conditions for tunnel construction, whether advanced by TBM or by blasting.

The author's experience with brittle failing rock in deep mining, underground construction, and Alpine tunnelling was previously presented in keynote lectures at GeoEng 2000 (Kaiser *et al.* 2000), summarizing a decade of collaborative research work on brittle rock failure, at the Rockburst and Seismicity in Mines Symposium (Kaiser 2005), introducing new means of complex data interpretation in seismically active mines, and at GEAT'06 (Kaiser 2006), focusing on recent experiences from deep Alpine tunnelling. This article briefly summarizes findings from previous studies, presents recent developments and highlights implications that are of practical importance, particularly with respect to design for constructability. Guidelines for support selection in brittle failing ground are given. Brittle failure processes at the tunnel face are briefly analyzed so that related construction issues can be anticipated.

Keywords: brittle failure, constructability, tunnelling, ground control, rock support, rockbursting.

Introduction

The theme of this conference is "rock mechanics in underground construction" which presumably involves rock mass characterization, design and construction; each component posing its own challenges. Contrary to other fields of science, in rock engineering when dealing with a natural material, it is difficult to obtain representative parameters for design, in part because of scale effects and in part because of the heterogeneous, discontinuous nature of rock. The issue of obtaining design parameters for design of structures in or on rock was eloquently discussed by Hoek (1999) in his lecture on "putting numbers to geology".

Difficulties in designing underground excavations are also often experienced because constitutive laws in numerical models do not necessarily reflect the actual behaviour of the rock. This is particularly true when dealing with brittle failure where the fundamental paradigm of the Mohr-Coulomb yield criteria $\tau = c + \sigma_n \tan \phi$, relating the shear strength τ to a cohesion c and a simultaneously acting frictional resistance $\sigma_n \tan \phi$, is not valid (Martin 1997 and Martin *et al.* 1999 , Kaiser et al. 2000). As intact rock is strained, cohesive bonds fail and frictional resistance develops at different rates and, as brittle rock "disintegrates" (Fig. 1.a). Furthermore, damage initiation and propagation occurs at different stress thresholds (Diederichs 2003) and the propagation of tensile fractures depends on the level of confinement (as established by Hoek 1968 and used to explain brittle failure by his collaborators (Kaiser *et al.* 2000)). A bilinear failure criterion is required to capture this dependence on confinement in materials that are prone to spalling (Fig. 1.b). Brittle failure by tensile spalling occurs when the stress path moves above the damage threshold to the left of the spalling limit.

Beyond these thresholds, the volumetric deformation characteristic of brittle failing rock changes drastically as geometric incompatibilities between fractured rock fragments leads

to high dilation (Fig. 2 (photo insert)). Most interestingly, while the depth of failure is essentially independent of the support pressure, the dilation of the broken rock is very sensitive to confinement and thus to the rock support characteristic or support pressure.

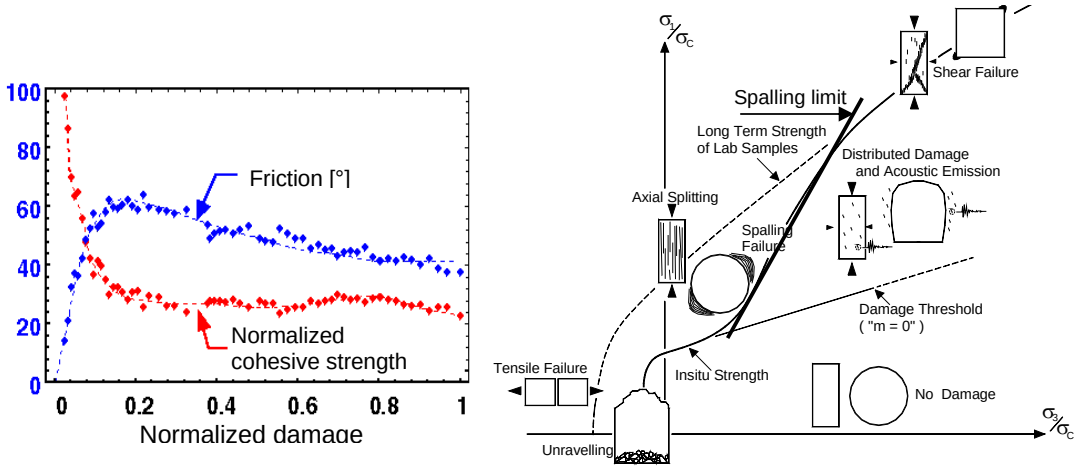

(a) (b)

Fig. 1 (a) Cohesion and frictional strength development as a function of plastic strain or damage (Martin 1997); (b) bilinear failure criteria (Kaiser *et al.* 2000) showing damage initiation threshold and spalling limit.

The development of dilation during the spalling of a triaxially loaded sample confined by 1MPa is shown in Fig. 2.a (Numerical simulation using ELFEN code). After peak, the dilation steadily increases to 4.5% at a total strain of roughly 3-times the elastic strain at peak. This dilation is however highly dependent on the confinement as illustrated by Fig. 2.b. For typical support pressures of <1MPa, the predicted dilation increases rapidly to values in the range of 7 to 10% at <0.1MPa. This is consistent with bulking factors *BF* derived from field measurements (Kaiser et al. 1996) showing >30% for unconfined floors and 1 to 10% depending on support type (Fig. 2.b).

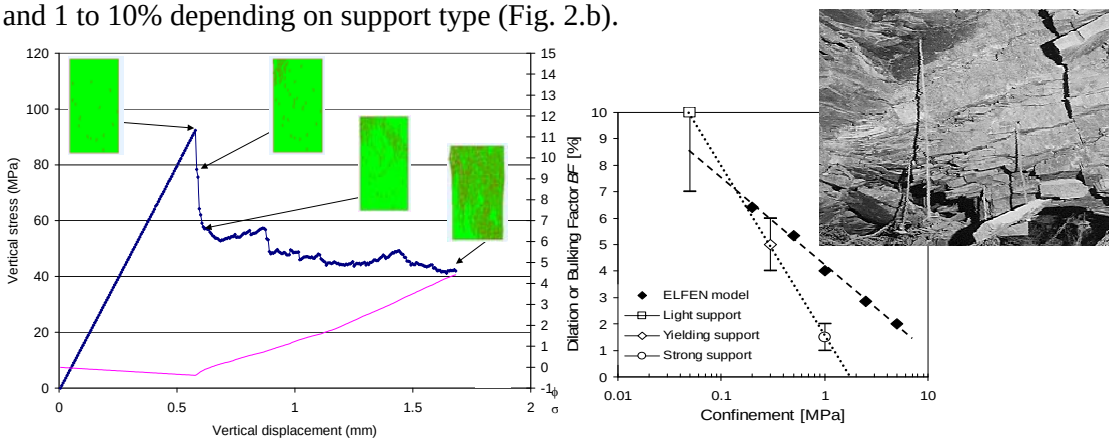

(a) (b)

Fig. 2 Photo insert shows rock fractured by dynamic loading (rockburst) with tensile fracturing and related volume increase (bulking); (a) simulated stress-strain and dilation of brittle failing rock using ELFEN (Cai 2006; unpublished report); (b) dilation as a function of confinement (dashed line: ELFEN model; dotted line: data from Kaiser et al. (1996).

As a consequence, serious deficiencies in predicted rock mass behaviour and resulting support designs must be expected when numerical models with constitutive models developed to simulate soil behaviour are applied to predict the behaviour of brittle rock. Even if underground excavations are designed based on continuum or with more sophisticated discontinuum models (UDEC, 3DEC, PFC, etc.), difficulties are encountered because of

serious limitations in modelling the transition from continuum to discontinuum behaviour. While advanced fracture mechanics codes (such as ELFEN) may eventually help to overcome these limitations, at present, more often then not, excavations and ground control measures are designed based on models with the serious limitations described above. More importantly, the practical implications of the transition from continuum to discontinuum behaviour are often not considered when selecting appropriate ground control methods (TBM shields, rock support, etc.). Such difficulties as drilling and grouting bolts in fractured rock, stabilizing ravelling rock behind a vibrating open TBM, setting ribs or steel sets on resulting irregular surfaces due to overbreak, often dominate constructability particularly from a construction time and equipment abuse perspective.

For good constructability, understanding the "post-peak" behaviour of a rock mass is therefore often of critical importance. If rock tends to unravel, it matters what the block size of the fractured rock mass is, what the available time to install support is, and whether the rock fails in a gradual or violent manner. By observing failure processes, it is possible to make predictions about the anticipated behaviour of tunnels and to anticipate situations that may lead to construction difficulties. Unfortunately, costly mistakes are often made because of a lack of understanding the actual rock mass behaviour under stress and of an over reliance on results of analyses or of experiences with similar excavations in lower stress environments.

In the author's opinion, the behaviour of highly stressed, brittle rock is often not anticipated, and thus not fully integrated into the design. Many lessons have been learned in recent years with respect to the behaviour of deep tunnels in brittle ground and it is the goal of this keynote to provide an improved framework for future tunnelling at depth.

1.1 *Robust engineering*

No matter how good the site investigation program and the engineering design analyses are, when tunnelling at depth in complex geological settings, it will not likely be possible to predict the exact response of the rock: the location, extent and depth of spalling, impact of support on rock mass dilation, etc.. In such situations, it is necessary to adopt a robust engineering approach that focuses on the construction process and ensures that all construction tools work well (Kaiser 2006). The need for robust tunnelling designs is not widely recognized and practiced as Teuscher (2006) reminded the engineers of the Alp-Transit project "… geology comprises all aspects of describing the rockmass, including its geomechanical behaviour" … (stress, strength, etc.) … "these parameters are the factors which determine the contractor's performance …". This comment reflects recent experiences showing that a design is only a good design if it is a robust design that can actually be implemented by the contractor without duress, such that the project can be completed in a timely and cost-effective manner.

Alternatively, the challenge of tunnelling within a framework of uncertainty could be managed by adopting an observational design/build approach (Peck 1969). Unfortunately, contractual arrangements are seldom conducive to adapt techniques in a truly responsive manner and, more often than not, lead to undesired delays and cost overruns.

Furthermore, for a successful observational approach, it is necessary to make the right observations, to properly interpret the findings and translate them into appropriate actions. This keynote presents qualitative observations that contribute to a better understanding of brittle rock mass behaviour which in turn will assist in robust engineering and adaptive tunnel design/construction. A qualitative, observational approach is particularly justified for deep tunnels in brittle rock. As Peck (1969) indicated, a measurement-based, quantitative approach is often not applicable when brittle failure processes predominate.

Robust engineering in brittle failing rock means to design for stress-driven rockmass degradation processes that affect constructability.

1.2 *Support engineering for constructability*

In brittle failing rock where stress-driven failure leads to a zone of fractured rock near an excavation (e.g., Fig. 3), engineering for constructability basically involves three aspects:

- Retention of broken rock near an excavation,
- Control of deformations due to the bulking of fractured rock, and
- Dissipation of energy if failure occurs in a violent manner.

These three aspects of broken rock management are reviewed here and the reader is referred to Kaiser et al. (1996), (2000), (2005) and Kaiser (2005) for details on related subjects.

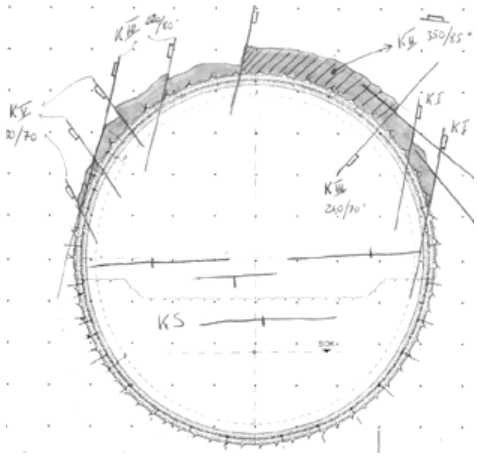

Fig. 3 Shallow stress-induced overbreak in tunnel excavated in moderately jointed rock.

2 Anticipating rock degradation

2.1 *Rock mass degradation and stress-driven rock "fragmentation"*

Rockmass behaviour and failure modes near underground excavations can be grouped according to stresslevel and degree of natural jointing (Hoek *et al.* 1995). In strong, hard rock, structurally controlled failure processes dominate at shallow to intermediate stress, while stress-driven behaviour dominates when the stress level is sufficient to cause failure of intact rock. If the rockmass surrounding the tunnel is heavily fractured, it tends to increase in volume and cause large wall deformations. Thus, deformation control measures are required to manage the ground.

At intermediate stress levels *SL*, typically when σ_{max} > ~0.8 UCS [a] or SL > 0.8, stress-driven rock fracturing processes start to overlap with structurally-controlled processes. From a constructability perspective, however, while stress-driven fracturing may not add much load to the support system, it may have serious impacts on overbreak and thus the development of loose ground. In addition, strain-bursting in massive to moderately jointed ground may lead to elevated risk levels (worker safety concerns).

At high stress levels, typically at *SL* > ~1.15 in strong, hard rock, deep seated stress-driven failure dominates. The rockmass surrounding the tunnel is heavily fractured, tends to increase in volume causing bulking related convergence, and deformation control measures such as rock reinforcements are required.

This keynote relates to conditions encountered at intermediate to high stress levels in massive to moderately jointed ground (for ground starting with *GSI* > 65; Fig. 4.a).

Stress-driven rock "fragmentation" is a tensile fracturing process (Kaiser *et al.* 2000, Diederichs 2003) in low confinement zones that creates broken rock of varying fragment size and shape distribution. For example, as illustrated by Fig. 4.b, a massive granitic rocks spalled to platy shapes with typical aspect ratios of 2:100:100mm to as high as 50:1000:1000 at the URL and to similar block sizes and shapes with aspect ratios as high

[a] $\sigma_{max} = 3\sigma_1 - \sigma_3$ is the maximum tangential stress at the wall of a circular opening in elastic ground, and UCS = σ_c is the laboratory uniaxial compressive strength of the intact rock. The stress level *SL* is defined as σ_{max} /UCS.

as 300:1500:>2000 at the Bedretto tunnel (not shown) after long-term wall degradation. When rockbursts are involved, the block sizes typically vary from dm^3 to $<m^3$ size with aspect ratios from cubic to platy. This degradation is plotted on the *GSI* chart (Cai et al. 2006; Fig. 4.a), showing that degradation transforms a rock mass of *GSI* >65 to a damaged, fractured rock mass of 55< *GSI* <35 and, most importantly, from a continuum or tight discontinuum, often with non-persistent joints, to a "loose" discontinuum with often continuous and open fractures as illustrated by the photos in Fig. 4.b to e.

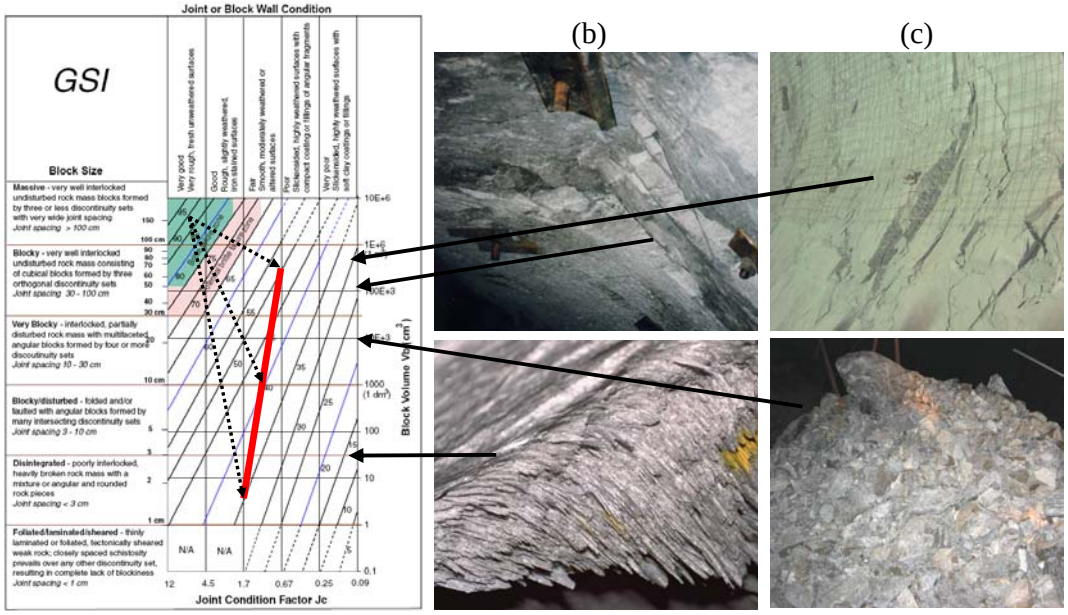

Fig. 4 (a) GSI-chart showing degradation paths for ultimate block sizes of 1.5, 10 and 70cm edge lengths; (b) spalling in back of Piora tunnel, Switzerland (image ~2m wide); (c) Lötschberg tunnel wall (slab ~ 30cm thick); (d) Spalling in notch at URL, AECL, Canada (image ~1m wide); (e) fragmented fall of ground due to rockburst (image ~2.5m wide)

2.2 *Ravelling of stress-fractured rock*

When rock is excavated, the stress path, though in a contorted manner (Diederichs *et al.* 2004), eventually ends in a nearly unconfined state (in the spalling zone of Fig. 1.b for brittle rocks). According to Bieniawski's standup-time chart (Fig. 5), for a 5 to 10m wide unsupported tunnel, nearly permanent stability with stand-up times of several months to a year can be achieved when *RMR* = 65±5 or *GSI* = 60±5 and acceptable short-term stand-up times for constructability of say 6-24 hours can be achieved when *RMR* = 40±5 or *GSI* = 35±5.

Thus, stress-driven fracturing and rock mass degradation can bring a stable, self-supporting rock mass to the brink of ravelling (compare Fig. 4.a and Fig. 5.b). According to Fig. 5.b, reasonable stand-up times and thus sufficient time to install support should be achievable if the joint spacing is >3cm with fair to good and >50cm for poor to fair joint condition. In other words, any process that degrades the rock mass to worse conditions will tend to lead to constructability problems as the fractured rock mass near the excavation will not be self-stabilizing (e.g., Fig. 3).

The limits given in Fig. 5.b, actually seem rather optimistic, as a 10m wide excavation in jointed rock with a joint spacing of 3 to 10cm would likely tend to ravel immediately after blasting or when emerging from the shield of an open TBM. Nevertheless, these charts

give an indication of how much rock mass degradation, due to stress, can be tolerated before serious construction problems must be anticipated.

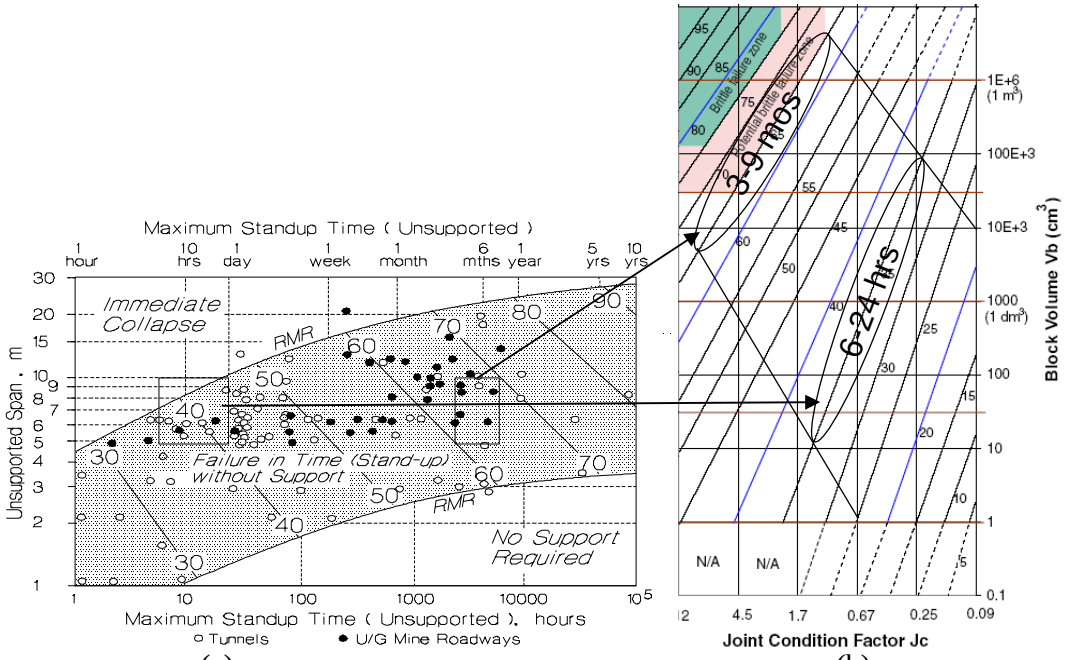

Fig. 5 (a) Stand-up time graph after Bieniawski (1989) from Hutchinson and Diederichs (1996) showing short- and long-term stability ranges for 5 to 10m wide excavations; (b) GSI chart with corresponding characteristics for 6-24 hours and 3-9 months stand-up time.

Other factors often dominate stability in the zone between long- and short-term stability (65<GSI<35). Of particular importance is the degree of stress relaxation (Diederichs and Kaiser 1999)) and the level of post-peak straining (Martin (1997) and Cai *et al.* 2006).

2.3 *Depth of failure*

One unique, from a constructability perspective very important, observation is that while stresses induce instability of the excavation wall and related ravelling of the fractured rock, this failure processes is mostly self-stabilizing (Fig. 3). Even if the excavation is unsupported, this process does not propagate beyond a finite depth of failure d_f unless the damage-causing stress changes (e.g., due to mining-induced stress changes). For this reason, it is possible to determine the depth of spalling type failure, normalized to the tunnel radius a, by the now well established semi-empirical relationship:

$$\frac{d_f}{a} = C_1 \frac{\sigma_{\max}}{\sigma_c} - C_2 = C_1 SL - C_2 \qquad (1)$$

Based on an extensive database of tunnels in varying geological settings, Martin *et al.* (1999)established the two constants as C_1 = 1.25 and C_2 = -0.51±0.1. Kaiser et al. (1996) showed that the constant C_1 depends on the level of dynamic stress increment due to a remote seismic event and found, supported by numerical modeling, that C_1 can be related to the induced ground motion (peak particle velocity *ppv*). Values for C_1 are listed in Fig. 6 for C_2 = 0.57. Other factors such as the frequency content of the seismic wave must be taken into account (for details refer to Kaiser et al. 1996). The anticipated ground motion depends on the event magnitude *(M)* and the distance *(R)* from the event as well as other parameters (see caption) as illustrated by Fig. 6.a.

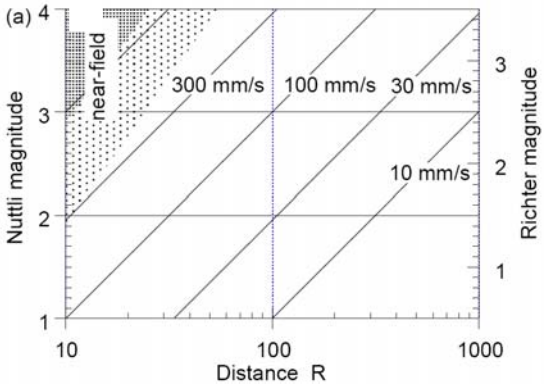

(a)

ppv [m/s]	C_1	Mean SL_o for $d_f = 0$
static	1.37	0.42
0.5	1.54 - 1.74	0.35
1	1.79 - 2.08	0.29
2	2.17 - 2.86	0.23
3	2.63 - 3.64	0.18

(b)

Fig. 6 Anticipated peak particle velocities for 50% confidence (average scaling law parameters: a^* = 0.5 and C^* = 0.1m^2/s; Kaiser *et al.* 1996); (b) C_1 for dynamic depth of failure determination and mean stress level SL_0 for d_f =0.

Accordingly, for example for a stress level of SL = 0.65, the normalized depth of failure d_f/a under static conditions of about 0.32, or d_f = 0.8m for a 5m wide tunnel, would increase to about 0.43 - 0.56 or 1.1 - 1.4m when affected by a seismic event causing a *ppv* of 0.5m/s.

2.3.1. *Variability of depth of failure*

When examining brittle failures underground, it is immediately evident that spalling is often localized and that the lateral extent and depth of failure varies greatly as illustrated by the data in Fig. 7.a. This is not surprising because even if the two constants C_1 and C_2 were truly constant, i.e., independent of the rocks proneness to spalling (Diederichs 2004), the *UCS* and the in-situ stress, and thus σ_{max}, are variable. After reprocessing the data by assuming a variable stress field (following the K_0-profile of Fig. 7.c based on the assumption that the horizontal stress decreases linearly from 22MPa at the portal to 32MPa at Chainage 2900 (interface between Leventina and Lucomagno Gneiss), much of the clustering is removed (Fig. 7.b) but d_f/a is still highly variable. Unfortunately, no reliable measurements are available to confirm the assumed stress profile. However, when back-calculating C_2 (assuming C_1 = 1.25), a consistent pattern emerges (Fig. 7.c). The mean value of C_2 is more or less constant over the full length of the tunnel at 0.52 (CoV = 17%).

Lab values of *UCS* typically show coefficients of variation *CoV* on the order of 25%. The in-situ stress may be highly variable in heterogeneous rock formations (e.g., near dykes) or relatively uniform in massive homogeneous rock formations. The anticipated effect of variability for a 15% for *UCS*, 10% for each of σ_1 and σ_3, and 17% for C_2, on the normalized depth of failure is shown in Fig. 7.d (Rosenbleuth (1981) assuming normal distributed parameters). Even though the mean normalized depth of failure is close to zero for the assumed parameters, it can be seen that a maximum of 0.45 (d_f = 1.15m) may be reached, and, most importantly from a constructability perspective, from the cumulative probability curve, that about 60% of the tunnel might not show any signs of failure (d_f = 0). In other word, about 40% of the tunnel should be expected to show stress-driven stability problems. When compared with the data of the Lötschberg tunnel (Fig. 7.d), it can be seen that the observed variability corresponds well. Both tunnels were excavated with an open TBM and are in comparable rock formations.

Eqn (1) predicts the mean depth of failure reasonably well if the relevant input parameters are well defined. When combined with standard statistical means and estimated *CoV*s, the anticipated frequency of occurrence as well as the range of depth of failure can be obtained to guide the excavation method and support selection.

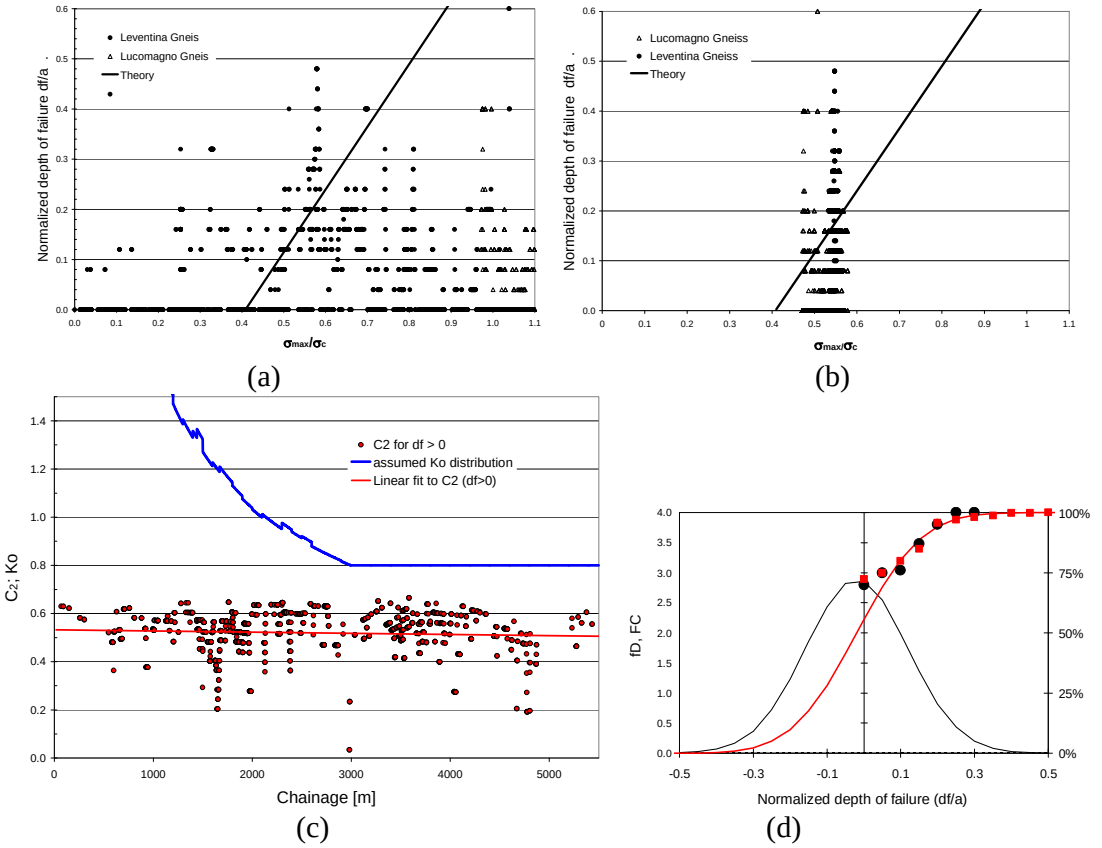

Fig. 7 (a) Normalized depth of failure records from Piora tunnel, Switzerland, assuming constant *UCS*, K_0 and overburden stress; (b) same assuming constant *UCS*, K_0-profile of shown in (c) and overburden stress; constant C_2 back-calculated assuming C_1 = 1.25 for measured d_f locations; (d) corresponding cumulative distribution curve with coefficients of variation = 17,15, 10% for C_2, *UCS*, and stress, respectively, compared with data from Piora tunnel (squares) and from Lötschberg tunnel (circles).

2.4 *Anticipated demands on support due to brittle rock failure*

For support selection to control stress-driven failure under *static loading*, three aspects can now be evaluated:

- the depth of potential unravelling can be constrained (e.g., d_f/a = 0 to 0.45 or d_f = 0 to 1.1m over 40% of the tunnel) and means to manage this ravelling potential can be chosen.
- the anticipated load demand can be estimated (e.g., at d_f * γ = 0 to 0.03MPa for the Piora tunnel) and the static factor of FS_L = load capacity/demand can be established (e.g., very light bolting would provide an adequate FS_L for this case).
- the anticipated deformation demand can be estimated (e.g., at d_f * *BF* (see above; *BF* = 1 to 10% with *CoV* of ~25% depending on support type). For example, for the Piora tunnel wall displacements of 11±6 mm, if well reinforced, to 110±60mm, if allowed to loosen with very light support, would be anticipated. Since the bulking is very sensitive to the applied support pressure, the anticipated deformations can be easily managed if a tight retaining system, e.g., shotcrete can be applied early.

The required bolt length is equal to the maximum d_f plus a safe anchor length. For split set bolts, the pick-up length (d_f) must be deducted from the bolts length to assess the hold-

ing capacity of the remaining anchor length. Other failure modes such as structurally controlled failures, of course, need to be assessed separately.

For support selection to control stress-driven failure under *dynamic loading*, the dynamic deepening of the failure zone as well as the shakedown and energy release (strainburst) potential must be considered.

- The dynamic deepening and thus the resulting potential depth of ravelling can be estimated for a design event magnitude as a function of the distance R to a potential event (e.g., Fig. 6.a for the assumed scaling law; $log(R\ ppv) = ML + (1.5 \pm 0.15) + 2\ logC^*$ with M_L = local Richter magnitude and constant C^* depending on static stress drop and desired confidence (Kaiser et al. 1996)). For the example presented above with a *ppv* of 0.5m/s, the mean static d_f/a = 0.32 would be expected to deepen to a mean dynamic d_f/a = ~0.5, with a maximum around 1.2 (Fig. 8.a). Thus, dynamic fracturing could locally deepen to as much as 3m with a corresponding static load increase to 0.08MPa and a wall deformation of between 30 and 300mm due to bulking depending on the effectiveness of the support. As shown by the cumulative distribution (Fig. 8.a), the potential for no failure at that location would be near zero.

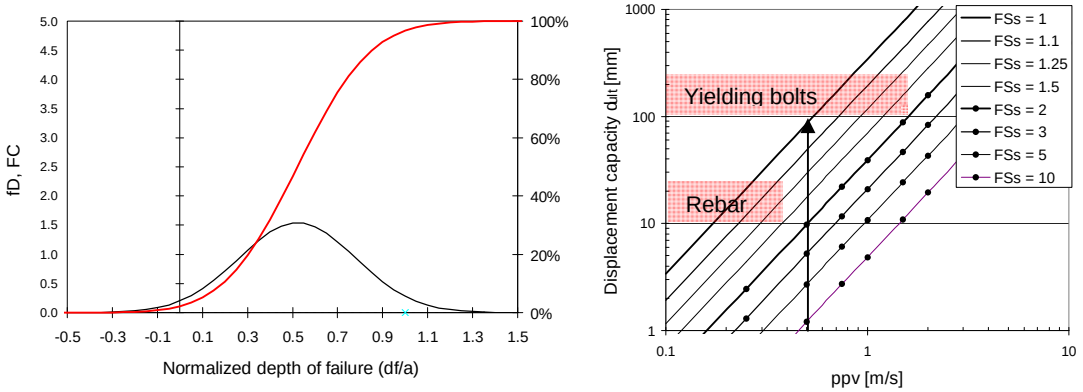

(a) (b)

Fig. 8 (a) Dynamic depth of failure distribution for *ppv* = 0.5m/s and conditions of Fig. 7; (b) ultimate support displacement capacity requirements as a function of static factor of safety FS_s (before shaking).

In addition to the dynamic deepening of d_f, the ground motion can lead to a shakedown failure of the broken rock. According to Kaiser et al. (1996), the survival limit of a support system depends on its static factor of safety FS_s (before shaking), the ground motion *ppv* and the ultimate displacement capacity d_{ult} of the support:

$$FS_s = 0.87\left[\left(\frac{ppv^2}{2gd_{ult}}\right)+1\right] \quad \text{or} \quad d_{ult} = \frac{ppv^2}{2g\left(\frac{FS_s}{0.87}-1\right)} \qquad (2)$$

The static factor of safety is the *FS* after dynamic deepening of the depth of failure zone. For *ppv* = 0.5m/s, standard grouted bolts (rebar) would survive if this factor of safety was higher than 1.25 (Fig. 8.b) or yielding bolts with a displacement capacity of d_{ult} >80mm would be required to (just) survive the event.

- The deepening process of the failure zone may occur incrementally by spalling of thin slabs (Fig. 4.c) or in a violent manner due to the sudden release of energy stored in the larger slabs. When energy is released the spalling process is called strainbursting. As Salamon (1984) showed, the release is largest when rock is "excavated" in a single step and zero when excavated in infinitesimally small steps. Thus, the worst case exists when the entire depth of failure zone is created in a single event. However, the energy

released and therefore the load on the rock support depends on the amount of energy dissipated by friction in the fragmented rock. Hence, it is difficult if not impossible to undertake accurate energy release calculations. Aglawe (1999), in an attempt to estimate the releasable energy, found that for a 4m wide circular tunnel in 200MPa rock, the maximum releasable energy was 0.05MJ/m2 at d_f/a =0.5. Considering that burst-resistant supports can at best dissipate 0.05MJ/m2, it follows that violent failure of slabs exceeding d_f/a = 0.5 would destroy the best possible burst-resistant support system. Furthermore, since the energy dissipation capacity of standard, non-yielding supports is ≤0.01MJ/m2, it follows that the support limit of a previously unloaded support ($FS_s=\infty$) is reached when a strainburst involves a normalized depth of failure in the following range: $<<0.1 < d_f/a <<0.5$, or $<0.25 < d_f <<1.25$m for a = 2.5m.
In other words, when strainbursting is anticipated or encountered, constructive means should be used to induce incremental spalling.

3 Face stability

The stress fracturing and bulking process illustrated by many examples above (Fig. 4) is visible only because the rock near the damage location collapsed and provided insight into the disintegrated rockmass. At the tunnel face, broken rock is either excavated with each round during drill and blast operations or is hidden in front of the face (ahead of a TBM).

Because of the constrained convergence pattern near the face, causing stress concentrations at the edge of the face and thus face parallel loading, the same processes as observed in the tunnel wall can happen at the tunnel face. The anticipated rockmass behaviour of a highly strained tunnel face was interpreted by Kaiser (2006). As illustrated by Fig. 9, two important processes lead to face instability: (i) surface parallel spalling (black zones in Fig. 9.b), and (ii) structurally controlled instability mechanisms (gray zones in Fig. 9.b) in response to the opening of joints due to the inward bulging of the face. These processes differentially strain the rock in the face and lead to a degradation that produces "blocky ground". Due to this stress-induced fracturing, the block size is generally of predominantly platy shape (Fig. 9.d).

There is now ample field evidence in support of the face disintegration process described above and this can be supported by numerical models using the brittle failure criterion introduced earlier (Kaiser 2006). Stress-driven spalling processes with or without inherent weaknesses (foliations or jointing) can lead to unstable "blocky" tunnel faces. While pre-existing joint sets may enhance the process of face degradation, the creation of a further "joint set" or fracture set that is sub-parallel to the face is the primary cause for the widely observed face instability problems evident at depth and in large tunnels. Kaiser (2006) also showed that the observed depth of face failure d_{ff} increases rapidly once an initiation threshold at overburden depth z/UCS ~ 4 is exceeded (z in m; UCS in MPa). At a stress level of z/UCS = 5 to 7, d_{ff}/a typically reaches 0.1 to 0.2. Most importantly, it was shown (Kaiser 2006) that face instability may occur at lower stress levels than when wall instability is first encountered; i.e., in brittle failing rock, face instability may occur at lower overburden stresses than wall instability.

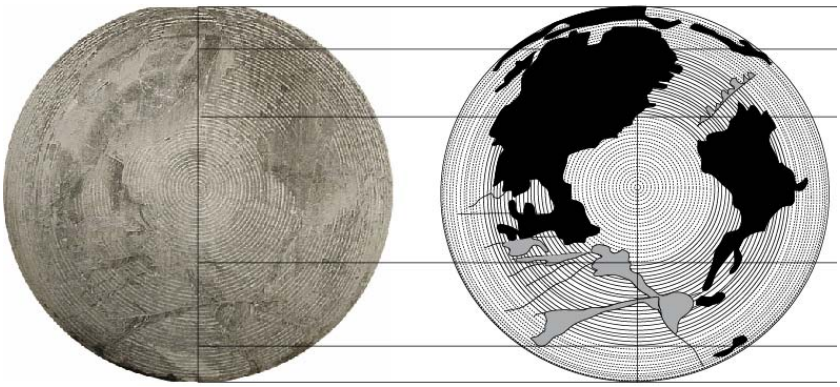

(a) (b)

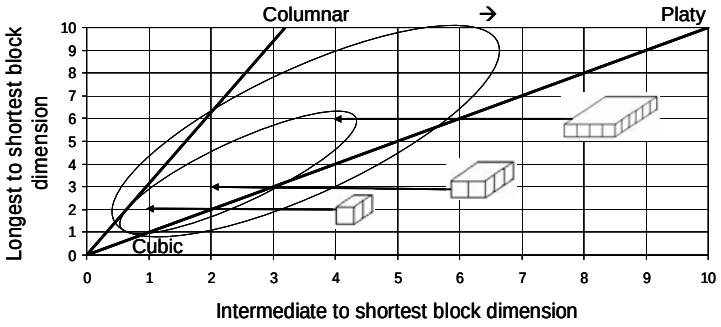

(c) (d)

Fig. 9 (a) and (b) Spalling of tunnel face in massive to moderately jointed rock (Weh and Bertholet 2006); (c) "blocky rock" rather than typical chips on conveyer; (d) observed, predominantly platy block shapes (shaded zones contain 65 and 99% of data).

From a constructability perspective, this finding is of great practical importance. It clearly demonstrates that the tunnel face can be more prone to stress-induced failure than the tunnel wall. Thus TBMs will have to act as rock breakers rather than disc cutters, leading to additional wear a of disks and cutter head as well as additional forces on the TBM, and may cause unexpected material handling problems.

This finding is also not in accord with some of the implicit principles behind current tunnelling standards or contractual arrangements (support and excavation classes). Contrary to the commonly encountered situation where wall instabilities slows tunnelling progress, in this situation, face instability may slow progress even though the walls are stable and may need little structural support.

Acknowledgments

Some of the studies presented in this article were partially funded by the Natural Sciences and Engineering Research Council of Canada and contributions of former graduate students* and long-term research collaborators* listed below are thankfully acknowledged.

References

*Aglawe, J.P. (1999). Unstable and Violent Failure around Underground Openings in Highly Stressed Ground. PhD. Thesis, Queen's University, 285p.

Bieniawski, Z.T. (1989). Engineering Rock Mass Classification, Wiley, New York.

*Cai, M., Kaiser, P.K., Tasaka, Y., and Minami, M. (2006). Determination of residual strength parameters of jointed rock masses using GSI system. *Int. J. of Rock Mech.*, 43(in press).

*Diederichs, M.S., Kaiser, P.K. and Eberhard, K.E. (2004). Damage initiation and propagation in hard rock and influence of tunnelling induced stress rotation. *Int. J. Rock Mech. Min. Sci.*, 41: 785-812

Diederichs, M.S., Villeneuve M. and Kaiser, P.K. (2004). Stress rotation and tunnel performance in brittle rock. Symp. Tunnelling Assoc. of Canada, Edmonton, 8p.

Diederichs, M.S. (2003). Rock fracture and collapse under low confinement conditions. *Rock Mech. & Rock Engr.*, 36(5):339-381.

Diederichs, M.S. and Kaiser, P.K. (1999). Tensile strength and abutment relaxation as failure control mechanisms in underground excavations; Stability of large excavations in laminated hard rock: the Voussoir analogue revisited. *Int. J. Rock Mech. Min. Sci.*, 36(1):69-96; 97-117.

*Hoek, E. (1999). Putting numbers to geology – an engineer's viewpoint. The Second Glossop Lecture, *Q. J. Engrg. Geol.*, 32: 1-19.

Hoek, E. (1968). Brittle Failure of Rock. In *Rock Mechanics and Engineering Practice*, John Wiley & Sons Ltd. London, 99-124.

*Hutchinson, D.J. and Diederichs, M.S. (1996). Cable bolting in Underground Hard Rock Mines, Bitech Publishers Ltd., Richmond, BC, Canada, 406 p.

Kaiser, P.K. (2005). Tunnel stability in highly stressed, brittle ground - Rock mechanics considerations for Alpine tunnelling. *Geologie und Geotechnik der Basistunnels*, Keynote lecture at GEAT'05 Symposium, Zürich, Switzerland, 183-201 (2006).

Kaiser, P.K., *Vasak, P. *Suorineni, F.T. and Thibodeau, D. (2005). New dimensions in seismic data interpretation with 3-D virtual reality visualization in burst-prone ground. RaSiM6, Perth, Australia, 33-47.

Kaiser, P.K., Diederichs, M.S., Martin, C.D., Sharp, J. and Steiner, W. (2000). Underground works in hard rock tunnelling and mining. GeoEng2000, Technomic Publ. Co., 841-926.

Kaiser, P.K., *McCreath, D.R. and *Tannant, D.D. (1996). Canadian Rockburst Support Handbook, Mining Re-search Directorate, Sudbury, Canada, 314 p.; also Drift support in burst-prone ground. *CIM Bulletin*, 89(998): 131-138.

Hoek, E., Kaiser, P.K. and *Bawden, W.F. (1995). Rock Support for Underground Excavations in Hard Rock. A.A. Balkema, Rotterdam, 215 p.

*Martin, C.D., Kaiser, P.K. and McCreath, D.R. (1999). Hoek-Brown parameters for predicting the depth of brittle failure around tunnels. *Canadian Geotechnical Journal*, 36(1):136-151.

Martin, D. (1997). The effect of cohesionloss and stress path on brittle rock strength. *Can. Geotech. J.*, 34:698-725.

Peck, R.B. (1969). Advantages and limitations of the observational method in applied soil mechanics. *Geotechnique*, 19(2):171–187.

Rosenbleuth, E. (1981). Two-point estimates in probabilities. *J. Appl. Math. Model.*, 5:329-335.

Salamon, M.D.G. (1984). Energy considerations in Rock Mechanics: Fundamental results. *J. South Afr. Inst. Min. Mettall.*, 84:233-246.

Teuscher, P. (2005). Presentation at *GEAT'05 Symposium*, Zürich, Switzerland (see Kaiser 2005).

Weh, M. and Bertholet, F. (2005). TBM-Vortrieb und spannungsinduzierte Abschalungen im Vortrieb Raron/Steg. Presentation at *GEAT'05 Symposium*, Zürich, Switzerland, 9p.

Keynote lecture presented at GEAT'05, Zurich, Switzerland

Tunnel stability in highly stressed, brittle ground – rock mechanics considerations for Alpine tunnelling

P.K. Kaiser

MIRARCO-Mining Innovation, School of Engineering, Laurentian University, Ontario, Canada
pkaiser@mirarco.org

ABSTRACT: Tunnelling in brittle rock at depth poses unique problems as stress-driven failure processes often dominate the tunnel behaviour. Experiences from tunnels at shallow to intermediate depth (to about 1500 m) are rarely adequate to foresee the response of a rockmass to drill-and-blast or mechanical excavation. Even if the geological conditions are properly and accurately described is it possible that the rockmass behaviour of a given rock type significantly differs at depth from that observed in shallower tunnels.
Observations of tunnel instability mechanisms are interpreted from a rock mechanics perspective based on deep mining and tunnelling experiences and by use of advanced numerical modelling techniques. In particular, observations of the tunnel face behaviour are carefully analysed to explain face instability processes encountered in large, deep tunnels. The influence of rock anisotropy (geological structures; schistosity; foliations or jointing) is briefly addressed. The observed differences in tunnel face and wall (or roof) stability patterns as well are examined.
Implications of lessons learned from these rock mechanics considerations are discussed with respect to design and constructability. Finally, apparent inconsistencies in tunnel behaviour, practical limitations of prediction methods, and deficiencies in current tunnelling standards are reviewed to provide guidance for future projects.

ZUSAMMENFASSUNG: Tunnelbau im spröden Gebirge und in grosser Tiefe stellt oft unerwartete Anforderungen dar, da Erfahrungen von ähnlichen Projekten mit geringer Überlagerung kaum genügen, um das Gebirgsverhalten richtig zu erkennen. Auch wenn die geologischen Verhältnisse richtig erkannt und beschrieben sind, ist es möglich, dass sich das Verhalten des Gebirges in der Tiefe grundsätzlich ändert, vor allem dann, wenn Sprödbruchvorgänge das Gestein verschlechtern.
Beobachtungen von angetroffenen Instabilitäten werden interpretiert und, an hand von neusten Erkenntnissen bezüglich Sprödbruchverhalten und entsprechenden numerischen Berechnungsmethoden beurteilt. Insbesondere werden Instabilitäten der Ortsbrust und der Einfluss von Anisotropien und Heterogenitäten diskutiert.
Die praktischen Bedeutungen der geotechnischen Ausführungen werden mit Bezug auf Sicherungsmethoden und Bauausführung präsentiert und Schwächestellen in Vorhersagemethoden sowie in Normen werden angezeigt.

1 INTRODUCTION

The main theme of this conference is focussed on „Geological Risks and Counter Measures“ and thus also on „Predictions and Reality“. As in most fields of science or engineering, it is difficult if not impossible to predict reality if we do not fully understand reality. Hence, if we want to make reliable predictions, it is important to understand the actual processes that control the real behaviour. This keynote is about understanding tunnel behaviour in highly stressed, brittle failing ground; i.e. understanding when tunnels become unstable rather than when tunnels are stable. By observing failure processes, it is possible to better understand reality, and thus to make predictions about the behaviour of tunnels in comparable situations. Unfortunately, when we step outside the world of common experience, we often overstep the boundary of current knowledge or understanding, and costly mistakes can be made because of a lack of understanding the actual behaviour of rock or because the rock behaviour may change (at depth) and behave in an unexpected manner.

1.1 Predicting rockmass behaviour

While many contributions to this conference focus on geological predictions and geological reality (the second theme of this conference), this contribution focuses on understanding the behaviour and then on predicting the response of the rockmass to tunnelling. When stepping out into an unknown world, in this case large Alpine tunnels at great depth, it is important to predict the behaviour of each geological entity (rock type and domain). Only if the behaviour is well understood in advance, is it possible to arrive at cost-effective engineering solutions with appropriate excavation and support methods. Otherwise, well established, „proven“ tunnelling technologies may fail to perform well as they do not fit the ground or have not been adapted to fit the actual rock behaviour.

As Hoek explained in his Glossop lecture (Hoek 1999), for this purpose, it is necessary to put numbers to the geology. While …“many geologists are uncomfortable with this requirement to assign numbers to geology … engineering design requires numbers … without these numbers the process of engineering design is not possible.” However, if we need to put numbers to geology, we have to understand the rock behaviour and its response to tunnelling so that we can define the numbers that are of importance. Throughout this lecture, examples are used to illustrate how massive to moderately jointed rock behaves when highly stressed, because stress-driven failure processes such as fracture propagation and rockmass damage affect and often dominate the in-situ behaviour and thus the respective engineering parameters.

As a consequence of the stress-related behavioural changes of the rockmass, established standards may no longer be fully applicable and the basis for contractual arrangements may change even if the geology, the rock type, is as predicted.

1.2 Matching design and rockmass behaviour

If it is not possible to predict the real rock behaviour, or if the rock behaviour was not predicted, risk must be managed in a „non-standard“ framework and by planning for uncertainty, e.g. by introducing several „lines of defence“ or by introducing a high level of flexibility in the construction process. In such cases, it is also important to operate in a flexible, risk-sharing framework as unexpected conditions can only be managed once they are actually encountered and understood.

Many speakers addressed and highlighted this eloquently in their contributions to this symposium. For example, to mention only a few, Lombardi concluded his presentation with several recommendations:

- Attempt to make the best possible prediction
- Be aware of variability in parameters
- Expect the unexpected and be prepared to deal with it
- Recognize the actual conditions early and throughout the project execution
- Respect the unexpected by ensuring sufficient flexibility in design and construction techniques.

Hufschmied … indicated that "risk assessment starts with risk identification (Gefährdungsbilder)", i.e. early rock behaviour identification. The same sentiment was expressed by Ehrbar confirming that "risk management starts with risk identification".

It is the author's opinion that the behaviour of highly stressed, brittle rock is often not well understood and anticipated, and thus not fully integrated into the design. Many lessons have been learned in recent years with respect to the behaviour of deep tunnels in brittle ground and it is time to take account so that future projects can benefit from the accumulated know-how. It is the goal of this keynote to analyse experiences with brittle rock failure in an effort to provide an improved framework for future tunnelling at depth.

1.3 „Robust engineering" versus „observational approach"

When stepping outside the world of experience, it may not be possible to anticipate the real behaviour and one has to be prepared for the „unexpected". In such situations it is either necessary to adopt robust engineering approaches and construction processes that work well „no matter what" or to „learn as we go" and adapt. The need for robust tunnelling designs is not widely recognized but Teuscher's comment … "geology comprises all aspects of describing the rockmass, including its geomechanical behaviour" … (stress, strength, etc.) … "these parameters are the factors which determine the contractor's performance …" clearly supports the need for robust designs.

For a robust engineering approach, all possible scenarios have to be anticipated and considered from a design and construction perspective such that the project can be completed in a timely and cost-effective manner with the assigned excavation and support tools (classes). Since this often leads to more costly solutions (e.g. use of shielded rather than open TBMs), there is a tendency to make compromises with respect to constructability (e.g. tunnel excavation size, support type and quantities, etc.).

Alternatively, the challenge of tunnelling within a framework of uncertainty can be managed by adopting an observational design/build approach (Peck 1969). In this case, new information gained from observations during project execution is integrated as a project proceeds. As a consequence, construction methods and techniques must be selected based on an incomplete picture and then adapted as new knowledge and information becomes available. The need for and benefits of an observational approach are described by Amberg (this conference), indicating that, when complex geological and difficult ground conditions are encountered, it is essential to design based on field measurements rather than on analytical or numerical predictive calculations alone. Unfortunately, contractual arrangements are seldom conducive to adapt techniques in a truly responsive manner leading to undesired delays and cost overruns.

What is often forgotten, is that there are two kinds of observations, qualitative/visual (rockmass behaviour) and quantitative/measured (displacements, stresses, etc.) observations. For a successful observational approach, it is necessary to make the right observations, to properly interpret the findings and to translate them into appropriate actions. This keynote focuses on qualitative observations that contribute to a better

understanding of rockmass behaviour which in turn will assist in supporting both robust engineering and adaptive tunnel design/construction. A qualitative approach is particularly justified for deep tunnels in brittle rock. As Peck (1969) already indicated, a measurement-based, quantitative approach is often not applicable when brittle failure processes predominate.

The observational approach brings benefits to a project when observations, whether qualitative or quantitative in nature, are translated in a timely fashion into action through effective construction practices within a flexible contractual framework that allows to respond to observations. Hence, it is necessary to „read the rock", understand the behaviour, and anticipate „the unexpected", then predict the changes in behaviour (putting numbers to geology), and adapt old tools to manage the now expected behaviour well. For example, once the stress-driven rockmass degradation process is properly understood, appropriate excavation and support techniques can be selected to ensure rapid and cost-effective tunnel advance. Systems that are designed for a mode of behaviour (e.g. structurally controlled instability) that is actually not encountered will most likely not perform well when the actual behaviour is significantly different (e.g. stress-driven spalling).

This keynote therefore presents an interpretation of observed rock failure processes, to explain geomechanics factors that affect constructability, and thus to assist in preventing delays and tunnelling cost overruns.

1.4 Anticipating rock behaviour

Typical rockmass behaviour and failure modes near underground excavations are described by the nine elements of the behavioural matrix shown in figure 1. In strong, hard rock, structurally controlled failure processes dominate at shallow to intermediate depth, or at low to intermediate induced stress (given on right side of matrix), while stress-driven behaviour dominates at depth when the stress level is sufficient to cause failure of intact rock. At high overburden, the rockmass surrounding the tunnel is heavily fractured, tends to increase in volume and cause large wall deformations. Thus, deformation control measures are required to manage the ground. The latter conditions may also be encountered at shallow depth, e.g. in regions where tectonic stresses from recent mountain folding sequences perturb the gravitational stress field (Himalayas, Andes, etc.; Carter et al. 2005) or where wide-scale continental drift stresses have not been released by thrust faults (e.g. in parts of the Canadian Shield).

- At shallow depth (top row in fig. 1), typically to around 750 m (when $\sigma_{max} < 0.4$ UCS; σ_{max} = maximum tangential stress near unsupported circular tunnel in elastic ground), structurally-controlled behaviour dominates in strong, hard rock. The severity of anticipated instability is dominated by the degree of jointing and the risk identification (Gefährdungsbild) is typically and appropriately described by joint set descriptions (orientation, spacing, roughness, persistence, etc.).
- At intermediate depth (centre row in fig. 1), typically when $\sigma_{max} > \sim 0.8$ UCS, stress-driven rock fracturing processes start to overlap with structurally-controlled processes. The degree of rockmass fracturing depends on the stress level and the stress orientation relative to existing rockmass weaknesses (non-persistent joints, foliations, etc.). At these depths, the rockmass starts to deteriorate when stresses are unfavourably oriented. The effects of stress at this intermediate stress level is typically ignored or overlooked for risk identification (Gefährdungsbild) as the assumption of persistent joint sets is considered to be conservative for support load determination. From a constructability perspective, however, while stress-driven fracturing may not add much load to the support system, it may have serious impacts on overbreak and thus the development of loose ground. In addition, strain-bursting

in massive to moderately jointed ground may lead to elevated risk levels (worker safety concerns).

- At great depth (bottom row in fig. 1), typically at more than 1500 m overburden in strong, hard rock, deep seated stress-driven failure dominates. The rockmass surrounding the tunnel is heavily fractured, tends to increase in volume or bulk causing bulking closure of the opening, and deformation control measures are required. This risk mode (Gefährdungsbild) is also typically anticipated and described by the ground-reaction curve concept.

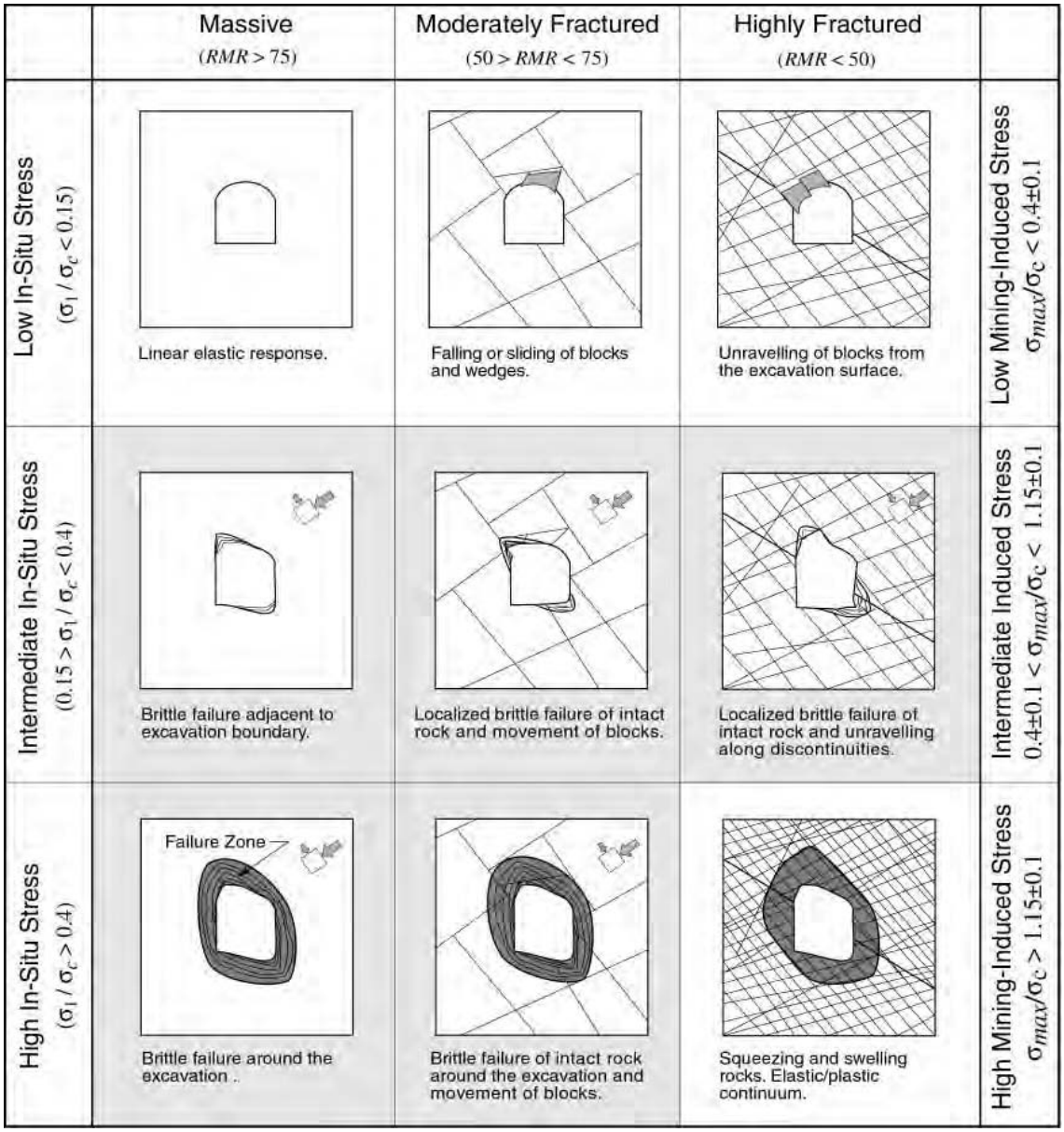

Figure 1. Rock failure mode matrix (Kaiser et al. 2000); σ_c = unconfined compressive strength of intact rock, and σ_{max} = maximum tangential stress near a circular opening = $3\sigma_1 - \sigma_3$.

This keynote focuses on conditions encountered at intermediate to great depth, in massive to moderately jointed ground (shaded matrix boxes in fig. 1 and for ground with GSI > 65; fig. 2).

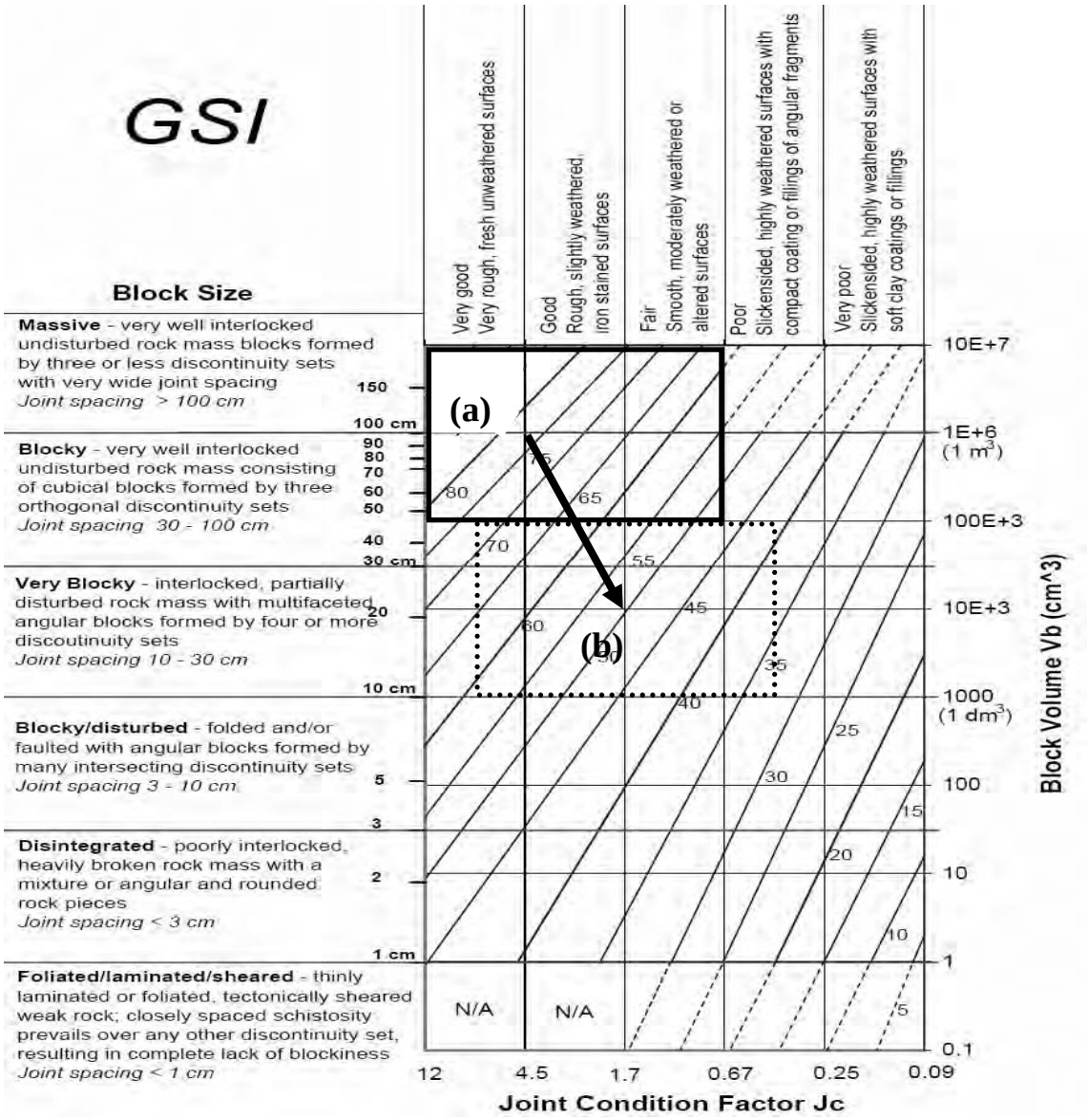

Figure 2. GSI chart – a. zone where brittle failure dominates massive to moderately jointed rock behaviour (Cai et al. 2004) and produces b. a stress-damaged rockmass with a reduced block size; arrow shown path caused by a block size reduction to 20% of its original size.

2 UNDERSTANDING AND MODELLING BRITTLE FAILURE

Brittle failure is a process that is dominated by induced tension leading to spalling rather than predominant shear failure. There are various processes that lead to such tensile failure in brittle rocks:

- Shear distortion in pure shear (fig. 3a) or at low confinement
- Stress-driven fracture propagation (Griffith crack propagation; fig. 3b)
- Extension strain-driven failure (Bai et al. 2000).

These processes are promoted by material and stress heterogeneities and are most prominent near excavation boundaries where the confinement level is low (σ_3 near zero). When the rock is sufficiently strained, tensile fractures tend to propagate and eventually form tunnel surface-sub-parallel fractures; called spalls as a result of a process called spalling. Figure 4 shows two examples of spalling: a. hour-glassing of a pillar, and b. notch formation at a tunnel wall. Both these examples were produced by

the second, stress-driven fracture propagation process, as illustrated by the superimposed model of crack propagation in figure 4.

Numerous efforts, e.g. Tang (1997) and many others, have been made to simulate this tensile rock failure process. For the design of underground excavations in brittle rock, however, it is important to realize that most commonly used failure criteria, such as the linear Mohr-Coulomb or the non-linear Hoek & Brown criteria, are not appropriate to simulate the behaviour illustrated by figures 4a, b. As described by Kaiser et al. (2000) and elaborated by Diederichs (2003), a bi-linear failure criteria with a spalling limit in the low confinement range as well as a tension cut-off is required to capture the spalling process (fig. 4c). While common failure criteria will predict shear failure near the excavation, the bi-linear criteria properly simulates the tensile failure processes near the excavation wall (circles in fig. 4d).

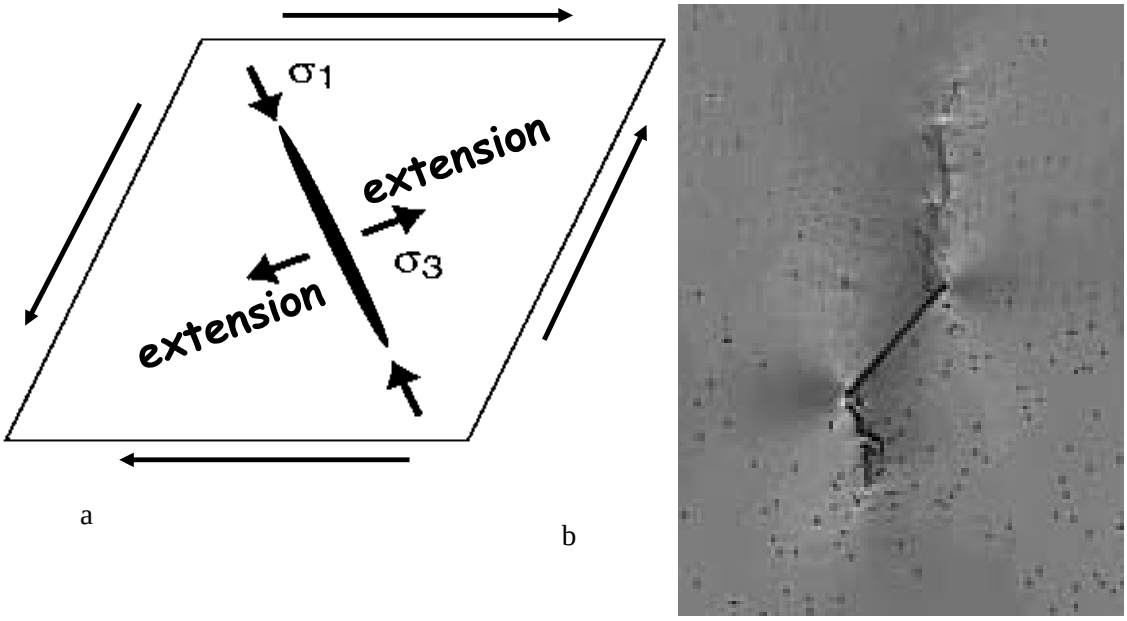

Figure 3. a. Shear stress-induced extension due distortion and related stress rotation; b. Griffith crack propagation (from simulation by Tang & Kou (1998) with RFPA™).

Most importantly, failure criteria commonly used in rock engineering do not predict stress-driven failure in the intermediate stress range (fig. 1; centre row) and thus do also not predict the related block size reduction in massive to moderately fractured or jointed rock where non-persistent joints tend to propagate due to tensile failure processes (fig. 3). As a consequence, the risk model (Gefährdungsbild) of moderately jointed rockmasses that are transformed into a continuously fractured rockmass with reduced block size due to spalling is seldom foreseen. However, this is frequently observed in the field as illustrated by (fig. 5). In this case, a massive, near horizontally bedded/foliated rock is disintegrated into a broken rockmass with plate-like blocks, a broken rockmass with little or no cohesive strength (Lockergestein).

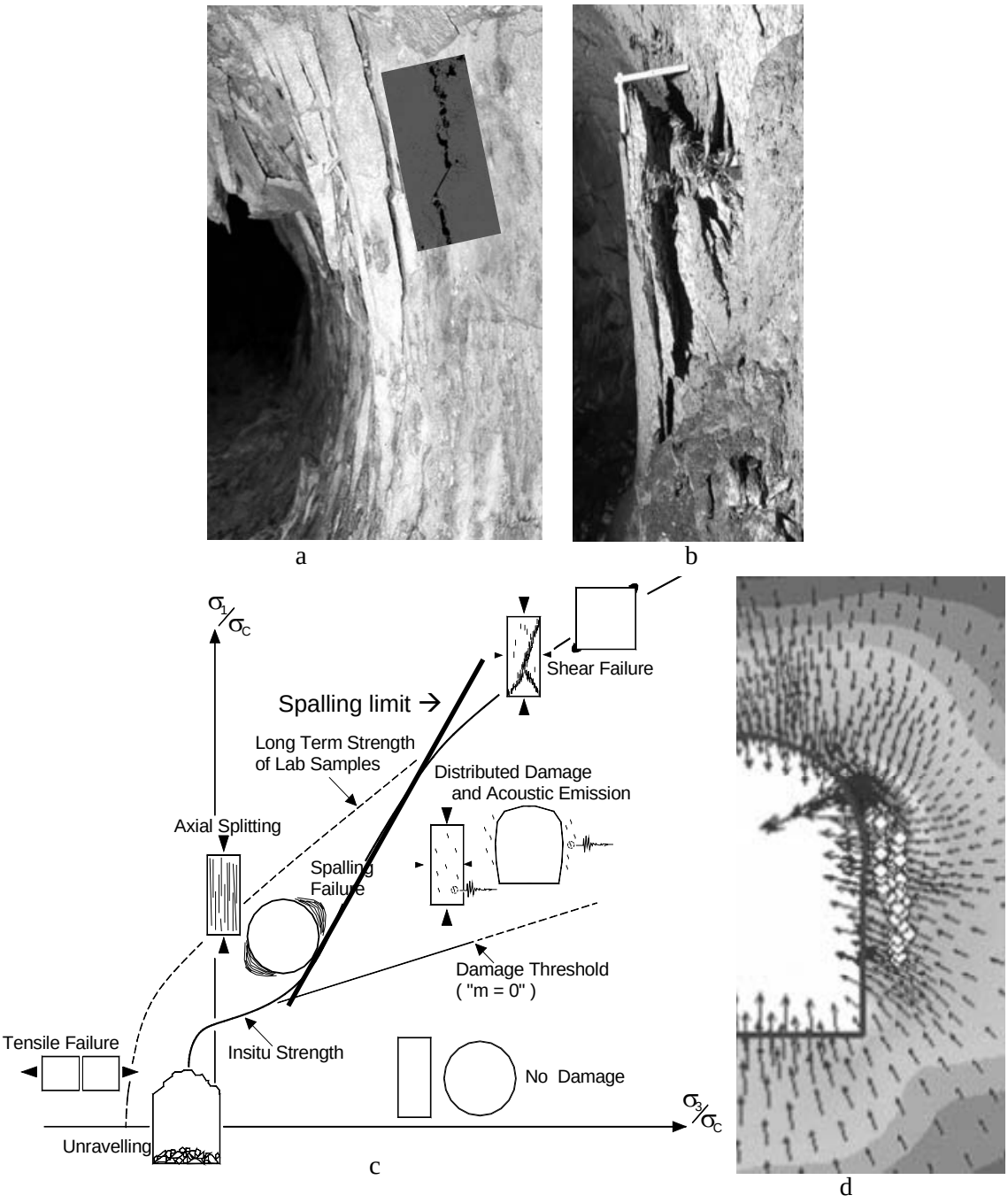

Figure 4. a. Hour-glassing of pillar with surface parallel spalling (Quirke mine, Canada;) with Griffith crack model (fig. 3) superimposed; b. tunnel wall spalling (Bedretto tunnel, Switzerland); c. bilinear failure criteria with spalling limit (Kaiser et al. 2000); and d. spalling of tunnel walls simulated with FEM model using brittle failure criterion parameters by Diederichs (2000).

Figure 5. Massive to moderately jointed rock with weak, near-horizontal foliation (Gneiss) showing stress-driven failure in the form of near-surface-parallel spalling.

2.1 Rockmass degradation

The effect of this stress-driven rockmass degradation process on the rockmass strength can best be assessed by reference to the rock classification example shown in figure 2 where the dotted area represents a damaged rock with blocks having an edge length of 20% of its original length (arrow from 1 to 0.2 m). The corresponding GSI reduction as shown by the arrow is from 85 to 55. This represents a rockmass strength reduction by approximately 75% (Hoek et al. 1995). While such a strength reduction on its own is already of practical significance, the fact that the behaviour mode changes from massive, stable to stress-degraded, „blocky“ ground has the most impact on tunnel construction, as such ravelling ground is more difficult to handle.

With a bi-linear failure criterion, a spalling limit, and a tension cut-off (fig. 4), it is now possible to simulate the frequently observed spalling, notching, or stress-driven overbreak process. It should be noted that this process starts to occur at relatively low stress levels ($\sigma_{max} > 0.4$ *UCS*; see right side of matrix in fig. 1), particularly in coarse grained rock types, and that its impact is often most evident when structural features such as joints, bedding planes or foliations, facilitate the stress-driven rockmass disintegration process.

From a practical perspective, it is therefore now possible to determine the depth of stress-induced rockmass disintegration and to anticipate stress-driven unravelling processes, a process that may affect both the performance of a TBM, particularly an open TBM, and the effectiveness of support systems that are installed without a shield.

3 ANTICIPATING THE „UNEXPECTED“

Stress-driven rockmass disintegration processes and their impact on tunnel stability, support performance, TBM performance, and thus contractor performance can now be anticipated.

3.1 Expected in-situ stress field

Because of the sensitivity of brittle rock to stress and stress concentrations caused by an excavation, the orientation of the in-situ stress field can often be determined from the location of stress-induced spalling. While other factors such as rockmass anisotropy, e.g. in foliated rocks such as gneisses, may also affect or even dominate the breakout process, the major principal stress typically acts in the direction perpendicular to the plane containing the deepest breakout. Qualitative observations at the deep Alpine tunnels in Switzerland, point to a predominantly vertical major principal stress, with spalling processes mostly observed in the tunnel walls, e.g. at the Lötschberg South Tunnels and the Bedretto Tunnel. At the St.Gotthard tunnel, including the Piora Exploration Tunnel, there is however evidence of sub-horizontal major principal stresses with spalling potential in the roof.

Since no systematic stress measurement campaigns were executed at either tunnel, the actual in-situ stresses are not known. Hence, for a robust design, it would be prudent to anticipate a non-uniform stress field with either sub-vertical or sub-horizontal major principal stresses (and possibly with stress rotation along the tunnel axis). Hence, *Ko* could range from < 1 to > 1 (likely range for St. Gotthard: $0.5 < Ko < 1.3$) and stress-induced spalling with related rockmass degradation would have to be anticipated in either the tunnel walls or the roof and floor. In areas of high (sub-) vertical stress, e.g. near valley walls, relaxation related loosening of the ground would also have to be anticipated in the roof.

Based on this uncertainty in the anticipated stress conditions, a robust engineering design would have to consider stress-driven rockmass degradation in both the walls and roof/floor, and would have to prescribe support and excavation techniques that are efficient in controlling broken ground in the walls and roof. Some floor heave due to bulking of fractured rock below the tunnel floor would also have to be anticipated.

3.2 Expected depth of failure at tunnel wall

By analyzing case studies of observed depths of failure from excavations damaged by rockbursts (Kaiser et al. 1996a, b) and from tunnels around the world failing in a progressive, non-violent manner (Martin et al. 1999), a robust empirical relationship between the depth of failure and the stress level at which this failure occurred was established for brittle rock where stress-driven spalling processes dominate the rockmass degradation or notch formation process. These studies show that the depth of failure, *df*, normalized to the tunnel radius a, is linearly proportional to the normalized stress level σ_{max}/σ_c (eqn 1), and that the failure process starts when σ_{max} exceeds about 40% of the rocks intact strength σ_c (see induced stress scale in fig. 1).

$$\frac{d_f}{a} = 1.25\frac{\sigma_{\max}}{\sigma_c} - 0.51 \pm 0.1 \qquad \text{(Martin et al. 1999)} \qquad (1)$$

where, $\sigma_{max} = 3\,\sigma_1 - \sigma_3$ is the maximum tangential stress at the wall of a circular opening in elastic ground, and σ_c is the laboratory uniaxial compressive strength of the intact rock.

3.2.1 Anticipated effect of rock strength and stress variability on depth of failure

As Lombardi indicated, one must be „aware of variability in parameters“ and „prepared to deal with its impact“. How significant the impact of the variability in rockmass strength on tunnel stability is can be illustrated by assessing its impact on the depth of failure. Even with well executed testing programs, σ_c typically is determined with a

standard deviation of at least 25%. In most tender documents, the defined coefficient of variation is actually much wider than 25%.

If the in-situ stress were well defined and most strength data (UCS) would fall within two standard deviations (rarely the case), the stress level σ_{max}/σ_c ranges between 67 and 200% of the mean stress level, and if in addition, the in-situ stress ratio ranges between 0.5 and 1.3 (see above), the stress level ranges non-symmetrically between 67 and 290% of the mean stress level case at $Ko = 1$.

Accordingly, the anticipated normalized depth of failure would be non-symmetrically distributed within the following range:

$$\frac{d_f}{a} = (0.84 \ to \ 2.90)\left(\frac{\sigma_{\max}}{\sigma_c}\right)_{mean\ at\ K_0=1} - 0.51 \pm 0.1 \qquad (2)$$

For example for a mean stress level of $\sigma_{max}/\sigma_c = 0.4$ at $Ko = 1$ with a corresponding normalized depth of failure of zero meters, the depth of failure should be anticipated to range from 0 to 0.65 a (or 0 to 3.25 m for a 10 m tunnel).

This finding is supported by statistics from many tunnels. For example, over a 2 km long section at the Lötschberg South tunnels, 70% of the tunnel was stable (without spalling) and the percentages of sections with spalling were 5, 1, 11, 8, and 5% for depths of failure of $df = 0.25$, 0.5, 0.75, 1.0, and 1.25 m, respectively. At the Piora Exploration Tunnel, along a 800 m long section in the Leventina Gneiss, 45% of the tunnel length showed no signs of spalling while the maximum depth of failure was 1.2 m or $df/a = 0.48$ in the zones which did spall.

These examples illustrate that, while we can anticipate stress-driven rockmass degradation and the mean depth of failure, the variability in available input parameters (e.g. the UCS given in tender documents) is too wide to accurately predict the anticipated range of depth of failure. Hence, robust engineering solutions must be adopted such that the entire range from stable tunnel roof and walls ($df/a = 0$) to deep-seated roof or wall failure ($df/a >> 1$) can be managed well.

3.2.2 Anticipated effect of overburden on depth of failure

According to equation 1, the depth of failure is proportional to the stress level and thus, if gravitational forces dominate, to the overburden depth[1]. However, it is well known that the ground becomes less forgiving as we proceed to greater depth. Hence, the practical consequences of increasing overburden or depth of failure are not directly proportional to overburden depth. First of all, stress-driven failure only manifests itself below a critical depth, below 1500 m for the parameters assumed to produce figure 6 (UCS = 200 MPa; $K_o = 1$) and in extreme situations below 700 m due to the assumed variability in stress and strength (same assumption as above). Consequently, as we proceed to greater depth both the longitudinal extent of a tunnel experiencing stress-driven failure and the severity of spalling (depth of failure) increase, particularly below 1500 m, for the parameters assumed here, where stress-driven instability is to be anticipated even under mean stress and strength conditions.

1 The stress level will not be proportional to the overburden depth if tectonic or other stress modifiers exist.

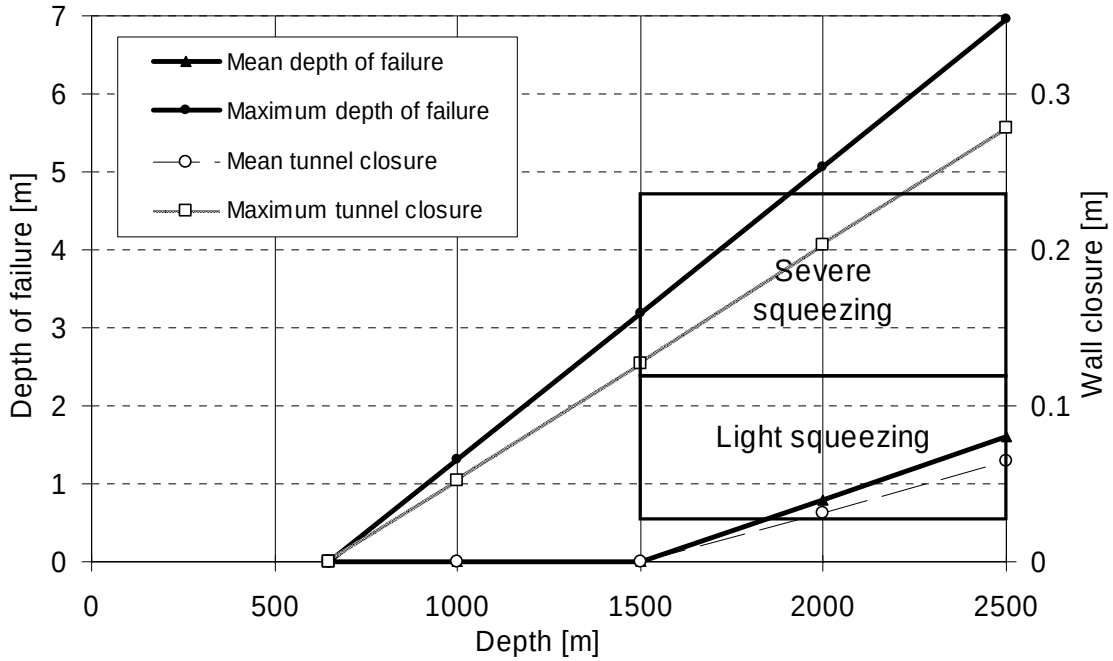

Figure 6. Depth of failure as a function of overburden depth for a set of mean stress and strength parameters that leads to stress-fracturing at 1500m depth (*UCS* = 200 MPa; K_o = 1); also shown is the maximum depth if the parameter range is two standard deviations for σ_c and a range of K_0 = 0.5 to 1.3.

3.3 Expected tunnel convergence due to rockmass bulking

When hard, brittle rock fails under stress, it disintegrates and massive to moderately jointed rock becomes „blocky ground“[2] (as described above and by fig. 2). Due to geometric incompatibilities, these rock pieces do no longer fit together perfectly and the rockmass volume increases rapidly due to geometric incompatibilities. This process is called bulking and the bulking factor BF typically ranges anywhere from near zero for highly confined rock to about 40% for unconfined bulking. As explained by Kaiser et al. (1996a), rock support does reduce the bulking factor but can seldom reduce it to less than 2 to 4% in hard brittle rock. To generate figure 6, it was therefore assumed that the bulking factor is 4% and the tunnel closure for the mean and maximum depth of failure is calculated and plotted. Accordingly, above a depth of 1500 m, the bulking related closure is typically between zero (mean conditions) and rarely > 12.5 mm; i.e. in general < 2.5% or elastic to lightly squeezing. Such convergences can normally be managed with conventional support techniques without significant impact on the construction process.

According to Hoek & Marinos (2000), difficult construction conditions demanding careful ground control measures are encountered when the strain exceeds 2.5% (fig. 6). Such conditions are not to be expected for the parameters assumed for figure 6 wherever the rock strength and stress correspond to mean conditions even at depths to 2500 m. However, with increasing depth beyond 1500 m, the chance of encountering deep seated failure (maximum depth of failure and related maximum tunnel closure; fig. 6) increases rapidly. Most important, when the rock is strained beyond 2.5%, the rockmass disintegrates totally, loosing much of its cohesive strength. Thus, below about 1500 m depth, the level of construction difficulty increases rapidly, in a non-linear manner with

[2] The term “blocky” is set in parentheses here because the rockmass is not naturally blocky due to persistent joint sets but has been transformed from massive or moderately jointed rock with non-persistent joints to “blocky” ground by the effect of stress.

depth, and rock support systems that can effectively control the related unravelling process must be adopted.

As a general rule, construction difficulties in brittle, hard rock must be anticipated when the originally massive to jointed rock is transformed to „blocky“, cohesionless rock (Lockergestein) and when large deformations due to rockmass bulking occur. An example that illustrates this state of transition from massive to „blocky“, bulking ground is shown in figure 7 (note the very massive state of the rockmass beyond the damaged rock; above white arrow in fig. 7a).

The same state of disintegration is visible in the pillar and tunnel walls shown in figures 4a, b and it would be reasonable to assume that the same process can occur ahead of the tunnel face if the near face convergence is sufficiently large to cause face spalling.

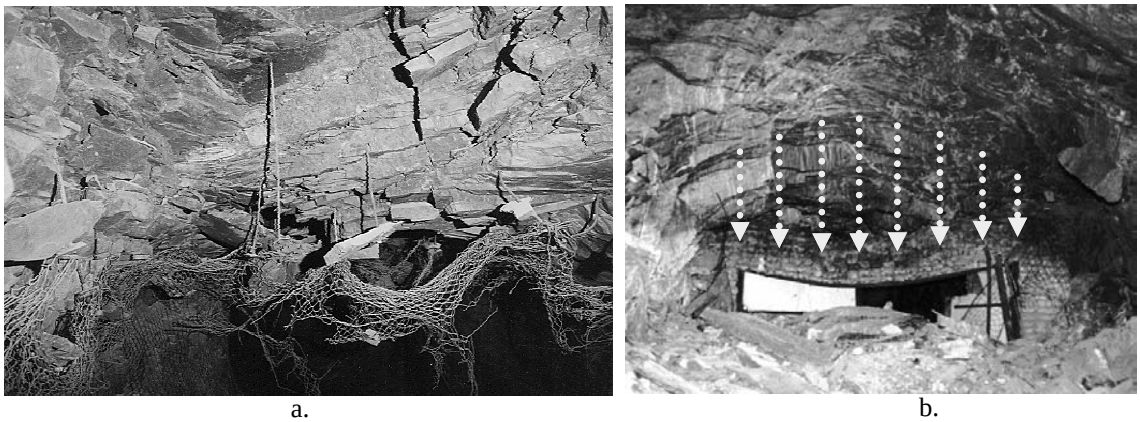

a. b.

Figure 7. Photos of stress driven failure: a. tunnel roof showing bulking due to stress-induced fractures opening because of lateral convergence (white arrow) (Lac Shortt Mine, Canada), and b. bulking related non-uniform convergence at vent door (Brunswick Mine, Canada).

4 TUNNEL FACE STABILITY

The stress fracturing and bulking process illustrated by figure 7 is only visible because the rock near the viewing point collapsed and provided insight into the disintegrated rockmass, otherwise it is mostly hidden behind the rock support. At the tunnel face, this broken rock is either excavated with each round during drill and blast operations or is hidden in front of the face (ahead of a TBM).

4.1 Face degradation process

Because of the constrained convergence pattern near the face, causing stress concentrations at the edge of the face and thus face parallel loading, it is reasonable to assume that the same processes could happen at the tunnel face. The anticipated rockmass behaviour of a highly strained tunnel face is illustrated by the photomontage shown in figure 8, illustrating two important characteristics leading to face instability: a. surface parallel spalling, and b. inward bulging of the face. These two processes differentially strain the rock and lead to rockmass disintegration and to „blocky ground“ in the face.

There is now ample field evidence in support of this qualitative description of the face disintegration process involving face parallel spalling (fig. 9c). Numerical models, using the brittle failure criterion introduced earlier, can reproduce the observed face spalling.

a. b.

Figure 8. Photomontage illustrating anticipated rockmass disintegration process ahead of a tunnel face: a. rotated tunnel roof showing slab formation and related opening of fractures; and b. anticipated non-uniform inward movement of the face (bulging) due to bulking ahead of the face causing non-uniform straining of rock ahead of tunnel face.

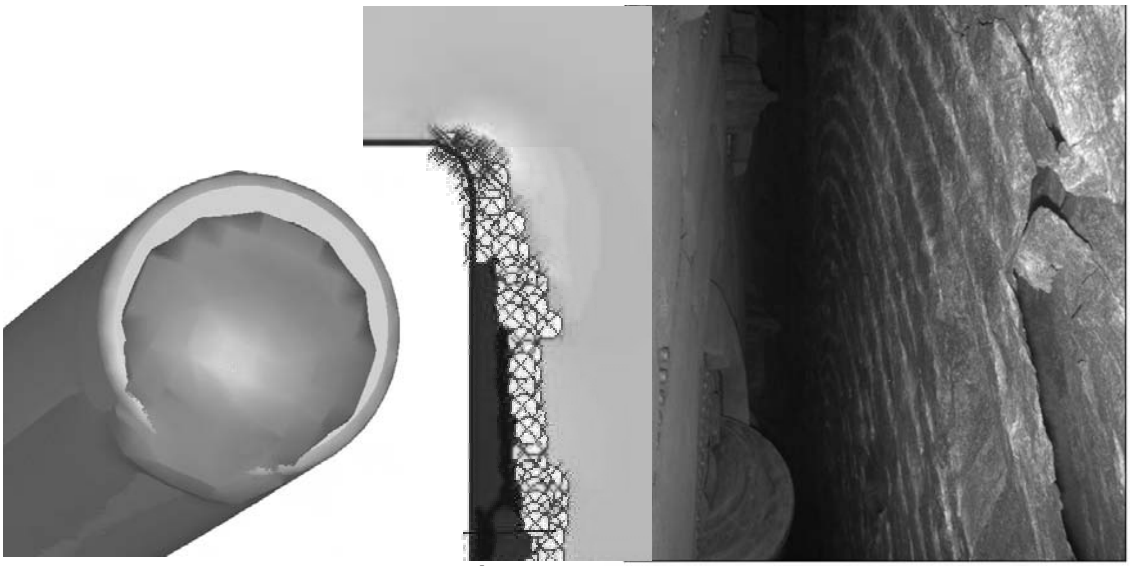

a. b. c.

Figure 9. Comparison of modeled and observed tunnel face conditions: a. 3D model showing zone of anticipated (vertical) foliation slip ahead of tunnel face; b. axisymmetric brittle rock model (fig. 4c) showing tensile failure zone in the face (circles) and shear failure (crosses) at the location of gauge cutters; and c. observed spalling of tunnel face in massive rock (courtesy: M. Weh).

The observed face parallel spalling is reproduced in figure 9b with circles and crosses indicating tensile and shear failure, respectively. This spalling process can be enhanced

and assume a non-symmetric pattern if weak foliations dip into the face. This is illustrated by figure 9a where ubiquitous joints are assumed to dip at 10 to 20º into the face. As a result, the failure zone is predicted to be deeper in the lower part of the face and also to affect the tunnel floor more than the roof. Again, there is ample field evidence in support of this interpretation (e.g. at the Amsteg lot of the St. Gotthard Tunnel).

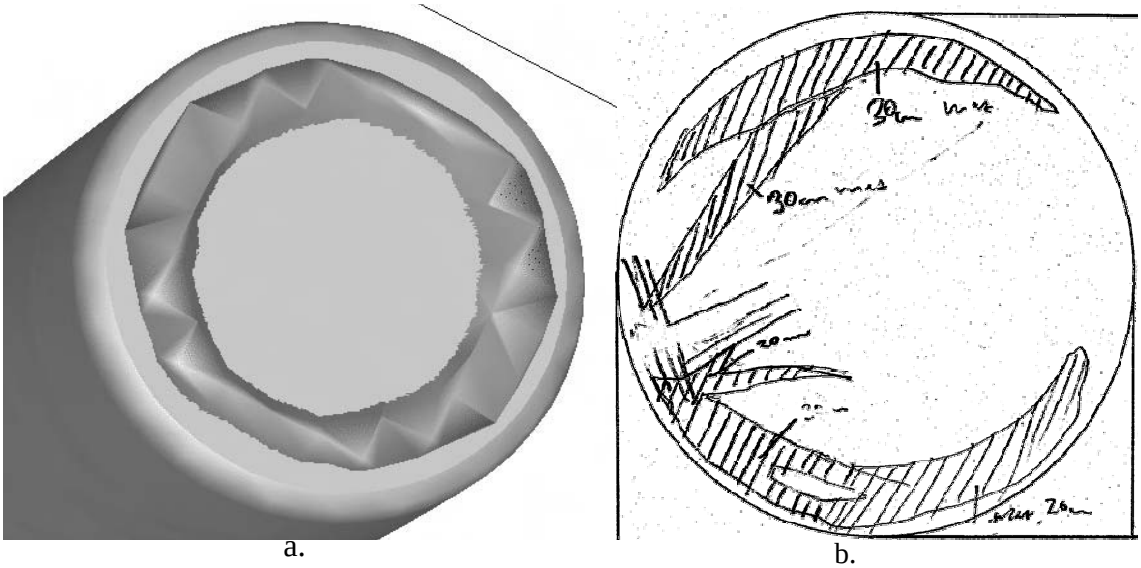

Figure 10. a. Predicted zone of face instability in foliated ground (elastic 3D ubiquitous joint model with vertical foliation) compared to b. face map record (courtesy: M. Weh).

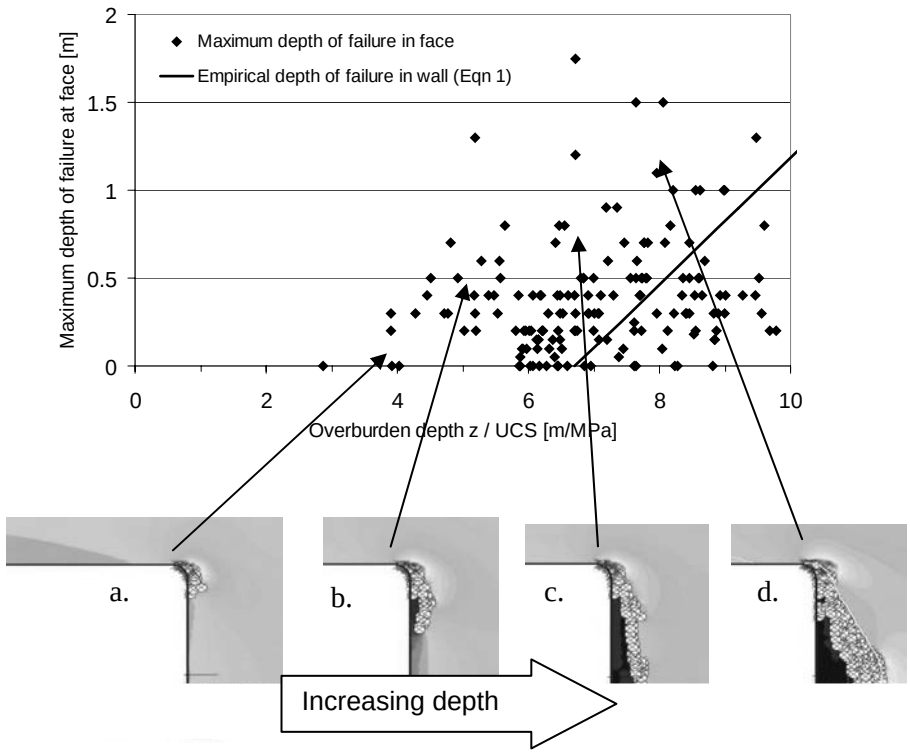

Figure 11. Measured spalling depth at tunnel face as a function of normalized depth z/UCS, compared to 3D axisymmetric model results for increasing overburden depth z (unpubl. data, courtesy Matrans).

Furthermore, characteristic circular face breakout patterns as illustrated by the face map of figure 10b can now be interpreted and reproduced by numerical models. Figure 10a presents isosurfaces of areas that are expected to fail when foliations are parallel to the tunnel face (3D elastic, ubiquitous joint model). Such face parallel weakness planes promote the propagation of fractures from the stress raisers at the edges of the tunnel face and thus accelerate the face damage process in the face (see also fig. 11).

In summary, stress-driven spalling processes with or without inherent weaknesses (foliations or jointing) can lead to unstable, „blocky“ tunnel faces. While pre-existing joint sets may enhance the process of face degradation, the creation of a further „joint set“ or fracture set that is sub-parallel to the face is the primary cause for the widely observed face instability problems evident at depth and in large tunnels.

4.2 Influence of depth

The effect of overburden depth on stress-driven face instability, i.e. depth of face failure d_{ff}, is illustrated by the data shown in figure 11. The observed depth of face failure in this 9.4 m wide tunnel (data from Lötschberg South Tunnels) increased rapidly once the initiation threshold at z/UCS = 4 was exceeded (z in m; UCS in MPa). At a stress level of z/UCS = 5, the depth of face failure typically reached 0.5 m and it reached or exceeded 1.0 m at z/UCS = 7.

Based on equation 1 (full line in fig. 11), failure at the tunnel walls would be expected when z/UCS = 7 is exceeded. In other words, this data illustrates that face instability may have to be anticipated before wall instability; i.e. in brittle failing rock, face instability occurs at lower overburden stress than wall instability. While at shallow depth, hoop stresses may enhance face stability over sidewall stability, particularly in foliated or blocky ground, at depth or higher stress, spalling and slabbing of the face occurs prematurely.

Results from axisymmetric, numerical models with brittle parameters (same assumptions as used for results shown in fig. 9) are shown as figures 11a-d to illustrate how failure in the tunnel face propagates as the overburden depth increases. This series of images show that failure initiates by shear failure at the stress raiser (circumference of tunnel face) but then propagates toward the centre of the tunnel face. At the point of face failure initiation (figs 11a, b), for this axisymmetric case, circular face breakouts (as frequently observed; fig. 10) are to be expected unless instability is dominated by structural weakness planes. As the stress level increases, spalling propagates toward the tunnel centre and eventually (fig. 11c) involves the entire tunnel face (again as observed in the field; fig. 9).

This revelation is of great practical importance. It clearly demonstrates that the tunnel face can be more prone to stress-induced failure than the tunnel walls. This is not in accord with some of the implicit principles behind current tunnelling standards or contractual arrangements (support and excavation classes). Contrary to the commonly encountered situation where wall instabilities slows tunnelling progress, in this situation, face instability may slow progress even though the walls are stable and may need little structural support.

5 EFFECT OF WEAKNESS ZONES

As indicated earlier, stress fracturing is largely a tensile failure process (figs 3, 4) that leads to spalling-type failure and rockmass degradation in low confinement areas near excavations. The extent and shape of low confinement zones (with low minor principal stresses) or relaxation zones are affected, if not dominated, by small and large scale

heterogeneities in the rock or rockmass. Hence, the location and extent of stress-driven rockmass degradation depends on the shape of the relaxation zone.

At a rockmass scale, relaxation is strongly influenced by stiffness or strength heterogeneities, e.g. due to weak or soft (fault) zones. A typical example of a tunnel with a weakness zone immediately above the tunnel roof is shown in figure 12a. Due to the assumed lower stiffness and strength of the weak zone, deep-seated relaxation is caused (even though the weak zone is only failing locally) and deep-seated tensile rockmass degradation occurs on both sides of the roof (as indicated by circles (o) representing elements failing in tension).

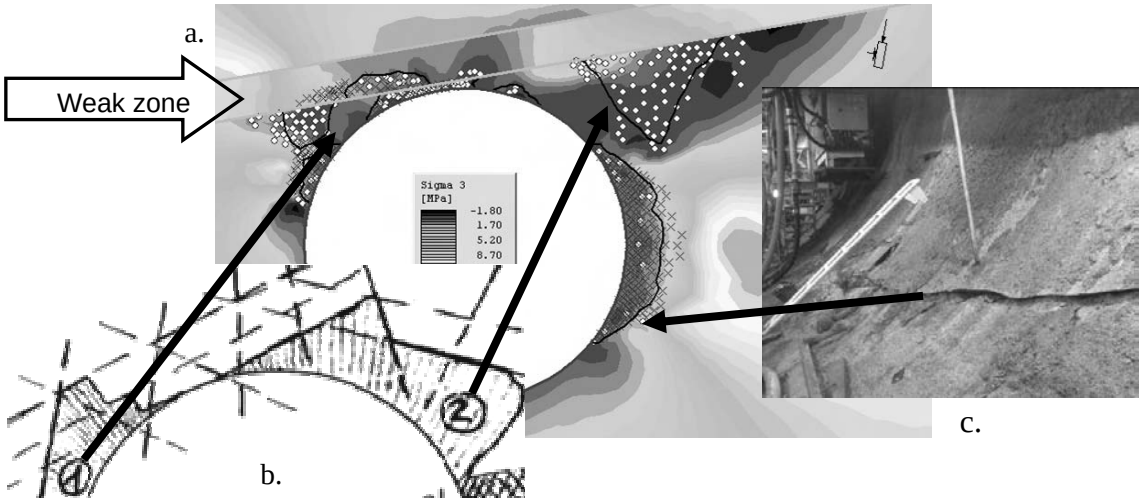

Figure 12. Numerical model of tunnel scenario with a weak, soft layer just above the tunnel roof: a. Minor principal stress contours with elements yielded in shear x and tension o. Superimposed are: b. typical overbreak record in roof and c. photo showing observed shear failure in lower part of the wall.

For the assumed stress state with a sub-vertical major principal stress, shear failure is induced in the walls (x; fig. 12a) and stress-driven rockmass degradation in the roof (o). Field evidence confirms this interpretation as illustrated by the superimposed photo of shear failure fig. 12c) and typical overbreak record (fig. 12b; courtesy: Girlanda, TAT).

This example illustrates that stress-driven rockmass degradation with associated loss of cohesion causing unravelling of an otherwise massive to moderately jointed rockmass must be anticipated near heterogeneities, faults or weakness zones. The effect of such heterogeneities can be felt by the tunnel even if such weak zones do not penetrate the tunnel.

Tunnelling situations, like the one illustrated by figure 12, with weakness zones near the tunnel wall or roof can therefore lead to difficult construction conditions. If such zones are encountered near the roof, deep-seated ravelling can occur even if the rockmass is massive to moderately jointed and standard bolting may be impractical due to the small block size in the disintegrated rock mass. If such zones are near the wall, gripper stability may be compromised, again because of deep stress-induced rock degradation. If such zones occur in or below the floor, unexpected floor heave may be encountered even if the weakness zone is not visible.

6 CONCLUSIONS

When stepping outside the world of common experience, costly mistakes can be made because of a lack of understanding of the actual behaviour of the rockmass or because

the rock may change its behaviour and behave in an unexpected manner. Many lessons have been learned in recent years and future projects can benefit from this accumulated know-how. This keynote focused on qualitative observations that contribute to a better understanding of rockmass behaviour in stressed ground to support robust engineering, adaptive tunnel design and construction. With a sound understanding of rockmass behaviour at depth, the „unexpected“ can be anticipated, changes in behaviour predicted, and old tools adapted to manage the now expected behaviour.

Brittle failure is a process dominated by induced tension leading to spalling rather than predominant shear failure, particularly in low confinement areas near underground excavations. As a consequence, a bi-linear failure criterion with a spalling limit is required for brittle rock to properly predict rockmass degradation processes near excavations. In this manner, it is now possible to anticipate the expected in-situ stress orientation and ratio and to design tunnels considering stress-driven failure processes. However, the uncertainty in the anticipated stresses along a deep tunnel is high and robust engineering designs must anticipate stress-driven rockmass degradation in the walls, roof and floor. Support and excavation techniques that are efficient in controlling broken ground are required. While we now can anticipate the mean depth of stress-driven rockmass degradation, the variability in available input parameters is typically too wide to accurately predict the depth of failure. Hence, robust engineering solutions must be adopted such that the entire range of tunnel behaviour, from stable to deep-seated roof or wall failure can be managed well.

When brittle rock fails under stress, it disintegrates and even massive rock can be transformed to cohesionless, broken ground (Lockergestein). Due to geometric incompatibilities, this broken rock is highly dilational and bulking factor typically range from 2% for well supported ground to about 40% for unconfined bulking. As a consequence, construction difficulties in brittle rock must be anticipated when the rockmass is transformed to broken, cohesionless rock and large deformations due to bulking occur.

Stress concentrations at the tunnel face cause face parallel spalling processes that may lead to unstable, broken ground in the tunnel face. The creation of a further „joint set“ or fracture set that is sub-parallel to the face is found to be the primary cause for the widely observed face instability problems evident at depth and in large tunnels. In massive to moderately, brittle rock, this face instability may occur before wall instability, i.e. at lower overburden stresses.

Finally, stress-driven rockmass degradation causing unravelling of rock must be anticipated near heterogeneities such as faults and weakness zones. The effect of such heterogeneities can be felt by the tunnel even if weak zones do not penetrate the tunnel. This can lead to difficult construction conditions with deep-seated ravelling, degradation of walls and floor heave.

As a consequence of stress-related rockmass behaviour change, established standards may no longer be fully applicable and the basis for contractual arrangements may change even if the geology is accurately predicted. Therefore, risk should be managed by planning for uncertainty with a high level of flexibility in the construction process.

REFERENCES

Bai, T., Pollard, D.D. & Gao, H. 2000. Explanation for fracture spacing in layered materials. Nature, 403:753-756.

Cai, M., Kaiser, P.K., Uno, H., Tasaka, Y., Minami, M. & Hibino, Y. 2004. Estimation of rockmass strength and deformation modulus using GSI system – a quantitative approach. *Int. J. of Rock Mech. & Min. Sc.*, 41(1):3-19.

Carter, T.G., Steels, D., Dhillon, H.S. & Brophy, D. 2005. Difficulties of Tunnelling under High Cover in Mountainous Regions. Proc. Int. AFTES Congress, Tunnelling for a Sustainable Europe, Chambery, 349-358.

Diederichs, M.S. 2000. Instability of Hard Rock Masses: The Role of Tensile Damage and Relaxation. PhD Thesis, University of Waterloo, 566 p.

Diederichs, M.S. 2003. Rock fracture and collapse under low confinement conditions, Rocha Medal Recipient, *Rock Mech. Rock Engr*., 36(5):339-381.

Hoek, E., Kaiser, P.K. & Bawden, W.F. 1995. Rock Support for Underground Excavations in Hard Rock. A.A. Balkema, Rotterdam, 215 p.

Hoek, E. 1999. Putting numbers to geology – an engineer's viewpoint. The Second Glossop Lecture, *Q. J. Engrg. Geol.*, 32:1-19.

Hoek, E. & Marinos, P. 2000. Predicting tunnel squeezing. *Tunnels and Tunnelling International.* Part 1 – 32(11): 45-51; Part 2 –32(12):34-36.

Kaiser, P.K., McCreath, D.R. & Tannant, D.D. 1996a. Canadian Rockburst Support Handbook, Mining Research Directorate, Sudbury, Canada, 314 p.

Kaiser, P.K., Tannant, D.D. & McCreath, D.R. 1996b. Drift support in burst-prone ground. *CIM Bulletin*, 89(998):131-138.

Kaiser, P.K., Diederichs, M.S. Martin, C.D. Sharp, J. & Steiner, W. 2000. Underground works in hard rock tunneling and mining. Keynote at GeoEng2000, Melbourne, Australia, Technomic Publishing Co., 1:841-926.

Martin, C.D., Kaiser, P.K. & McCreath, D.R. 1999. Hoek-Brown parameters for predicting the depth of brittle failure around tunnels. *Canadian Geotechnical Journal*, 36(1):136-151.

Peck, R. B. 1969. Advantages and limitations of the observational method in applied soil mechanics, Ninth Rankin Lecture. *Geotechnique*, 19(2):171–187.

Tang, C.A. 1997. Numerical simulation of progressive rock failure and associated seismicity. *Int. J. of Rock Mechanics and Mining Sciences*, 34(2): 249-261.

Tang, C.A. & Kou, S.Q. 1998. Crack propagation and coalescence in brittle materials under compression. *Engineering Fracture Mechanics*, 61(3-4):311-324.

New Dimensions in Seismic Data Interpretation with 3-D Virtual Reality Visualization for Burst-prone Mines

P. K. Kaiser, P. Vasak and F. T. Suorineni
MIRARCO – Mining Innovation/Geomechanics Research Centre, Laurentian University, Sudbury, Ontario, Canada
D. Thibodeau
INCO Technology Centre, INCO Limited, Sudbury, Ontario, Canada

ABSTRACT

3-D virtual reality (VR) visualization has opened new opportunities for complex 3D (x, y, z), 4D (x, y, z, t) or even nD data interpretation. The integration of common earth models (3D geologic data), mine models (3D excavations and stress), extraction models (1D time sequencing or mine sequencing) and nD monitoring data (e.g., seismic event parameters) into a common mining process model provides a platform for experts in various fields to better design, evaluate, monitor and modify mine plans throughout a mine's life; from feasibility, through operation, to closure. Viewing seismic data in a stereoscopic VR environment within a mining process model offers data interpretation processes previously unavailable at lower dimensionality. MIRARCO has developed data analysis and viewing processes specifically designed to enhance microseismic and seismic data interpretation in a collaborative, immersive VR environment; bringing mine personnel and expert consultants together to evaluate data and make strategic decisions for cost effective and safe mining.

Seismic events cause immediate hazards (rockbursts) and microseismicity causes gradual hazards through its cumulative effect in rock mass degradation. The focus of this paper is on understanding seismicity from a mine safety and mine planning perspective; in particular, how seismic migration patterns relate to the rockmass response to mining.

The benefits of innovation in seismic data interpretation are significant, e.g., for hazardous work area identification, allowing better formulation of re-entry policies and workforce allocation planning, as well as allocation of effective support systems to strategic areas of elevated risk. Better understanding of the overall response of a mine to extraction also facilitates mine planning and design, assisting in reducing production costs and thus in enhancing profitability.

1 Evolution of Virtual Reality Technology

Making sense from huge amounts of complex data with unknown patterns and multiple interrelated parameters is a challenging task that requires tools to detect patterns and trends. The human mind is highly developed to use visual perception in every day life. Hence, it is imminently obvious that there should be a potential in exploiting this ability for complex, multi-dimensional data processing using scientific visualization (www.ncsa.uiuc.edu). Scientific visualization enables data to be presented in dynamic images in order to reveal intrinsic patterns and dependencies. Scientific visualization was made possible by high performance computing and computer graphics starting in the 1970's. This evolution was the brainchild of Douglas Engelbart in the 1950's who first envisioned that computers should not just be used for number crunching but as tools for digital display. The idea gradually transformed computer graphics to produce virtual reality (VR) environments, as we know them today. Virtual reality is the result of a demand for interactivity in computer visualization.

VR applications started in the military for real time display of radar defence systems data. Pioneering industries in the use of 3D visualization are the aerospace, automotive and biomedical industries (Tyler 2003). The oil industry pioneered the use of VR in the earth sciences and reservoir engineering fields. The late application of 3D visualization in the oil and gas (O&G) industries is attributed to the lack of suitable software to drive these large environments in interactive data analysis (Zeitlin, 2003). An international consortium was established by the O&G industry in 1998 (Schlumberger et al, 2002) to demonstrate the impact of VR for the industry. A first prototype of VR for the O&G industry was available in late 1998 (Fröhlich and Göbel, 1999). The overall goals of the international consortium were to apply and evaluate virtual environment technology for reservoir discovery, for the characterization of oil

fields and for the management of oil extraction. MIRARCO recognized the same barriers in the use of VR for the mining industry and embarked on a strategic R&D program to assist mining in the adoption of VR.

VR environments were also created to enable multi-disciplinary collaboration, to generate synoptic views of data from multiple sources and to support strategic planning by multi-disciplinary teams (Fröhlich and Göbel, 1999). The international consortium proved that with VR an "Earth scientist could dive under the surface and fly around a reservoir, detecting interesting features in the data that would be less obvious on a small desktop computer monitor" (Polyakov, 1999) and that multi-disciplinary collaboration was possible. There are many forms of VR (desks, walls to caves, with or without haptics, etc.). However, due to similarities between O&G and mining applications, MIRARCO opted for collaborative, immersive VR (CIVR) as the most appropriate VR format for mining. With multi-dimensional models different data from various sources can be integrated and interpreted in CIVR by a multi-disciplinary team in a more effective manner than ever before. Most importantly, CIVR accelerates the pace of discovery, improves communication, reduces the risk for error and makes the decision making process more efficient and convincing ("seeing is believing").

Several success stories have been told in the O&G industry following the use of VR applications. One such anecdotal story stems from the Schlumberger ConocoPhilips Ekofisk field in the North Sea (Norsk Hydro, 2003). In a jack-up drilling campaign involving 5 wells, extensive water influx was observed in the overburden of the first well resulting in the abandonment of the well at 8000 ft sub sea. A second well was successfully drilled after overcoming the same water influx situation but which was successfully controlled with increased mud weight with no loss situation. The next two wells were drilled without encountering the high water pressure situation. An alternative well plan for the first abandoned well was made but also had to be abandoned for the previous reason. Drillers and management were reluctant to make further trials, but giving up the well meant a loss production opportunity, as this was a one time drilling campaign. With the use of VR, team members pooled experiences together using data from various sources in an integrated manner to plan a well trajectory in the overburden with little risk of hitting the high-pressure water. The well was successfully drilled yielding revenue of 18 million dollars that otherwise would have been lost.

VR application to science and engineering therefore offers many advantages and benefits:

- Facilitates the use of visual perception, a capability that only humans master
- Enhances ability to integrate complex and/or large volumes of data from different sources
- Provides increased understanding of complex data sets and simplifies critical decision making
- Encourages interdisciplinary team collaboration and brainstorming
- Reduces time in data understanding and interpretation
- Connects geographically remote experts (through linked VR centres) for problem solving at much reduced cost and with great time savings
- Provides a great strategic planning, negotiating and public relations tool based on the principle of "seeing is believing". Management and investors are more easily convinced when they instantly see what they would have to read in lengthy reports, articles or papers.

2 Application of VR in Mining

Mines are complex environments and solving mining problems require an integrated approach. Mines collect data from exploration to recovery and closure; including data from boreholes, geological mapping, rockmass characterization, rock engineering properties, orebody geometry delineation, excavation and infrastructure layout design, support performance observations, seismicity, costs and much more. Unfortunately, this data is rarely integrated and properly analysed, and as a result, we rarely have a grasp of the larger picture of a mine's performance. By learning how to turn data into information, or by adopting technology to assist in this process, much can be gained as illustrated by the success story of the O&G industry.

The key for a more efficient use of data is to provide planning and design teams a means to first identify areas where data is either "weak" or missing in order to make decisions, and then to provide a means for fast and effective data integration and processing. This can best be accomplished within a collaborative, immersive visualization framework where teams of sector experts (geologists, planners, designers, operators, managers and eventually financiers) can work together to gain a real advantage by quickly establishing the 'big picture', resulting from a greater understanding of the data, and thus the value of a property. VR application offers the best opportunity for understanding complex, varied and large volumes of data in a central setting. However, as indicated earlier, the late adoption of VR technology in earth

sciences and mining engineering is a result of a lack of suitable, sector-focused tools and processes, as well as a lack of skill in making the technology work for the mining industry. Furthermore, data is not structured and stored for interactive data analysis. Recent development in the software sector (Datamine, FracSIS, GoCAD, etc.) has removed some of these obstacles and has paved the way for the use of VR in mining. For these and other reasons, the mining industry has been late in taking advantage of the VR technology.

Through extensive industry consultation, MIRARCO identified a need for a R&D program supporting the adoption of VR in mining and with funding from the Canada Foundation for Innovation (CFI, matched by the Ontario Innovation Trust (OIT)) was able to open a state-of-the-art Virtual Reality Laboratory (VRL) (Figure 1) at Laurentian University. The VRL constitutes the anchor facility of a multidisciplinary research approach bringing disciplines from exploration to mine site rehabilitation together through a Centre for Integrated Monitoring Technology (CIMTEC). This research program is designed to meet the needs of the mineral exploration, mining and geotechnical industries, and is the first VR facility fully dedicated to the mineral industry sector.

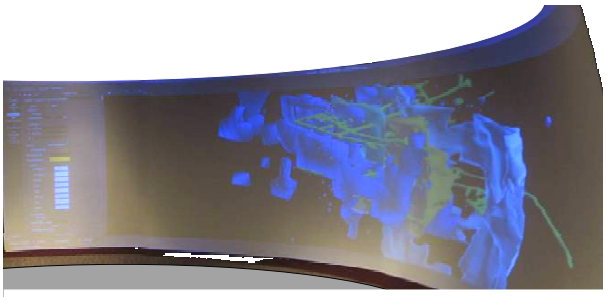

Figure 1: View of double curved screen with image of mining blocks, drifts and geology used for seismic data interpretation (see Figure 2)

This facility builds on technologies developed and proven for the O&G industry. Several visualization packages are used to "map" data from multiple sources to a single, world coordinate system. The system projects dynamic stereo images onto a 8 x 22 foot double-curved screen, providing up to 20 persons with the sense of full data immersion. Subsurface excavations, infrastructure, geology, hydrology, geochemistry, geomechanics, cost and time can all be combined to provide a holistic overview of a mine property. Inherent complexities of three-dimensional data can be viewed with a true sense of depth and spatial relationship. The scale of the screen, combined with the depth perception provides an immersion that increases the participants' overall understanding of spatially complex data relationships and accelerates data comprehension as well as transfer of experience and knowledge.

The power of VR environments lies in the illusion of being in a virtual world and individuals can see and feel their data as being part of it. The large size and extent of images combined with the depth perception in VR centres allow interpreters to see details without losing the broader perspective. Data and images can be rotated in any direction, magnified to various scales and sliced in arbitrary directions for detailed viewing, analysis and interpretation.

The benefits of VR in geomechanics design of underground excavations were presented by Henning et al. (2003). Figure 2 includes geological data (dyke, waste stringer, orebody), geometry of excavations (stopes and development drifts, stress in voxet with a movable stress plane), stress-driven dilution potential, and seismic data. Even if the image is enlarged, it is practically impossible to interpret and relate this data without stereo VR.

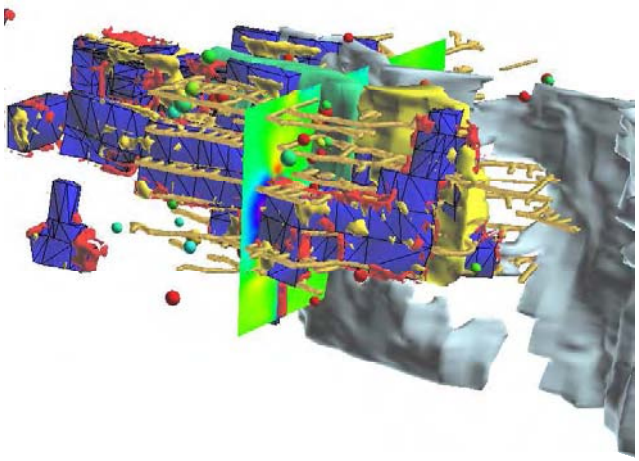

Figure 2: Integrated data image of mining block (scale: top to bottom about 300m)

3 Use of VR for Seismic Data Interpretation

Data fusion provides a "new" view of existing data. It enhances the identification of hidden relationships or discovery and explanation of complex data interdependencies. Seismic and microseismic data patterns are complex, come in large volumes from several years of seismicity monitoring, and each event involves more than a dozen measured or interpreted parameters (seismic moment, stress drop, source size, location in space and time, etc.). The interpretation of seismic data therefore constitutes one of the most complex forms of mining data and thus requires an integrated approach to data interpretation. Most importantly, proper data interpretation depends on bringing together experts with vastly different backgrounds and expertise, including experts from

seismology, geology and structural geology, geomechanics, (geo-) statistics and mining engineering. Collaborative, immersive VR therefore lends itself ideally for seismic data interpretation.

The Canadian Rockburst Handbook (Kaiser et al.1996) provides the background for understanding of seismicity and its effect on rock support. It also provided a general approach for the development of seismic data interpretation tools for support design in deep level hard rock underground mines. The Rockburst Handbook was the result of a 5-year study of the Canadian Rockburst Research Program (CRRP) funded by the Mining Research Directorate (MRD, CAMIRO and its Canadian and international, industrial sponsors), the Ontario Ministry of Northern Development and Mines and the Natural Sciences and Engineering Research Council (NSERC). The study reviewed worldwide support practices in burst-prone grounds and developed fundamental knowledge for the understanding of seismicity-induced failure mechanisms. An empirical database of rock damage and support performance under actual rockburst conditions was compiled and used to establish important relationships between seismic source magnitude and distance, initial excavation conditions, amount of rockburst damage and predicted support performance. Scaling laws (relationship between seismic source parameters, distance and ground motion) were established for major underground mines in the Canadian Shield. A seismic hazard map concept was developed in the form of Mine Map Overlays (MMO) to project anticipated hazards to mine infrastructure at various development or production levels.

The implementation of this approach was, however, hampered by severe limitations in overcoming the threshold of data integration and interpretation. It was simply too time-consuming to build realistic geological models, combine them with stress models and superimpose the effect of seismicity (rockmass degradation and dynamic loading) at that time. Now, with advanced computing, data integration and visualization capabilities in a VR environment, these barriers and obstacles have been removed.

The approach adopted for seismic data interpretation in this paper separately examines the effects of large seismic events (rockbursts) and those of microseismic events (rockmass degradation). Seismic events cause sudden and large scale hazards with immediate consequences whereas microseismicity cause long-term hazards through its cumulative effects in degrading the rockmass due to cumulative rockmass damage.

Understanding seismic events from mining safety and enhanced production point of view enables identification of zones of potential seismic activity and the characteristics of seismic aftershocks. This in turn enables one to estimate consequences of additional loading on mine structures in order to select appropriate support systems based on the level of anticipated hazard and location. Through the power of the VR the Geomechanics Research Centre (MIRARCO) has developed various approaches to interpret seismic and microseismic data patterns. Many of these approaches are supported by plug-ins developed for GoCAD™ or other software packages.

The power of the VR for the interpretation of seismic data is the ability to display large volumes of data and different types of data in a multi-dimensional form (e.g. event magnitude, damage location, damage intensity (seismic clustering; Falmagne, 2000; Falmagne et al., 1998)) and, most importantly, in time sequence (called time-links below).

4 New dimension in seismic and micro-seismic data interpretation

4.1 Background

The results presented in this paper are the outcome of a joint collaboration between INCO Mines Technology Department and INCO's Creighton Mine, and MIRARCO, Sudbury, Ontario. Creighton Mine has been in operation for over 100 years and long-range plans are under review to mine well below the 2,500-m horizon. Associated with this long history of operation and depth are both stress and structurally related seismic activities monitored by a full-waveform Hyperion Microseismic System (ESG, 2000) since November 1995.

Creighton Mine has de-stressing and extraction sequence protocols in place to mitigate stress-induced seismicity such as strain and pillar bursts. The gains of the de-stressing procedure are further enhanced with proactive designs and installed support that minimizes the effects of any dynamic stress-induced events. In general, stress-driven seismicity is well understood and controlled. However, Creighton mine, as most other mines, is significantly affected by discrete geological features as shown in Figure 3. The influence of these structures, shears, faults and dykes, is complex and less understood, particularly the mine-wide interaction between mining blocks needed to be investigated in more detail.

Experience at the mine, supported with several years of seismic monitoring records, shows that both microseismicity (MS) and seismicity are often located along these discrete, characteristic geological structures (Vasak and Neumann, 1999). Planes of seismic activity include geological "planes of weakness" (e.g., shears, faults, weak contacts and

dykes) and features attracting stress (e.g., strong dykes, contacts with stiffness contrast). The role of these geological structures in causing seismicity is poorly understood and they are often only linked to seismic activity after the fact.

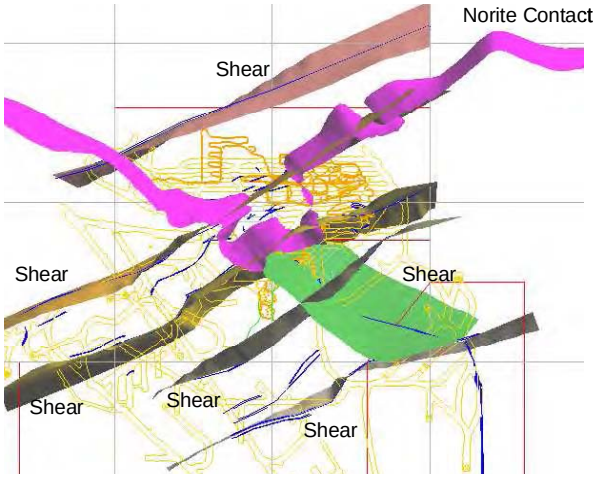

Figure 3: Major geological structures at Creighton Mine (Vasak et al., 2004)

There is a need for a better understanding of the interaction among the discrete geological structures (faults and shear zones), ubiquitous joint zones and mining-induced stresses, for both economic and safety reasons. To arrive at a better understanding of the complex stress and structural geology conditions at the mine, the micro-seismically active structures had to be identified in space, from the vast microseismic records accumulated at the mine over the years, and the time sequence in activating zones of seismic activity had to be understood.

Large magnitude events are often interpreted as fault-slip events along pre-existing structures. This interpretation may be valid for some of the observed events when these events are clearly associated with large-scale geological structures, as is typical for earthquake scenarios. However, in mining, such structures are often created gradually as mining creates degrees of freedom for movements along weakness planes. Hence, microseismicity may be associated with smaller-scale, non-continuous structures that contain rock bridges. Only after sufficient deformation has accumulated are large-scale features created. Structures, which deviate from the typical fault-slip mechanism model and involves fracture of intact rock, must also be readily identified from the MS data. Details of sources of seismic and microseismic events can be found in Vasak et al. (2004).

In the VRL, we are now able to better examine the evolution of complex and large volumes of seismic and microseismic data and understand the spatial and time evolution better than ever before. The VR technology has enabled us to develop procedures and tools to effectively interpret seismicity and its impact on workplace conditions. This procedure is illustrated by Figure 4, showing how seismic data is used to identify zones of rockmass damage (volumes of degradation), active planes (planar features of degradation or movement), time evolution (seismic matrix and probability tree), and impact on mine (hazard maps and monitoring); all to enhance work place safety and to assist optimal production decision making.

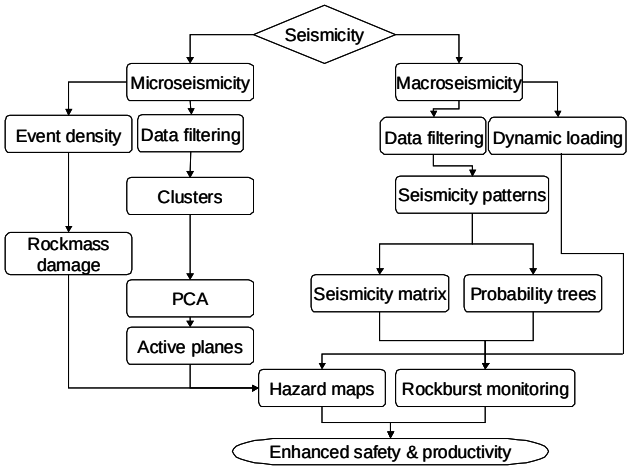

Figure 4: Procedure for interpretation of seismic and microseismic data (PCA = principal component analysis)

4.2 Seismic data visualization and utilization: Time-link and Probability trees

Our interpretation of seismic event sequences presented here is based on the hypothesis that subsequent events may be related, i.e., subsequent seismic events can be "connected in space" and visualized as a time sequence chain. This chain or time sequence vector string is called "Time-links" (Figure 5).

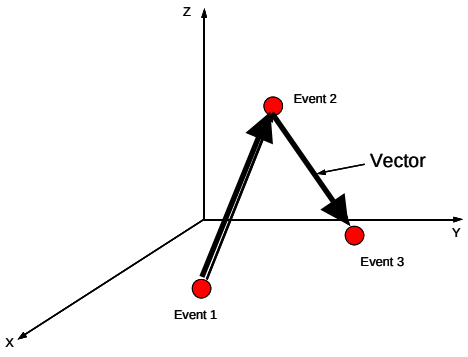

Figure 5: Time-link concept showing event-connecting vector string

Of course, it is extremely important to disconnect unrelated events, e.g., those that are related to a blast rather than a precursor. To ensure that seismic events are not blast-induced or related, blast events and any seismic events occurring within blasting times are filtered out from the database and not connected (broken links). Connections between events may also have to be broken if there is no physical or geological reason for linkages. Redundant links can be identified by experienced workers such as the ground control engineer at the mine.

Time-links enable tracking of seismic migration patterns and can be related to changes in mining geometry. The time-link concept is used to interpret seismic migration patterns visually as illustrated for a given time window by Figure 6.

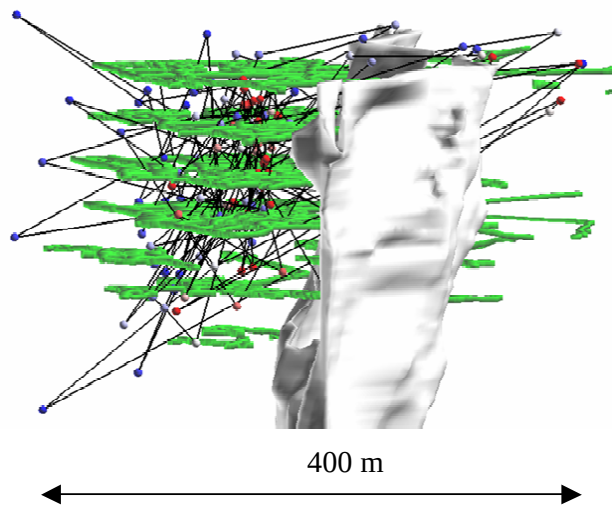

Figure 6: Time-links showing linkage of stress-induced activity in the immediate stoping area (area with high event density in centre of image) to relatively remote seismicity in hanging wall (left) and behind or inside dyke (right)

In geomechanics, it is often assumed that seismicity is primarily related to stress changes and changing mine geometry (ore extraction). While the seismicity in the hanging wall (Figure 6) may well be related to stress changes due to mining in an orebody (not shown) on the left side of the developed zone, the seismicity inside or behind the dyke is remote (>100 m) from any mining and cannot be explained by excavation-induced stress changes (the stress change calculated by continuum models at these locations is <<1%). However, cause and effect can be clearly detected by visual inspection of time-link images.

The observed interdependence of seismicity can be attributed to deformation-controlled processes. This can best be understood by a railway analogue. When the locomotive starts to move, cars in the immediate vicinity react while cars at the end of the train do not yet know that the locomotive is moving. They eventually will "get connected" and feel the pull of the engine. The opposite is true when the train decelerates. Similarly, there is a periodic pull-push effect when the extraction ratio in a mine increases. The resulting interaction process is illustrated by the time-links. In other words, the large-scale response of a mine to mining can be effectively visualized even if it cannot be modelled[1].

We introduced two means to characterize the above-described interaction or "cause and effect" process: (1) seismic migration matrices, and (2) probability trees.

4.2.1 Time-link matrix

Figure 7 shows time-link and seismic migration patterns at Creighton Mine after filtering blast-related and other unrelated events.

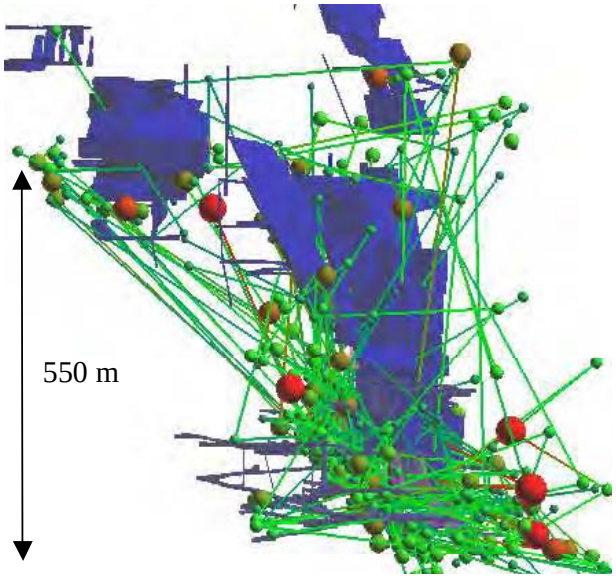

Figure 7: Seismic migration patterns after filtering blast and other unrelated events (Vasak and Thibodeau, 2003)

A close examination of the seismic data reveals that the mine can be divided into blocks characterized by typical, interrelated seismic migration patterns (Figure 8). Events migrating within blocks are associated with short inter-event distances and time intervals whereas longer inter-event distances and time intervals characterize inter-block event migration.

Migration of events within and outside blocks can be statistically examined and seismic migration matrices

[1] Note: This process cannot be simulated by continuum models; discontinuum models, like 3DEC, could simulate this process but the required block geometry is normally not sufficiently known (see below: active plane detection).

and probability trees established (Table 1 and Table 2)[2].

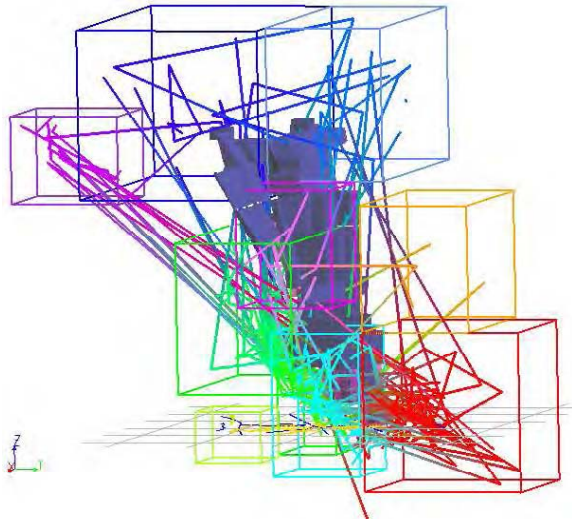

Figure 8: Seismic blocks based on seismicity migration pattern

Table 1 Seismic migration matrix for four seismic blocks; considering events ≥ 2.2 Nuttli magnitude

Aftershock Activity Matrix for Defined Regions	Block #1	Block #2	Block #3	Block #4
Block #1				
Probability	***0.57***	***0.14***	***0.29***	
Inter Region Probability		***0.33***	***0.67***	
Distance (feet)	370	1430	590	
Delay (hours)	7.258	3.078	0.524	
Relative Mn change	-0.95	-1.50	-1.15	
Block #2				
Probability		***0.64***		***0.18***
Inter Region Probability				***0.50***
Distance (feet)		98		622
Delay (hours)		0.069		10.253
Relative Mn change		-0.74		-1.05
Block #3				
Probability			***1.00***	
Inter Region Probability				
Distance (feet)			128	
Delay (hours)			4.425	
Relative Mn change			-0.85	
Block #4				
Probability		***0.43***	***0.14***	***0.43***
Inter Region Probability		***0.75***	***0.25***	
Distance (feet)		294	138	140
Delay (hours)		1.308	9.756	1.429
Relative Mn change		-0.93	-1.00	-0.27

A seismic migration matrix is a summary of statistical seismic inter-block activity information. It provides information about anticipated aftershock characteristics such as location in space, distance from main event, delay time and magnitude. An example of a seismic migration matrix is shown in Table 1. In this example Block 1 and Block 2 have about as many aftershocks within as between other blocks. Block 3 is the most seismically active with 100% of the time-links within the block. Seismicity in this block has no impact on other parts of the mine. Block 4 shows the highest aftershocks migrating to other blocks (57%).

4.2.2 Probability trees

Probability trees provide a means for more detailed tracking of seismic event behaviour within and between blocks in the seismic matrix. A probability tree generated for a given seismic block tracks the likely location in space of its aftershock, the distance to aftershocks from the main event, the time-lapse between major event and aftershock, and the probable magnitude of the aftershock. Table 2 is an example of a probability tree for Block 1 of the seismic matrix shown in Table 1. Fields in Table 2 again provide: number of time-links, interregional probability, distance, delay and the anticipated change in magnitude relative to magnitude of the event in the source block.

Table 2 Probability tree for seismic Block 1 using events ≥ 1 Nuttli Magnitude)

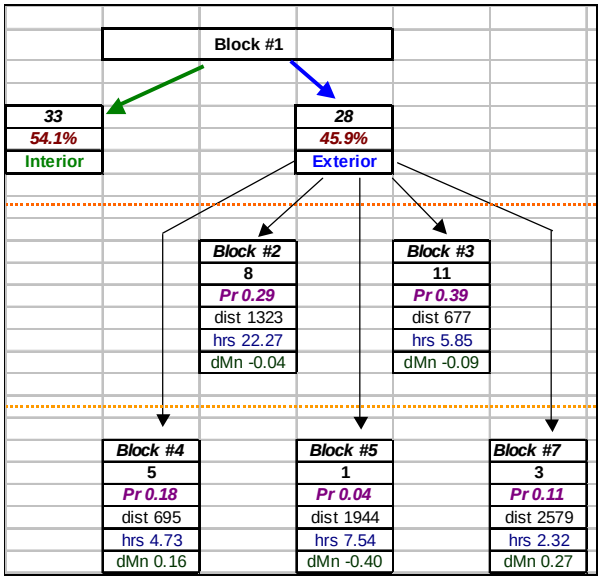

By nature, seismic migration pattern matrices and probability trees identify hazardous work areas in the event of seismic activity based on historical data. They can be used to formulate re-entry policies to enhance worker safety and to support work force allocation during periods of seismic activity as long as data from the past is representative of the future. Hence, seismic pattern matrices and probability trees should be frequently updated and calibrated to remain useful.

[2] Fields in tables provide number of time-links, interregional probability, distance, delays and anticipated change in magnitude relative to magnitude of event in source block).

5 Seismic Hazards

In underground mining, there are two fundamental hazards to be considered: (1) rockmass degradation due to rockmass damage by micro-seismic and seismic events, and (2) dynamic loading or shakedown due to seismic wave propagation.

5.1 Rockmass degradation due to micro-seismicity (MS)

Such degradation can be diffuse (density increases with time) or along planar features (as seismically active planes develop with time).

The following analysis approach for MS data is based on the hypothesis that MS and seismic events are time and spatially related and occur in natural clusters. Spatial plots of microseismic events, shown as migrating clouds (e.g., Figure 9), illustrate mining-related stress migration but do not reveal the full impact on the rockmass and on excavation stability unless proper "filtering", data integration and visualization techniques are used to identify interrelated patterns and trends. Based on research work by Falmagne (2001) on the effect of event clustering and related rockmass damage, we adopt here a novel way of combining space-time event density, agglomerative hierarchical clustering (AHC) and principal component analysis (PCA) in a VR environment for the identification of high-density zones (consequence of cumulative MS effects) and for the identification of planes of microseismic activity (active planes).

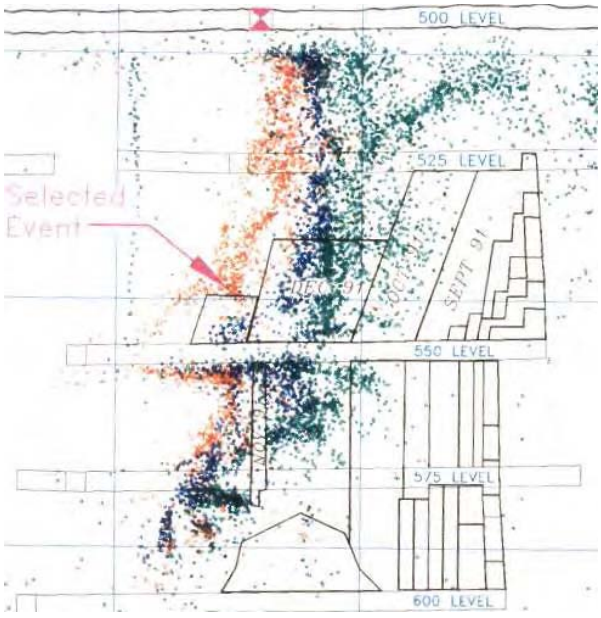

Figure 9: Unprocessed microseismic data as clouds of points in 3D space evolving during three mining steps (green to blue to red)

5.1.1 Diffuse micro-seismicity – rock mass degradation

The MS (or crack) density is used to identify areas of rock mass degradation as a result of cumulative damage by MS events. Each microseismic event implies a new crack or extension of an existing crack. Some filtering out of random events (outliers) or events that are due to stress near drifts or other infrastructure may be required to identify mining-induced MS density patterns (particularly, if the primary objective is to examine structurally induced seismicity).

Filtering is also important for the application of the principal component analysis (PCA), a method routinely used in microseismic data analysis. The success of a PCA in defining realistic planes of seismic activity depends on how well natural clusters are identified. In well-defined clusters there should be little or no random objects between them. The presence of random objects between clusters results in chaining or merging of unrelated clusters.

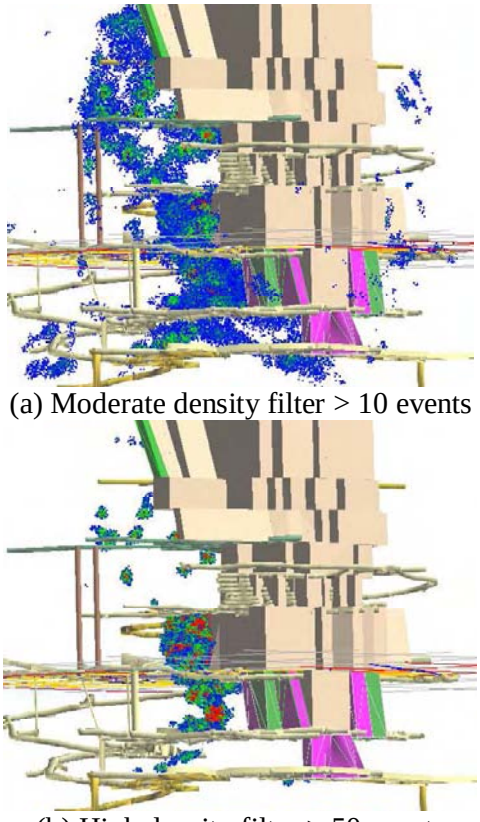

(a) Moderate density filter > 10 events

(b) High density filter > 50 events

Figure 10: Effect of density counts on cluster size

A microseismic density number is assigned to each event and is defined as the number of MS counts in a search sphere of 10-m radius. Events with no neighbours or low number of events (defined by analyst) are dropped (cause no significant rock mass

damage). Discrete clusters emerge after the filtering as shown in (Figure 10). Clusters become more discrete with increasing number of neighbours of events. Discrete clusters identify areas of significant rockmass degradation

5.1.2 Identification of seismically active planes

As indicated above, to understand the time-linkages between internal and remote seismic responses, it is necessary to identify (geological) structures that may transmit deformations over long distances. Seismically active planes (SAP) certainly form part of the rockmass structure that is (currently) being deformed. Hence, identification of such SAPs is important to establish a discontiuum model of a mine.

Principal component analysis (PCA) is a common statistical procedure used to transform a number of possibly correlated variables into a smaller number of uncorrelated variables (Johnson and Wichern, 1992). It is based on examining the variance-covariance structure of the data where the first principal component accounts for as much of the variability in the data as possible, and succeeding components account for as much of the remaining variability as possible (Johnson and Wichern, 1992). The application of this method is ideal if there is a good correlation between at least two variables. Poor correlation and large variability in the variables cannot reduce the dimensionality of a data set.

In our context, for a highly scattered MS cloud with no dominant spatial trend, little benefit is gained by doing PCA without pre-processing (cluster identification). As a matter of fact, PCA analysis can be misleading in microseismic data analysis if applied to raw dataset in which planes are not isolated (i.e. planes intersect or are parallel and close to each other). For example, PCA analysis cannot define intersection or closely spaced, sub-parallel, planar clusters. It can also not adequately define the correct planar clusters when chaining (random events between natural clusters) is present due to the tendency of cluster merger.

The application of statistical clustering procedures as pre-processing tools improves the reliability of PCA. This is illustrated Figure 11.a and b where PCA was first directly applied to data containing two intersecting planar clusters (Figure 11.a). In this case, PCA sees the two datasets as one and gives one solution that does not represent the data.

After a clustering algorithm (Ward, 1963) was applied to define the two clusters that make up the data, the PCA correctly identifies the two planar features (called activity planes) (Figure 11.b).

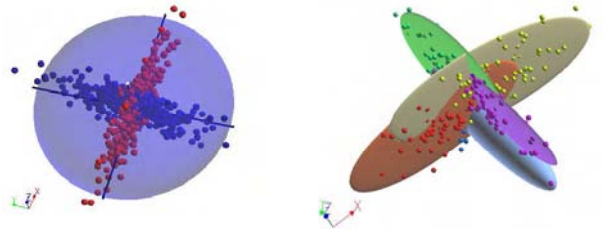

(a) PCA applied to all data fails to define planar features

(b) PCA applied after cluster analysis defines two active planes

Figure 11: PCA and cluster algorithm applied to define active planes

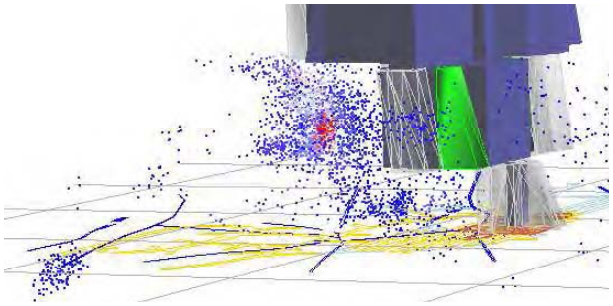

(a) Filtered MS density

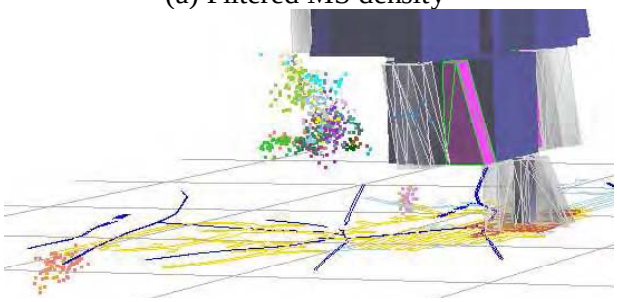

(b) Clusters defined by Ward variance method

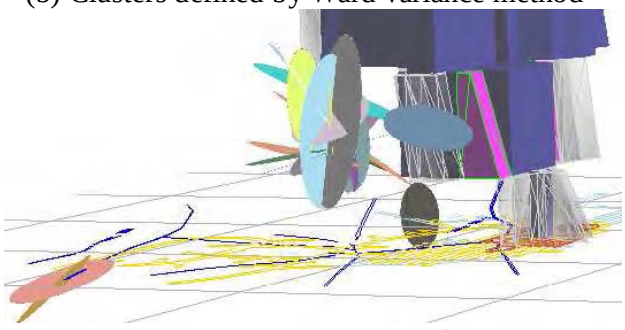

(c) SAPs determined by PCA on defined clusters

Figure 12: Procedure used to determine representative seismically active planes (SAPs).

In our research, we adopted hierarchical clustering using the Ward Variance Euclidean (WVE) method to define natural MS clusters (Vasak et al. 2004). WVE was found to be robust compared to other clustering algorithms, i.e., it is less affected by data shape.

An example of SAP determination by applying PCA after cluster analysis is shown in Figure 12. Only

microseismic data from a limited mining block is shown here.

This procedure was subsequently applied to data from an area of the mine where there was concern about future rockburst activity and the resulting 247 SAPs are shown in Figure 13. This figure highlights how visualization can be combined with trend detection tools to assist data interpretation (and eventually model building). The general trend of these SAPs was then compared with structures observed and mapped underground in the mine (Figure 14).

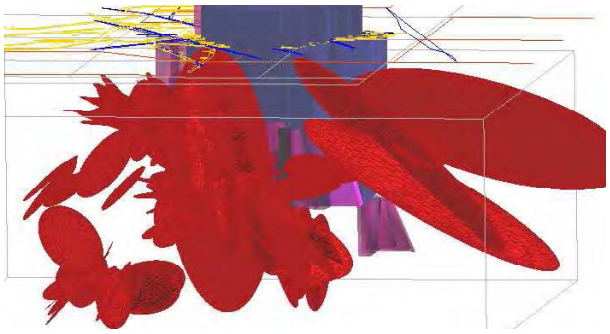

Figure 13: Seismically active planes determined by PCA on 247 microseismic clusters

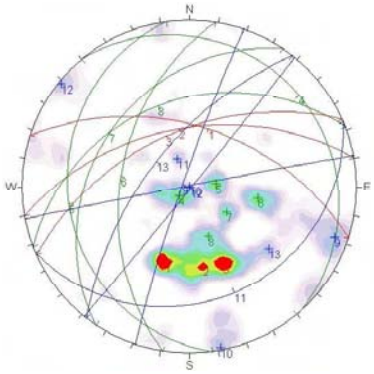

(a) Seismically active planes

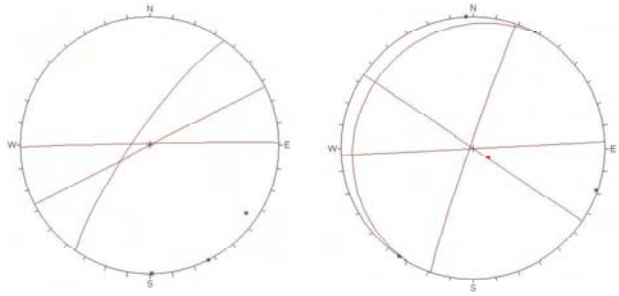

(b) Observed structures and late shears (right)

Figure 14: Comparison of SAPs and observed structures

Note that not all structures are visible or mapped underground, possibly as a result of scale or lack of access, but most likely because these SAPs do not necessarily consist of single structural features (i.e., they represent echelon fracture systems). Despite these limitations there is a fair correspondence between the seismically active planes determined by the above-described procedure and the observed structures.

5.2 Damage caused by dynamic loading due to seismicity

When a rockburst occurs additional loading in the form of dynamic stress waves are imposed on the walls of mine infrastructure and supports. Marginally stable rockmasses may be induced to fall by dynamic acceleration. Mine structures that were already close to failure (factors of safety close to one) could be triggered to fail by strain bursting or by seismically induced falls of ground as a consequence of this additional loading. The rockmass near structures with higher factors of safety would not fail but the surrounding rockmass will be further damaged and the factor of safety will be reduced.

The consequences of dynamic loading are rockmass fracturing and bulking, as well as shakedown in blocky rockmasses. In the following, we only deal with the effect of dynamic stress (Kaiser et al., 1996; for seismically induced falls of ground refer to same publication). The dynamic far-field stress change modifies the stress near an excavation (by $\Delta\sigma^d$) causing rotating stress concentrations as shown schematically for a circular excavation by Figure 15.

Figure 15: Superposition of dynamic and static stresses increases overall stresses around excavations in the event of seismicity (Kaiser et al., 1996).

The dynamic stress increment (Eqn 1) can be large if the excavation is close to the epicentre of the seismic event. The maximum dynamic stress increment $\Delta\sigma^d$ is given by:

$$\Delta\sigma^d = n\, c_s\, \rho\, ppv_s \qquad [1a]$$

where c_s and ppv_s are the velocity and peak particle velocity of the shear wave, respectively. The multiplier n depends on the dynamic wave incidence angle: $n = 4\cos 2\theta$ where θ is the angle between the direction of the incident wave and any location on the excavation walls ($-4 < n < +4$). Consequently, the maximum dynamic stress increment $\Delta\sigma^d_{max}$ is:

$$\Delta\sigma^d_{\max} = \pm 4\, c_s\, \rho\, ppv_s \qquad [1b]$$

Taking into account the static stress at the excavation boundary, the resultant maximum stress for a shear

wave arriving at an angle θ is obtained by superposition:

$$\sigma_{\max}^{(s+d)} = 3\sigma_1 - \sigma_3 + n\, c_s\, \rho\, ppv_s \qquad [2]$$

Since the *ppv* depends on the magnitude of the event M_N and the distance R from the epicentre of the event, the amount of dynamic loading imposed on a mine structure depends on these two factors.

Sharma and Judd (1991) empirically established a relationship between peak ground acceleration *ppa* at the surface, overburden depth and damage severity using earthquake data from around the world. The amount of damage suffered by a target depends on the intensity of ground motion, which is measured by particle displacement, frequency, *ppa* or *ppv*. Peak particle acceleration and peak particle velocity are the ground motion measurement parameters commonly used. Peak particle acceleration is related to peak particle velocity. In civil engineering design *ppa* is traditionally used to design for dynamic loading because building codes (www.eqhazmaps.usgs.gov) describe how much horizontal force a building or other structure should be able to withstand during an earthquake. In mining or seismological context *ppv* is commonly used because most seismic monitoring systems measure *ppv* (www.scotland.gov.uk).

Scaling laws can be established to estimate seismic induced damage based on dynamic stress concentration. A scaling law (Eqn 3) relating event magnitude (M_N on Nuttli scale), *ppv* (m/s) and distance to event (R in metres) was established from data from Canadian mines (Kaiser et al., 1996):

$$ppv = \frac{c^* 10^{a^*(M_N+1)}}{R} \qquad [3]$$

For Creighton Mine, Kaiser et al. (1996) determined constants a* and c* as 0.3 and 0.5, respectively. Figure 16 shows the corresponding relationship between M_N, R and *ppv*. The equivalent maximum induced stress change $\Delta\sigma^d_{max}$ at the excavation wall ranges from ~50MPa (for ppv = 3m/s) to ~1 MPa (at ppv = 0.03m/s).

Locations with seismically induced damage are plotted in Figure 16 and were used to calibrate the approach described above and then used to establish hazard maps (note: some are related to stress others to shakedown).

6 Seismic Hazard Maps

The objective of monitoring seismicity at mines is to enhance worker safety and to reduce risk in general, e.g., to minimize production interruptions. These goals can be achieved by various means, all involving some form of data analysis to produce practically useful outputs (e.g., re-entry policies, stoping sequences, etc.). Here we focus on means to identify hazards related to infrastructure, i.e., the development of hazard maps.

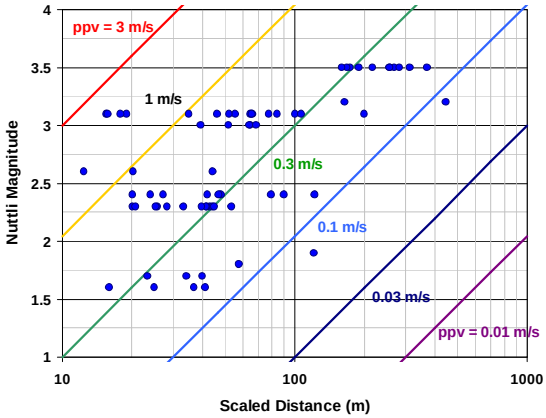

Figure 16: Ground motion intensity chart for site-specific parameters; locations experiencing damage to excavations are also shown.

Hazard maps provide an overall picture of the stability conditions in a mine for planning and operational control purposes. They show hazardous areas in the mine by identifying degraded rockmass zones, seismically active structures such as faults, and areas of high impact by seismic waves (dynamic stressing). Degraded zones of rock, if close to excavations and infrastructure crossing seismically active planes or active fault zones will require higher support levels and mining sequences must be properly managed to minimize impact on hazardous areas. When planning, new mine infrastructure may be located outside hazardous zones if this is economically acceptable.

In this study, three hazard factors were used to develop hazard maps:

- MS degradation with MS density as an indicator of level of rockmass degradation
- Seismically active planes as indicators of both localized rockmass degradation and rockbursts source potential
- Dynamic loading due to seismic stress

More factors will be included in the future.

6.1 MS degradation hazard

The space-time density procedure was used to define four density levels shown in Table 3. The four MS density levels correspond to four hazard levels due to reductions in rockmass quality RMR (Bieniawski, 1973).

Table 3 Site-specific hazard rating of MS degradation factor (ratings must be calibrated at each mine)

No. of MS events, R=5m	Change in RMR ΔRMR (from RMR=85)	Rating	UCS_{rm}	Hazard impact
<5	0	Very Good	100	Negligible
5 - 10	-15	Good	40	Low
10 - 50	-25	fair	20	Moderate
≥ 50	-35	Fair to poor	10	High

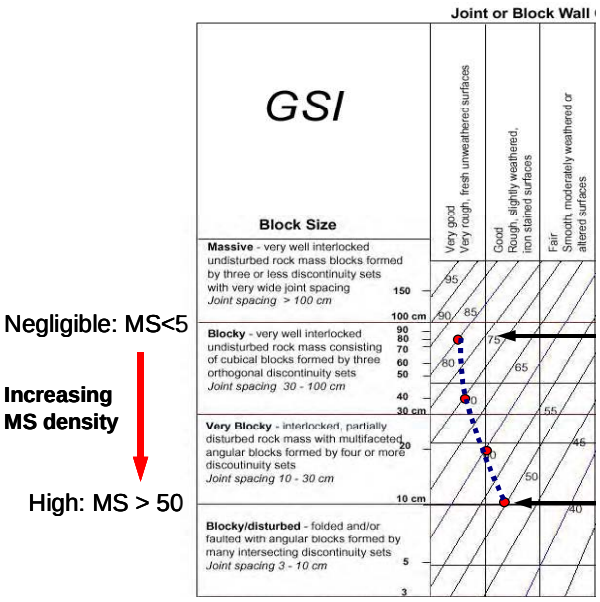

Figure 17: Effect of increasing MS degradation on rockmass quality

Increasing MS or induced fracture density levels causing rockmass degradation can be primarily viewed as a gradual reduction in block size. This is illustrated schematically in Figure 17 by example on the Geological Strength Index (GSI) chart (Hoek et al., 1995; Cai and Kaiser, 2003).

In this manner, the degradation process and impact on critical infrastructure can be visualized as shown in four time windows by Figure 18. This figure clearly shows how infrastructure is gradually impacted by rockmass degradation and where potentially additional rock support might have to be placed.

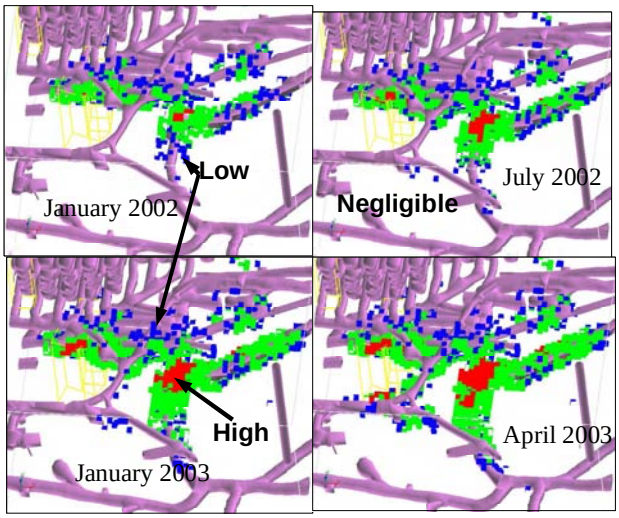

Figure 18: MS degradation hazard rating evolution (blue to red = low to high degradation hazard)

6.2 Seismically active plane (SAP) hazard

The hazard posed by SAPs increases as degrees of freedom for movement increase and thus when SAPs interact amongst themselves and with excavations. The mere presence of SAPs alone is a sign of potential hazard. Discrete structures are often signs of loosening as reflected in the stress reduction factor *SRF* in the Q-system (Barton et al., 1974). When SAPs intersect near an excavation, wedges or wedge-like structures may form and thus increase the hazard for falls of ground.

The hazard posed by the SAPs can be viewed as short to medium-term and represents a tendency of planes to slip or wedges to form. The SAPs may be discrete features or zones of ubiquitous fracturing. Generally, the higher the numbers of planes present at one location in the rock mass, the higher the hazard for drift instability, but also for fault-slip type movement (or rockbursting). Hence, the intersection lines of SAPs provide a means to rate and locate the hazard levels due to localized seismic activity. The intersection lines corresponding to Figure 13 are shown as in Figure 19.

If the active planes are considered as analogous to zones of (ubiquitous) joints, then the hazard levels can be estimated using the joint set number (J_n) in the tunnelling quality index or Q-system (Barton et al, 1974) (Eqn 4). Increasing J_n indicates reduction in Q and implies an increasing degree of freedom for block movement, hence, increasing hazard.

$$Q = \frac{RQD}{J_n} \bullet \frac{J_r}{J_a} \bullet \frac{J_w}{SRF} \qquad [4]$$

where RQD is the rock quality designation, J_n joint set number, J_a the joint alteration number, J_w joint water reduction factor and SRF stress reduction factor. Table 4 shows the assumed relationship between number of joint sets and their equivalency in terms of SAPs and the adopted hazard impact rating.

Table 4. Hazard rating for SAPs

Joints				Faults	
No. of joint sets	Equivalent No. of SAPs	Jn	Impact rating	# of faults	SRF
Random	Random	1	Negligible	0	1
1	Close to a SAP	2	Low	1	2.5
1+ random	1 SAP intersecting	3	Moderate	2	5
2+ random	At least 2 SAPs intersecting	6	High	≥ 3	7.5

.

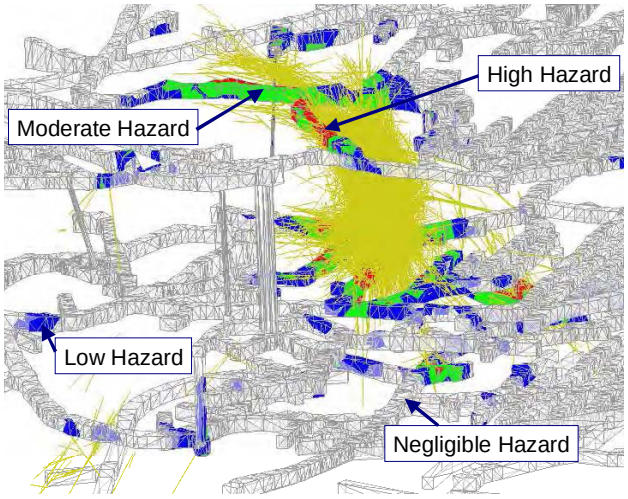

Figure 19: Active planes impact rating assuming, planes are ubiquitous joints.

These hazard impact ratings have been painted on drifts or other mine infrastructure in Figure 19. Similar hazard maps can be generated using active planes or faults numbers or *SRF* ratings. Again, visualization of this nature provides an immediate image of potential hazard locations. This provides the ground control engineer a tool to focus inspection and possibly support rehabilitation efforts.

6.3 Dynamic stress hazard

Table 5 presents the adopted dynamic stress impact rating and indicates the dynamic stress equivalents.

Table 5 Dynamic stress hazard rating

Hazard	Impact rating			
	Negligible	Low	Moderate	High
Seismicity ppv (m/s)	<0.1	0.1 – 0.3	0.3 - 1	≥1
Dynamic stress equivalent $\Delta\sigma^d$ (MPa)	< 3	3 - 10	10 - 32	≥ 32

Figure 20 presents a typical dynamic stress impact hazard map for a seismicity threshold at 3.5-Nuttli magnitude. The figure shows the iso-surface containing historical events exceeding the threshold and the corresponding hazard levels on two selected sections in the mine. Again, visualization assists in identifying potentially hazardous locations.

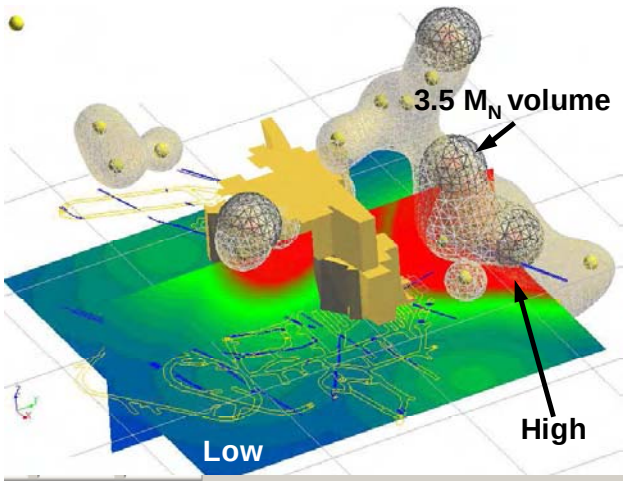

Figure 20: Stress hazard map for a threshold at 3.5 Nuttli magnitude

6.4 Combining individual hazards to form overall hazard maps

The previously described individual hazards do not act independently and it is thus necessary to combine hazards to account for all possible hazard factors at a given location. Such maps should show effects of individual factors as well as the combined hazard.

A hazard map accounting for MS degradation, SAPs and stress effects is shown in Figure 21. Table 6 shows the rating of the individual hazard factors and preliminary, combined hazard factor ratings used in the development of this combined hazard map. Table 7 provides the combined impact factor ratings. Four hazard levels are identified as 1 (Negligible) to 4 (High).

As indicated in the table headings, the proposed ratings are preliminary in nature. Further research and

field calibration is required to verify and improve the rating system.

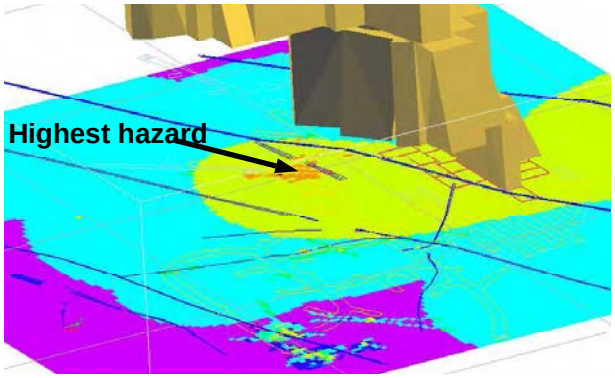

Figure 21: Composite hazard map with 3.5 Nuttli magnitude event

Table 6 Preliminary rating of combined hazard factors

Hazard factor	Hazard rating description			
MS degradation	Negligible (N)	Low (L)	Moderate (M)	High (H)
SAPs	Negligible	Low	Moderate	High
Dynamic stress	Negligible	Low	Moderate	High
Hazard rating weighting	0	1	2	3

Table 7 Preliminary composite hazard ranking matrix

Combined impact rating description		Combined ratings	Hazard ranking
Negligible	1	(N, N, N)	1
Low	2a	(L, N, N)	2
	2b	(L, N, N)	3
	2c	(L, L, N)	4
Moderate	3a	[M, (L or N), (L or N)]	5
	3b	[M, M, (L or N)]	6
	3c	(M, M, M)	7
High	4a	[H, (N, L or M), (N, L or M)]	8
	4b	[H, H, (N, L, or M)]	9
	4c	(H, H, H)	10

Nevertheless, Figure 21 illustrates how the results of such a hazard assessment process can be visualized and quickly and effectively communicated to those working underground and making operational decisions. Since the maps can be up-dated in real time, they can also be used to guide re-entry protocols. They can form an integral part of a sound emergency preparedness program.

The seismic hazard map concept and applications discussed above can be specifically applied to drifts. In assessing drift performance and support demand both stress and drift orientation (direction) are to be considered. Seismic hazard is an additional factor that can be added in burst prone grounds. The following section discusses a methodology for quickly identifying drifts at risk for both planning and rehabilitation purposes.

7 Drifts at Risk

Support demand depends on a wide range of factors, including initial and induced stress conditions, stope geometry, mine sequencing, rockmass quality, geological domain characteristics, joint set properties and time. Seismicity is another factor that can be added as shown above. Typically, these factors will vary significantly across a given mining horizon.

To address the needs of industry, MIRARCO completed the first stage of a Drifts@Risk suite of tools for use in Laurentian University's VR facility. These tools encapsulate some of the research of the Geomechanics Research Centre on geomechanics mine design during the last decade. The Drifts@Risk modules enable engineering, geology and production teams to apply these techniques in a matter of minutes allowing comparisons with visual or quantitative field observations.

Drifts@Risk is a wizard developed to assess stress-(depth-of-failure) and wedge-related instability of mine drifts. Drift geometry, geological structures, and results from stress analyses are combined to determine risk levels (Drifts@Risk) and then visualized in a similar manner to hazard maps; except, in this case, the drifts are painted according to the anticipated support (as defined below) rather than hazard type (Figure 22):

- less than standard support required (LS) - blue
- standard support adequate (SS) - green
- rehabilitation anticipated and heavy support (HS) required - yellow
- rockburst potential high; special burst-resistant support recommended (RS) – red

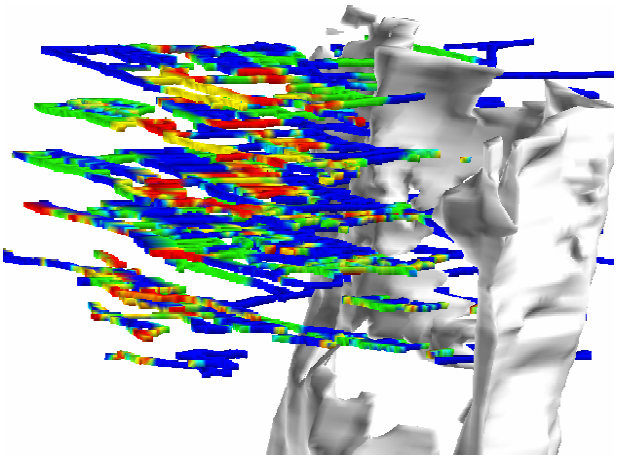

Figure 22: Drifts@Risk visualization by anticipated support type

Drifts@Risk allows mine engineers to evaluate several aspects of geomechanics design of an orebody, including:

- Placement of infrastructure: facilitated by quick means to evaluate geomechanics influences in an interactive manner within a VR framework.
- Support selection: based on selected site-specific geomechanics constraints, the portion of the total drift lengths that fall into pre-defined Risk Level categories can be determined (Feet@Risk). This is illustrated by Figure 23 for a drift affected by mining nearby stopes in 8 mining steps. Heavy spalling and some rockbursting are immediately anticipated. As mining progresses, the length of drift affected by bursting grows to about 70m in mining step 2. After step 3 significant yielding is anticipated, requiring deformable support over a length of about 140m.

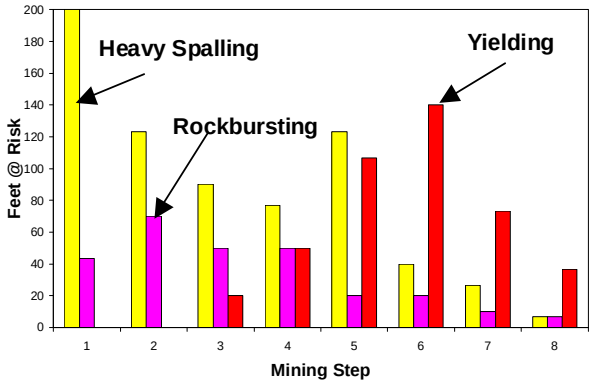

Figure 23: Feet@risk (see below) as mining passes drift (Alcott et al. 1999)

- Support costing: based on support chosen for anticipated hazard types and levels.

Traditionally, many mine operations have relied on a systematic, standardized support design approach, which tends to over-look variability on support demand. As a result, sections of the drift may be over-supported (conservative design) whereas other sections may be inadequately supported for long-term demand (costly rehabilitation may be required).

To assist in support design, a Feet@Risk module was developed which builds on Drifts@Risk stability results. The Feet@Risk analyzer determines the portion of the total drift length that fall into predefined Risk Level categories (representing a range of support-type categories), the selection of which is dictated by combinations of stress damage or wedge failure characteristics (and possible seismicity in burst-prone mines). The support categories are painted onto the infrastructure, as illustrated by Figure 22, to visualize support requirements along the drift. The resulting images can then be utilized by the ground control staff during underground inspection to first calibrate the approach and then assist in evaluating local risk levels and support requirements.

A support category analysis for one of the levels in Figure 22 is presented in Figure 24. The anticipated support and rehabilitation costs can readily be determined based on such information by multiplying lengths by support costs for each support type. Comparisons between two levels showed that the support costs (for initial installation only) for a favourable layout was about $400,000 lower than for a level with a less favourable layout.

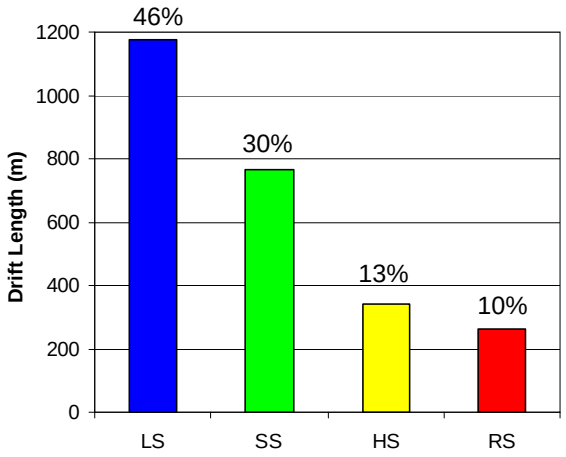

Figure 24: Feet@Risk based on Drift@Risk procedure (Henning et al., 2003)

Scheduling of development and advance rate estimates can be optimized considering total lengths of drift requiring a specific support type and timing within the production schedule.

The benefits of such integrated data analyses procedures can be significant, including less over-

support, reduced rehabilitation demand, and improved budgeting of material and labour expense. Worker safety is also enhanced as potential hazards can be proactively avoided.

8 Concluding Remarks

3D virtual reality visualization has become a critical element of integrated data processing. As illustrated above, visualization combined with mine modelling, integrating complex mining-induced stress fields, rockmass variability (geology and structures), cumulative microseismicity effects, that alters the virgin rockmass, and effects of seismicity, allows us today to gain critical insight into the response of an orebody to increasing levels of extraction. It allows us to identify and understand the evolution pattern of rockmass degradation, the mobilization of weakness zones (seismically active planes), time-links in seismic patterns, and their distribution and impact on operations (hazard levels).

With 3D VR, we have succeeded in advancing our understanding of the complex nature of mirco-seismic and seismic event migration. VR combined with an appropriate software environment allows us to fuse large volumes of data and to visualize what normally is presented in graphs and tables and thus only accessible to the patient reader or the expert. By presenting geomechanics data in a visual form, communication is enhanced and miners, engineers and management can simultaneously understand the result of advanced science and engineering.

The ability to rapidly integrate complex data sets and to analyse them visually has enabled us to develop procedures and tools that offer new dimensions in the interpretation of seismic data. It has also allowed us to calibrate models more effectively and to translate research results into practically useful tools.

The benefits of these new techniques to a mine are significant:

- in locating critical mine structures (detailed layout design)
- in making preventative support decision and in prioritizing of support logistics
- in enhancing workplace safety by identify hazardous areas in space and time and in developing advanced re-entry policies
- in real-time processing of seismic data to implement such policies as part of emergency preparedness and due-diligence procedures.

Future work aims at incorporating other hazard factors and at the development of risk maps. Risk assessment requires knowledge of factors of safety, which require a handle on both demand and capacity. Hence, it will be necessary to introduce factors that relate to the self-supporting capacity of the rock (rockmass quality) and to the capacity of the support (Support element capacities and behaviour as well as support condition). In this manner, we will eventually, be able to manage risk in a well-informed manner and assess the cost / benefit of both support and mining practices better.

9 Acknowledgement

The research work would not have been possible without the support of INCO Ltd., particularly the INCO Mines Technology Department and Creighton Mine. Special thanks are directed to: Steve Wood, Larry Lauzon, Al Punkkinen, Chris Meandro, Steve Audette and Dr. Robert Tan from Creighton Mine; Brian Maynard, Samantha Espley and Robert Barclay from the INCO Mines Technology Department. Additional support was provided through the following agencies: the Northern Ontario Heritage Fund Corp. (NOHFCo), The Natural Sciences and Engineering Research Council (NSERC) the Ontario Research and Development Fund (OR&DCF), and the Canada Foundation for Innovation (CFI)/ Ontario Innovation Trust (OIT). In addition to the co-authors many current and former students and staff of MIRARCO have contributed to this research and are thankfully acknowledged: B. Anderson, J. Alcott, L. Cotesta, A. Dasys, V. Falmagne, J. Henning, A. Verma and many more.

10 References

Alcott, J.M., P.K. Kaiser, M. Gauthier, D. Nelson and P. Mah, (1999) SHARK: Stability Hazard and Risk Assessment at Placer Dome's Campbell Mine. C*olloque de Contrôle de Terrain*, Val-d'Or, 9 p

Barton, N., Lien R., and Lunde, J., (1974) Engineering classification of jointed rock masses for the design of tunnel support. *Rock Mech.* 6, 189-236.

Bawden, W. F. and Coulson, A.L., (1993) Structural and geomechanical study of Creighton Mine with increased attention focused on the levels below the 6600 level. *Rept. No. MD005*, Queen's University, Kingston.

Bieniawski, Z.T., (1973) Engineering classification of rock masses. T*rans. S. African Institute of Civil Eng. 15*, 335-344.

Cai, M., Kaiser, P.K., Uno, H., Tasaka, Y., and Minami, M., (2003) Estimating rockmass strength and deformation modulus using GSI system – a quantitative approach. *Int. J. Rock Mech. Min. Sci.*, 41(1): 3-29.

ESG (2000) Engineering Seismology Group – Validation of real-time source parameter calculation at Creighton Mine, Sudbury, Canada. *Report Submitted to Inco Mines Research and Mining Research Directorate of Canada, Report* #ESGQN95-01, 22 p.

Falmagne, V., (2001) Rockmass degradation and micro-seismicity, *Ph.D. thesis*, Department of Mining Engineering, Queen's and in Collaboration with School of Engineering at Laurentian University, Sudbury, Ontario, Canada, 401 pp.

Falmagne, V., Kaiser P.K. and C.D. Martin C.D., (1998) Microseismic monitoring and rock mass degradation. In *CD-ROM Proc 100th* Canadian Institute of Mining, Metallurgy and Petroleum publications, Montreal, 8 p.

Fröhlich, B. and Göbel, M. (1999) Virtual reality in the oil and gas industry. In *ERCIM News 37*, Online Edition.Fröhlich, B. and M. Göbel, 1999. Virtual reality for oil and gas industry. ERCIM News, Online Edition.

Henning, J.G., L. Cotesta and P. K. Kaiser, (2003) Geomechanics Design of Underground Excavations Utilizing Virtual Reality. In *Proceedings, 4th International Conference on* Computer Applications in the Minerals Industries (CAMI), 8-10 September 2003, Calgary, Alberta.

Hoek, E., Kaiser P.K. and Bawden W.F., (1995) Support of underground excavations in hard rock. A.A. Balkema, Rotterdam.

Johnson, R.A. and Wichern, D.W., (1992) Applied multivariate statistics. *Englewood Cliffs*, NJ, Prentice-Hall, 642 p.

Kaiser, P.K., McCreath, D.R., and Tannant, D.D., (1996) Canadian rockburst support handbook. *Geomechanics Research Centre*, Laurentian University, Sudbury, Ontario, Canada.

Norsk Hydro, (2003) Case study: Inside reality 3D virtual reality technology. In *Schlumberger Information Systems*: www.sis.slb.com.

Polyakov, V., (1999) Virtual reality in the oil and gas industry. In *ERCIM News 37*, Online Edition: SEED.

Schlumberger F.E., Volz, W., Dorn, G., Fröhlich, B. and Roberts, D.M., (2002) Future trends in oil and gas visualization. In *Proceedings of the Conference on Visualization*, Boston, Massachusetts, pp.567-570.

Sharma, S. and Judd, W.R., (1991) Underground opening damage from earthquakes. *Engineering Geology* 30: 263-276.

Tyler, T., (2003) Q&A Roundtable Editorial. In *Virtual Roundtable of Leading Industry Experts: Visualization, Vol. 5.*

Vasak, P. and Thibodeau, D., (2003) Seismicity used to identify and monitor active weakness planes in relation to assessment. *Paper presented at the eastern Section Annual Meeting, Seismological Society of Americ*a, 19-21 October, University of Toronto, Toronto, Ontario, Canada.

Vasak, P., Suorineni, F.T., Kaiser P.K. and D. Thibodeau, (2004) Hazard Map Approach Using Space-time Clustering Analysis of Mining-induced Microseismicity. *CIM- AGM*, Edmonton.

Vasak, P., Suorineni, F.T. and Verma, A., (2004) Identification of seismically active structures for hazard assessment at Creighton Mine. *Report Submitted to INCO Mines Technology Department*.

Vasak, P. and Neumann, M, (1999) Full-waveform microseismic monitoring. *Report Submitted to Technical Advisory Committee, CAMIRO Mining Division*, Rept #11, 109 p.

Ward, J.H., (1963) Hierarchical grouping to optimize an objective function. *J. Am. Stat. Assoc*: 58, pp.236-244.

www.archive.ncsa.uiuc.edu

www.eqhazmaps.usgs.gov

www.scotland.gov.uk

www.seed.slb

Zeitlin, M.J., (2003) In Virtual Roundtable of Leading Industry Experts: Vol. 5.

UNDERGROUND WORKS IN HARD ROCK TUNNELLING AND MINING

P. K. Kaiser[1] M.S. Diederichs[2], C. D. Martin[3], J. Sharp[4], and W. Steiner[5]

ABSTRACT

The rock mass around an underground opening is subjected to a unique stress path that results in low radial confinement and both tangential loading and unloading conditions near the wall. As a result, the rock mass strength near underground excavations is controlled by failure mechanisms dominating at low confinement. Hence, when constructing underground works in hard rock, two general scenarios are encountered: (1) structurally controlled gravity-driven failures; and (2) stress-induced failure with spalling and slabbing. The former process is predominant when both the radial and the tangential stresses are low, where as the latter is prevalent when high tangential stresses drive rock mass failure. Whereas structurally controlled failures are most frequently observed at shallow depths and slabbing failure is commonly found at great depth, mining and tunnelling experience shows that these failure processes may be encountered at essentially any depth. In this keynote the authors provide an overall framework for assessing the stability of underground openings in hard rocks, regardless whether the excavations are required for mining, nuclear waste or civil engineering applications.

For the prediction of stress-induced slabbing, a bi-linear failure envelope cut-off is introduced. The resulting failure envelope, combined with numerical modelling, is used to determine the depth of failure near excavations and in pillars, and to examine the effect of rock mass bulking of the failed rock on the displacement demand for support selection. An assessment of rock mass relaxation on structurally controlled failure processes is made with respect to support demand and support capacity. This keynote also includes a brief review of violent failure processes, i.e., rockbursting. Where possible, examples from mining and civil engineering projects are provided to illustrate the design challenges of underground excavations in hard rocks. Guidelines for support design are provided.

The findings presented here are intended to assist the practitioner in arriving at more economical solutions and to provide a basis for further research to advance the state of knowledge in this field.

1.0 INTRODUCTION

In both civil and mining engineering, the need to construct underground excavations at great depth is challenging engineers and at the same time opens new frontiers. In mining, depths of 4 km have long been exceeded in South Africa and mining at depths in excess of 2.5 km with elevated horizontal stresses are forcing the Canadian mining industry to arrive at more cost-effective mining methods. The need for more rapid transport links in Europe demand tunnels at the base of the Alps, with tunnelling at overburden depths exceeding 2 km. Underground works at great depth, i.e., in highly stressed ground, provide therefore a natural focus for this keynote lecture. At these depths, the ground is much less forgiving and careful engineering is required to lower the risk to acceptable levels both in terms of safety and economy.

Nevertheless, large permanent underground openings close to surface, for hydropower developments, hydrocarbon storage, transportation structures, water treatment and holding tanks and civil defense openings,

[1] MIRARCO – Mining Innovation, Geomechanics Research Centre, Laurentian University, Sudbury, Ontario, Canada P3E 2C6; Ph +1-705-673-6517; Fx +1-705-675-4838; pkaiser@mirarco.org

[2] Innovative Geomechanics, 105 William Street, Waterloo, Ontario, Canada N2L 1J8; Ph +1-519-578-5327, Fx +1-519-746-7484, ingeom@attglobal.net

[3] Department of Civil Engineering, University of Alberta, Edmonton, Alberta, Canada T6G 2G7; Ph +1-780-492-2332, Fx +1-780-492-8198, dmartin@civil.ualberta.ca

[4] Geo-Engineering Consulting Services, Coin Varin, St. Peter, Jersey, U.K. JE3 7EH; Ph +44-153-448-1234, Fx +44-153-448-1315, geoengineering@cinergy.co.uk

[5] B+S Ingenieur AG, Muristrasse 60, CH-3000 Bern 16, Switzerland; Ph +41-31-352-6911, Fx +41-31-352-7205, w.steiner@bs-ing.ch

still pose new challenges. Even more demanding applications include the disposal of nuclear waste and containment structures for liquids and gases under high pressure. Hence, one section is dedicated to a review of current and future trends in permanent civil engineering underground works. It also focuses on structurally controlled stability concerns when constructing caverns in moderately to highly fractured ground. The final section, addresses some of the challenges facing the civil construction industry when tunnelling at depth.

1.1 Scope

This keynote lecture deals primarily with trends and challenges of underground works in hard rock, in particular with the behaviour of brittle rock. In mining, ever increasing international competitiveness has forced the industry to find innovative and better means to mine at depth. Lessons learned from this environment, where control of the failure process is paramount for economic survival, can also assist in creating permanent structures for civil engineering applications in a more economic manner.

Because of the structure of this conference, the authors have intentionally excluded issues related to excavations in soft rock, underground openings in rocks with pre-dominantly time-dependent behaviour (swelling or squeezing), excavation techniques by blasting or mechanical cutting, and risk or hazard assessment methods. We hope that these and other topics related to underground works are covered elsewhere.

Excavations in hard rock can be categorized into nine classes as illustrated by the matrix of instability modes in Figure 1.1. This keynote covers the entire spectrum described by the matrix from excavations in hard rock at shallow to great depth, and from intact to highly fractured rock ([row 1; column 1] to [3; 3]).

This article is structured into five sections, contributing to an understanding of brittle hard rock failure, the stability assessment of excavations in brittle failing rock, and rock support to control the broken ground when rock mass failure cannot be prevented.

Experience from recent research is summarized in Sections 2 to 4, with primary contributions by M.S. Diederichs, P.K. Kaiser, and C.D. Martin. These sections are addressing critical issues for excavations at moderate to high stress, and in massive to moderately jointed rock (Figure 1.1; shaded matrix elements [1 to 3; 2] and [1 to 2; 3]). Because failure around underground openings occurs where the confining stresses are very low or tensile, the failure criteria discussed in Section 2 are restricted to predict the stability of underground openings and not the behaviour of confined rock. Furthermore, the content of companion sections 3 and 4 are restricted to hard, brittle failing rock, where elastic stress calculations provide an accurate measure of induced stress and where progressive spalling is the dominant failure mechanism.

Section 5 deals with shallow structures of large span, permanent excavations (caverns), with J. Sharp as main contributor (Figure 1.1; matrix elements [2 to 3; 1] and [2 to 3; 2]). Based on an assessment of past experience, the need to fully understand and foresee the likely ground response and its potential behaviour as the primary support component for the underground structure, is explored. Practical guidelines are presented.

In Section 6, some challenges facing the civil construction industry when tunnelling at great depth are addressed, with W. Steiner as primary contributor (Figure 1.1; matrix elements [1 to 3; 2] and [1 to 3; 3]). This section is building on recent experiences from the exploration and planning phases for deep alpine tunnels in Europe.

1.2 Acknowledgements

This research was supported by the Natural Sciences and Engineering Research Council of Canada, the Ontario Government with a grant to the Chair for Rock Mechanics and Ground Control, the Canadian Mining Research Organization (Mining Division), and the hard rock mining industry of Northern Ontario. This article also draws on research work that was undertaken at AECL's Underground Research Laboratory and summarizes work of many graduate students and research staff of the Geomechanics Research Centre at the Laurentian University over a period of more than ten years. Their contributions, especially of those mentioned in the list of publications, are gratefully acknowledged. Directly or indirectly, Dr. E. Hoek has stimulated much of our work and deserves special recognition for his contributions and encouragements. Section 5 contains summary data from a program supported by UK Nirex. Their support and contribution are gratefully acknowledged. Many people made this section possible through published data and discussion. Particular acknowledgements are due to Professor L. Endersbee, Dr. S. Bandis and R. MacKean for both past and present contributions in this field. Experience from civil tunnels in Switzerland draws on the

experience from many individuals in contracting and consulting whose work has been referenced. Their information and support is gratefully acknowledged.

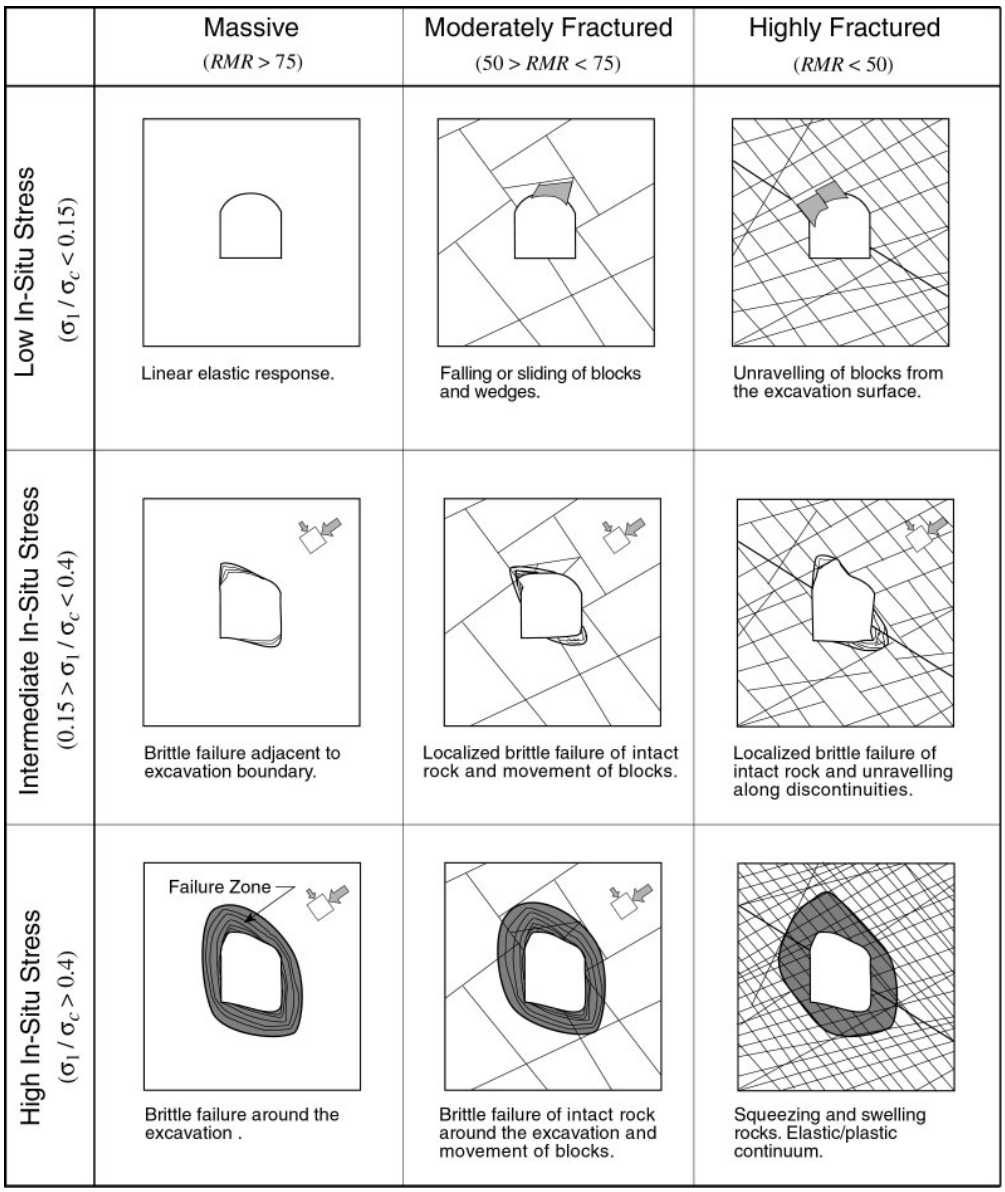

Figure 1.1: Tunnel instability and brittle failure as a function of rock mass rating and the ratio of the maximum far-field stress σ_1 to the unconfined compressive strength σ_c (Martin *et al.* 1999; modified from Hoek *et al.* 1995)

2.0 CHARACTERIZATION AND BEHAVIOUR OF HARD ROCK

Failure of underground openings in hard rocks is a function of the in situ stress magnitudes and the characteristics of the rock mass, i.e., the intact rock strength and the fracture network (Figure 1.1). At low in situ stress magnitudes, the failure process is controlled by the persistence and distribution of natural fractures. As the in situ stress magnitudes increase, the natural fractures become clamped and the failure process becomes brittle and is dominated by new stress-induced fractures growing parallel to the excavation boundary. One of the key parameters characterizing brittle failure in hard rocks is the stress magnitude required to initiate and propagate these stress-induced fractures through intact or tightly clamped fractured rock. Initially, at intermediate depths, these stress-induced fractured regions are localized near the tunnel perimeter but at great depth the fracturing involves the whole boundary of the excavation (Figure 1.1). Unlike ductile materials in

which shear slip surfaces can form while continuity of material is maintained, brittle failure deals with materials for which continuity must first be disrupted through stress-induced fracturing before kinematically feasible failure mechanisms can form.

The purpose of this section is to deal with the fundamental processes of brittle failure in hard rocks that are relevant when assessing excavation stability for ground control and rock support.

2.1 Fundamental characteristics of brittle rock masses

The analysis of underground openings for brittle failure requires knowledge of three variables: (1) the in situ stress boundary condition, (2) the rock mass strength, and (3) the geometry of the excavation(s).

2.1.1 Intact and rock mass strength

The strength of intact rock is determined from laboratory tests on cylindrical samples and the strength of a rock mass assessed using empirical approaches or by back-analyzing case histories where examples of failure have been carefully documented. One of the most widely used empirical failure criteria is the Hoek-Brown criterion (Hoek and Brown 1980). Since its first introduction, the criterion has been modified several times, most recently by Hoek and Brown (1998). The generalized form of the criterion for jointed rock masses is defined by:

$$\sigma_1 = \sigma_3 + \sigma_{ci}\left(m_b \frac{\sigma_3}{\sigma_{ci}} + s \right)^a \qquad \text{(Eqn 2.1)}$$

where σ_1 and σ_3 are the maximum and minimum principal stresses at failure respectively, m_b is the value of the Hoek-Brown constant m for the rock mass, s and a are constants which depend upon the characteristics of the rock mass, and σ_{ci} is the uniaxial compressive strength of the intact rock pieces (Figure 2.1).

For hard rock, Hoek and Brown (1998) recommend a value of 0.5 for a. In order to use the Hoek-Brown criterion for estimating the strength and deformability of jointed rock masses, three properties of the rock mass have to be estimated. These are: (1) uniaxial compressive strength σ_{ci} of the intact rock pieces in the rock mass; (2) Hoek-Brown constant m_i for these intact rock pieces; and (3) Geological Strength Index *GSI* for the rock mass. *GSI* was introduced by Hoek *et al.* (1995) to provide a system for estimating the rock mass strength for different geological settings. It can be related to commonly used rock mass classification systems, e.g., the rock mass quality index Q or the rock mass rating *RMR*.

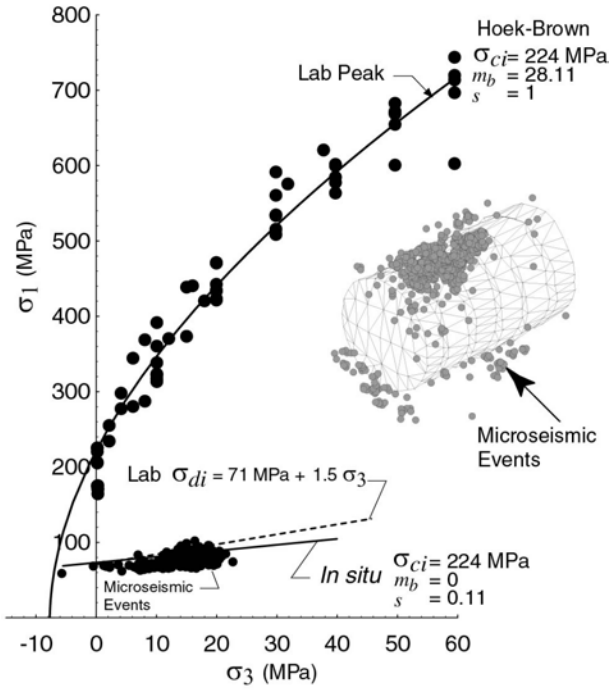

Figure 2.1: Example of the Hoek-Brown criterion using laboratory samples and the parameters required to fit damage initiation based on microseismic events

The origin of the Hoek-Brown criterion is based on the failure of intact laboratory samples and the reduction of the laboratory strength is based on the notion that a jointed rock mass is fundamentally weaker in shear than intact rock. While the concept is sound, the application of the Hoek-Brown criterion to brittle failure has met with limited success (Nickson *et al.* 1997; Martin *et al.* 1999). Pelli *et al.* (1991) showed that in order to fit the Hoek-Brown criterion to observed failures, the value of m_b had to be reduced to unconventionally low values and Martin *et al.* (1999) found that m_b should be close to zero with a value of s = 0.11 ($1/3\sigma_{ci}$). Similar findings were reported by Stacey and Page (1986), Wagner (1987), Castro *et al.* (1997), Grimstad and Bhasin (1997) and Diederichs (1999) who all showed, using back-analyses of brittle failure, that stress-induced fracturing around tunnels initiates at approximately 0.3 to 0.5 σ_{ci} and that it is essentially independent of confining stress. Hence, while the traditional Hoek-Brown parameters may be appropriate for estimating the shear strength of ductile rock

masses around tunnels and slopes at shallow depths, there is growing evidence that the same approach is not appropriate for estimating the strength of hard rocks around tunnels at depth. The fundamental difference between the two modes of failure is that at shallow depths slip along discontinuities or shearing of the rock matrix dominates the failure process, while at depth stress-induced fracturing dominates.

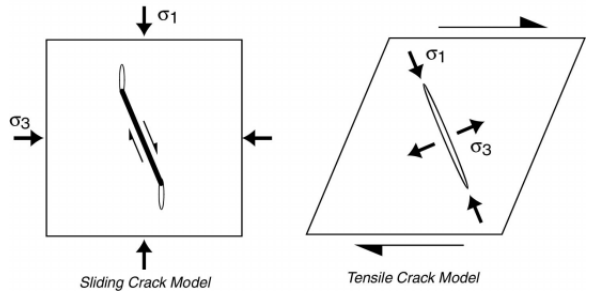

Figure 2.3: Mechanisms for damage initiation

Since the early work of Brace *et al.* (1966) laboratory studies have shown that in unconfined compression tests, damage initiation occurs at 0.3 to 0.5 of the peak strength. Starting with the pioneering work of Griffith (1924) many researchers, e.g. Horii and Nemat-Nasser (1986) and Kemeny and Cook (1987), have associated this damage with slip and proposed sliding crack models to simulate brittle failure (Figure 2.3). However, as pointed out by Lajtai *et al.* (1990) this initiation of damage in laboratory samples is not caused by shear-induced slip as only lateral dilation of the cylindrical samples is recorded with no axial shortening. Lajtai *et al.* (1990) suggested that damage initiation was caused by tensile cracking. Figure 2.3 illustrates two possible mechanisms causing damage initiation when rock containing a flaw is subjected to deviatoric stress. Because of the molecular bonding structure, rocks are fundamentally weaker in tension than in compression. Hence, during compression or shear loading, tensile cracking will dominate the failure process provided tensile stresses are generated internally and exceed the tensile strength. This concept was explored by Diederichs (1999) and conditions causing tension in a compressive stress field are discussed later.

The microscope work by Tapponnier and Brace (1976) has shown that the length of the cracks, at the initiation stage in the damage process, is approximately equal to the grain size of the rock. Hence, to track the failure process numerical models should be able to simulate the grain scale. Cundall *et al.* (1996) developed the particle flow code *PFC* that can be used to represent rock by considering particles as mineral grains. *PFC* treats the rock as a heterogeneous material bonded together at contacts with each contact point acting like a pair of elastic springs allowing normal and shear relative motion. When either a tensile normal-force or a shear-force limit is reached, the bonds break and cannot carry tension thereafter. Broken contacts, which remain in contact, can generate frictional shear resistance in response to normal stress. Diederichs (1999) used *PFC* to explore the damage initiation in simulated samples of Lac du Bonnet granite. In this work, the accumulation of both tensile bond breaking and bond slip were tracked as loads were applied.

A typical axial stress versus axial strain curve from these simulations is shown in Figure 2.2. The stress-strain curve shows the characteristic damage initiation at about 0.3 to 0.4 of the peak strength and rapid strain softening immediately after peak. Also shown in Figure 2.2 are the incremental snap-shots of crack growth. Note that even though the sample is confined with 20 MPa, the total amount of

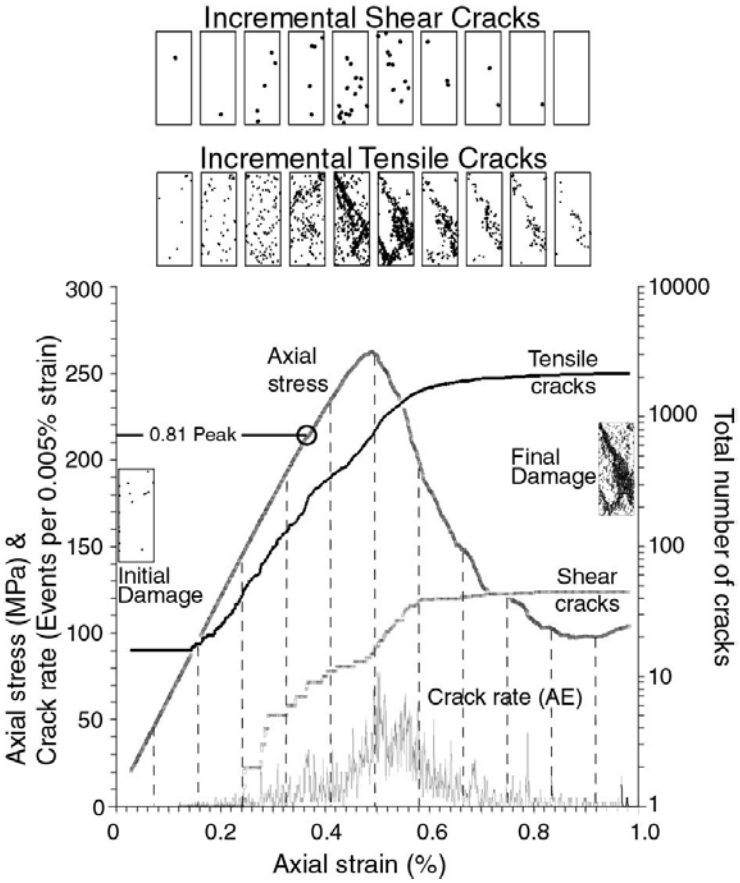

Figure 2.2: Example of axial stress versus axial strain from a bonded disc model (after Diederichs 1999). Also shown are the number of tensile and shear cracks, as well as the crack rate per unit strain.

tensile cracking dominates shear cracking by a ratio of approximately 50:1 and that there is very little new crack growth after the macro-scale failure zone has formed. Heterogeneity (both in grain size and material properties) is key in generating tensile stresses in a compressive stress field.

Furthermore, Diederichs (1999) demonstrated that for a system in which unstable propagation of individual cracks is prevented (as is the case with *PFC*), a consistent statistical relationship exists, for a range of confining stresses, between the stress required for crack initiation and the stress level at which a critical density of accumulated cracks results in crack interaction and yield (yield stress / initiation stress = 2 for the model). This ratio is similar for polycrystalline rock such as granite in laboratory testing of cylindrical samples (Brace *et al.* 1966). The crack interaction threshold is defined as the first point of axial non-linearity or, for uniaxial tests, of volumetric strain reversal. While crack initiation is dependent on a critical stress threshold, crack interaction is dependent on a critical crack density. In laboratory tests where the loading path is monotonic, this critical crack density is reached when the maximum stress value reaches twice the crack initiation stress. In a rock mass surrounding underground openings, the loading path is quite different and the critical crack density is reached at stress values that are considerably less than the laboratory value. In the limit, the critical crack interaction becomes coincident with crack initiation. This causes the in situ yield strength (crack interaction) to drop to the stress level required for crack initiation (0.3 to 0.5-times σ_c). This in situ strength drop is widely observed in massive and moderately jointed hard rock masses.

It is often argued that tensile failure cannot occur in a confined state. However, most rocks and rock masses are heterogeneous at the grain or rock block level and this introduces internal stress variations as illustrated by Figure 2.4 on results from a bonded disc model of a sample confined at 5 MPa. The fourth quadrant presents the minor principal stress state inside the sample and it can be seen that large zones of tension are created due to heterogeneity. Despite the applied boundary confinement of 5 MPa, internal tension in excess of 6 MPa is locally observed.

When continuum models are adopted to determine the stability of an excavation, uniform stresses are predicted (implicit in homogeneous continuum models) with mostly confined conditions near excavations, unless irregular geometries or high in situ stress ratios cause tension zones. Figure 2.5 illustrates that this is not the case in heterogeneous rock masses. Here, the average stresses sampled within smaller regions of the overall confined specimen (20 MPa) are shown for applied axial stress levels of 80 and 250 MPa, respectively. As the axial stress increases, the variability in both the local major and minor principal stress increases as well and half of the sampling points experience lower confinement than the applied boundary stress.

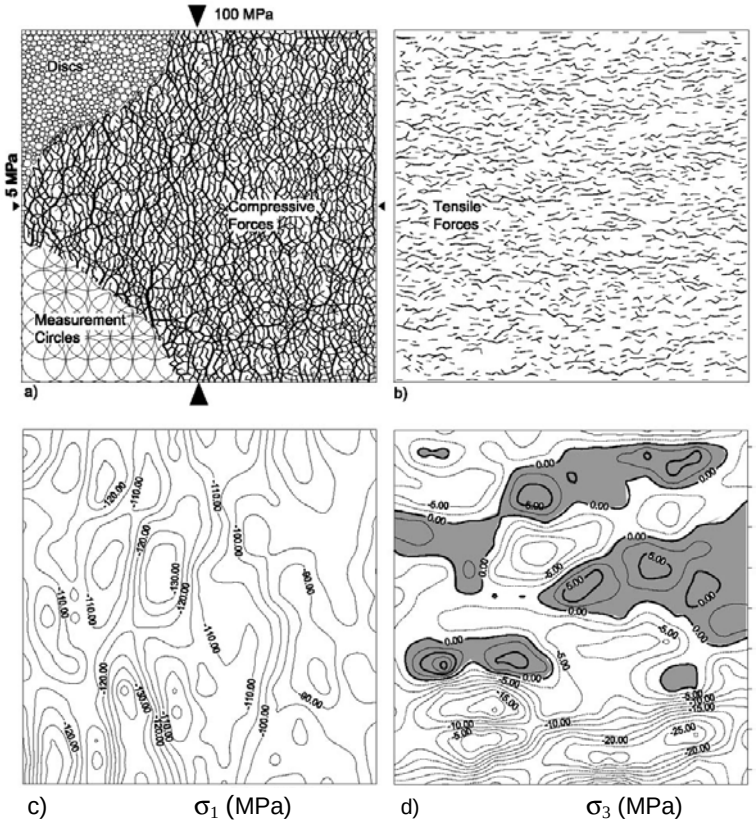

Figure 2.4: Bonded disc model demonstrating stress heterogeneity: (a) disc assembly with compressive contact forces and stress sampling circles; (b) tensile contact forces; c) averaged vertical stresses (compression negative); (d) averaged lateral stresses with shaded tensile zones (Diederichs 1999)

This issue of tensile stresses and thus tensile failure in a compressive stress field was also addressed from a different perspective by Cai *et al.* (1998). Conventionally, the interpretation of near-excavation micro-seismic data is based on models assuming shear failure as a dominant source of energy release (e.g. Brune 1970). It is found that these models are often unsuccessful in interpreting near-boundary micro-seismic behaviour (Feignier and Young 1992). Stimulated by the qualitative observation that shear models provide unrealistically large source sizes for micro-seismic events, a tensile cracking model was developed by Cai *et al.*

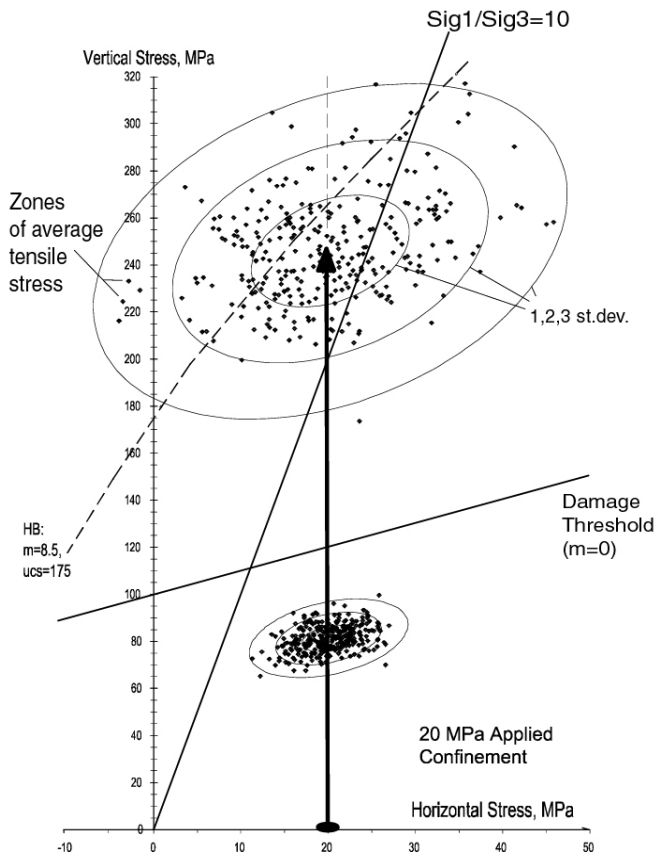

Figure 2.5: Internal stress variations at an external confinement of 20 MPa (Diederichs 1999) leading to localized, internal low or tensile confining stress zones

(1998) and evaluated on data from the Underground Research Laboratory *URL* (Collins and Young, 2000).

This tensile failure model produces realistic fracture sizes, sizes that correspond more closely with field observations. The findings are summarized in Figure 2.6 (a) comparing calculated source sizes predicted by the tension and shear model as a function of seismic energy. This tension model fits better with the established empirical relationship and, more importantly, predicts sizes that are consistent with visual observations of at least one to two orders of magnitude smaller sizes. While it is difficult to obtain data on actual source size distribution, it can be indirectly demonstrated that the tensile model produces more realistic source sizes.

In Figure 2.6 (b), source locations and sizes for micro-seismic events recorded around a test tunnel in massive Lac du Bonnet granite are shown as circles rotated into the cross-sectional plane. Visible instability (slabbing) is to be expected when fractures interact or cluster sufficiently to create continuous fractures (Kaiser *et al.* 1997; Falmagne *et al.* 1998). Clustering leading to one-sided notch formation is evident in Figure 2.6 (b). The sources in the upper notch interact to the observed depth of failure whereas they do not interact in the floor where the notch is much less distinct. Hence, indirectly the observed notch formation at the URL supports the tensile failure model in an overall compressive stress field, and demonstrates that the tensile model is able to better estimate the damage accumulation and the eventual size of the failure zone (Cai *et al.* 1998).

Tensile stresses near the boundary of the tunnel can exploit grain-scale cracks leading ultimately to stress-induced slabbing and spalling, commonly associated with brittle failure (Figure 2.7). The depth and extent of

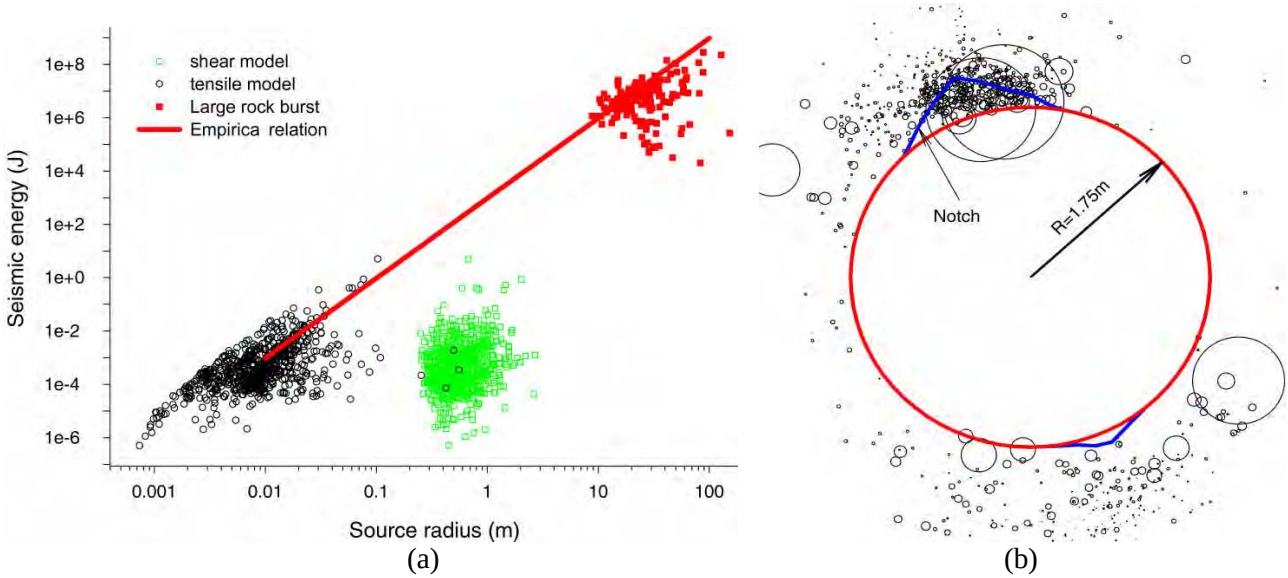

Figure 2.6: (a) Source radius versus seismic energy for shear (Brune) and tensile model; (b) source size clustering near notch of mine-by experiment tunnel at URL (Pinawa, Canada) (after Cai *et al.* 1998)

Figure 2.7: Example of the stress-induced slabbing and spalling that occurs during brittle failure around deep excavations (after Ortlepp 1997)

the tensile region and the magnitude of the tensile stresses can affect the thickness and extent of the slabs. Evidence from laboratory tests and field studies suggest that brittle failure is a phenomenon that occurs when the confining stress is either tensile or very close to zero. Under such conditions the initiation of damage becomes a key indicator for determining whether brittle failure is possible. Below this damage-imitation threshold, underground openings in hard rock masses remain stable.

2.2 Site characterization

A site characterization program for a deep tunnel begins by compiling the geological and geotechnical information for the proposed route and as the design moves forward, detailed information is required of the individual rock units, discontinuities, groundwater, etc. From Section 2.1, it is evident that brittle failure is dominated by stress-induced fracturing of intact rock. Hence, the strength and deformation characteristics of this intact rock, as well as the in situ stress magnitudes, are essential for the design of underground openings in hard rock. The importance of discontinuities and water and other factors are discussed separately.

2.2.1 Sample disturbance of intact rock

At first glance, it would appear that obtaining samples of hard rocks for laboratory testing would be a straightforward task. For deep tunnelling excavations it is routine to core samples at depths greater than 500 m and in the mining and petroleum industry samples often come from depths of several kilometres. It is generally recognized, in the petroleum industry, that softer rocks, i.e., shales, siltstones, etc., are susceptible to sample disturbance and that this process affects their laboratory properties (Santarelli and Dusseault 1991).

The process of drilling a core sample from a stressed rock mass induces a stress concentration at the sampling point. When this stress concentration is sufficient, grain-scale microcracking occurs and the accumulation and growth of these microcracks ultimately may lead to core discing. Martin and Stimpson (1994) showed that the accumulation of these microcracks is progressive and a function of the stress environment, i.e., increasing depth. They also showed that the accumulation of these microcracks:

- reduces the uniaxial compressive strength,
- decreases the Young's modulus,
- increases the Poisson's ratio,
- increases the porosity and permeability, and
- reduces the P-wave velocity.

Martin and Stimpson (1994) suggested that sample disturbance started to affect the laboratory properties of Lac du Bonnet granite when the ratio of far-field maximum stress to the uniaxial compressive strength was greater than 0.1. When this ratio reached approximately 0.3, the uniaxial compressive strength and tensile strength of Lac du Bonnet granite were reduced by nearly 30 and 60%, respectively. It is important to recognize this phenomenon and to take it into account when using design criterion that rely on properties affected by sample disturbance.

2.2.2 In situ stress

The design of an underground excavation requires in situ stress as an input parameter; hence there is little debate about the need for stress measurements. The more challenging question is: What stress measurement techniques are best suited for deep excavations in hard rocks? AECL's URL is often described as an excellent example of a site where the in situ stress state is known with confidence (Amadei and Stephansson 1997). While this is true, the in situ stress state at the URL was not determined using only one of the method listed in Table 2.1. In fact, most of the traditional indirect measurements failed below 300 m depth to give consistent results and in most cases gave erroneous results (Martin 1990). Combining all the results from the various techniques mentioned in Table 2.1 enabled the development of a valid stress tensor below 300 m depth. One finding from this combination of methods is that large-scale methods using back-analysis techniques give consistently more reliable results than 'small-scale' traditional methods.

Table 2.1: Stress measurement techniques tried at AECL's URL summarized from Martin *et al.* (1990)

In situ stress-Method	Technique	
Indirect	Triaxial Strain Cells	- Modified CSIR - CSIRO - Swedish State Power Board - Sherbrooke Cuis Cell
	Biaxial Strain Cells	- CSIR Door Stopper - Modified Door Stopper - USBM Gauge - Bock Slotter
	Hydraulic Fracturing	- Maximum stress
Direct	Hydraulic Fracturing	- Minimum stress
Large-scale back-analysis	Convergence	
	Under-excavation	
	Mine-by Experiment	
	Depth-of-failure	

Wiles and Kaiser (1990) showed that even for very good rock mass conditions, such as at AECL's URL, ten overcore tests were needed to provide statistically significant results and that with less than ten measurements, the results were very erratic and with less than five measurements little confidence can be placed on the mean stress. Figure 2.8 from Martin *et al.* (1990) demonstrated that a single large-scale stress measurement technique gave the same results as the mean of the ten overcore results referred to by Wiles and Kaiser (1994). They attribute the variability in overcore results to the systematic errors in the measurement technique and not to the variability in stress. Stress measurement techniques must be designed to reduce this variability.

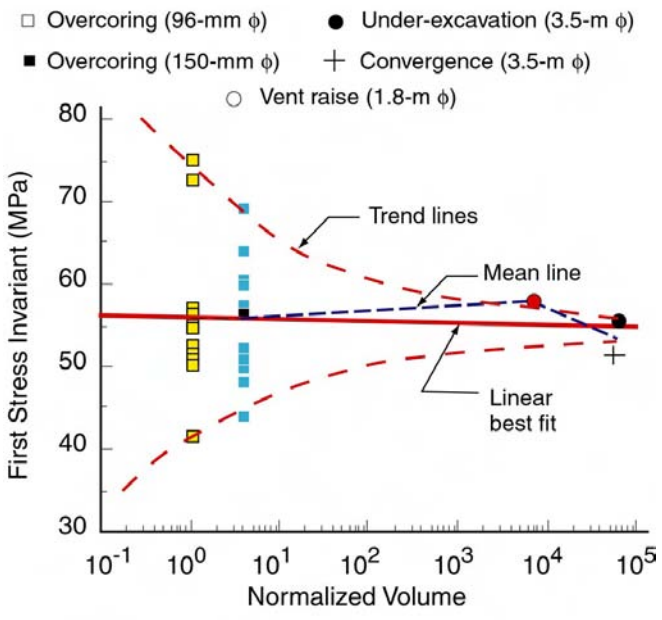

Figure 2.8: Effects of scale on stress variability, data from Martin *et al.* (1990)

The findings from the in situ stress characterization program that was carried out at the URL from 1980 through to 1990 can be summarized as follows:

- Traditional methods are suitable for shallow depths, i.e., where the ratio of the far-field maximum stress to the uniaxial laboratory strength is less than $\sigma_1/\sigma_c < 0.15$.
- Where the ratio of $\sigma_1/\sigma_c > 0.15$, the rock mass response will be non-linear and any traditional method that records the non-linear rock mass response and requires the interpretation of these non-linear strains will give erroneous results if interpreted using linear elastic theory. The severity of the error will depend on the magnitude of the ratio above 0.15.

The URL experience indicates that when $\sigma_1/\sigma_c > 0.2$, the results are extremely difficult to interpret and when $\sigma_1/\sigma_c > 0.3$, they are basically meaningless. In the Canadian Shield these limits occur at depths of approximately 1000 m to 1500 m, respectively. Wiles and Kaiser (1990) showed how the under-excavation technique could be used to overcome these limitations.

- Where the horizontal stress magnitude is the maximum stress, hydraulic fracturing produces sub-horizontal fractures and these are difficult if not impossible to interpret. Because hydraulic fracturing only provides the minimum stress, hydraulic fracturing results tend to reflect some component of the vertical stress and the minimum horizontal stress. In addition, the pressures required to fracture the rock at depths greater than 1000 m are beyond the capabilities of most hydraulic fracturing equipment, particularly for 75-mm-diameter boreholes or less.
- Large scale observations and back-analysis of failures, similar to those observed in borehole breakouts and orepasses, using the depth and extent of failure can reduce the variability that plagues small-scale measurements, such as overcoring, and provide consistent stress orientations and magnitudes.

2.2.3 Stress change

For stability assessment, it is the maximum induced stress near an excavation wall that determines whether failure occurs. These mining-induced stresses, of course, are directly related to the in situ state of stress, but the geometry of the opening and nearby excavations, within the zone of influence, often have a dominant effect on the maximum stress concentration at the excavation wall.

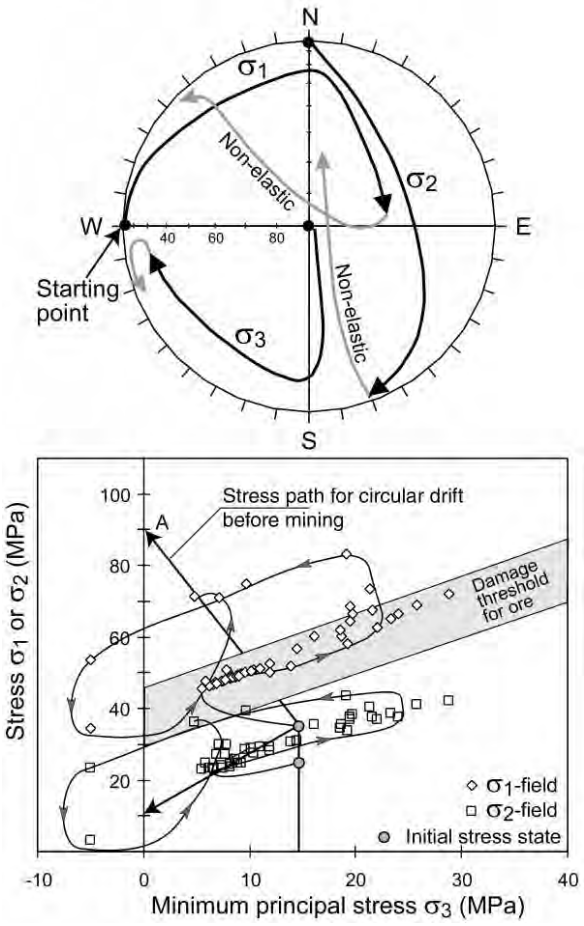

Figure 2.9: Stress change observations at Winston Lake mine (after Kaiser *et al.* 2000)

A mining example from the Canadian Shield is used to illustrate the importance of mining-induced stress change. The effects of stope advance was recorded by stress change cells in the hanging wall and near a top sill drift at the Winston Lake mine (Kaiser *et al.* 2000; Figure 2.9). The lower hemisphere stereonet in this figure shows the measured stress path for the three principal stresses in the hanging wall and it can be seen that these stresses undergo a stress rotation of between 90 and 180 degrees. Also shown is when the stress path, according to a comparison with stresses from elastic 3D modelling (Kaiser *et al.* 2000), deviates from elastic rock mass behaviour.

The influence of such stress changes on the stress concentration factor *SCF*[6] can best be illustrated by example of a circular excavation experiencing a stress change $\Delta\sigma$ (Figure 2.10). For a tunnel in a virgin in situ stress field of (σ_3/σ_c = 0.2; σ_1/σ_c = 0.25), the minimum and maximum stress level at the wall are 0.3 and 0.55, respectively. If this tunnel ex-periences a stress increase $\Delta\sigma$ in the major principal stress (from 0.25 to 0.4), the minimum and maximum stress level at the wall change to 0.2 and 1.0, respectively, as illustrated by the second graph in Figure 2.10.

[6] defined as the maximum tangential stress at the excavation wall normalized by the laboratory uniaxial compressive strength: $SCF = \sigma_{max}/\sigma_c$, where $\sigma_{max} = 3\sigma_1-\sigma_3$.

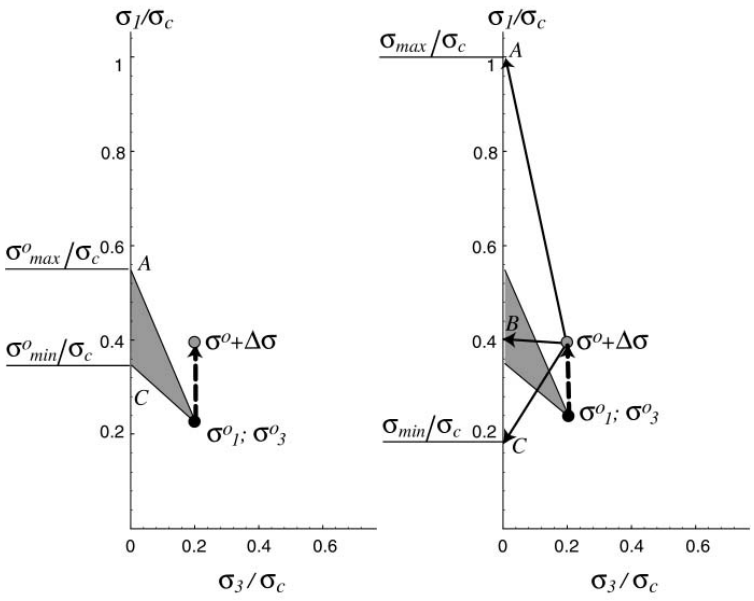

Figure 2.10: Stress path for circular excavation experiencing stress change (increase in major principal stress)

The stresses measured above the top sill drift at Winston Lake mine are shown in Figure 2.9, and compared to a damage threshold (discussed later) and to the 2D stress path for a circular excavation (before mining-induced stress change). It should be noted that the 2D stress path is conceptual with the starting and end-points being independent of the loading conditions. In reality, 3D effects near the face of the drift will result in distinctly non-linear stress paths. At an in situ stress level of [0.16; 0.36], the stress concentration at the wall of the top sill drift, before mining started, would reach 1.02-times the minimum strength of the ore (90 MPa) (Point A in Figure 2.9). In other words, the calculated maximum tangential stress was roughly equal to the rock strength and, hence, must have exceeded the damage threshold long before the drift was subjected to additional stresses induced by the mining front. Because the stress cell was placed at some distance from the wall of the drift, the measured stresses should never reach Point A, the maximum predicted for the wall.

As mining approaches the cell location, the axial stress σ_2 generally increases but stays at all times below the damage threshold. While the major principal stress σ_1 increases steadily till a maximum is reached at about 80 MPa, the minor principal stress σ_3 first drops to less than 5 MPa, then increases to in excess of 25 MPa, and finally drops rapidly to below zero when the damage threshold is exceeded. Consequently, as a result of mining-induced stress changes, the top sill drift experiences large variations in stress, initiating failure when the deviatoric stresses near the top sill exceed the damage threshold. After this point, the confining stress σ_3 drops off rapidly providing further evidence of failure.

2.2.4 Site characterization considering mining-induced stresses

Since the induced stresses near an excavation wall start the failure process and not the in situ stress directly, the mining-induced stress concentration factor σ_{max}/σ_c (or damage index D_i (Martin *et al.* 1999)) serves as a more appropriate indicator of excavation behaviour. Using this indicator, the relative in situ strength ranges, shown on the left margin of Figure 2.11, can be replaced by the mining-induced stress concentration ranges summarized in Table 2.2 and shown on the right margin of this figure. The ranges given for each stress domain indicate that the predominant behaviour mode also depends on: rock type, grain size, degree of jointing, and the level of heterogeneity in the rock mass.

As can be seen from Figure 2.10, the normalized minimum stress (Point C) is also affected by stress change and may approach zero or negative (tensile) values in typical mining scenarios. In other words, there are locations around an excavation where the tangential (clamping) stresses become tensile. Since this means that stresses relax relative to the original stress state, the term "relaxation" is used throughout this article to describe conditions where a negative stress change leads to a reduction in tangential stresses near an excavation.

Table 2.2: Ranges of mining-induced stress concentration to identify applicable stress regime (Figure 1.1 and Figure 2.11)

Low mining-induced stress	$\sigma_{max}/\sigma_c < 0.4\pm0.1$
Intermediate mining-induced stress	$0.4\pm0.1 < \sigma_{max}/\sigma_c < 1.15\pm0.1$
High mining-induced stress	$\sigma_{max}/\sigma_c > 1.15\pm0.1$

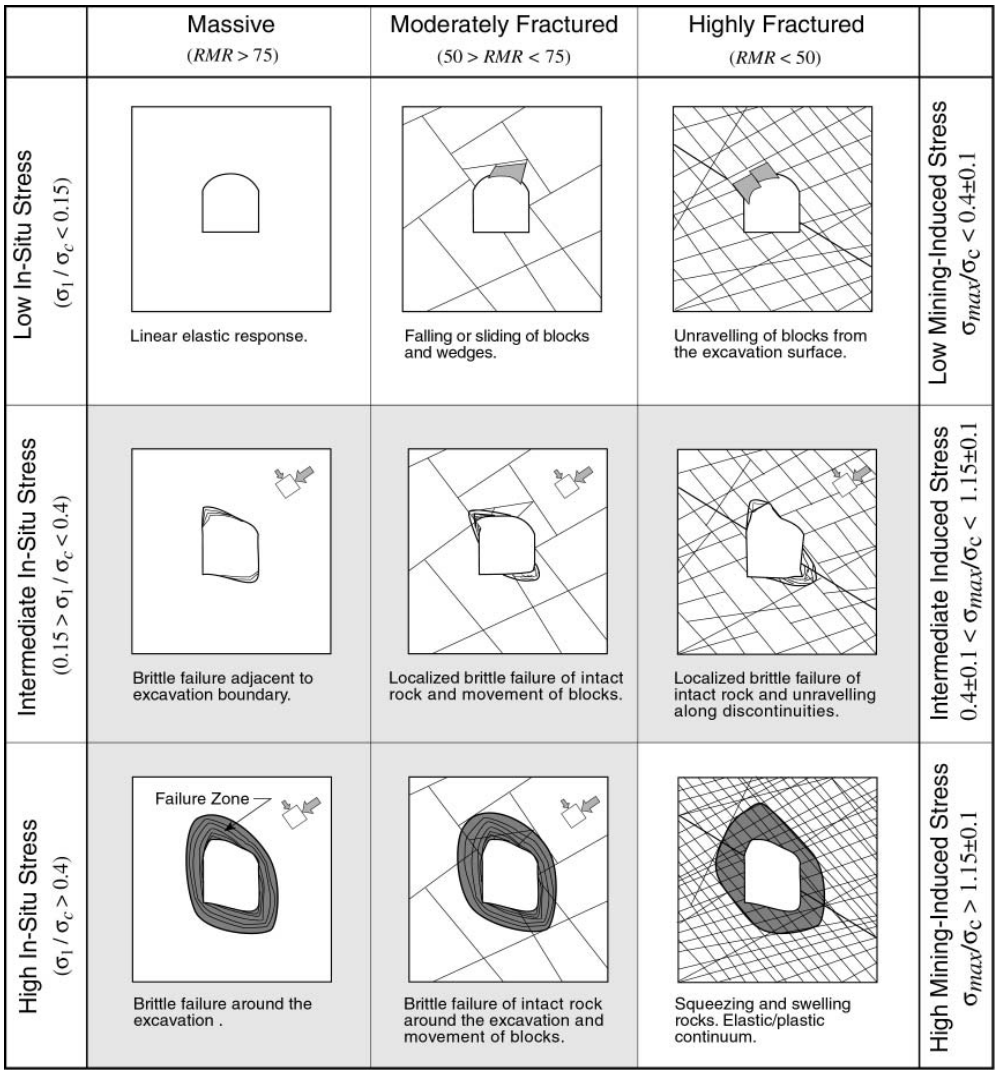

Figure 2.11: Examples of tunnel instability and brittle failure (highlighted gray squares) as a function of Rock Mass Rating and the ratio of the maximum far-field stress σ_1 to the unconfined compressive strength σ_c (modified from Martin *et al.* 1999). Also shown are corresponding ranges of mining or excavation-induced stress concentrations σ_{max}/σ_c.

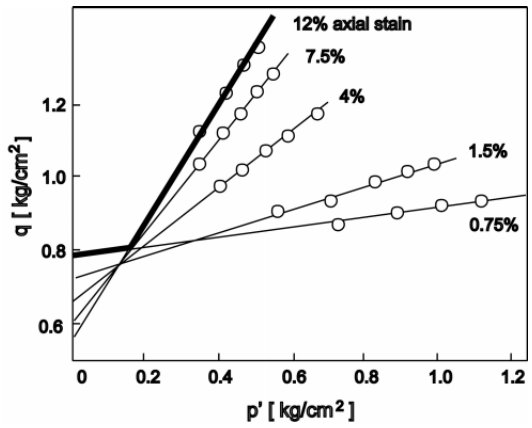

Figure 2.12: Bilinear envelope for stiff clay (developed as a function of axial strain) illustrating transition from a cohesive to a frictional yield mode (after Schmertman and Osterberg 1968)

2.3 Brittle rock mass failure envelope

In conventional usage, the Hoek-Brown and the Mohr-Coulomb strength envelopes assume that both cohesion and friction contribute to the peak strength, and are mobilized instantaneously and simultaneously. This is certainly valid at high confinement levels, when the rock behaves in a ductile manner ($\sigma_1/\sigma_3 < 3.4$ according to Mogi (1966)) and cohesion and frictional strength components can be mobilized simultaneously. Diederichs (1999) suggests that this behaviour results from the condition of all-round compressive strain at the point of crack initiation (i.e. without extension strain cracks cannot extend or dilate allowing coincidental friction mobilization). However, Martin *et al.* (1999) argue that the assumption of instantaneously and simultaneously mobilized cohesion and friction is not correct for brittle rocks in a compressive stress field at low confinement. In these conditions, cracks dilate or open after initiation and

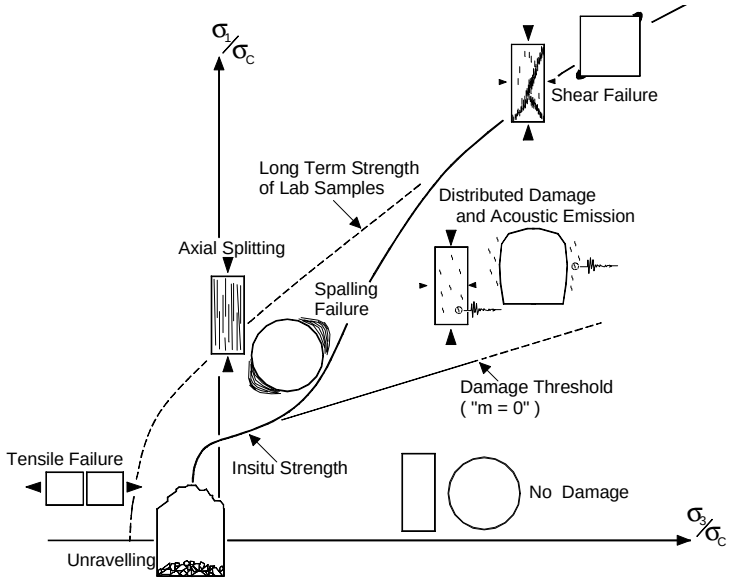

Figure 2.13: Schematic of failure envelope for brittle failure, showing four zones of distinct rock mass failure mechanisms: no damage, shear failure, spalling, and unravelling (after Diederichs 1999)

this inhibits the coincidental mobilization of friction and cohesion. This notion is also supported by the laboratory findings of Martin and Chandler (1994). Hajiabdolmajid *et al.* (2000) suggest that brittle strength mobilization can be reasonably represented as a two-stage process, with the pre-peak behaviour dominated by the cohesive strength of the rock material, and the residual strength controlled by the mobilized frictional strength within the damaged rock. In short, the frictional strength cannot be mobilized until the rock is sufficiently damaged to become essentially cohesionless.

2.3.1 Bi-linear failure envelope cut-off

At low confinement levels, the accumulation of significant rock damage, equivalent to loss of cohesion, occurs when the principal stress difference $(\sigma_1-\sigma_3)$ = 1/3 to 1/2 σ_c is reached or exceeded. This is equivalent to a bi-linear failure envelope cut-off starting at $\phi = 0$ (Mohr-Coulomb) or $m = 0$ (Hoek and Brown) as discussed by Kaiser (1994).

The concept of a bi-linear failure envelope is not unknown to the soil mechanics community (cap model and critical state soil mechanics), e.g., for over-consolidated clays. It is also consistent with the findings of Schmertman and Osterberg (1968) summarized in Figure 2.12 (tests on Jacksonville Sandy Clay). For this material, the cohesive strength component dominates at low strains and at low confinement (p'), whereas the frictional strength component dominates at large strains and high confinement.

For brittle rock, the strength envelope can also be represented by a bi-linear failure envelope cut-off as illustrated schematically by Figure 2.13. Below a damage threshold (m = 0), the rock is not damaged and remains undisturbed. When this threshold is exceeded, seismicity (acoustic emissions) is observed and damage accumulates, leading eventually to macro-scale shear failure if the confinement level is sufficiently high, preventing unstable crack or fracture coalescence (e.g., in confined cylindrical test samples).

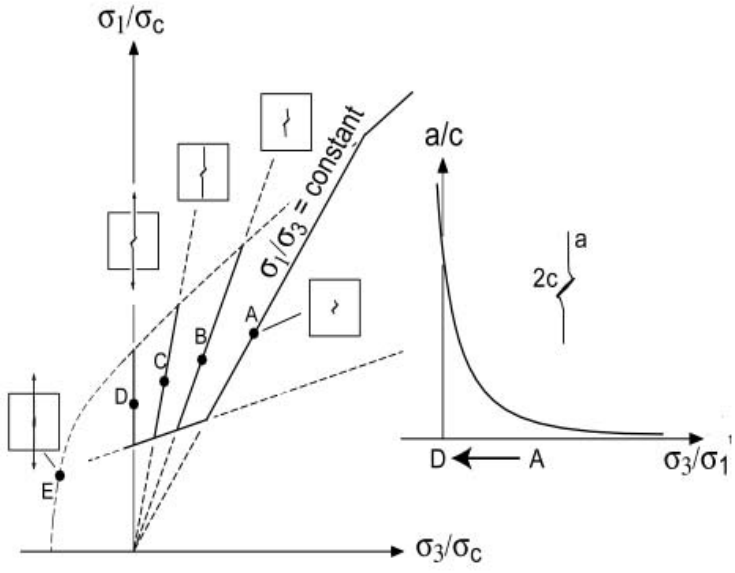

Figure 2.14: Schematic diagram illustrating preferential crack propagation at σ_1/σ_3 = constant

Spalling limit

When a stress path reaches the low confinement zone and exceeds the damage threshold, however, crack and fracture coalescence leads to spalling with preferentially surface parallel fractures (axial splitting with fractures parallel to the maximum principal stress). As a result, the in situ rock mass strength is significantly lower than predicted from laboratory tests, where this mode of failure is retarded due to the particular state of stress in cylindrical samples. If tension is generated, rock fails due to the tensile failure of rock bridges and unravelling mechanisms dominate.

The stress space, therefore, can be divided into four regions (Figure 2.13): no damage, shear failure, spalling and tensile failure.

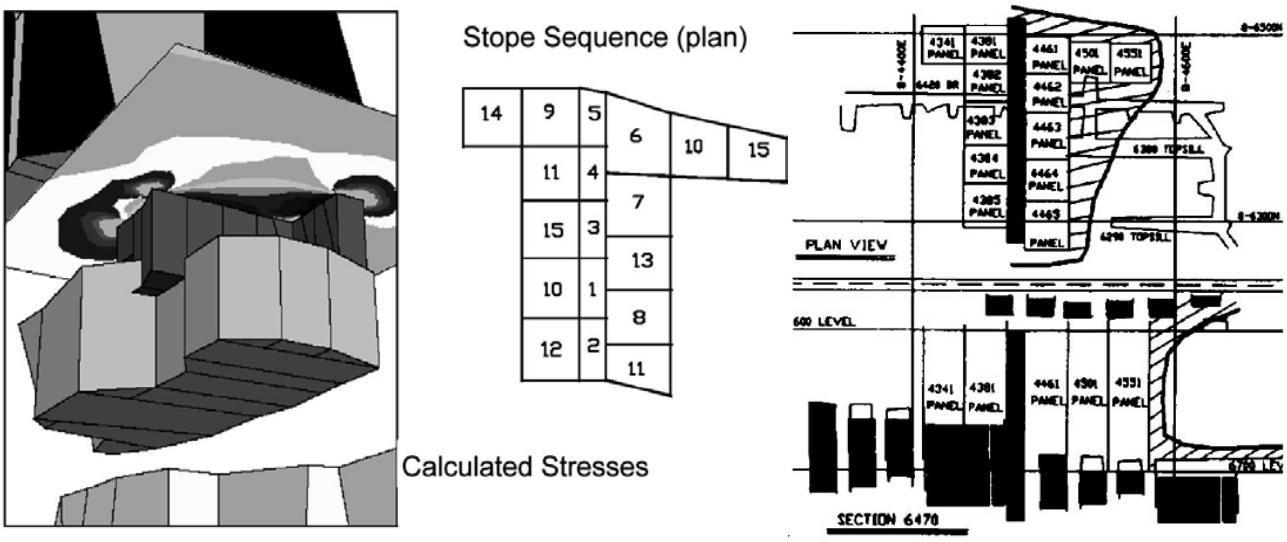

Figure 2.15: Case example from Creighton Mine, Sudbury: Elastic model of staged mining geometry (left); Stope sequence (centre); damage/yield zone from field observations by Landriault and Oliver (1992) at one mining stage (hatched zones in right part of figure)

As the stress path enters the low confinement area, near the excavation boundary, fracture propagation becomes highly sensitive to confinement. Figure 2.14 illustrates that, as σ_3/σ_1 approaches zero (Point A to D), the tendency for cracks and fractures to propagate and coalesce increases exponentially. As the stress path moves from A toward E and the stress ratio σ_3/σ_1 increases and eventually reaches zero, the crack length $2(a+c)$ increases in the direction of the major principal stress. Hence, moving from A to D, the potential for coalescence and thus spalling grows rapidly. Essentially, lines of constant σ_1/σ_3 represent lines of equal coalescence potential. The damage and cohesion loss process is non-linear and accelerates as σ_3 approaches zero or a tensile state in the radial direction.

As was shown by Figure 2.4, heterogeneity introduces internal tensile zones. Inside these tensile zones, the potential for crack propagation is therefore very high, higher than predicted based on the applied, uniform stress ratio σ_1/σ_3. When a boundary stress ratio of $\sigma_1/\sigma_3 = 10$ is exceeded, localized tension is encountered (see Figure 2.5), promoting unstable failure and spalling.

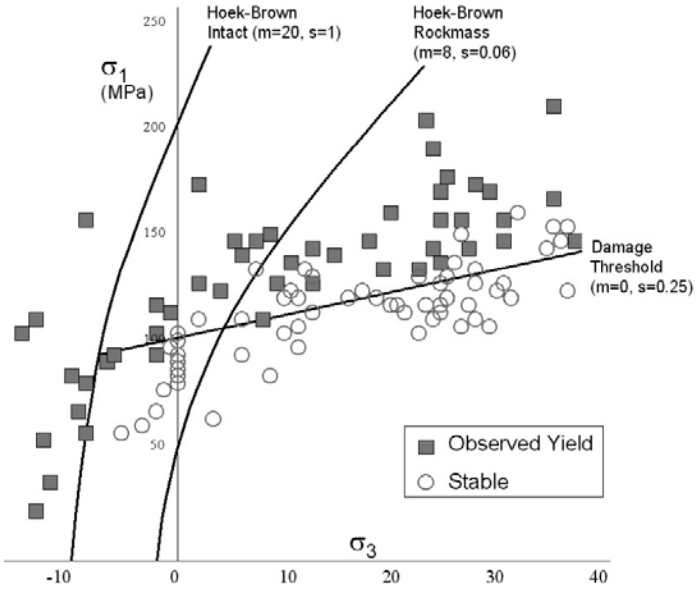

Figure 2.16: Comparison of yield observations with Hoek-Brown failure envelopes and with $m = 0$ damage threshold (after Diederichs 1999)

Damage threshold

Martin *et al.* (1999) showed that the concept of the damage threshold ($m = 0$) is applicable to a wide range of rock mass strengths. This damage threshold can be established from acoustic emission measurements (Figure 2.1), from field observations of rock mass deformation monitoring (Castro 1996), or from borehole fracture surveys (Diederichs 1999). For example, during the mining of a stoping sequence at Creighton mine (Figure 2.15), the extent of the damage zone was established from borehole camera observations and the state of stress, inside and outside this damage zone, was calculated using a 3D elastic model. The stresses inside the damage zone are plotted in Figure 2.16 as squares and the stresses outside, in the stable zone without damage, as circles. A $m = 0$ line with $s = 0.25$ provides a lower bound limit for conditions of visible damage, called observed yield.

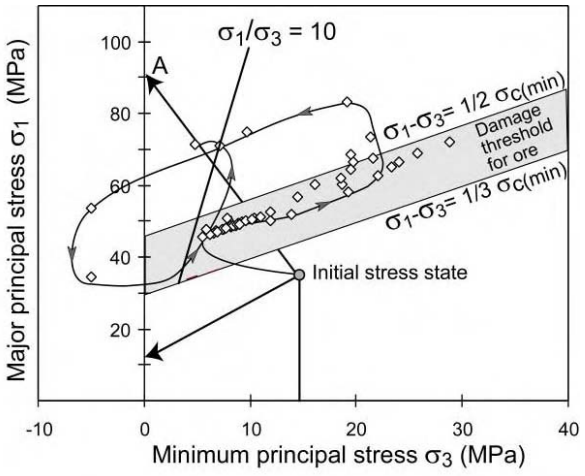

Figure 2.17: Principal stress change above top sill drift at Winston Lake mine (from Figure 2.9; after Kaiser *et al.* 2000)

Case example – Winston Lake mine

When a stress path exceeds the damage threshold and the spalling limit (σ_1/σ_3), brittle failure will occur even if the long-term rock mass strength is not yet reached. Such a stress path was anticipated at Winston Lake mine as indicated by the arrow from the initial stress state to Point A in Figure 2.17. It is important to note that the actual stress path is not expected to follow this line. The path, measured at Winston Lake mine by a stress cell at some distance from the back of a top sill drift, is shown in this figure. Initially, the measured stresses hovered around the stress expected at the stress cell location (around σ_3 = 10 MPa and σ_1 = 50 MPa). Then, as mining influences the drift, both σ_1 and σ_3 increase more or less proportionally (similar behaviour has been observed near the mine-by tunnel at the URL (Martin 1997)). Shortly after the stress path exceeds the damage threshold, σ_3 suddenly starts to drop, indicating the onset of spalling failure. Such spalling is associated with the opening of surface parallel fractures (as can be seen in the photo presented in Section 4 (Figure 4.6)). As a result, the confining stress locally drops to zero. Kaiser *et al.* (2000) describe the details of this failure sequence. It is of interest to note that rock bolts and cables in the back of the drift were able to stabilize the fractured rock mass as indicated by compressive long-term stress conditions at the end of the stress path. This monitored stress path supports the notion that failure occurs in brittle rock when the stresses reach the bi-linear failure envelope cut-off, i.e., before reaching the confined long-term rock mass strength.

2.4 Summary

Because spalling occurs in brittle rock, when the tunnel boundary stresses exceed the damage threshold, failure can be predicted using a bi-linear failure envelope cut-off as shown schematically in Figure 2.18. In terms of the Hoek-Brown failure criterion, the first portion of the brittle strength envelope is modelled using the so-called brittle strength parameters: m = 0, s = 0.11 to 0.25. Substituting these values into the Hoek-Brown equation leads to the principal stress equation (σ_1–σ_3) = 1/3 to 1/2 σ_c, a yield criterion that is appropriate to define the damage threshold. This damage threshold depends on the degree of damage or fracturing and the level of rock mass heterogeneity.

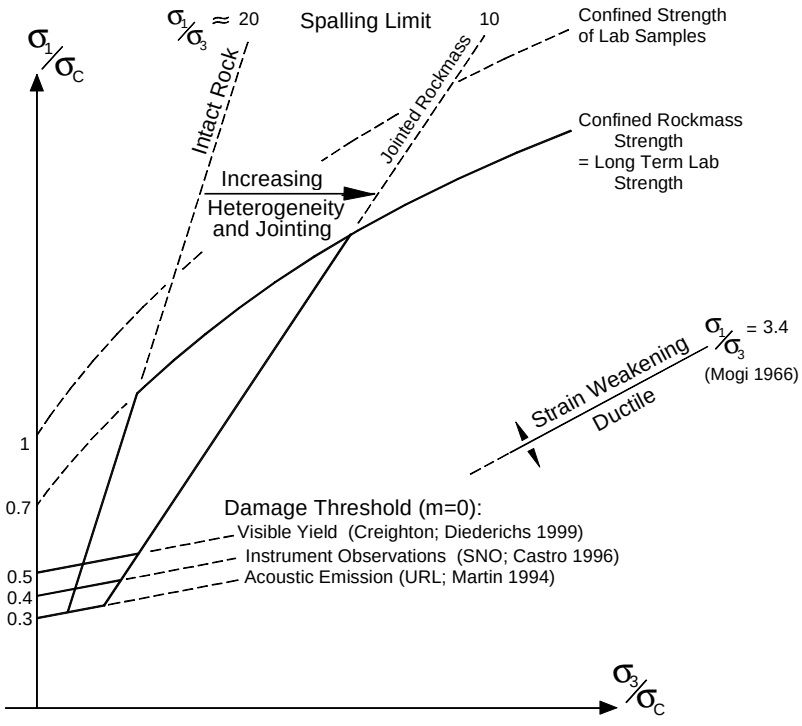

Figure 2.18: Example of the bi-linear failure envelope cut-off for hard brittle rock. The limits for the application of the m = 0 portion of this failure envelope are given by the σ_1/σ_3-ratio.

Above this threshold, the confined rock mass strength envelope, as determined from laboratory tests, is cut-off by the spalling limit at σ_1/σ_3 = 10 to 20. It depends on factors promoting internal tensile stresses and thus also on rock and rock mass heterogeneity and the level of natural jointing.

This bi-linear failure envelope cut-off constitutes the underlying framework for much of the remainder of this article, where it is demonstrated on various examples, from stopes to tunnels to pillars, that the behaviour of brittle rock cannot be properly described by conventional yield criteria, unless a bi-linear cut-off as shown in Figure 2.18 is introduced.

3.0 STABILITY OF HIGHLY STRESSED EXCAVATIONS

In this section, two key issues affecting the stability of underground excavations in hard rock are addressed: (1) stress-induced failure causing slabbing and spalling, and (2) rock mass relaxation promoting gravity-driven failures. At depth or in highly stressed ground, the latter situation may be aggravated by stress-induced rock mass pre-conditioning in the form of stress-induced rock damage. The role of rock mass relaxation around an underground opening caused by ground movements at some distance from the excavation is of particular importance in mining where multiple openings are common. It is less relevant in civil engineering because adjacent openings are typically separated by a distance greater than the zone of influence of individual excavations and because excavations are staged to promote arching and to maintain compression in the rock.

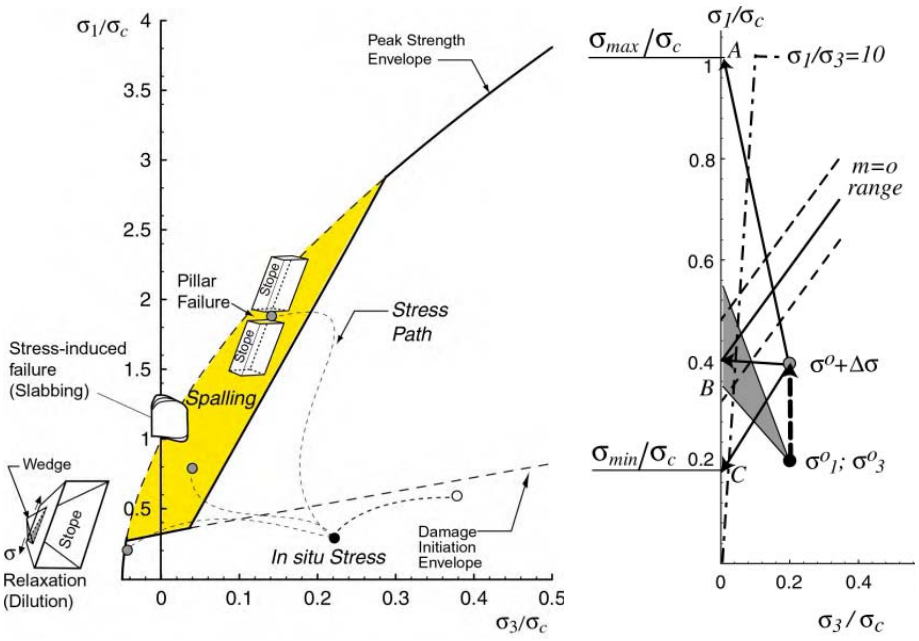

Figure 3.1: Illustration of stress path and resulting modes of failure

Distinct modes of failure around underground openings caused by different stress paths are illustrated in Figure 3.1. This concept was used by Martin *et al.* (1999) to assess the potential for ground control problems around mine openings. The importance of stress change on the stress path and the ultimate state of stress at the excavation wall is already mentioned in Section 2 (Figure 2.10). As illustrated for a circular excavation by the graph on the right in Figure 3.1, points near the excavation wall (e.g., Point A) may experience a stress increase leading to spalling, whereas other locations (e.g., Point C) may experience a stress decrease (relaxation). This notion of stress path leading to different failure modes will be further explored in this section. Because of the sensitivity of hard rock to stress change, a good understanding of the failure processes and stress path helps to assess the potential for caving of stopes, for dilution, and to adequately support the development tunnels. This section also deals with some special challenges of pillar design and violent failure during rockbursting.

3.1 Stope design

Underground open stopes are typically of a scale where interaction with rock mass structures is inevitable. Even at depth, it is therefore necessary to consider the rock mass as a whole when predicting the potential for instability around open stopes. The stability graph method originally developed by Mathews *et al.* (1981) and later modified by Potvin (1988), is an empirical system for open stope stability assessment. It considers the rock mass quality, defined by conventional parameters common to tunnelling classification, as well as special stress, structure and geometry parameters.

The stope face size and geometry is defined by the 'hydraulic radius' *HR*, equal to the area of a stope face divided by the face perimeter, and the rock mass quality. Inherent stability is quantified by the stability number *N'*:

$$N' = Q' \bullet A \bullet B \bullet C = RQD/Jn \bullet Jr/Ja \bullet A \bullet B \bullet C \qquad \text{(Eq 3.1)}$$

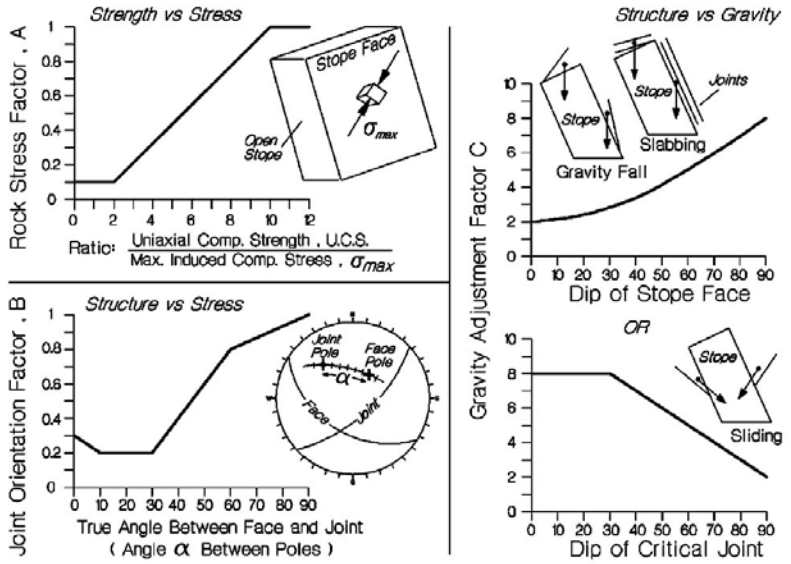

Figure 3.2: Stress (A), structure (B) and gravity (C) factors for calculation of the stability number *N'*

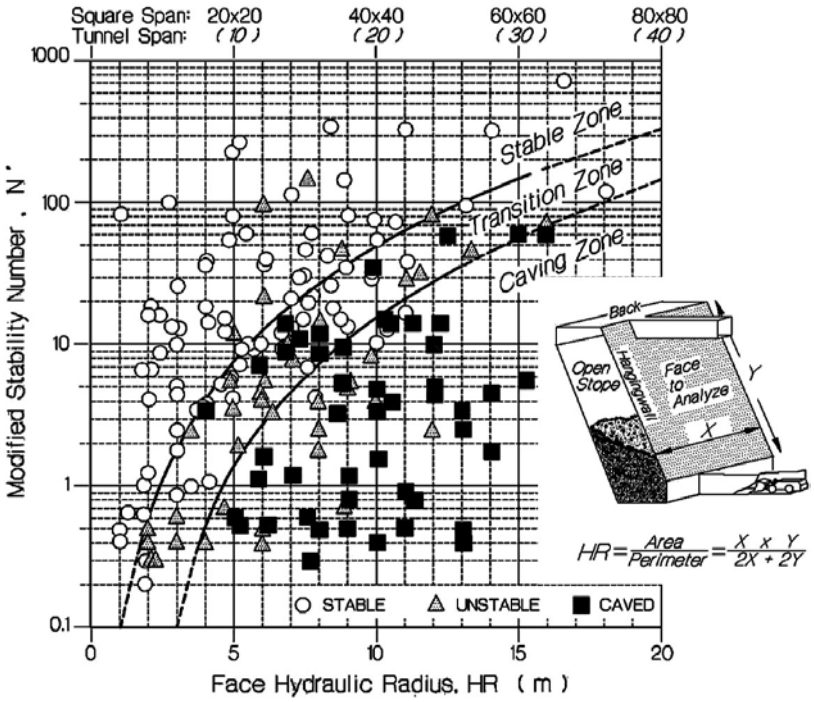

Figure 3.3: Stability chart with unsupported stope database from Potvin (1988) and Nickson (1992). Curves represent upper and lower no support limits.

where *RQD, Jn, Jr* and *Ja* are defined by Barton *et al.* (1974) and factors *A, B* and *C* by Potvin (1988) as shown in Figure 3.2.

Based on several hundred cases, Potvin (1988) and Nickson (1992) empirically related *HR*, to the rock mass stability number *N'*. The upper boundary of the transition zone shown in Figure 3.3 describes the more conservative predictive limit for instability. For rock masses with stability numbers that plot above this upper limit, stability is predicted. This technique has found wide application in Canadian mining operations and has been calibrated by many mines to take account of site-specific conditions. Kaiser *et al.* (1997) identified one fundamental deficiency, i.e., the sensitivity to stress change and loss of tangential confining stress in the walls of a stope. This condition happens frequently in cases of re-entrant geometry, multiple lens mining and in most hangingwall/footwall situations (in steeply dipping ore bodies common to Canadian mining).

Even at depth, the modelled (elastic) stresses tangential to the stope walls are often tensile (Diederichs and Kaiser 1999; Martin *et al.* 1999). In reality, this manifests itself through open joints normal to the boundary and is analogous to an outward displacement of the stope abutments. Actual abutment movements are also often induced, e.g., during bottom-up mining (Kaiser *et al.* 2000; Kaiser and Maloney 1992; Maloney *et al.* 1992), and may lead to significant stress reductions in the stope walls, particularly in hard rock.

Figure 3.4 illustrates the effect of this abutment relaxation on the no-support limit of the stability graph in Figure 3.3. Here the stability graph has been replotted with respect to *log(HR)* and relationships for various relaxation levels, derived by Diederichs and Kaiser (1999) using a calibrated voussoir arch analogue, are shown. Positive displacements correspond to abutment relaxation and move the no support limit up and to the left. In other words, relaxation caused by only tens of millimetres significantly reduces the maximum stable size for a stope in a given rock mass quality. The influence of relaxation is particularly dramatic when major rock structures (faults) intersect stopes (Suorineni *et al.* 2000).

Diederichs and Kaiser (1999) converted the abutment deformation from Figure 3.4 to an equivalent average tensile stress acting parallel to the stope face. This results in the modified stability limits shown in Figure 3.5 where tension is plotted positive. Also plotted in Figure 3.5 are data from stope backs (roof) and hangingwalls from a Canadian hard rock mine (Greer 1989). The stope backs shown in the lower part of the

graph are in compression and instability of these faces is therefore adequately predicted using the conventional no-support limit. The hangingwalls at this mine, however, are reported to be in tension (Bawden 1993). The destabilizing effect of this tension can be accounted for, using an adjustment for tension, by a modified stability graph *A*-factor that is applicable for tensile boundary stress conditions only:

$$A = 0.9 \cdot e^{11\frac{\sigma_r}{\sigma_c}} \quad \text{(for } \sigma_T < 0\text{; Diederichs 1999)} \qquad \text{(Eq 3.2)}$$

The impact of moderate relaxation (e.g., 5 to 10 MPa of average elastic tension parallel to the boundary) is approximately equivalent to a 30% to 50% reduction in maximum stable span or *HR*. Clearly, the neglect of this relaxation for complex openings at depth has major negative economic consequences.

An even simpler approach for instability prediction is illustrated by the case example presented in Figure 3.6. For blocky ground around underground open stopes or ground that has been preconditioned by high stress (stress-induced rock mass damage), the extent of structurally controlled unravelling can be predicted, using mine-wide 3D elastic models such as Map3D™[7], by the spatial limits of tension zones ($\sigma_3 < 0$) (Martin *et al.* 2000). Good model control (mesh and gridding) is essential for this type of analysis to avoid spurious tensile calculations near openings.

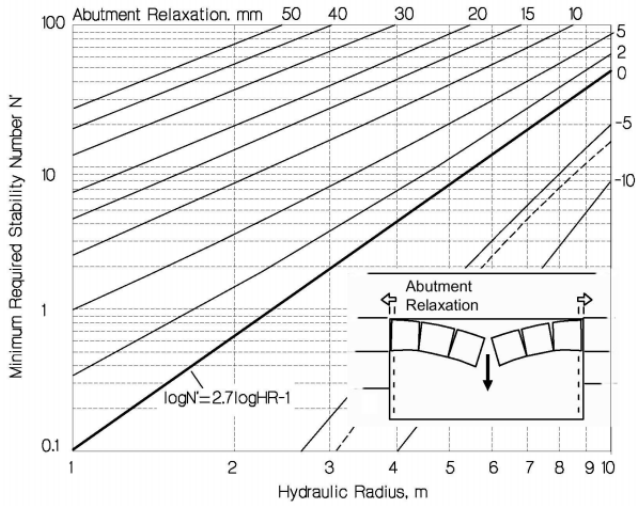

Figure 3.4: Replotted upper-bound no-support line (solid line labeled with log function; lower-bound shown as dotted) and the translation of this upper limit due to relaxation equivalent outward displacement of abutments (after Diederichs and Kaiser 1999)

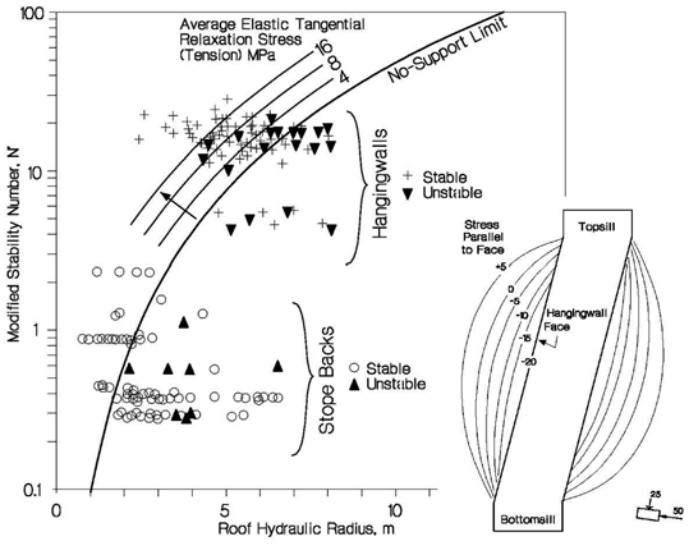

Figure 3.5: Comparison between confined backs and relaxed hangingwalls. Walls at depth can experience strong relaxation equivalent to elastic tension as shown in inset example. The translated no-support limits due to tension are shown for three stress/tension levels (after Diederichs 1999).

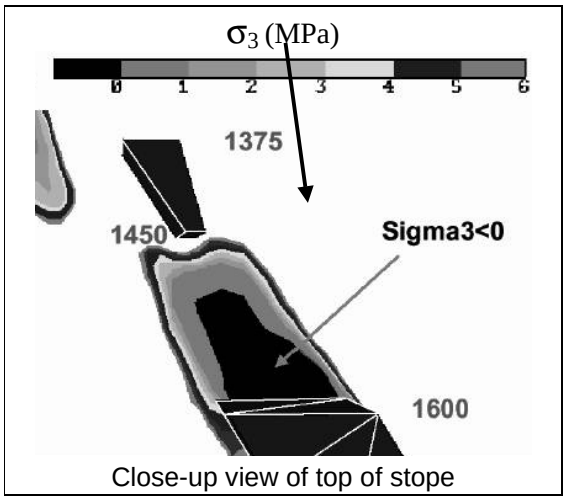

Figure 3.6: Comparison between zone of elastic tension above a back (relaxation due to complex geometries) and the observed extent of caving predicted using MAP3D

[7] Available from Mine Modelling Pty. Ltd.; visit http://www.map3d.com or www.mirarco.org

3.2 Drift or tunnel design

Two stress scenarios are also considered with respect to the stability of tunnels and drifts: (1) stability in relaxed ground, and (2) stability in over-stressed rock.

3.2.1 Drift instability in relaxed ground

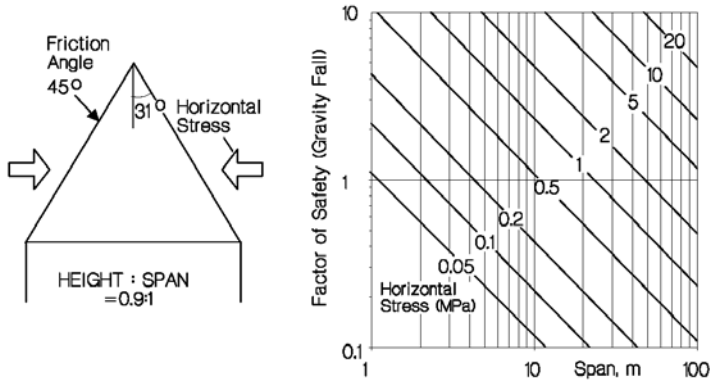

Figure 3.7: Effect on wedge stability of small amounts of confining/horizontal stress

Stress relaxation or confinement loss can also occur above the roofs of tunnels in the vicinity of large mine openings or where complex intersection geometries are present. Relaxation combined with favourably oriented joint sets can form potentially unstable wedges. The stabilizing effect of stress has long been recognized but Diederichs (1999) illustrated that even a small amount of confining stress has a significant impact for such wedges (Figure 3.7). For example, a wedge with a height to span ratio of 0.9:1, as shown in Figure 3.7, can be fully stabilized over a span of 10 m by only 0.5 MPa of horizontal stress acting across the back (friction angle of 45° is representative for moderately rough, planar joints). In fact, for any isolated drift of standard geometry (circular, rectangular, arched) with a span of 10 m at a depth of more than 40 m in undisturbed or unfaulted ground, a roof wedge with a cone angle of less than the friction angle (average joint dip steeper than friction angle) will be inherently stable. This rule of thumb is illustrated in Figure 3.8.

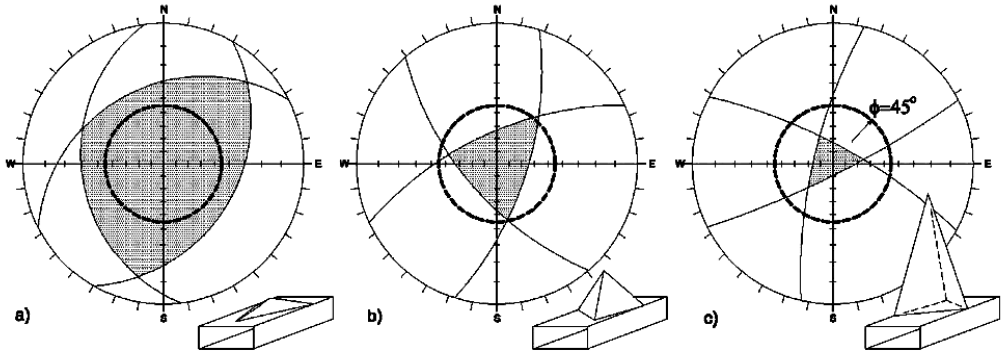

Figure 3.8: Identification on lower hemisphere stereo nets of clamping stability for simple wedges: (a) shallow wedge released in all conditions; (b) wedge with apex angle close to friction angle - stable if confined; (c) steep wedge stable unless relaxation is extreme (after Diederichs 1999)

This stabilizing confinement, however, can be lost in situations where: a stope is mined near the drift; a shallow fault is nearby; an intersection is created; or in a sill undergoing active mining (Figure 3.9). Such geometry- or structurally-induced relaxation may also lead to delayed failure and can be particularly dangerous in active mining areas.

For tunnel intersections, horizontal confinement loss is induced by a disruption of stress flow in two directions, not just around the initial drift. Intersections at depth also increase midspan displacement (elastic displacement in an intersection is 1.5 to 2-times the initial roof displacement). This additional deflection increases the zone of tension or relaxation in the roof at midspan allowing larger joint defined blocks to be released as shown in Figure 3.10. For this reason, intersections often require substantially higher support capacities, i.e., cablebolting. Discrete wedge identification or a semi-empirical approach to structural hazard assessment, taking relaxation into account is a prudent measure when designing intersections (Diederichs *et al.* 2000).

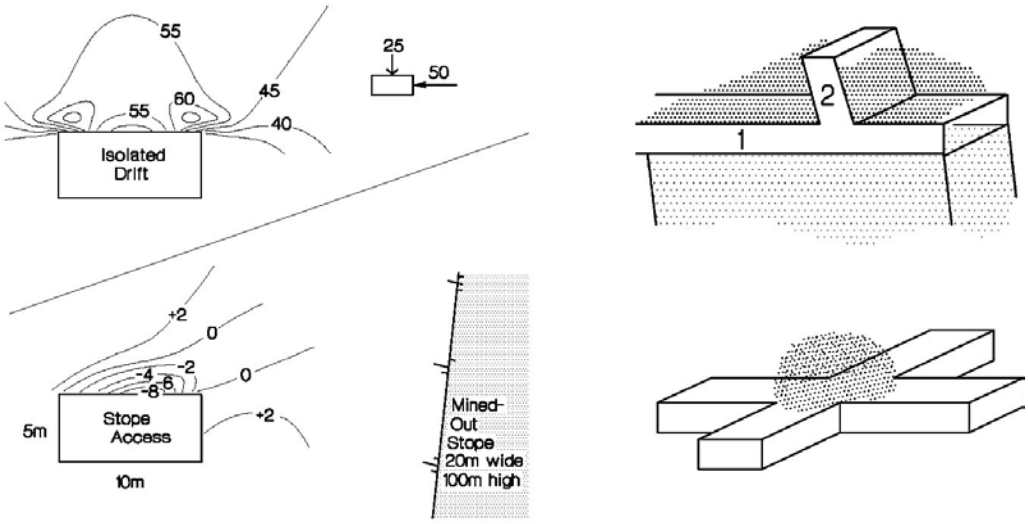

Figure 3.9: Relaxation or equivalent elastic tension (negative values (MPa)) in an access drift after nearby mining (left), adjacent to a new mining panel (top-right) and above an intersection (lower-right). Such relaxation can lead to wedge fallout or rockmass instability.

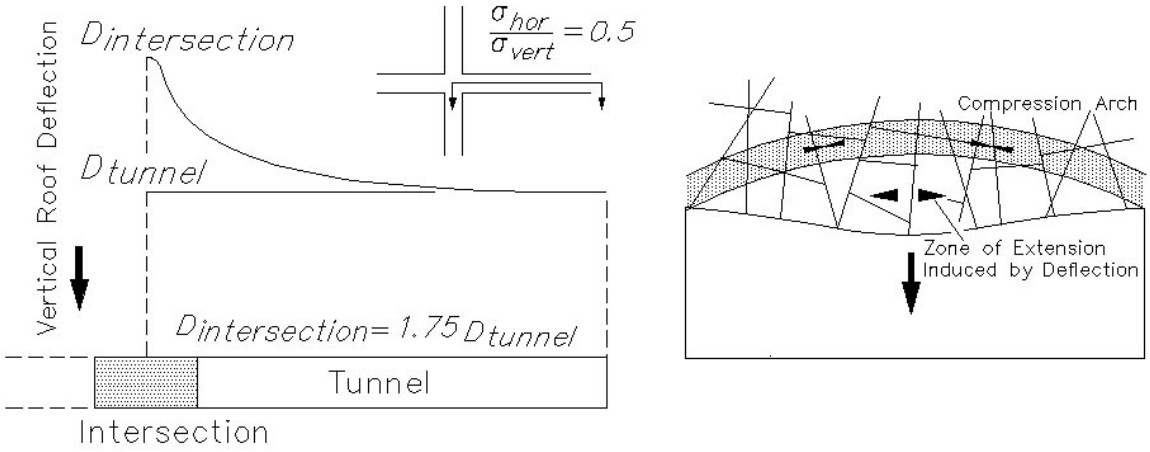

Figure 3.10: Increased roof deflections due to intersection creation (left) with consequent increase in zone of lateral extension or relaxation (right)

3.2.2 Drift instability in highly stressed ground

In highly stressed ground, failure around a tunnel is initiated by localized yield or by spalling or slabbing when the tangential stresses near an excavation exceed the rock mass strength. In mining, most tunnels are of rectangular shape with slightly arched backs and stress raisers, at sharp corners of excavations, often initiate this spalling process (Figure 3.11). Semi-circular fractures propagate until a more stable (nearly circular or elliptical) excavation shape is established. The detached material between the excavation boundary and the fractures emanating from the stress raisers is called "baggage" (Kaiser and Tannant 1999) because it needs to be held in place unless it is removed to create a geometrically more stable excavation shape (arched backs). Vasak and Kaiser (1995) corroborated numerically that this baggage formation is inevitable at depth for openings and pillars with sharp corners and that this instantaneous process is distinct from the subsequent progression of damage beyond this baggage zone. Martin *et al.* (1999) explored and provided guidelines for conditions when arched backs should be adopted. They showed that flat roofs are more stable at intermediate in situ stress conditions while arched backs are beneficial at great depth, because the demand on the support is reduced as the baggage is eliminated or at least significantly reduced. However, if the stress concentration near the curved wall exceeds the rock mass strength failure will further propagate until a new equilibrium is reached at some depth of failure d_f (see insert in Figure 3.11).

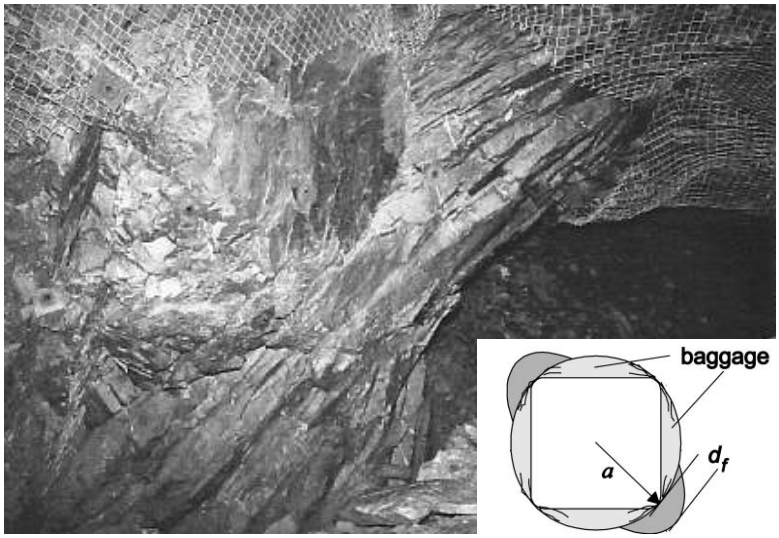

Figure 3.11: Baggage formation by curved fracture propagation from stress raiser (corner of excavation)

Attempts to predict either the onset of this brittle failure process or the maximum depth to which the brittle failure process will propagate, using traditional failure criteria based on frictional strength models, have not met with much success (Wagner 1987; Castro 1996; Grimstad and Bhasin 1997; Diederichs 1999). One approach, which attempts to overcome this deficiency, is to model the failure process progressively by using iterative elastic analyses and conventional failure criteria. The initial zone of failure is removed, and the analysis is then repeated based on the updated tunnel geometry. This incremental excavation sequence is intended to simulate the progressive nature of brittle failure. However, this process is not self-stabilizing, and as a result, over-predicts the depth of failure by a factor of 2 to 3. Pelli *et al.* (1991) found that localized failure could only be properly predicted if unusually low *m*- and high *s*-values (Hoek-Brown parameters) were adopted in numerical failure simulations.

Martin and Chandler (1994) demonstrated in laboratory experiments that in the brittle failure process peak cohesion and friction are not mobilized together and that most of the cohesion is lost before peak friction is mobilized. They postulated that around underground openings the brittle-failure process is dominated by a loss of the intrinsic cohesion of the rock mass such that the frictional strength component could be ignored. This eventually lead to the development of brittle parameters for the Hoek-Brown failure criteria (Martin *et al.* 1999). The applicability of this approach as a general criterion for estimating the depth of brittle failure is illustrated here for tunnels and in the following section for pillars. It was also demonstrated that it is applicable to dynamic loading conditions, i.e., to predict the depth of failure during rockbursts (Vasak and Kaiser 1995).

By analysing case studies of observed depth of failure from excavations damaged by rockbursts (Kaiser *et al.* 1996) and from tunnels around the world failing in a progressive, non-violent manner (Martin *et al.* 1999), an empirical relationship between the depth of failure and the stress level was established for brittle rock. These studies show that the depth of failure normalized to the tunnel radius *a* is linearly proportional to the normalized stress level σ_{max}/σ_c, as summarized by Equation 3.3. In this ratio, σ_{max} is calculated as the ratio of maximum tangential stress at the wall of a circular opening, placed at the drift location and in the same in situ or mining-induced stress field. This value is divided by the laboratory uniaxial compressive strength σ_c.

$$\frac{d_f}{a} = 1.25\frac{\sigma_{\max}}{\sigma_c} - 0.51 \pm 0.1 \qquad \text{(Martin } et\ al. \text{ 1999)} \qquad \text{(Eq 3.3)}$$

The stress level defined in this manner is identical to the stress concentration factor *SCF* introduced by Wiseman (1979). Figure 3.12 presents the data used to arrive at the linear best fit represented by Equation 3.3.

It is of practical importance to realize that in hard rock σ_{max} and therefore the depth of failure is insensitive to the support pressure applied at the excavation wall (for an extreme support pressure of 2 MPa the depth of failure is only reduced by 2 to 3%).

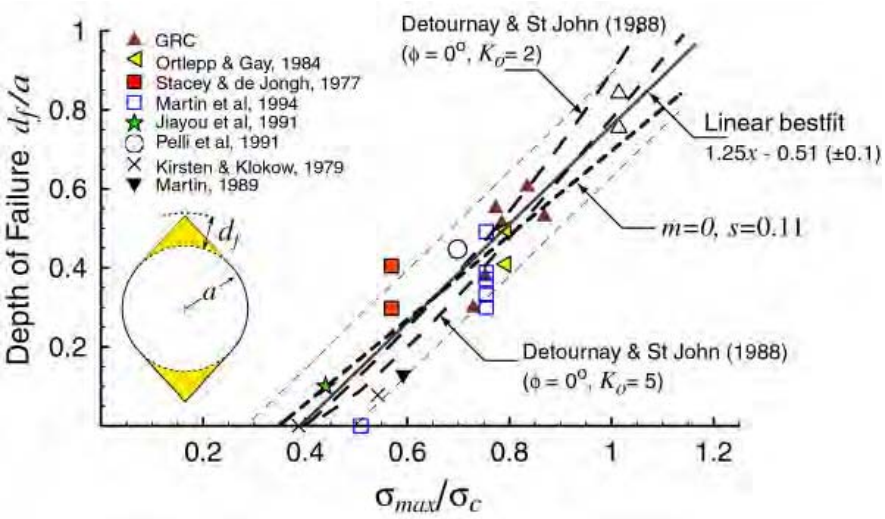

Figure 3.12: Depth of failure data compared to predictions utilizing brittle rock parameters (m or $\phi = 0$)

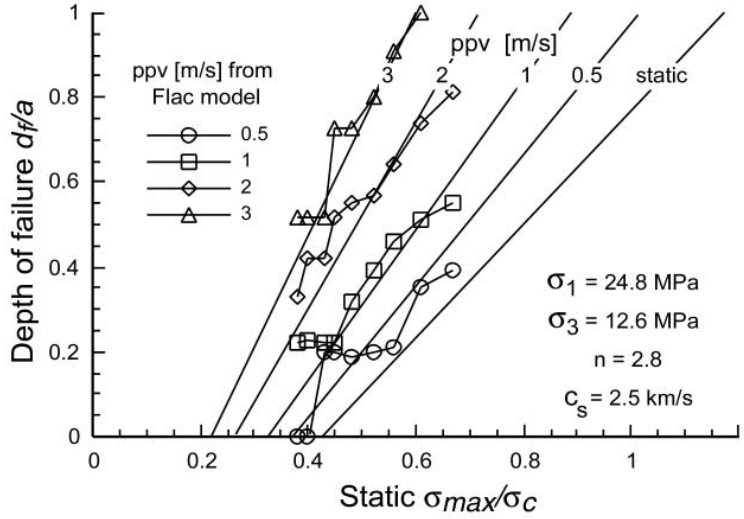

Figure 3.13: Example of predicted or simulated dynamic deepening of depth of failure as a function of ground motion level (peak particle velocity *ppv* = 0 to 3 m/s) at the location of a drift; $n = 4 \cos\theta$, a factor that depends on incident angle θ, and c_s = shear wave propagation velocity (after Kaiser *et al.* 1996)

Martin *et al.* (1999) demonstrated using PHASE2™[8] that this empirical relationship (Eqn 3.3) could be predicted utilizing the proposed brittle Hoek-Brown parameters ($m = 0$; $s = 0.11$) in elastic numerical models (Figure 3.12).

Utilizing equivalent brittle parameters ($\phi = 0$ and a rock mass strength $q = \sigma_c \sqrt{s}$), this interdependence can also be predicted for tunnels in deviatoric stress fields with the closed-form solutions presented by Detournay and St. John (1988). Figure 3.12 illustrates for a range of $K_o = 2$ to 5 that the maximum depth of failure is insensitive to the stress ratio. Only for high stress levels (>0.8), does the empirical relationship (Eqn 3.3) tend to underestimate the depth of failure. On the other hand, the depth of failure predicted by Detournay and St. John (1988) is under-predicted by about 50% if conventional parameters with friction angles on the order of 30 to 45° are applied.

Dynamic loading of an excavation can drastically enlarge the depth of failure, i.e., during strain bursts induced by dynamic stress increments. When a dynamic wave propagates through rock, it induces a stress change that is magnified by the excavation. The effect of this dynamic stress wave can be predicted by superimposing static and dynamic tangential stresses (Kaiser *et al.* 1996). Figure 3.13 illustrates this for a specific example whereby theoretical predictions of depth of failure are compared with results from FLAC™[9] modelling.

Using the empirical or analytical depth of failure relationships presented earlier in combination with the method introduced in Section 2 for mining-induced stress level calculation, this provides an effective means to assess the impact of stress and stress change on the stability of a tunnel in highly stressed ground. Figure 3.14 shows the depth of failure chart, rotated to align with the stress level axes of the principal stress space. Also shown here is the stress state of the example introduced in Section 2. When a stress path exceeds both, the damage initiation threshold ($m = 0$) and the spalling limit $\sigma_1/\sigma_3 > 10$, the severity of instability is reflected by the corresponding depth of failure. The dashed arrows indicate how the maximum depth of failure

[8] Available from Rocscience Inc., 31 Balsam Ave., Toronto, Ontario, Canada M4E 3B5, http://www.rocscience.com

[9] Available from Itasca Consulting Group, Inc.708 South Third Street, Suite 310 Minneapolis, MN 55415, USA, http://www.itascacg.com

increment Δd_f is obtained for an excavation experiencing mining-induced stress change $\Delta\sigma$. For the scenario introduced in Section 2, the depth of failure would increase due to mining-induced stress change by more than threefold from 0.2 to 0.7.

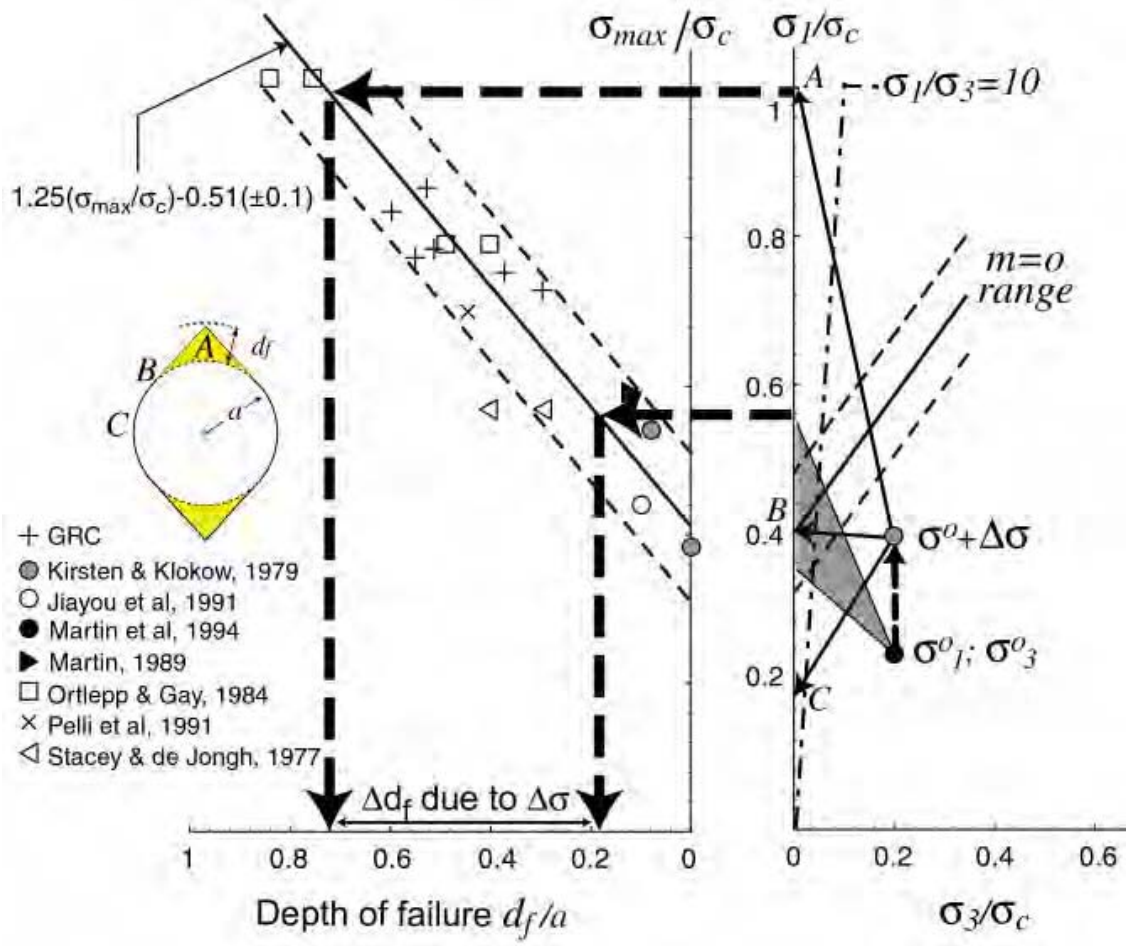

Figure 3.14: Depth of failure chart (Figure 3.12) combined with stress space chart (Figure 2.10)

3.2.3 Estimation of shaft overbreak

A practical application of the depth of failure logic developed above is the estimation of the breakout area that will evolve around a borehole, tunnel or shaft. For example, a 9.5 m diameter concrete lined shaft is being considered for a deep mine in the Canadian Shield. One of the concerns for the shaft is the extent and depth of spalling failure that can be expected, as this void will have to be replaced with concrete. Two approaches were used to estimate the possible extent of this failure: (1) well bore breakout data from acoustic televiewer logs and (2) the depth of failure logic.

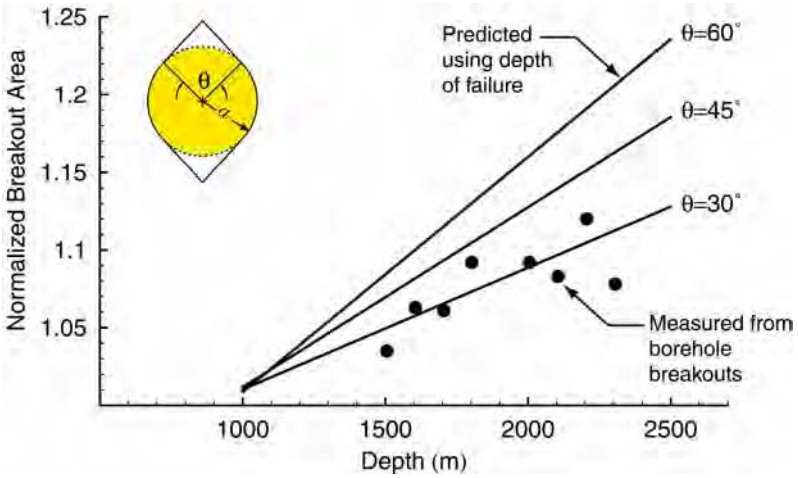

Figure 3.15: Comparison of overbreak area estimates using depth of failure logic (Eqn 3.3) and measured overbreak from televiewer

From acoustic televiewer surveys carried out in the vicinity of the future shaft, the cross-sectional area of breakout was determined and normalized to the borehole cross-sectional area based on a nominal borehole diameter of 76 mm. This was then compared to the depth of failure relationship given by Equation 3.3 assum-

ing a typical in situ stress relationship with depth for the Canadian Shield (Herget 1993). The estimated depth of failure assumes that the breakout has a triangular shape and is constrained by Equation 3.3 and the breakout angle θ. Figure 3.15 compares the results from both approaches. Experience from tunnels suggests that the breakout angle can range from 30 to 60° while the televiewer logs recorded an average breakout angle of 40°. Despite the difference in the diameters of the borehole (76 mm) and the tunnel (9500 mm), both methods show the same trend with the borehole providing a lower bound estimate. For a 10 m diameter shaft, advanced to a depth of 2500 m, this suggests that about 30,000 tonnes of extra muck would have to be hoisted and the cost of extra concrete would be on the order of one million dollars (assuming \$100/m^3 for in-place concrete).

3.3 Pillar design

Pillars can be defined as the rock between two or more underground openings. Hence, all underground mining methods utilize pillars, either temporarily or permanently, to safely extract ore. Observations of pillar failures in Canadian hard rock mines indicate that the dominant mode of failure is a progressive slabbing and spalling process, suggesting that pillars should be designed by application of the brittle rock parameters introduced earlier . The design of pillars in these rock masses can follow three approaches:

- attempt to numerically simulate the slabbing process using appropriate constitutive models;
- use empirical pillar stability graphs and pillar formulae; and
- select a rock mass strength criterion based on an evaluation of rock mass characteristics and calculate the pillar strength to stress ratio at each point using continuum models.

Here, we will focus on the second and third approach, particularly using the recently developed Geological Strength Index *GSI* and the Hoek-Brown failure criterion. Case studies from the Elliot Lake uranium mines are used to demonstrate that the conventional Hoek-Brown parameters based on *GSI* do not accurately predict the strength of hard rock pillars, but the brittle Hoek-Brown parameters *(m_b = 0, s = 0.11)* do show good agreement with observations. It will be demonstrated that the conventional Hoek-Brown failure envelopes over predict the strength of hard-rock pillars because the failure process is fundamentally controlled by a cohesion-loss process in which the frictional strength component is not mobilized. As explained earlier, this process is not reflected in the conventional Hoek-Brown strength parameters and therefore does not properly simulate the near wall slabbing process.

3.3.1 Pillar failure observations

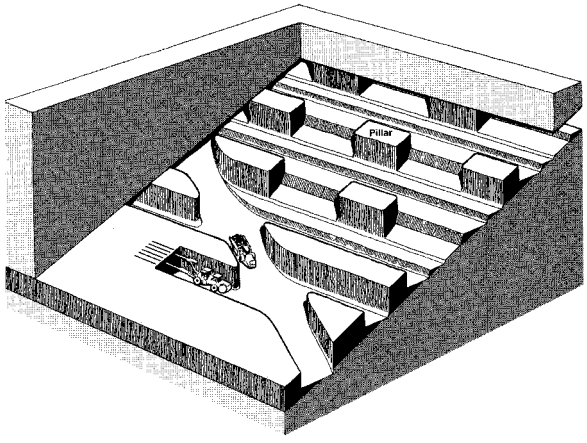

Figure 3.16: Illustration of the room-and-pillar mining method. In order to use trackless equipment, transport drifts must cut across the orebody if the dip exceeds 20%.

The Elliot Lake uranium orebody was actively mined from the early 1950s through to the mid 1990s. The shallow (10 to 20°) dipping tabular deposit was characterized by uranium bearing conglomerates separated by massive quartzite beds 3 to 30 m thick (Hedley and Grant, 1972; Coates *et al.* 1973). Mining was carried out using room-and-pillar and stope-and-pillar methods. An example of room-and-pillar mining with trackless equipment is given in Figure 3.16. At Elliot Lake, the mine was laid out with long (76 m) narrow rib pillars formed in the dip direction.

Pritchard and Hedley (1993) compiled, via detailed mapping, the progressive nature of hard-rock pillar failure that was observed in the Elliot Lake mines (Figure 3.17). Their observations clearly show the initiation of spalling and the gradual loss of the pillar's load carrying capacity as the pillar developed an hourglass geometry. They suggested that the peak strength of the pillar was reached by Stage II in Figure 3.17 when axial splitting, i.e., extension fracturing of the pillar, was observed. Furthermore, they noted that in the early (pre-peak strength) stages of pillar failure at Elliot Lake stress-induced spalling, dominated the failure process while in the latter stages (post-peak strength), after spalling had created the typical hour-glass shape, slip along structural features such as bedding planes and joints played a more dominant

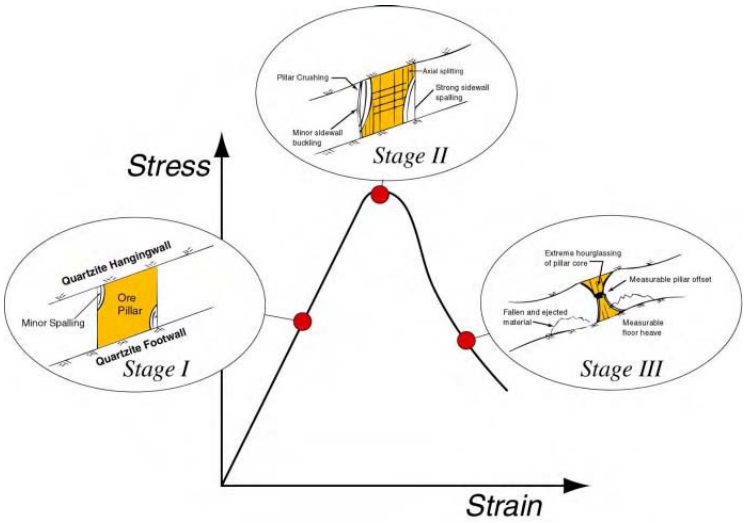

Figure 3.17: Observations and illustration of the progressive nature of hard-rock pillar failure (sketches from Pritchard and Hedley (1993))

role in the failure process. These observations are in keeping with the laboratory findings of Hudson *et al.* (1972) and Martin and Chandler (1994) who demonstrated that the development of the shear failure plane in laboratory samples also occurs after the peak strength is reached. Numerical crack accumulation and interaction studies by Diederichs (1999) show consistent results.

3.3.2 Empirical pillar strength formulas

Following the Coalbrook disaster of 1960, in which the collapse of 900 pillars resulted in the loss of 437 lives, a major coal-pillar research program was initiated in South Africa. Using the back-calculation approach Salamon and Munro (1967) and Salamon (199) analyzed 125 case histories involving coal pillar collapse and proposed that the coal-pillar strength could be adequately determined using the power formula:

$$\sigma_p = K \frac{W^\alpha}{H^\beta} \qquad \text{(Eq 3.4)}$$

where σ_p (MPa) is the pillar strength, K (MPa) the strength of a unit volume of coal, and W and H are the pillar width and height in metres, respectively. The notion that the strength of a rock mass is to a large part controlled by the geometry of the specimen, i.e., the width to height ratio, has since been confirmed by extensive laboratory studies, e.g., Hudson *et al.* (1972) and Ormonde and Szwedzicki (1993).

One of the earliest investigations into the design of hard-rock pillars was carried out by Hedley and Grant (1972). They analyzed 28 rib pillars (3 crushed, 2 partially failed, and 23 stable) in massive quartzite and conglomerates in the Elliot Lake room and pillar uranium mines. Since 1972 there have been several additional attempts to establish hard rock pillar strength formulas, using the back calculation approach. These are summarized in Figure 3.18 showing the predicted pillar strength from the various formulas using a pillar height of 5 m. The pillar strengths in Figure 3.18 have been normalized to the laboratory uniaxial compressive strength σ_c.

What is surprising, and must be conceptually incorrect, is that all pillar strength equations have an asymptotic strength value as the pillar width to height ratio increases. Clearly very wide pillars should have very high strength and the curvature should be convex upward. The asymptotic shape, however, makes sense if it is assumed that stability of pillars is actually defined by the severity of failure at the pillar wall, i.e, the pillar skin behaviour.

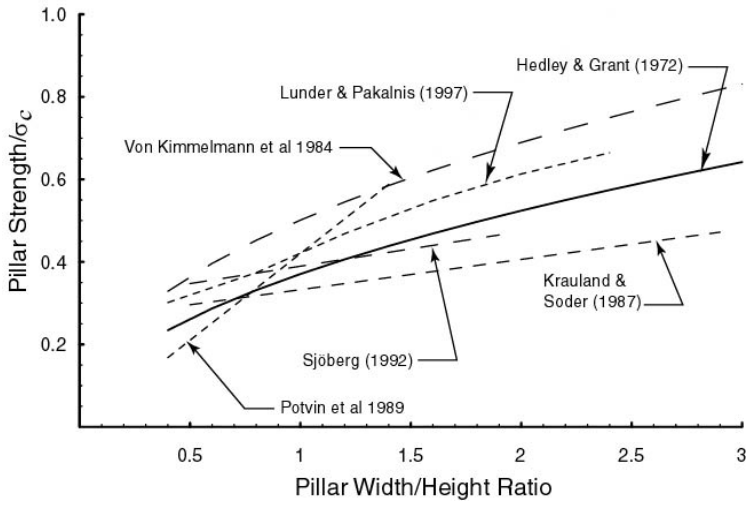

Figure 3.18: Comparison of various empirical hard rock pillar strength formulas

By utilizing the maximum pillar skin stress calculated by Obert and Duvall (1967) for rib-pillars as a function of pillar stress and introducing them in Equation 3.3 (with $a = H/\sqrt{2}$), the pillar stress for a given depth of failure normalized to the pillar height H can be obtained. Lines of constant depth of failure normalized to the pillar height are shown in Figure 3.19 together with data of Lunder and Palkanis (1997). The shape of these curves is also asymptotic and similar to those provided

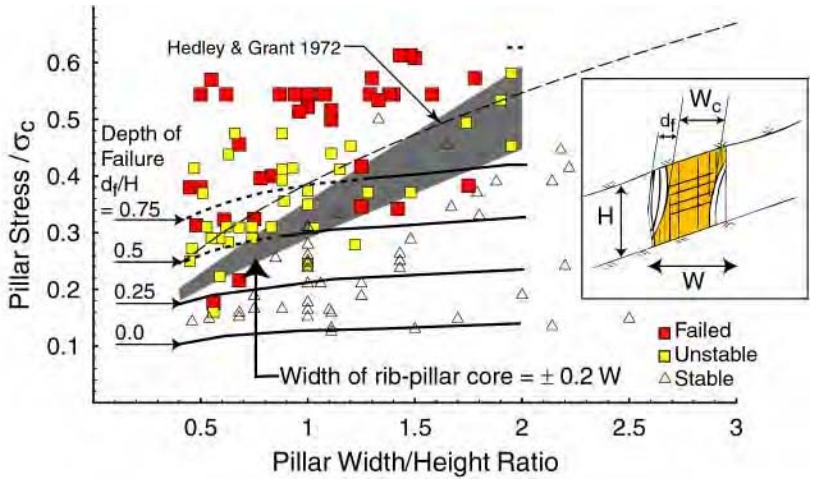

Figure 3.19: Comparison of data and selected empirical pillar equations with predicted depth of failure d_f/H (valid for rib-pillars only) and zone of predicted near-zero pillar core width (shaded area)

by most pillar equations. These considerations illustrate that the various pillar equations actually provide empirical guidelines to ensure that the stresses at the pillar wall are not excessive, i.e., that the depth of spalling is limited such that there remains some load-bearing core in the pillar. According to Figure 3.19, two narrow pillars were classified as "failed" when the depth of failure reached 20 to 35% of *H*. Most pillars rated as "unstable" or "failed" fall beyond an estimated depth of failure of 50% of the pillar height. The upper bound to the group of "unstable" pillars can roughly be described by a predicted depth of failure equal to the height of the pillar (not shown because it implies through-going spalling for $W/H < 2$).

Furthermore, the width of the non-failed pillar core W_c can be estimated as (W-$2d_f$), ignoring the fact that some stress redistribution occurs. The predicted range of near zero core width, i.e., when the spalling process reaches the center of the (rib-) pillar, is shown in Figure 3.19 by the shaded zone. It can be seen that all but a few cases of pillars rated as "failed" or "unstable" fall above this zone. It follows that the depth of failure equation (Eqn 3.3) can therefore be used to assess pillar failure. When the calculated depth of failure reaches half the pillar width, the pillar must be rated as unstable with a high potential for complete failure.

3.3.3 Pillar strength using Hoek-Brown brittle parameters

In the following, the Hoek-Brown brittle parameters, $m_b = 0$ and $s = 0.11$, introduced by Martin *et al.* (1999) will be adopted to further investigate pillar stability. The fundamental assumption in using these brittle parameters is that the early stages of failure is dominated by cohesion loss associated with rock mass fracturing, and that the confining stress dependent frictional strength component can be ignored, as it cannot be mobilized when hour-glassing occurs. This approach is clearly not applicable to simulate the final stages of failure in wide pillars where the frictional strength component can be mobilized and dominates the behaviour of the core of a pillar.

Martin and Maybee (2000) used PHASE2 and the Hoek-Brown brittle parameters to evaluate pillar stability over the range of pillar *W/H*-ratios from 0.5 to 3. The analyses were carried out using a constant horizontal to vertical stress ratio of 1.5 and the results are presented as heavy, solid lines in Figure 3.20 for a Factor of Safety *FOS* equal to 1 and 1.4. A pillar was considered to have failed when the core of the pillar had a *FOS* = 1. The same approach was used to establish when the pillar core reached a *FOS* = 1.4. The empirical pillar strength formulas of Hedley and Grant (1972) and Lunder and Palkanis (1997) as well as the database of Lunder and Palkanis (1997) are shown in Figure 3.20 (Note: beyond a pillar *W/H*-ratio of 2.5 there are no recorded pillar failures).

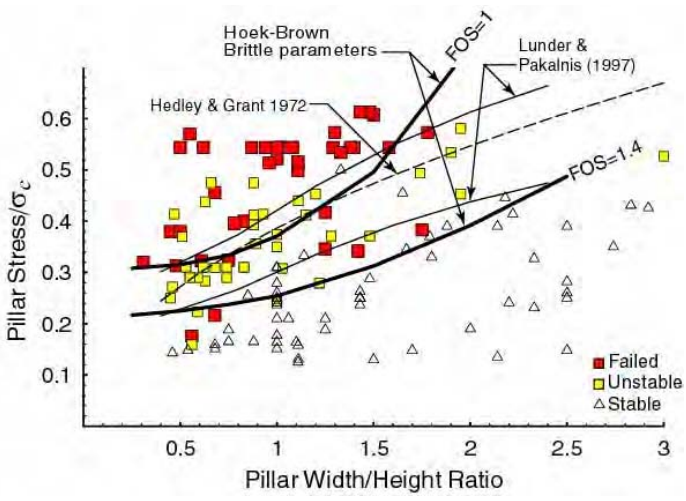

Figure 3.20: Comparison of the pillar stability graph and PHASE2 modeling results using the Hoek-Brown brittle parameters (modified from Martin and Maybee (2000))

According to Figure 3.20 there is only a small deviation between the predicted *FOS* = 1 line using the Hoek-Brown brittle parameters and the empirical stability lines proposed

by Hedley and Grant (1972) and Lunder and Palkanis (1997) for pillars with *W/H* of 0.5 to 1.5. However, for wider pillars, *W/H* of 1.5 and 2.5, the empirical formulas suggest only a modest increase in pillar strength whereas the predicted brittle stability line suggests a significant increase in pillar strength. This predicted increase in pillar strength is more in keeping with observations as the number of pillar failures decreases significantly once the pillar *W/H*-ratio increases beyond 1.5. Most importantly, in contrast to the empirical stability lines for pillars with *W/H* < 0.75, the predicted pillar strength is essentially constant. This is consistent with field observations, except for special cases of pillars subjected to shear loading as discussed in the following section.

3.3.4 Strength of pillars under inclined loads

The Quirke Mine, which was brought into production in 1969, was one of several mines in the Elliot Lake Camp that used room-and-pillar stoping to extract the dipping uranium bearing reefs to depths of 1050 m. Figure 3.21 shows the general arrangement of the stopes and rib pillars (Hedley *et al.* 1984). The reefs were 3 to 8 m thick and dipped to the south at approximately 20°. Coates *et al.* (1973) reported that the uniaxial laboratory strength of the reefs and the massive quartzite that overlay and underlay the reef averaged 230 MPa. They also reported that in the east-west direction (strike) the horizontal far-field in situ stress is 2 to 2.5-times the vertical stress and in the north-south direction (dip) the horizontal far-field in situ stress is about 1.5-times the vertical stress.

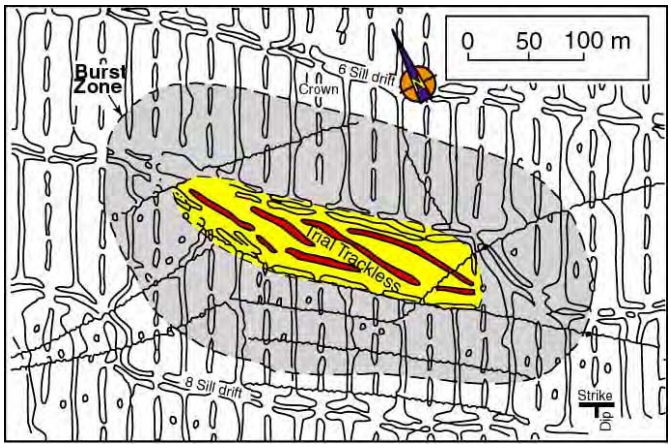

Figure 3.21: Stope and pillar layout at Quirke mine

The rock mass quality of the pillars in the Quirke mine can be classified as Very Good *Q'*= 40 to 100 (C. Pritchard, pers. comm.). Hoek and Brown (1998) suggested that the Geological Strength Index *GSI* can be related to *Q'* by:

$$GSI = 9 \ln Q' + 44 \qquad \text{(Eq 3.5)}$$

indicating that the rock mass strength can be characterized by *GSI* ranging from 77 to 85. A *GSI*-value of 80 was used to establish the parameters for the Hoek-Brown failure criterion (Table 3.1) for the Quirke mine pillars.

In 1978, a trial trackless area was mined out as shown in the center of Figure 3.21 and illustrated by Figure 3.16. Shortly after mining of the stopes in the trackless area started, deterioration of surrounding pillars was observed and some 13 months later rockbursting began. Hedley *et al.* (1984) provides a detailed account of the rockburst history and mining sequence. For the most part, there was a gradual deterioration of the pillars oriented along the strike of the orebody near the trackless area, similar to that described in Figure 3.21. Pillars that were oriented in the dip direction of the orebody remained relatively stable.

Table 3.1 Parameters used in the PHASE2 modelling to estimate the strength of the Quirke mine pillars assuming an elastic brittle response.

Parameter	Description	Value
Rock type	Quartzite	
Intack rock strength	σ_{ci} =	230 MPa
Geological Strength Index	*GSI* =	80
Hoek-Brown constants	m_i =	22
	m_b =	10.7
	s =	0.108
	m_r =	1
	s_r =	0.001

The Quirke mine pillars typically have *W/H*-ratios varying from 0.5 to 1.7 and dip at 20°. To examine the effect of this inclination on pillar strength, a series of elastic analysis were carried out using the Hoek-Brown parameters given in Table 3.1 and the Hoek-Brown brittle parameters. Figure 3.22 shows the results for rib-pillars oriented parallel to the dip of the orebody with maximum stress horizontal. Both failure criterion indicate that these dip pillars are stable.

Figure 3.23 shows the numerical modeling results for the pillars oriented parallel to strike compared to the pillar failure observations made by Pritchard and Hedley (1993). For these strike pillars, the traditional Hoek-Brown criterion

predict that the strike pillars are also stable while the Hoek-Brown brittle parameters clearly show that the strike pillars are unstable. Note that the Hoek-Brown brittle parameters show the initiation of failure in corners of the pillars in keeping with the observations reported by Pritchard and Hedley (1993). This example nicely illustrates the difficulties of using the traditional Hoek-Brown parameters for assessing brittle failure and the success of the Hoek-Brown brittle parameters in matching field observations.

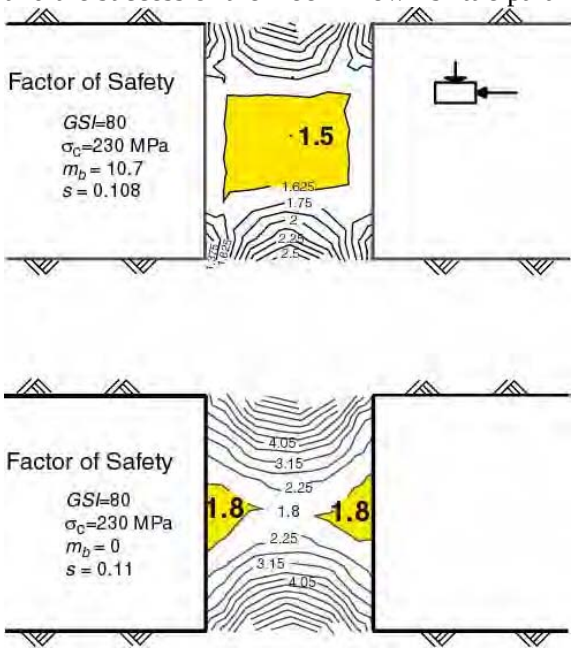

Figure 3.22: Comparison of the pillar factor of safety using the Hoek-Brown conventional parameters (m_b = 10.7, s = 0.11) and the Hoek-Brown brittle parameters (m_b = 0, s = 0.11)

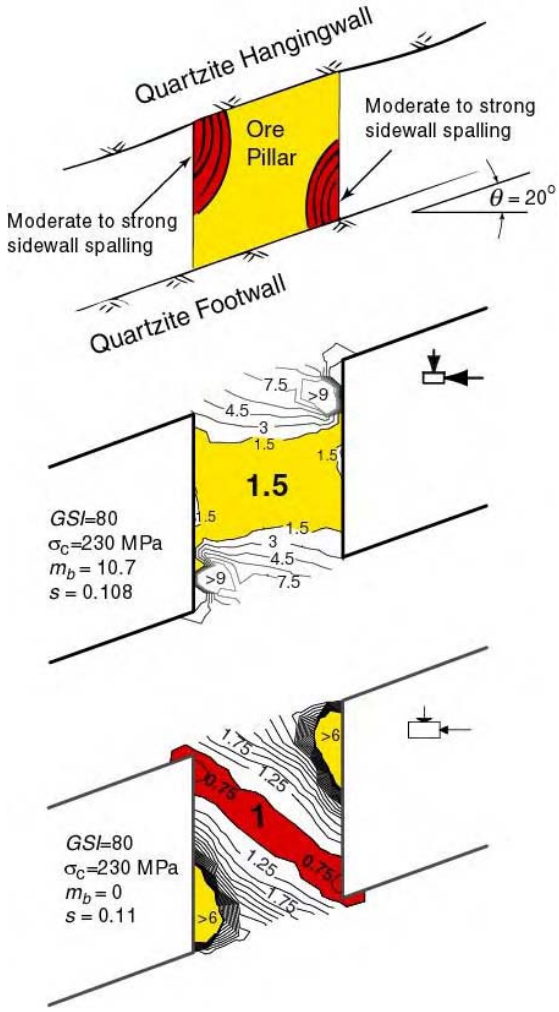

Figure 3.23: Comparison of observed pillar failure with predicted failure (factor of safety less than 1) using Hoek-Brown conventional parameters (m_b = 10.7, s = 0.11) and brittle parameters (m_b = 0, s = 0.11)

From a practical perspective, this example illustrates that the pillar strength can be significantly reduced when, during late stage mining, relative movements of hanging-wall and footwall inflict shear stresses on pillars. We suspect that several of the pillars with data points that fall below the predicted failure curves in Figure 3.20 were affected by shear. Furthermore, for wide pillars with W/H > 2, this study shows that pillar stability is dominated by skin failure, a fact that should be taken into account when designing wide pillars and when estimating energy release values for pillar bursts. In other words, bursts of wide pillars may not involve the entire pillar but only the skin of the pillars.

3.4 Rockbursting

When mining in hard brittle rock under high stress, rock will tend to fail in a violent manner; i.e., it will burst. A rockburst is defined as damage to an excavation that occurs in a sudden or violent manner and is associated with (not caused by) a seismic event. There are basically three classes of rockbursts: (1) fault slip, (2) pillar, or (3) strain bursts.

1. Fault slip burst – is a rockburst caused by the sudden, earthquake-like movement along a weakness in the rock mass (e.g., a fault) that causes a sudden change in the stress field within the volume of influence and radiates energy in the form of ground vibration. Unless a fault intersects an excavation, damage is triggered or caused by (1) stress-induced failure due to a dynamic stress increment, (2) acceleration of marginally stable rock blocks, called seismically-induced ground falls, or (3) energy transfer to such blocks causing rock ejection.

2. Pillar burst – occurs when static or dynamic stresses exceed the rock mass strength and lead to the sudden failure of an entire pillar or part of a pillar; its skin.
3. Strain burst – is encountered when static or dynamic stresses exceed the rock mass strength in the wall of an excavation. In this case, the damage consists of the brittle, violent failure of the unsupported or supported rock mass near the excavation wall. The term "brittle" implies that failure is associated with a sudden loss of rock mass strength near the excavation and the term "violent" implies that energy is released during this failure process. For civil engineering applications, this class of rockburst is most relevant.

From an engineering perspective, however, this classification is not very useful as it mixes causes and effects, and often implies a measure of severity that is not relevant from an excavation design perspective. Fault slip may be the cause for a seismic event but a pillar or a strain burst could be the consequence of engineering significance. Fault slip events are often most violent in terms of event magnitude but a pillar burst may be most damaging to an underground excavation.

For tunnelling, it is more meaningful to categorize rockbursts by *trigger mechanism*, *damage mechanism* and *severity*.

3.4.1 Rockburst trigger mechanisms

There are two trigger mechanisms for rockbursts:

1. Remotely triggered rockburst - where a remote seismic event, e.g., an earthquake or a fault slip event, triggers and causes damage to an excavation at another location; and
2. Self-initiated rockburst – where the seismic event and the damage location are essentially identical.

The first type occurs in seismically active regions or in mining and is discussed by Gürtunca and Haile (1999). In the following, we focus primarily on the second type, the self-initiated rockbursts. These rockbursts occur when the stresses near the boundary of an excavation exceed the rock mass strength, and failure proceeds in an unstable or violent manner. Failure is sudden and violent if the stored strain energy in the rock mass is not dissipated during the fracturing process. This occurs when the stiffness of the loading system is softer than the post-peak stiffness of the failing rock (Jaeger and Cook (1969); Brady and Brown (1993)). In general, pillars with low *W/H*- ratio are loaded by a soft loading system where the imposed deformation was excessive relative to the deformation needed to fail the pillar wall.

Whether self- or remotely triggered, the rock fails when stresses exceed the strength. The stresses causing failure may be a combination of some or all of the following:

- gravitational stresses,
- excavation-induced stresses
- dynamic forces due to ground vibrations (inertial forces during acceleration or deceleration), and
- dynamic stress increments due to dynamic straining of the ground (caused by strain waves).

When these stresses exceed the capacity of the unsupported or supported rock, even temporarily, failure is initiated or triggered. Hence, the potential for rockbursting is best defined in terms of the stress level (or a stress-to-strength ratio, i.e., $\sigma_{wall}/\sigma_c = \sigma_{max}/\sigma_c$; see earlier).

3.4.2 Rockburst damage mechanisms

When failure is initiated, three distinct damage mechanisms may be encountered as illustrated by Figure 3.24 and described in more detail by Kaiser *et al*. (1996):

1. Seismically induced rock falls (or falls of ground) caused by seismic shaking, which creates acceleration-enhanced gravitational forces. This mechanism is most critical when marginally stable conditions exist, e.g., due to the forming of wedges by continuous geological structures. Increasing the holding capacity of the support can stabilize them.
2. Fracturing with rock mass bulking – occurs when static and dynamic stresses exceed the rock mass strength. In brittle rock, fracturing of the rock mass around an excavation is associated with a sudden volume increase or bulking of the failing rock. This bulking can be reduced by rock reinforcements as discussed earlier but the support system must also include deformable retaining and holding components to prevent unraveling of the broken rock between bolts.
3. Ejection of rock – can be caused by two mechanisms. For rockbursts triggered by a remote event, energy can be transferred from the seismic source to a marginally stable block of rock near an ex-

cavation (momentum transfer). This type of failure has been identified as a frequent cause for damage in deep South African mines (e.g., Gürtunca and Haile (1999)). During a self-initiated rockburst, part of the strain energy stored in the failing rock annulus may be converted to kinetic energy, leading to rock ejection.

3.4.3 Rockburst damage severity

Once failure is triggered, the severity of the damage depends on two factors: (1) the volume of rock involved in the failure process and (2) the energy that is released during the failure process (Aglawe 1999). The latter provides a measure of the violence of failure. The volume of failing rock depends on the extent of the excessively stressed zone of rock around an excavation or the depth of failure, and the releasable energy depends both on the stress at failure and the system response or the system stiffness during failure.

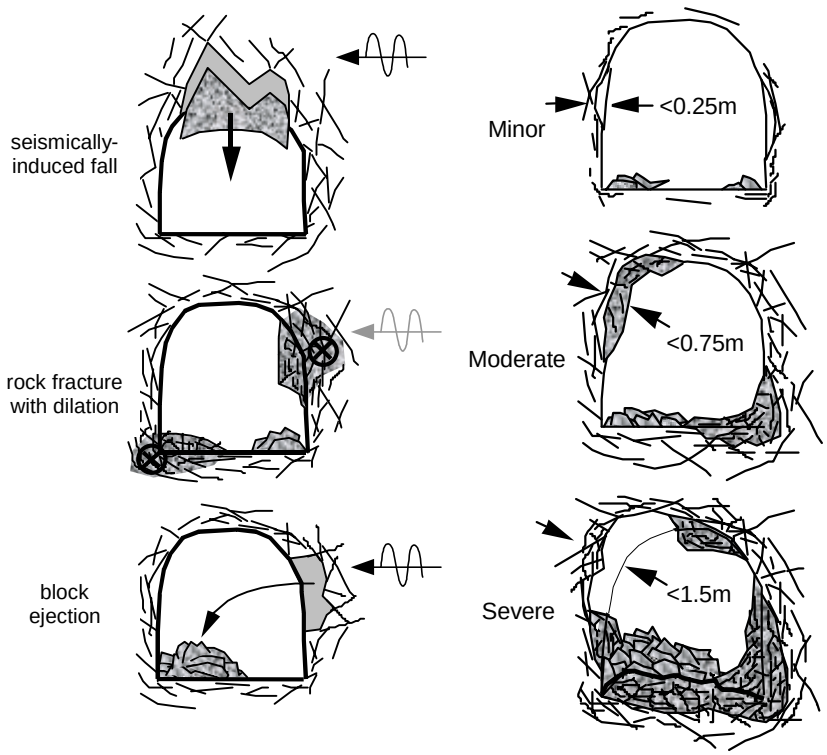

Figure 3.24: (a) Rockburst damage mechanisms; (b) Levels of rockburst damage severity (thickness of rock loosened or fractured is shown by arrows)

Because of the limited ability of rock support to resist rockburst damage, and the large amounts of energy that can be stored in hard rock under high stress, it takes relatively little failing rock to create conditions that classify as severe from a practical perspective. Failure around tunnels involving less than a 0.25 m thickness of fractured rock classify as minor damage; those involving about 0.75 m of failing rock as moderate damage, and those involving on the order of 1.5 m or more as severe damage (Figure 3.24(b)). The justification for this rating is given in Kaiser and Tannant (1999). It is largely guided by the maximum capacity of economically feasible support systems.

3.4.4 Violence of failure

The violence of failure in terms of energy release can be described either by the ejection velocity or the energy content of a volume of rock that is ejected. Since the kinetic energy must be dissipated by the rock support, it is more meaningful to consider the energy content per square metre of tunnel wall. Burst-resistant rock support systems typically have energy dissipation capacities between 5 and 20 kJ/m^2 with a practical maximum of about 50 kJ/m^2 (Kaiser *et al.* 1996).

The energy for rock ejection is some percentage of the total releasable energy of the failing rock annulus near the tunnel wall. The releasable energy is the total stored strain energy that is released if a block of rock is removed and includes the strain energy from within the block and from the surrounding rock mass. It depends on the stress level, the system stiffness (Aglawe 1999), and the volume of the failing rock, which is defined by the depth of failure d_f. Because the depth of failure is proportional to the tunnel radius for a given stress level, it follows that the releasable energy per unit area of tunnel wall increases as the tunnel size increases. Hence, larger tunnels require support with a higher energy dissipation capacity (Kaiser and Tannant 1999). For typical tunnel sizes and from an energy dissipation point of view, severe rockburst conditions can be expected when the failure depth exceeds 1.5 m. This provides the third justification for the severity classification presented in Figure 3.24(b).

3.5 Summary

Two modes of failure dominate the stability of deep underground excavations in hard rock: (1) stress-induced failure causing slabbing and spalling, and (2) rock mass relaxation promoting gravity-driven failures. Recognizing each mode of failure requires an understanding of the stress path the underground opening will follow.

It is shown that the depth of stress-induced failure can be estimated by setting the Hoek-Brown strength parameters to their so-called brittle values ($m = 0$, $s = 0.11$ to 0.25). The s-values for the brittle parameters should be calibrated with actual failures. The $m = 0$ approach can be used to estimate the depth of failure from both the static and dynamic loading of brittle failing rock. Furthermore, it is also demonstrated that these parameters can be used to assess the stability of pillars when uniaxially loaded or stressed by inclined loads. This practical approach to determine the extent of stress-induced spalling captures the fundamentals of brittle failure described in Section 2.

Strainbursts are defined as damage to an excavation resulting from a violent release of stored strain energy. The amount of damage is a function of the tunnel size and the stress magnitude. From an energy dissipation point of view, considering the maximum capacity of practically feasible support systems, severe rockburst conditions can be defined as conditions when the failure depth exceeds 1.5 m.

All rock masses contain fractures at some scale. If these fractures are not tightly clamped failure around the underground opening is dominated by gravity-driven relaxation of loose blocks. At depth, the shape of the underground opening can promote this rock mass relaxation. The importance of boundary parallel confining stress loss and the destabilizing impact of abutment relaxation on structurally dominated or laminated rock masses is highlighted. Such relaxation can be taken into account using existing empirical tools modified for use in relaxed ground. Recognition of the impact of confinement loss is particularly critical when assessing the stability of inclined stope walls, drift intersections and areas of complex and reentrant excavation geometry.

It should be noted that, fundamentally, failure around underground openings occurs where the confining stresses are very low or tensile. Hence, the stability criteria discussed in this section are restricted to predict the behaviour of underground openings. Furthermore, the content of this and the companion sections are restricted to hard, brittle failing rock where elastic stress calculations provide an accurate measure of induced stress conditions and where progressive spalling is the dominant failure mechanism.

4.0 SUPPORT OF HIGHLY STRESSED EXCAVATIONS

In highly stressed ground, rock support needs to control the failure process. However, it must be recognized that the strength of the support, e.g., concrete, is lower than the strength of the hard rock. Hence, control of the failure process basically means retention of the self-supporting capacity of the broken rock near the excavation without attracting undue stresses to the support components. For this and other reasons, rock support systems frequently consist of various elements, such as bolts, mesh, shotcrete, spray-on liners, etc., each fulfilling a different function.

When mining at depth in hard rock, failure often occurs in a violent manner in the form of strainbursts or seismically induced falls of ground. Hence, rock support needs to resist both static and dynamic loads. The interested reader is referred to the Canadian Rockburst Support Handbook (Kaiser *et al.* 1996) for a detailed treatment of support design in burst-prone ground. In this section, the authors primarily address two support design issues related to static loading: 1) support of highly stressed ground, i.e., control of the stress-induced fractured rock inside the depth of failure zone, and 2) support of relaxed ground, i.e., structurally controlled modes of failure and failure of pre-conditioned or stress-damaged ground due to mining-induced relaxation.

4.1 Design considerations

4.1.1 Support functions

Support systems are commonly comprised of various support components: bolts, mesh, shotcrete, spray-on linings, etc. Bolts are used to hold rock in place or to reinforce the rock mass; mesh is used to retain loose or broken rock; and shotcrete fulfils a combination of these functions. It holds by adhesion; strengthens the rock by preventing relative movements at the shotcrete/rock interface; and acts as a “supermesh” by provid-

ing a stiff retaining component with substantial bending or flexural capacity. The role each element plays is complex and depends on the ground-support interaction behaviour (McCreath and Kaiser 1992).

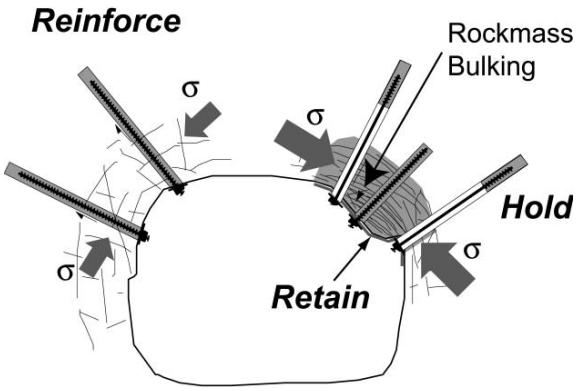

Figure 4.1: Three primary functions of support elements (Kaiser *et al.* 1996)

Each support component in a support system is intended to perform one of the three functions illustrated in Figure 4.1: (1) reinforce the rock mass to strengthen it and to control bulking, (2) retain broken rock to prevent key block failure and unravelling, and (3) hold key blocks and securely tie back the retaining element(s) to stable ground. While each support element may simultaneously provide more than one of these functions, it is convenient to consider each function separately:

1. The goal of *reinforcing* the rock mass is to strengthen it, thus enabling the rock mass to support itself (Hoek and Brown 1980). Reinforcing mechanisms generally restrict and control the bulking of the rock mass, thus ensuring that interblock friction and rock mass cohesion are fully exploited. Typically, reinforcing elements such as grouted rebars or dowels behave as stiff support elements, but other types, such as Split Sets, yielding Swellex or cone bolts, behave as ductile or yielding elements under high stress or deformation conditions.
2. While *retaining* broken rock at the excavation surface may be required for safety reasons, it may also become essential under high stress conditions to avoid the development of progressive failure processes that lead to unravelling of the rock mass. Qualitative observations indicate that full aerial coverage by retaining elements becomes increasingly important as the stress level increases (McCreath and Kaiser 1992). Retaining elements may be either stiff or strong, such as a cast concrete liner or a closed-ring shotcrete membrane, or they may be soft and able to yield, such as chain-link or welded-wire mesh, or isolated, slotted or flat shotcrete panels. Certain elements may undergo a transition from stiff to ductile behaviour at large differential displacements, (e.g., mesh-reinforced shotcrete).
3. The *holding* function is needed to tie the retaining elements of the support system back to stable ground, and to prevent gravity-driven falls of ground. Under certain conditions, a high strength anchorage into deeper-lying stable rock can provide this function, such as grouted cablebolts or resin-grouted dowel. However, under conditions of large imposed (relative) displacements between the anchor and the head of the holding element, a yielding element is required. The ability to yield may be enhanced by a special sliding mechanism (e.g., cone bolt or Split Set), by a highly ductile material (e.g., yielding SuperSwellex), or by a combination of both.

These three support functions gain increasing importance as the ground conditions worsen. For example, in good rock and at low stress, the holding and reinforcement functions are most important whereas in fair to poor rock, all three functions must be integrated (Figure 4.2). At intermediate to high stress, the retaining function is always required. This is automatically realized when appropriate stress reduction factors are used to characterize the ground (refer ahead to Figure 4.33**Error! Reference source not found.** for details). In very poor ground (Q < 1; Barton *et al.* 1974) large deformations must be anticipated and support components must retain their functionality over a large displacement range. In other

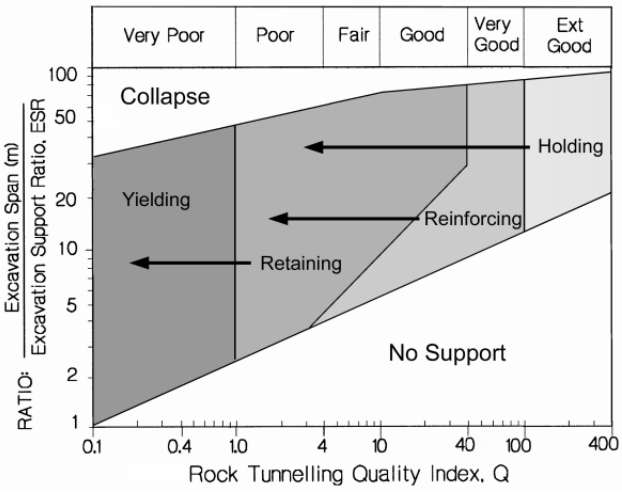

Figure 4.2: Support functions within stability graph for excellent to very poor rock.
Arrows indicate that the required support functions are cumulative, i.e., for poor ground, the support needs to hold, reinforce and retain, and for very poor ground, the support must fulfill these three functions while yielding.

words, the support must have superior yielding characteristics. Again, in highly stressed ground this zone may be reached in ground that would be characterized as good or excellent under low stress conditions. In the domain requiring yielding support, it is necessary to design the support system such that it can yield without building up excessive stresses but, most importantly, the support system must contain reinforcement elements that control the bulking process.

When designing support for mines, it must be recognized that mining-induced stresses alone can reduce the rock mass quality index (e.g., *Q*) from its virgin state by more than one order of magnitude, thus changing the support function requirements in otherwise identical rock conditions. To define an appropriate support function for mining applications or for any excavation with complex geometry, it is therefore paramount to select a stress reduction factor (Barton 1994) that takes mining-induced stresses rather than the in situ stresses into account (for details see Figure).

4.1.2 Support functions of shotcrete

Directly or indirectly, shotcrete can contribute to all three support functions noted above but only if properly integrated into the support system:

1. Holding - shotcrete resists load by adhesion, thrust and bending resistance. If shotcrete forms a continuous support arch or ring, it can hold rock in place by building thrust forces in the arch and if it adheres well to the rock mass, its holding capacity is substantially increased by the combined arching action of rock and shotcrete.
2. Reinforcement - shotcrete as a surface support component does not directly reinforce rock. However, if we define the effect of reinforcement as strengthening the broken rock, then shotcrete has an equivalent effect. It increases the rock mass strength by increasing the confining stresses and, more importantly, by preventing loosening of the rock mass or broken rock. Furthermore, contrary to mesh, it also prevents relative shear of rock blocks further enhancing the self-stabilizing effect.
3. Retention - when combined and connected to proper holding elements (rock bolts or cables) shotcrete provides a stiff and high capacity retaining function. In well-jointed or blocky rock, shotcrete prevents ravelling between bolt heads, locks in-place key blocks, assists in transferring loads onto bolts, and helps to maintain the integrity of rock blocks. In this case, shotcrete works as a high capacity, very tight mesh (called "supermesh").

In burst prone mines, shotcrete assumes one additional function: energy dissipation. Because energy dissipation is in part proportional to the mass of the support and the energy required to deform the support, shotcrete dissipates large amounts of energy (see later) and can be utilized as an effective component of a burst-resistant support system.

Shotcrete may also serve other functions that are not covered here, e.g., protection of rocks susceptible to rock mass degradation (weathering, slaking, etc.) and reduction of wall roughness (for ventilation, sealing, etc). Seldom does shotcrete fulfil all these functions and for an economic design, the designer must decide which function the shotcrete is expected to perform (Barrett and McCreath 1995). For example, a heavy shotcrete arch may serve the function of holding loose rock in place, eliminating the need for bolts, whereas a thin, bolted shotcrete layer may only serve to retain rock (the bolts are expected to carry the load). A lack of understanding which function the shotcrete is intended to serve may be the cause of poor shotcrete design.

4.1.3 Sources of deformation – rock mass bulking

In brittle failing rock, the process of stress-induced fracturing near excavations is associated with substantial dilation (volume increase) resulting from three sources: (1) dilation due to new fracture growth, (2) shear along existing fractures or joints, and more importantly, (3) dilation due to geometric incompatibilities when blocks of broken rock move relative to each other as they are forced (squeezed) into the excavation. This dilation process, called rock mass bulking, produces large, permanent, radial deformations in the fracture zone and consequently at the excavation wall. Figure 4.4 illustrates the bulking process near an excavation damaged by mining-induced stress.

The bulking process can be quantified by a bulking factor *BF*, defined as the percentage increase in radial deformation due to fracturing inside the failure zone extending to the depth of failure d_f. Contrary to the depth of failure, which is largely independent of the support pressure, the amount of bulking inside the failure zone strongly depends on the support type, characterized by the distributed support capacity, as illustrated by Figure 4.3. This figure is based on a limited number of qualitative and quantitative field

observations from extensometer measurements (e.g., Hepworth 1984) on overstressed tunnels in brittle rock, supported by various support systems (Kaiser *et al.*1996). Unconfined rock can increase in volume by as much as 30 to 60% (e.g., in the unsupported floor of a drift) but confinement and rock reinforcement drastically reduces bulking. An effective reinforcement system providing a distributed support capacity of >200 kPa can reduce bulking to less than 3%.

Ranges for three typical support types providing distributed support capacity from (<50) to (>200) kN/m^2 are indicated in Figure 4.3: light support – standard (mechanical) bolting with mesh; yielding support – frictional bolts with mesh but without grouted rebar, and heavy support – strong support with rock mass reinforcement (including grouted rebar).

It is important to realize that it is not the support pressure alone that controls the bulking process. As illustrated by Figure 4.10, rock reinforcement, e.g., by grouted rebar, prevents the opening of fractures and thus reduces bulking much more effectively than pressure applied at the tunnel surface alone.

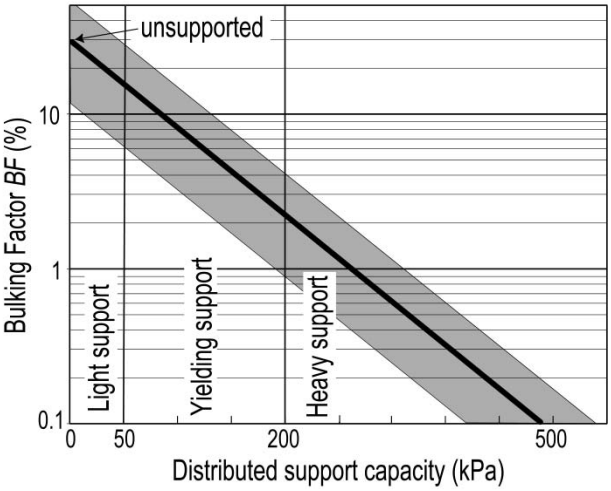

Figure 4.3: Bulking factor as a function of distributed support capacity (trend line with range of ±3 standard deviations) (after Kaiser *et al.* 1996)

Figure 4.4: Wall convergence due to bulking reflected in deformation of ventilation door (courtesy T. Villeneuve)

4.1.4 Estimation of rock mass bulking

Based on the range of bulking factors given in Figure 4.3, it is now possible to establish ranges of anticipated wall convergence as a function of the depth of failure d_f and the applied support type (Figure 4.5). The convergences in this figure are normalized to the radius a of the excavation and do not include elastic deformations due to tunnel advance. Hence, Figure 4.5 presents a means to estimate the anticipated, non-elastic convergence due to rock mass bulking in a failure zone extending to a depth d_f. It can be seen that the amount of convergence attributed to rock fracturing is significant for depths of failure exceeding 10 to 20% of the tunnel radius and that rock reinforcement (heavy bolting with grouted rebar) can reduce the tunnel wall convergence by at least half an order of magnitude.

Figure 4.6 presents a view of a lightly supported drift back that experienced bulking during a rockburst. The depth of failure is roughly equal to the length of the mechanical bolt. Several open fractures (>5 mm) as well as localized shear zones causing bulking deformations in the radial direction are clearly visible. The depth of failure is approximately 1 m (beyond the baggage zone) or 0.3 to 0.4a. Hence, the anticipated bulking factor for a light support is between 2 to 5 % and the corresponding wall deformation about 35±10 mm. This predicted deformation is equal to the ultimate displacement capacity of short mechanical bolts (20 to 50 mm; Kaiser *et al.* 1996) and it is therefore not surprising that the drift back partially collapsed (front portion of Figure 4.6).

By combining the bi-linear failure envelope cut-off in stress space (Section 2), the depth of failure prediction capability (Section 3), and the interrelationship of rock mass bulking and support (Figure 4.3 and Figure 4.5), it is possible to provide a simple approach for support system selection in overstressed brittle rock. This is illustrated in Figure 4.7.

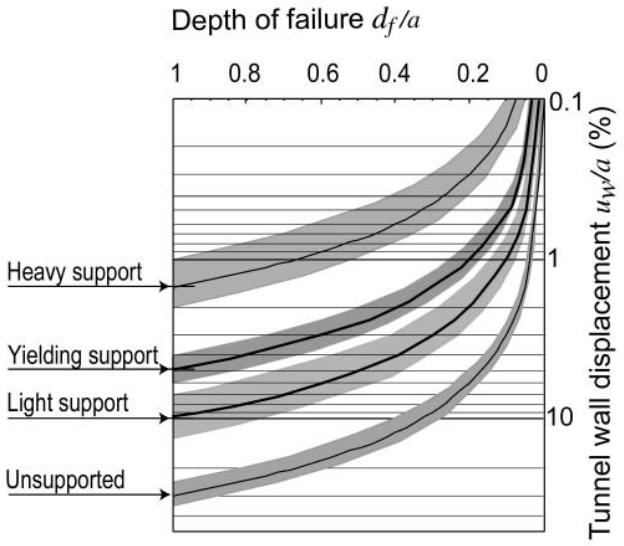

Figure 4.5: Normalized tunnel wall convergence due to rock mass bulking as a function of depth of failure and applied support system

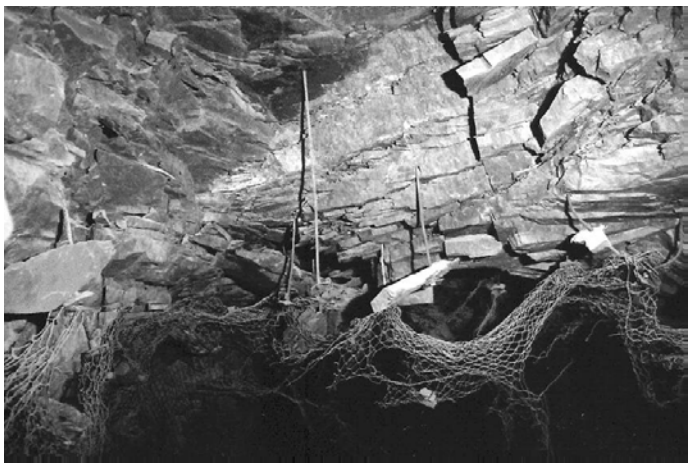

Figure 4.6: Localized volume of moderately jointed rock that bulked due to damage by a small strainburst behind a light support system of welded-wire mesh and mechanical bolts. The rock mass was loaded tangentially, creating surface parallel fractures that opened during the failure process. The depth of failure is slightly less than the length of the mechanical bolts.

For the example introduced in Section 2, mining-induced stress change brings this excavation from a low intermediate to a high intermediate state of stress (σ_{max}/σ_c = 0.55 to 1.0; Figure 2.11). The shaded range in the stress space represents the stresses around the excavation for the original, pre-mining state of stress. As a consequence of mining and induced stress change, the depth of failure is predicted to increase from 0.18 to 0.72*a*. If the deformations are to be kept below 3% of the tunnel radius *a*, a yielding support system with a distributed support capacity of about 150 kPa would be required. 5 to 10% convergence would have to be anticipated with a light support system. For example, in a tunnel with a radius of 2.5 m, this mining-induced stress change would increase the wall convergence from 20 to 65 mm with a yielding support, and from 50 to 150 mm with a light support system.

Several other practically useful observations can be obtained from Figure 4.7. From the principal stress space and depth of failure chart, it can be seen that this tunnel will only fail locally between Points A and B (see insert). Between Points B and C, the depth of failure is zero, and thus the bulking related deformation is also zero. In other words, the curves in the convergence chart provide information about the differential deformation around the tunnel, from zero at Point B to the maximum at Point A. For the selected example, the yield support would experience differential deformations from 0 to 65 mm. This differential displacement demand often leads to deformation incompatibilities between the ground and the support system, causing localized stress concentrations that damage individual support components.

For tunnels experiencing burst conditions, the dynamically induced depth of failure can be obtained as a function of induced ground motion *ppv* from Figure 3.13, and the burst-induced deformations can be obtained from the convergence chart in Figure 4.7.

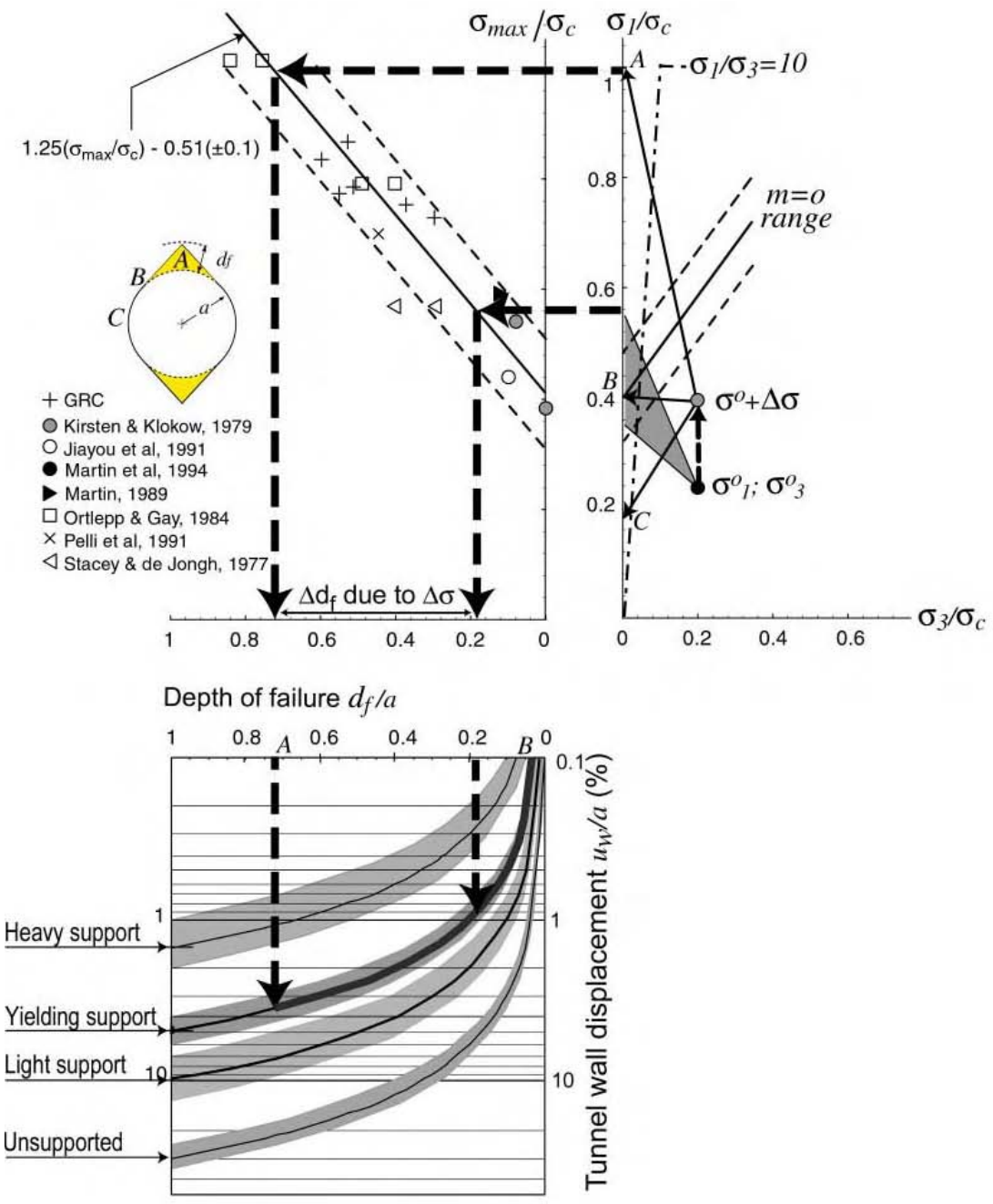

Figure 4.7: Combination of stress concentration factor (stress path chart), depth of failure chart, bulking and convergence chart for support selection to control failing ground in overstressed brittle rock

4.2 Rock mass reinforcement

Rock reinforcement has two primary functions: (1) to prevent rock mass deterioration by preventing failure of rock bridges and loss of interlock, and (2) to control and minimize rock mass bulking.

4.2.1 Retention of self supporting capacity of rock mass

The first function of reinforcement is to retain as much as possible the rock's self-supporting capacity (Hoek and Brown 1980). If shear strain is dominating the rock mass behaviour, reinforcement can improve the self-supporting capacity by maintaining interlock and preserving a high composite dilation angle along rough joint surfaces. This is particularly important in ground subject to dynamic disturbances. In this case, the passage of a seismically or blast-induced wave can cause "asperity jump" or the loss of interlock. The residual static strength would thereafter be considerably reduced. A stiff reinforcement acts to limit this reduction by minimizing normal and shear displacements across or along joint surfaces or newly formed fractures.

Figure 4.8: View across stope showing stress-induced fracturing around drift and effective stabilization of baggage and fractured rock by grouted rebar

In highly stressed rock, fractures form from nucleation cracks and flaws, creating surface-parallel fractures. This rock mass degradation process as a result of fracture propagation can be effectively arrested by stiff support components that prevent the opening of fractures. Figure 4.8 presents a unique view of onion skinning around a drift entering a stope.

In a more heavily jointed rock mass, reinforcement still plays a role, limiting the localization of strains and preventing continuous shear surfaces from forming. Inelastic shear strain, distributed throughout the rock mass as small discontinuous slips, requires a greater total amount of dilation to propagate than a single through-going shear plane. The distribution of shear strain results in a higher degree of internal resistance. Stiff reinforcement acts to minimize the degree of destabilizing strain localization.

Reinforcement also acts to preserve rock bridges formed by incomplete joint plane formation. Joints are often assumed to be fully persistent for stability analyses even though this is normally not the case in moderately jointed rock masses. Where these rock bridges exist and where they can be preserved by careful blasting and the use of stiff tendon reinforcement, the self-supporting capacity of the rock mass, through these rock bridges, can be quite significant under tensile loading as shown in Figure 4.9.

These values for rock mass tensile strength were calculated by Diederichs (1999) using fracture mechanics approaches modified after Kemeny and Cook (1987). A detailed comparison to conventional support systems is given in Table 4.1. These rock bridges, while unstable under sustained tensile load beyond the critical levels indicated in this figure, can fail in a stable fashion if the tensile strains are controlled as discussed by Ingraffea and Atkinson (1987). A stiff reinforcement normal to these bridges acts to limit the propagation of the fractures and the rupture of the rock bridges.

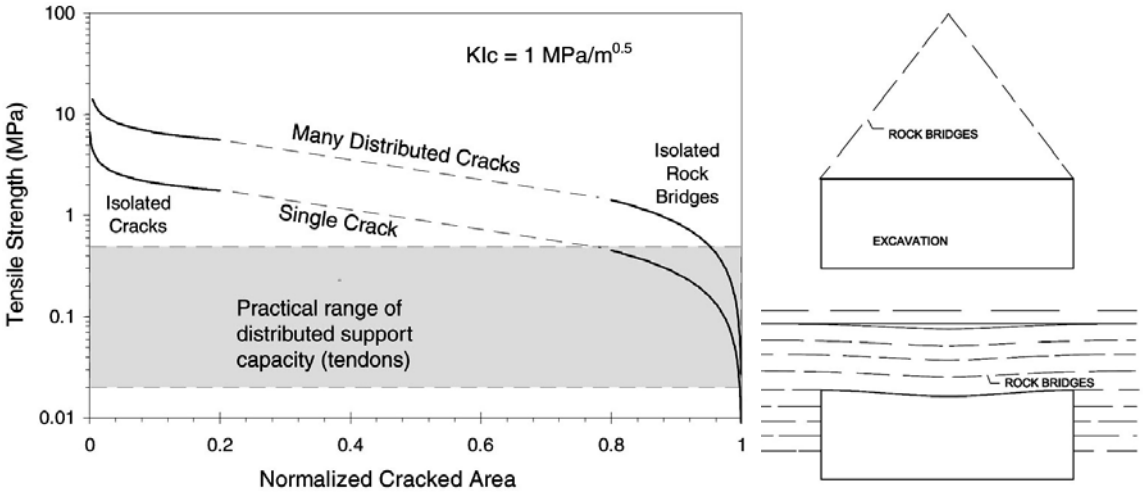

Figure 4.9: Distributed load capacity of rock bridges compared with range of economically practical tendon support (e.g. bolts, cablebolts, etc). Calculated range of tensile strength based on granite (Diederichs 1999).

Table 4.2: Support patterns and equivalent rock bridge area

Support Type	Support Pattern (m x m)	Equivalent Pressure (kPa)	Maximum Supported Thickness (m)	Capacity Equivalent Rock Bridge Area (% of cross-section area)
Rockbolts	2 x 2	20	0.7	0.1-0.2
Rebar	1.3 x 1.3	60	2.0	0.4-1.2
Single strand cablebolts	2 x 2	65	2.2	0.5 to 1.4
Double strand cablebolts	2 x 2	130	4.3	1.2 to 5
Double strand cablebolts	1.3 x 1.3	300	10	3.5 to 12
Double strand cablebolts	1 x 1	500	17	5.0 to 20

Note: 1% rock bridge area is equivalent to a 10 cm by 10 cm rock bridge per 1 m^2 total area.

It is prudent to include stiff fully-coupled reinforcement components such as resin-grouted rebar in a composite support system. Even if a rebar breaks in discrete locations along the shaft (as shown in Figure 4.10), the remaining segments continue to act to suppress shear localization and to preserve rock bridges, lessening the demand on the holding components of the support system.

The preservation of rock bridge capacity in hard rock masses is particularly important at the excavation face. If careful blasting is employed, the installation of full support can be delayed. Perhaps only a spray-on lining or a thin shotcrete layer is required for worker safety at the heading. Without the installation of a stiff tendon reinforcement, the rock bridges may eventually rupture freeing unstable wedges and laminations. In many cases, however, the installation of the reinforcement can be delayed several rounds. In a mining or tunnelling environment, this allows for the simultaneous installation of permanent support along with heading development and drilling for the next round (the two crews now occupy different space in the tunnel). In a typical mine, this represents a time saving equivalent to a full crew-shift and has a significant economic impact for mine development.

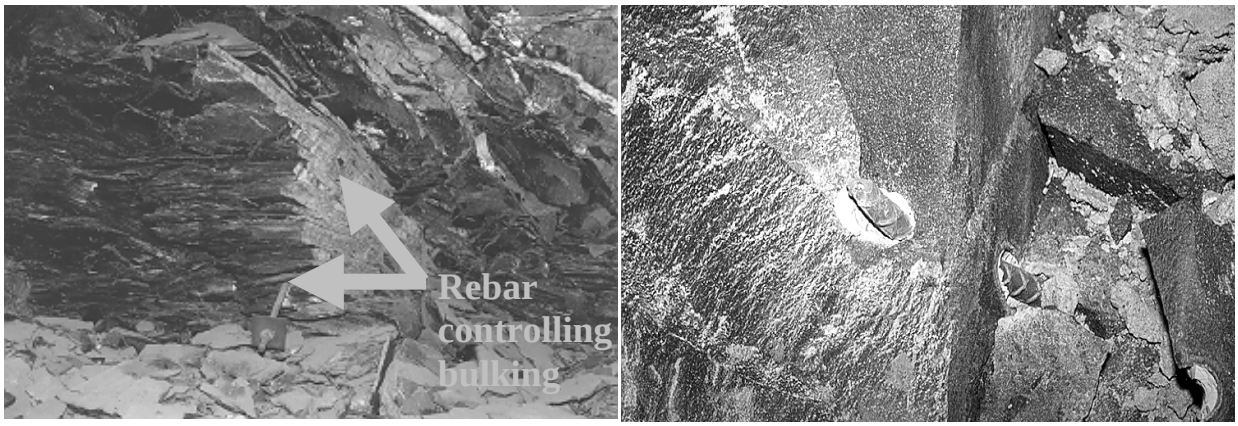

Figure 4.10: Grouted rockbolt (rebar) limiting rock mass dilation (bulking) during failure of brittle, laminated rock. Such rebars are effective in controlling bulking, even if they fail to fulfill their holding function

4.2.2 Minimize displacement demand on support

The second function of reinforcement is to control the rock mass bulking. As illustrated by Figure 4.10, rock reinforcement, e.g., grouted rebar, prevents the opening of fractures, and thus bulking, very effectively. Despite the fact that the entire pillar wall has failed in this laminated rock, the fully grouted rebar prevents the opening of fractures and the total disintegration of the rock mass. Consequently, in intermediate to highly stressed rock, when large deformations due to bulking are anticipated, fully grouted rock reinforcements should be utilized to minimize bulking and the associated radial deformations. For example, by reducing rock mass bulking, shotcrete applied to the surface of a tunnel will be deformed less and thus be stressed to a lesser extent. Even if the rock bolts fail due to excessive localized straining inside the zone of failed rock, they are still very beneficial for deformation control as they restrain bulking everywhere except at the fracture point. In other words, rock reinforcements are essential in highly stressed ground to control defor-

mations such that cost-effective holding and retaining system components perform well. Contrary to common arguments that grouted rebar is too stiff, for example for burst-prone ground, and therefore should not be used, the need to minimize deformations in brittle failing ground justifies the use of grouted rebar. However, the rebar must in such situations be combined with yielding bolts or plain cablebolts to ensure adequate holding capacity when the rebars break.

From a practical perspective, it is most important to recognize that while failure cannot be prevented and the depth of failure cannot be reduced by the support, the bulking process and thus the wall deformations can be minimized by a combination of rock reinforcement and wall support.

4.3 Holding - rock support by cablebolts

In the context of this work, the holding function of the rock support encompasses the action of resisting gravity forces on kinematically free wedges, slabs or stress-damaged zones of rock, the limits of which extend away from the excavation boundary. Most of the holding function is fulfilled by rockbolts and similar tendon support. Here, the authors focus on the use of cablebolts, factors that affect the effectiveness or capacity of cablebolts, and factors that influence the demand on the support.

Grouted cablebolts, each consisting of one or more multi-strand steel cables grouted into a borehole can perform a reinforcing function in soft rocks. The system stiffness of a cement-grouted cablebolt is considerably less than that of a resin-grouted rebar. As such cablebolts are less effective for suppressing or limiting the propagation of fractures in stressed hard rock or for maintaining intimate contact of joint surfaces. They do however, possess significant load capacity and are extremely useful where longer tendon support is required. Cablebolts represent the only practical support mechanism for open stopes. As an example of a holding support system in hard rock, the use of cablebolts is examined here in more detail. A comprehensive overview of cablebolt support and installation practice is presented by Hutchinson and Diederichs (1996).

4.3.1 Empirical design

Cablebolt support can be highly effective in moderately jointed or blocky ground at low to moderate stress levels (Figure 4.11). Cablebolts, without additional face retention such as straps or large plates, are less effective in controlling the unravelling of a highly damaged or heavily jointed rock mass. The lower stiffness of the cablebolt system results in less ability to control the propagation of excavation induced stress fractures.

The zone of cablebolt effectiveness in Figure 4.11 can be extended if the cablebolts are used in combination with surface retention (as discussed next) or if rock mass disintegration is controlled by a primary system of grouted rebars. The latter combination is commonly used in the backs of large open stopes where face access is available. Cablebolts can fulfill the roles of holding, reinforcement and retention, depending on the rock mass condition, the joint spacing and on the cablebolt spacing as shown in Figure 4.12.

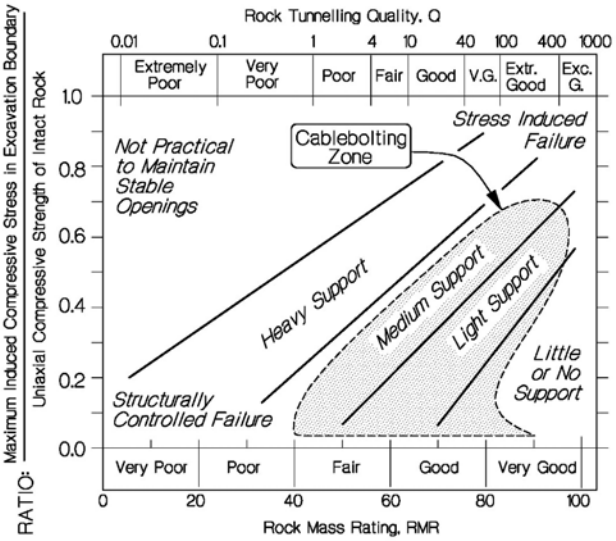

Figure 4.11: Empirical limits of cablebolt support as a stand alone system (Hutchinson and Diederichs 1996)

For the purposes of cablebolt array design, recall the stability graph for open stopes discussed in Section 3. Above the upper no-support limit (low *HR* or high *N'*) open stopes can remain unsupported without significant instability. Below a lower limit (high *HR* or low *N'*), defined by Nickson (1992) the stope face is deemed unsupportable. The intervening transition zone represents the zone of cablebolt effectiveness and efficiency. Cables can perform a number of overlapping functions within this zone. Based on case examples, three main subdivisions can be defined. Near the upper no-support limit, as shown in Figure 4.12, reinforcement is the key mode of support, as the cablebolts serve to maintain integrity between interlocking blocks or laminations to create a stable arching function. Near the lower limit, arching is assumed to be lost and cablebolts act only to hold the disintegrated rock mass in place.

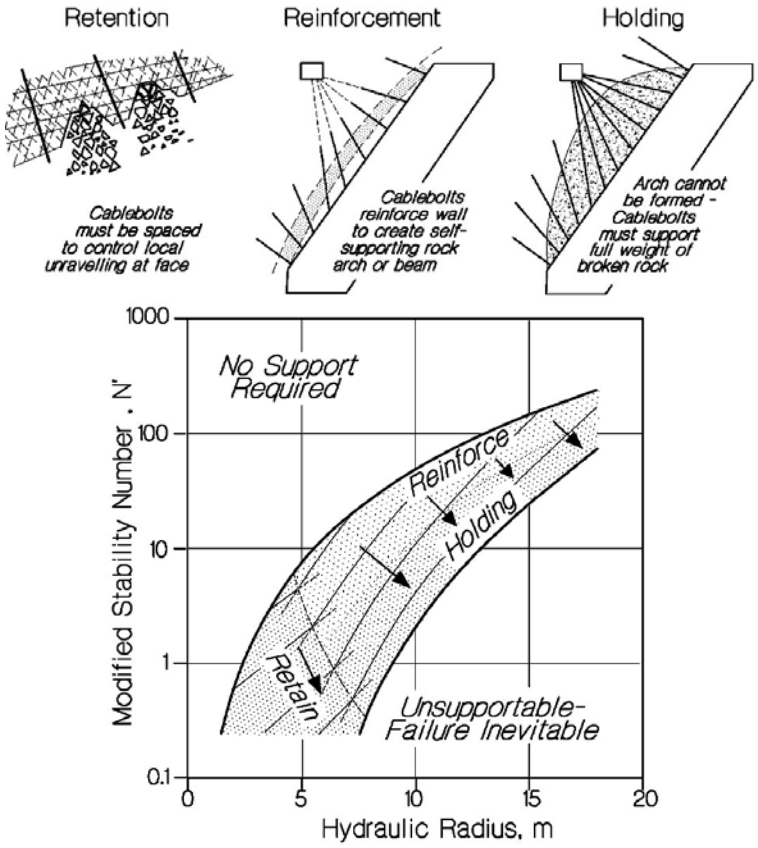

Figure 4.12: Support modes for cablebolt arrays within stability graph (*N'* and *HR*; Diederichs 1999)

For very low quality rock masses (*N'* < 1), the cablebolt spacing must be very tight to prevent the rock mass from unravelling unless additional support such as rebar or shotcrete is used.

Based on a semi-analytical approach outlined in Diederichs (1999), these general mechanistic zones form the basis of cablebolt spacing guidelines for regular arrays as shown in Figure 4.13. In these guidelines, the limiting cablebolt spacing required for stability reduces (more cablebolts are required) as the primary function moves from reinforcing to holding based on the decreasing ability of the rock mass to support itself (at lower *N'* or higher *HR*). Retention demands limit the spacing for low quality rock masses (low *N'*) unless the cablebolts are accompanied by a tighter pattern of rockbolts, rebar or by a layer of shotcrete.

4.3.2 Effect of relaxation on holding demand

These cablebolt spacing guidelines apply to the conditions assumed in the stability chart calculations. Recall, however, that this empirical tool does not, in its conventional form, consider the impact of confinement loss or abutment relaxation. Relaxation, caused by adverse geometry, adverse in situ stress ratios or abutment yield can lead to a loss of arching or self supporting capacity within the rock mass. In this case, this loss must be replaced by more holding capacity as shown in Figure 4.14. In this example, derived from a Voussoir beam analysis (Diederichs 1999), an outward movement of the abutments (analogous to tangential confinement loss or relaxation) must be compensated for by an increase in applied bolt (or cablebolt) support.

In addition, a loss of confining stress adjacent to a roof or wall of an excavation can release steeper (and therefore larger) wedges than would normally occur under moderate clamping. In the example shown in Figure 4.15, a cone with an apex angle slightly less than the friction angle approximates a wedge pyramid. Under moderate clamping or confinement the wedge is stable. For a 20 m span a loss of 2 MPa of clamping stress mandates the implementation of a standard double-strand cablebolt pattern to maintain stability.

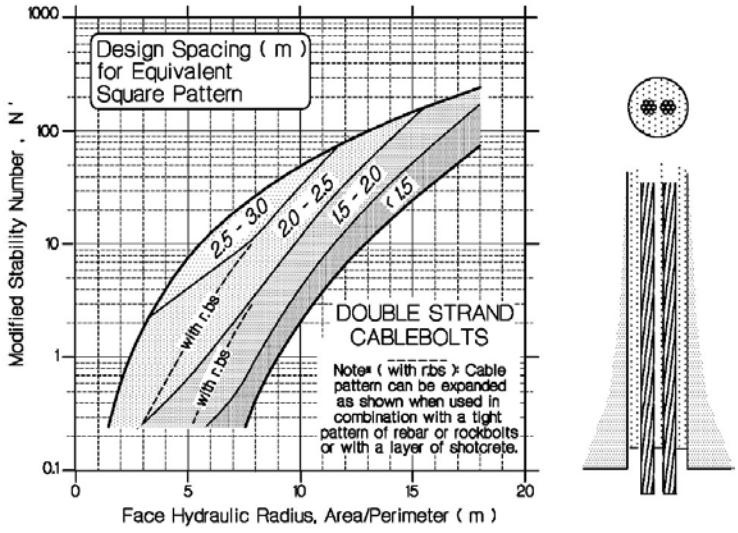

Figure 4.13: Guidelines for cablebolt spacing based on three dominant support modes

In the empirical stability chart, this increased demand is reflected in a translation of the no support limit up and to the left. That is, support is required for smaller spans or higher quality rock masses if abutment extension or relaxation is present. Likewise, the cablebolt spacing recommendations within the supported transition zone in Figure 4.13 translate due to the presence of relaxation. Figure 4.16 illustrates modified guidelines for cablebolt

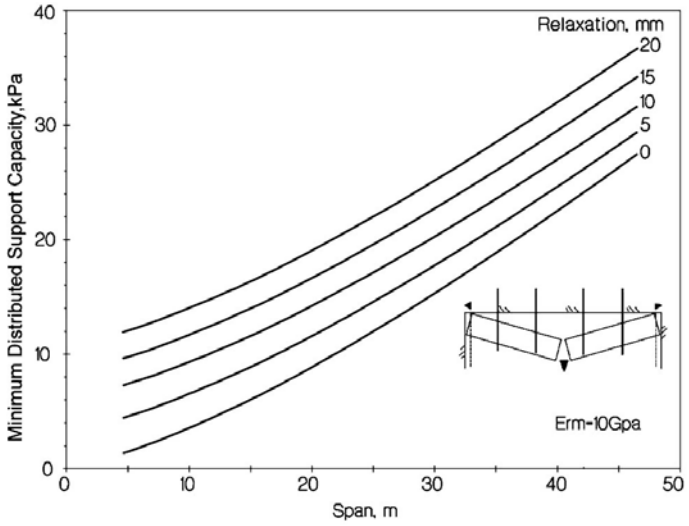

Figure 4.14: Increase in minimum stabilizing support requirements due to abutment relaxation

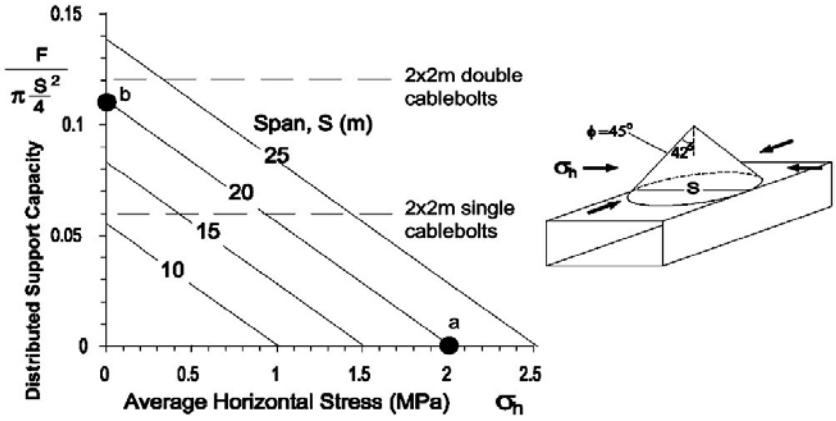

Figure 4.15: Increase in cablebolt support demand due to loss of confining stresses (cablebolt capacities shown assume use of modified or

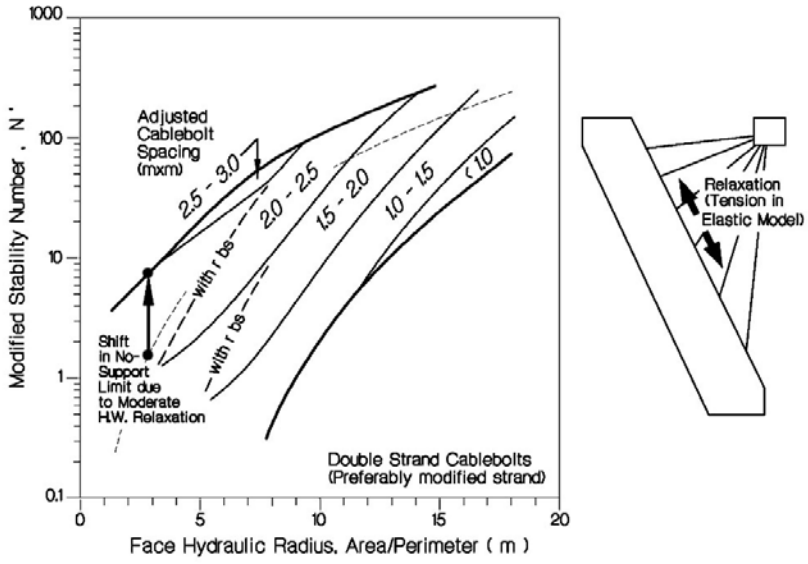

Figure 4.16: Impact of lateral extension (equivalent boundary tension of 10 MPa) on cablebolt spacing recommendations. Compare to Figure 4.13

spacing in ground subject to moderate relaxation (here equivalent to 10 MPa of elastic tensile stress).

That the effect of relaxation has a drastic effect can also be illustrated by comparing support limits recommended by the two empirical stability chart systems; the Mathew-Potvin or *N'*-system, and Barton or *Q*-system. Figure 4.17 shows superimposed no-support limits (calculated as described by Kaiser *et al.* 1997) and maximum supported excavation limits. Whereas the no-support limits (for *ESR* = 3 to 5) and the unsupported transition zone (Figure 3.3 and 3.4) correspond reasonably well, the limit for supported ground according to the Mathew-Potvin approach (Figure 4.13) falls much lower than the upper limit for supportable excavations (labelled "Maximum support limit" in Figure 4.17) according to the *Q*-system. This large deviation in empirical design limits can be attributed to various factors including different support quality standards, excessive cablebolt spacing without proper surface fixtures, and the fact that relaxation is seldom encountered in civil applications, whereas abutment relaxation often dominates in mining.

4.3.3 Effect of relaxation on cablebolt capacity

The guidelines presented in Figure 4.16 are based on the assumption that the capacity of the cablebolt is not affected by boundary-parallel relaxation. Unfortunately, this is not the case for plain strand grouted cablebolts. Kaiser *et al.* (1992) clearly demonstrated that a stress decrease, normal to the cablebolt, after installation results in a loss of frictional bond strength and therefore a loss of load transfer capacity. This leads to the familiar site of stripped cablebolts hanging from the back or wall of open stopes after a ground fall, which apparently occurs without load transfer to the cablebolts. Figure 4.18 illustrates the theoretical impact of stress decrease on cablebolt bond strength.

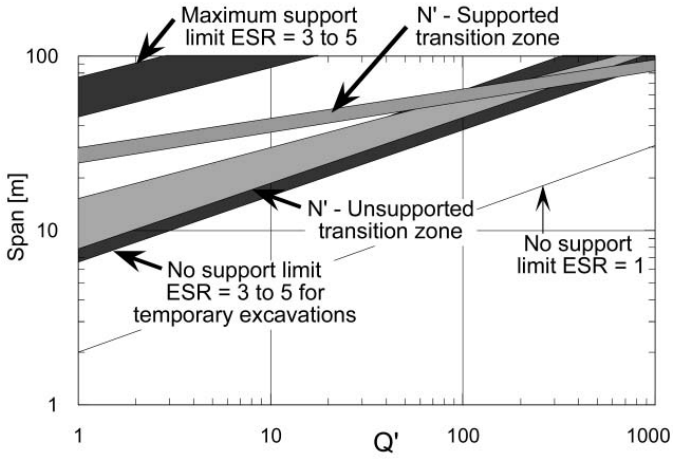

Figure 4.17: Comparison of stability charts using *N'* (Mathews-Potvin approach) and Q' (Barton approach)

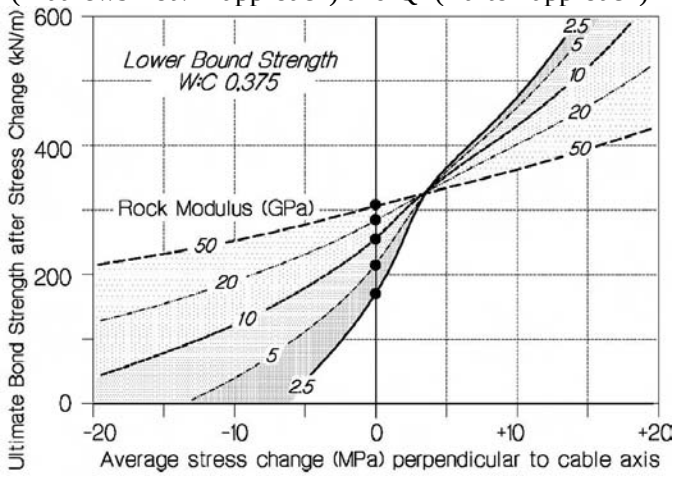

Figure 4.18: The impact on cablebolt bond strength (load transfer/embedment length) of induced stress change in rock mass after installation (after Hutchinson and Diederichs 1996)

The main reason for this sensitivity to stress change is that the grout tends to pull away from the cablebolt surface as the hole diameter expands in response to a drop in rock stress. This interface separation is of the same magnitude as the dilation that occurs during cablebolt pullout. This problem has been recognized for some time now. One solution is to ensure that all cablebolts are plated with barrel-wedge anchors. This is not always possible, however, since access is not available to many cablebolted faces such as hangingwalls of open stopes (in these cases cablebolts are installed remotely from a drift in the hangingwall). The best alternative to minimize stress change sensitivity is to use modified strand cablebolt geometries such as bulbed strand cables. The bulbed strand increases the amount of dilation necessary for cablebolt pullout. This increase compensates for the interface separation that occurs during stress decrease and preserves the bond strength and load transfer capacity. Such strands should be used, for example, in all hanging wall applications or anywhere stress drop is anticipated.

4.4 Rock retention

The retaining components of a support system typically consist of mesh, shotcrete, and more recently of spray-on linings (Figure 4.19). The primary difference between these systems is that the later two adhere to the rock, providing resistance to relative movement at the support/rock interface. This adhesion and shear resistance contributes significantly to the self-supporting capacity and integrity of the liner/rock arch.

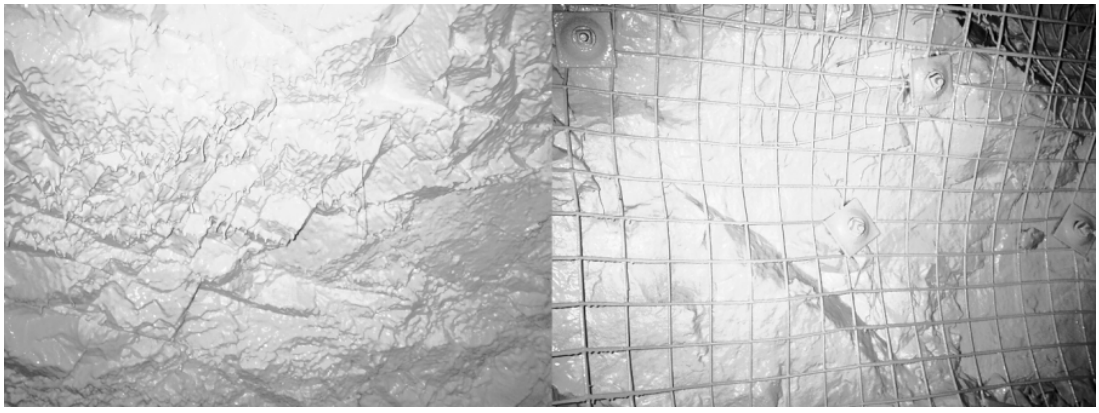

Figure 4.19: Sprayed-on polyurethane (Mineguard™) used to support a narrow-vein stope without the use of bolts or mesh and a top sill drift above bulk mining stopes with mesh and bolts

4.4.1 Test set-ups

Initially, central loading tests on panels of retaining elements (from 1.5x1.5 to 1.8x3.6 m in size) were conducted to obtain the retention capacity of individual retaining elements under static or dynamic (impact)

loading (Tannant *et al.* 1996). This mode of loading is most appropriate to assess the capacity to retain loose rock or rock ejected during rockbursts. Dynamic tests were conducted by dropping a cylindrical weight onto panels supported by posts (bolts) as shown in Figure 4.20.

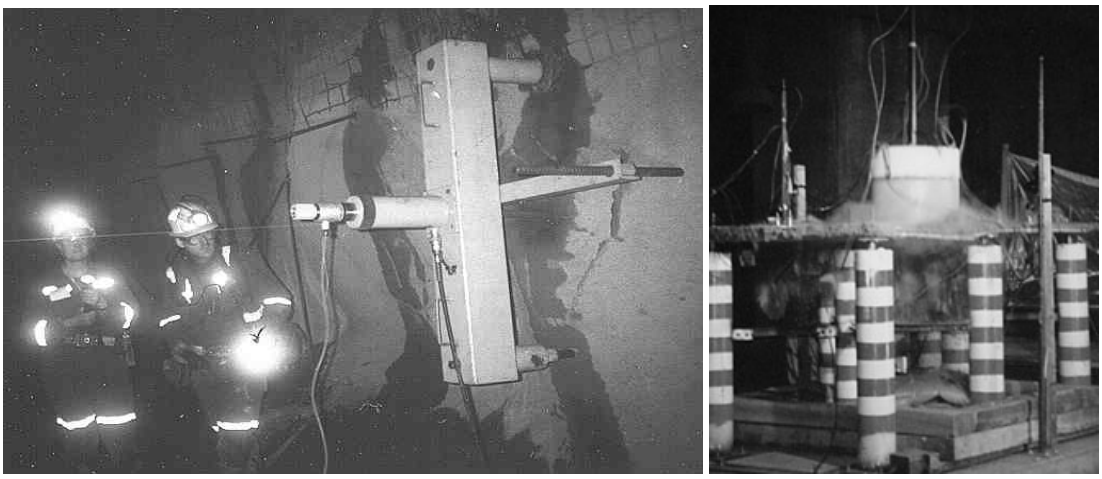

Figure 4.20: Field test set-up for static plate pull tests and impact test facility (at time of impact)

SRK (1996) has conducted similar static loading tests on panels supported at 1x1m bolt spacing and with distributed loads applied by a pressure cushion. As will be discussed later, the two systems produce distinctly different stress and strain distributions in the panels and thus results cannot be compared directly. Distributed load tests, producing uniform extension strains, create conditions most favourable for steel-fibre reinforced shotcrete.

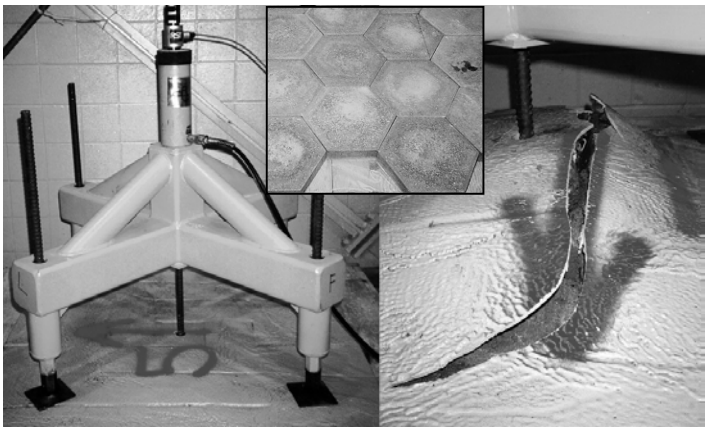

Figure 4.21: Pull test on polyurethane-coated square blocks and ruptured membrane at large central deflection (Espley-Boudreau 1999); most results presented here are from tests with 50 mm thick hexagonal blocks; see insert)

More recently, recognizing the importance of interface shear resistance, adhesion and the tensile capacity of the retaining elements, a standard test frame for laboratory and field use with a 1.2 m-square bolt spacing was developed. This frame is shown in Figure 4.20 during shotcrete testing underground and in Figure 4.21 during laboratory tests on spray-on membranes. In this laboratory set-up, the bending resistance of a 50 to 90 mm thick layer of rock (concrete blocks) is integrated into the support system. This testing system was designed to evaluate the performance of membrane liners for the support of jointed or fractured rock. Test panels were made by spraying polyurethane or shotcrete over an arrangement of inter-locked concrete blocks. The test panels were loaded with a 300-mm pull plate (Figure 4.21) and the loads and displacements were recorded (Espley-Boudreau 1999).

4.4.2 Mesh or screen

Since mesh is widely used in mines, its load capacity, deformability, and energy dissipation potential serves as a basis for comparison. Results from tests by Tannant *et al.* (1997) are reproduced in Figure 4.23. The energy dissipation capacity is summarized in Figure 4.22,

These typical results illustrate the high deformation capacity of mesh. The full capacity is only mobilized after substantial deformations; >100 mm for weld mesh and 400 mm for chain link mesh. For support in burst-prone ground, chainlink mesh is often used to retain broken rock. As can be seen from Figure 4.22, it has clearly superior energy dissipation capacity, though only at very large deformations. Expanded metal

mesh demonstrates comparable characteristics but tends to corrode more readily and thus is no longer in wide use.

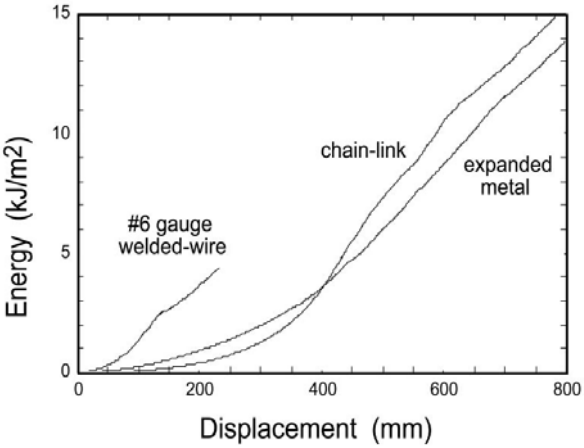

Figure 4.22: Energy dissipation capacity for static mesh types shown in Figure 4.23

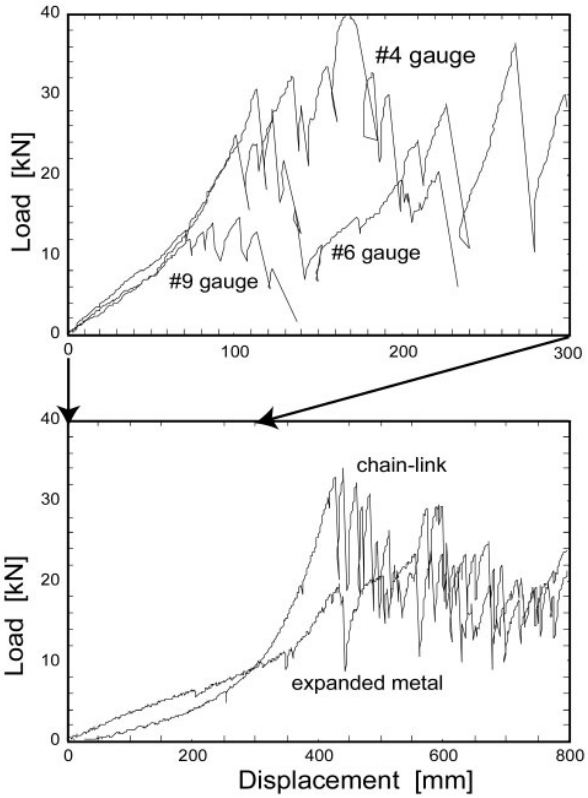

Figure 4.23: Mesh pull test data: #6 to #9 weld mesh compared to light chain-link and expanded metal mesh (Tannant *et al.* 1997)

4.4.3 Shotcrete

Much has been published about the pros and cons of various types of shotcrete reinforcement (fibres vs. mesh) but it is worthwhile to revisit this issue. In general, it can be concluded that fibre-reinforced shotcrete performs best when deformations are relatively small and when the shotcrete is uniformly strained. Mesh-reinforced shotcrete performs best when large deformations causing extension cracking are encountered and localized cracking due to strain localization occurs. It performs poorly when sheared or stressed in compression.

The failure process in shotcrete is often progressive and localized in nature, especially when adhesion loss and flexural bending occur. In such situations, often encountered in mining, point load tests are more representative of in situ conditions than distributed load tests because the former cause stress and strain localization near the loading plate. Typical results from static pull-tests with mesh- and fibre-reinforced shotcrete are summarized in Figure 4.22. The effect of the adhering rock (50 mm concrete blocks) almost doubles the capacity of the shotcrete (compare Curves A and B). This is largely attributed to the fact that the adhering blocks effectively double the total beam thickness. Adding another 53mm of shotcrete to increase the thickness by 85% only adds about 30% to the load capacity (Curve C).

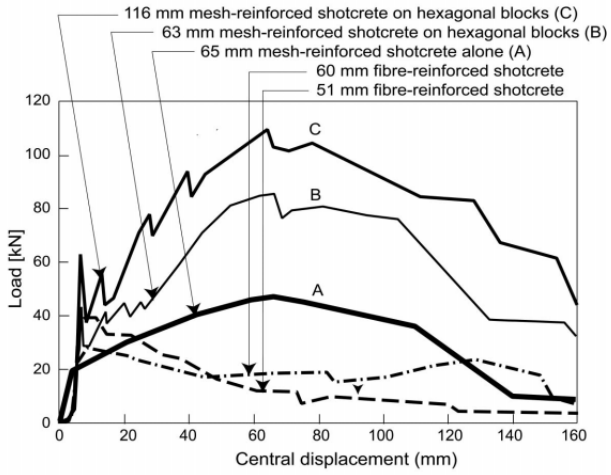

Figure 4.22: Summary of shotcrete panel test data: mesh-reinforced shotcrete alone and on hexagonal blocks; fibre-reinforce shotcrete on hexagonal blocks (modified from Espley-Boudreau 1999)

As introduced earlier, distributed load tests (SRK 1996) create uniform stress and strain distributions in the test panels. Because short fibres have a limited extension capacity, these distributed load tests create very favourable conditions for fibre-reinforced shotcrete. Only if uniform loading can be ensured are such tests truly representative of in situ behaviour. Ranges of results from distributed load tests by SRK

(1996) are reproduced in Figure 4.23. These tests suggest that fibre-reinforced shotcrete is superior to mesh-reinforced shotcrete, at least for central deflections of <60 mm. As will be shown next, only if loading is uniform will fibre-reinforced shotcrete demonstrate such superior behaviour with fibre-reinforced shotcrete exhibiting almost double capacity at centre deflections of 20 to 40 mm. At very large deflections exceeding 60 to 100 mm, however, the mesh-reinforced shotcrete performs better because the fibre-reinforced shotcrete continues to lose its load bearing capacity as fibres pull out.

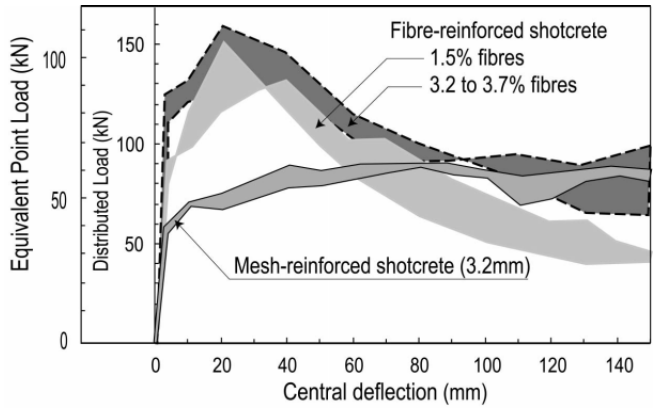

Figure 4.23: Distributed load tests on shotcrete panels (1x1m bolt spacing) (after SRK 1996)

On first sight, these results seem to be in conflict with the results presented by Kaiser *et al*. (1996) and those from Espley-Boudreau (1999) on fibre-reinforced shotcrete shown in Figure 4.22. In this case, loads were applied centrally and fibre-reinforced shotcrete was applied overtop of hexagonal blocks. Because localization occurred at the block boundaries, the fibre-reinforced shotcrete performance is clearly inferior, even at relatively small deformations (>20 mm). The difference can be attributed to the test system, one causing strain localization, the other uniform straining. To compare results from the two test set-ups, the equivalent point load must be calculated (shown as a secondary axis labelled Equivalent Point Load in Figure 4.23) and then further adjusted for the shorter bolt spacing (1 rather than 1.2 m) and for the somewhat higher shotcrete quality. After an approximate load adjustment for these factors, the two sets of test results have been superimposed in Figure 4.24.

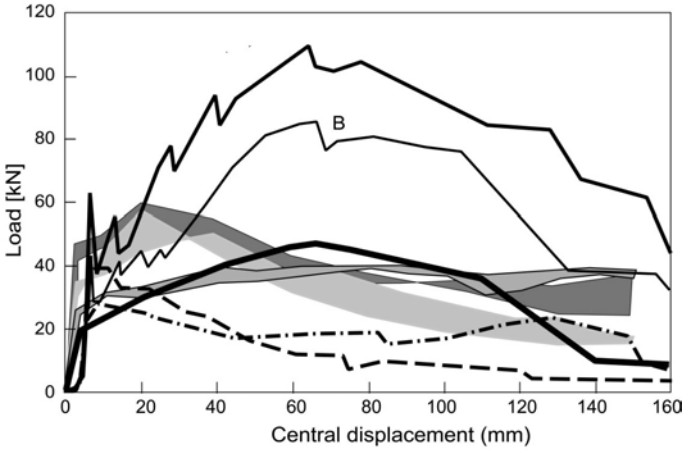

Figure 4.24: Superposition of data from Figures 4.25 and 4.26 after adjustment for test configuration, geometry and shotcrete quality

It can be seen that the two test results are now more alike but the distributed load tests still produce higher capacities for fibre-reinforced shotcrete at small deflections (<60 mm). These capacities are roughly double those obtained from tests causing localization at block boundaries (dashed lines). Most importantly, it can be seen from Figure 4.24 that the high tensile strength of the mesh becomes most beneficial in blocky ground (represented by the test set-up with concrete blocks) leading to superior performance of mesh-reinforced shotcrete (Curve B) for central deflections exceeding 30 to 50 mm.

Hence, the selection of an appropriate reinforcement largely depends on the anticipated type and amount of deformation. If shotcrete is applied such that straining is limited and uniform, fibres will perform well. On the other hand, when adhesion failure occurs and shotcrete has to act as a retaining system with high tensile capacity, mesh-reinforced shotcrete will perform better. Fibre-reinforced shotcrete, on the other hand, will have superior compressive strength characteristics. When shotcrete is expected to fail (in compression) and sustain large deformations, e.g., at stress raisers, mesh reinforced shotcrete will perform better. This latter conclusion arises not because of its load capacity but because the mesh will continue to provide some retaining capacity even after very large deformations.

The observation that distributed load tests produce superior fibre-reinforced shotcrete performance is not just important for test data interpretation but it is also of practical relevance. If shotcrete is allowed to debond and sag, such that central, point loading becomes dominant, the performance will move from distributed toward point loading, and the shotcrete capacity is significantly reduced. It is therefore paramount that shotcrete, particularly thin layers, be well bolted and, ideally, applied in a slight arch shape such that sag and localized loading is prevented.

For support in burst-prone ground, it is reasonable to assume that the support system must be able to dissipate energy from localized loading. Because of its mass, shotcrete plays an important role in energy dissipation. Kaiser *et al.* (1996) published results of an extensive investigation on the energy absorption capacity of shotcrete and the reader is referred to this publication for details. Nevertheless, Figure 4.25 summarizes the essence of these tests (Tannant and Kaiser 1997) and compares shotcrete with mesh. Results from static and dynamic tests are shown for comparison. Mesh-reinforced shotcrete can dissipate substantial amounts of energy, long before it is severely damaged (at about 0.3 to 0.4 m central deflection). When compared to static loading tests, shotcrete was able to dissipate roughly twice as much energy. Most importantly, it retained a significant self-supporting capacity even after dissipating more than 10 to 20 kJ/m^2 (Tannant *et al.* 1996). While only a limited amount of testing was conducted on fibre-reinforced shotcrete panels, its ability to dissipate energy was significantly lower (largely because of strain localization during impact testing). It is for these reasons that mesh-reinforced shotcrete is often preferable for support in burst-prone ground of moderate to severe burst potential.

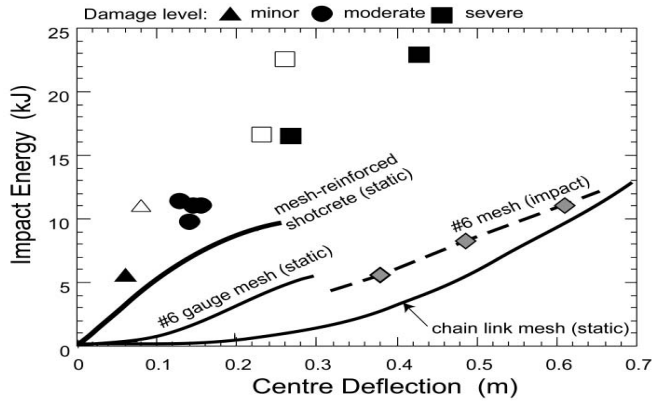

Figure 4.25: Energy dissipation capacity from impact tests on mesh-reinforced shotcrete (Kaiser *et al.* 1996); empty symbols for 75 to 90 mm and full symbols for 60 to 70 mm thick shotcrete

4.4.4 Spray-on linings

Driven by a need to automate the mining process and to reduce support costs, innovative means to support the ground such as spray-on linings are under development. Many manufactures are producing spray-on products of varying characteristics. Findings from a product called Mineguard™ are reported here for the simple reason that this product has been most widely tested (in Canada) and compared through consistent testing procedures with both mesh and shotcrete.

Polyurethane linings have been tested extensively (Espley-Boudreau 1999; Figure 4.21) and used by INCO Ltd. to support ground in narrow-vein mining stopes and to protect mesh and bolts on the backs of top sill drifts exposed to blasts (Figure 4.19). Typical results from tests of Mineguard™ over concrete blocks are presented in Figure 4.26 for three examples: 2 to 3 mm and 8 to 12 mm thick Mineguard™, and 2 to 10 mm Mineguard™ over #6 gauge mesh (2 test curves shown). Earlier presented results from shotcrete over blocks and mesh over hexagonal blocks are shown for comparison.

From the two tests with Mineguard™ over mesh, it can be seen that this type of support produces a very tough support system that is roughly equivalent to 116 mm of mesh-reinforced shotcrete. This conclusion is only valid as long as at least 50 mm of rock adheres to the spray-on lining. 8 to 12 mm of Mineguard™ alone produces about double the capacity of 60 mm of fibre-reinforced shotcrete, again as long as 50 mm of rock adheres. The main difference between Mineguard™ and

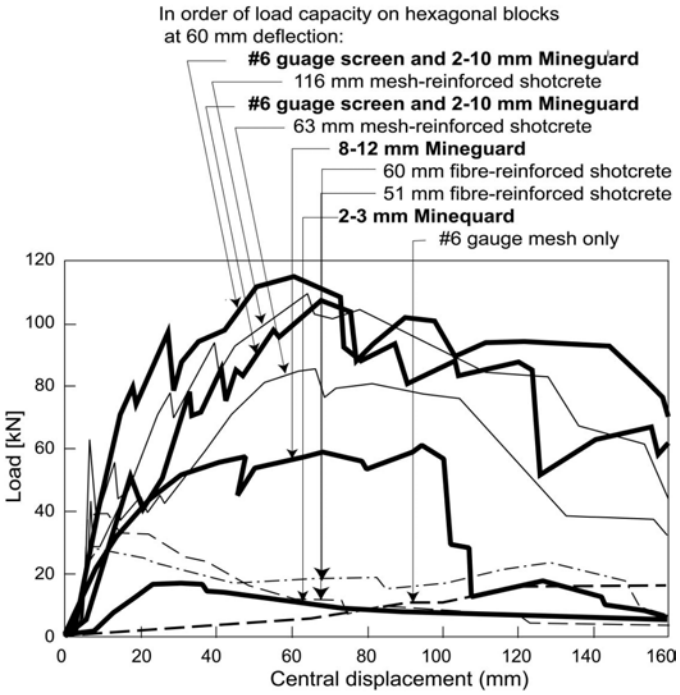

Figure 4.26: Test results from pray-on lining tests of polyurethane-coated blocks compared with mesh and shotcrete test data (after Espley-Boudreau 1999)

fibre-reinforced shotcrete is that Mineguard™ does not provide the early stiffness of shotcrete at < 20 mm deflection.

These tests demonstrate the importance of creating a near-continuous membrane in order to provide effective support for fractured rock (blocks). When the lining failed to bridge the gaps between blocks, the resulting support capacity was severely compromised. The adhesive strength between the lining and the blocks is another important property (Espley-Boudreau 1999). An extensive field testing program was undertaken by INCO Ltd. (Espley-Boudreau 1999) and some preliminary findings have been published by Tannant *et al.* 1999.

In summary, when used over bolts, the Mineguard™ effectively replaces many of the roles of shotcrete. However, because of the thin skin nature of spray-on linings, it does not provide the bending resistance that shotcrete offers. However, if the liner and rock forms a thin arch as in the test set-up with hexagonal blocks, this weakness is eliminated and spray-on linings can compete with shotcrete.

4.5 Use of empirical methods for support design in brittle failing rock

Most empirical tunnel design methods have been developed with data from civil engineering structures and gradually yielding ground. In brittle rock, failure often occurs in a violent manner (rockbursts) and is associated with extensive bulking. For design of support in burst-prone ground, the reader is referred to Kaiser *et al.* (1996). However, independent of the violence of the failure process, it is necessary to assess whether excessive deformations, which could damage the support, may be encountered and to determine whether the deformation compatibility limit of a support system may be exceeded.

4.5.1 Deformation compatibility of support and ground

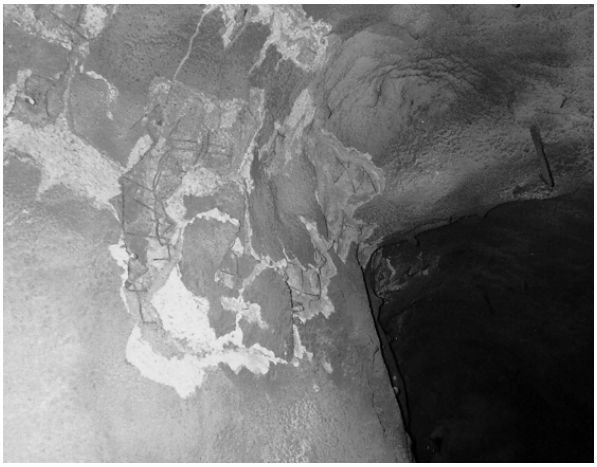

Figure 4.27: Damage to a shotcrete arch due to deformation incompatibility during minor rockburst

In mining, matters are complicated by the fact that mining-induced stress changes and related rock mass failure causes additional deformations, deformations that are not encountered in civil engineering excavations (caverns and single or twin tunnel situations). Unless a drift or tunnel is remote from a mining zone or the mining-induced stress changes do not cause rock mass failure, additional deformations must be anticipated as described earlier (Figure 4.7). These post-support deformations are often the cause for poor performance of shotcrete, particularly in burst prone ground as illustrated by Figure 4.27. This support failed because of deformation incompatibility between ground motion demand and displacement capacity of the support. Rock mass fracturing and bulking behind the shotcrete caused radial convergences that in turn created high compressive hoop stresses within the shotcrete, bringing it to failure. If the shotcrete was not continuous (e.g., longitudinally slotted), such damaging hoop stresses would not have built up and spalling would not have damaged the shotcrete. It is therefore necessary to determine whether damaging deformations are to be expected such that a sufficiently compliant or yielding support system can be selected.

For shotcrete in particular, the deformed shape of the excavation boundary often no longer matches the initial shape of the liner and debonding or flexural failure is induced. In other words, when large deformations are anticipated shotcrete is to be applied in such a manner as to prevent deformation incompatibility. Appropriate installation techniques preventing "self-destruction" of shotcrete are: longitudinal slots or gaps in shotcrete arches to break the flow of hoop stresses, or flat wall shotcrete panels that are free to move without causing constraints at panel boundaries (corners) (Kaiser and Tannant 1997; Figure 4.28). When shotcrete is applied as panels or slotted arch segments, it must be held in place by rock bolts or cables that are able to survive the deformations imposed on them by the bulking rock mass and the deforming shotcrete. This is called a yielding support system (see Figure 4.2).

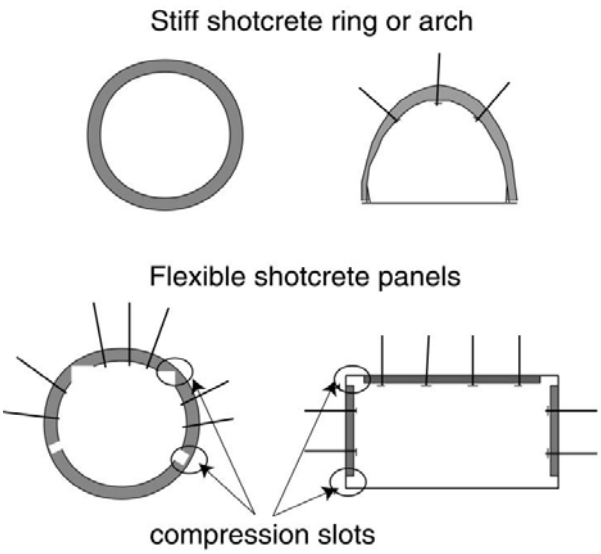

Figure 4.28: Shotcrete as a support ring, support arch, or flexible retaining in form of curved or flat panels

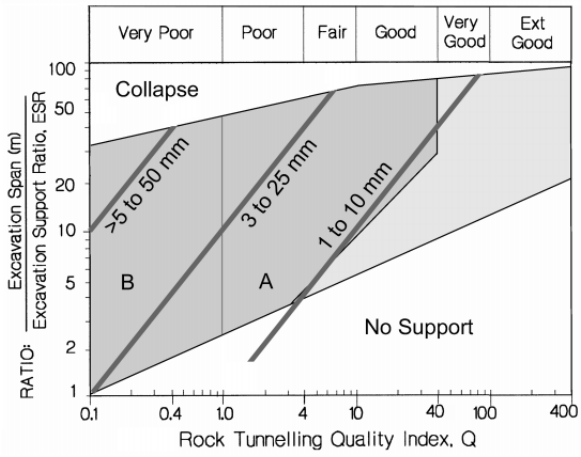

Figure 4.29: Deformation limits observed from well supported excavations superimposed on stability chart (after Kaiser 1986)

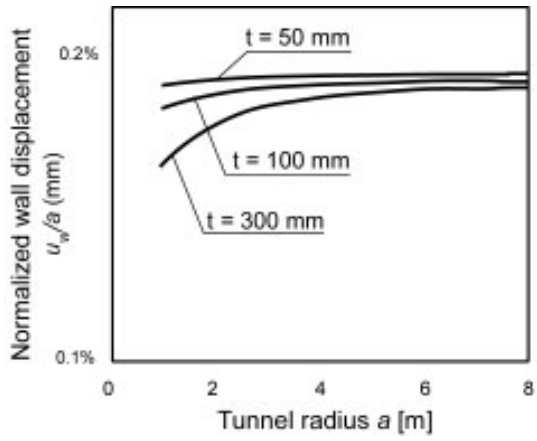

Figure 4.30: Deformation capacity of a shotcrete ring at peak load (without shrinkage allowance) (Kaiser and Tannant 2000)

The same rationale can be applied to other support components (rock bolts, cablebolts, etc.). If the strength of a bolt is not sufficient to prevent bulking inside the failure zone, it must have sufficient deformation capacity to yield. However, as explained earlier, even fully coupled (grouted) rock reinforcements that fail inside the fractured rock zone, still contributes significantly to the overall support capacity of a well-designed support system as bulking control measures.

4.5.2 Use of stability chart to assess deformation compatibility

Kaiser (1986) presented deformation limits from field observations on well-supported caverns and large tunnels. These limits are reproduced on the stability chart in Figure 4.29, defining zones where deformations are expected to exceed 1 to 10, 3 to 25, and 5 to 50 mm, respectively. For comparison, the deformation capacity of a closed shotcrete ring is shown in Figure 4.30. Consequently, for typical tunnels sizes, when Q falls below about 1, the wall displacements must be expected to exceed 0.2% of the excavation radius. A closed shotcrete ring, for example, would not be able to withstand the anticipated deformations. As a general guideline then, excavations falling to the left of Q = 1 must be designed in such a manner that the support system is compatible with large deformations and can deform without attracting destructive loads, i.e., that it can yield (refer also to Figure 4.2).

While it is difficult to accurately predict ground deformations, selecting appropriate stress reduction factors can indirectly be used to assess the impact of deformations on support performance.

Figure 4.33 presents stress reduction factors as a function of stress level σ_{max}/σ_c based on recommendations by Barton (1994). In massive to moderately jointed, brittle rock, the depth of failure is also related to the stress level (see Section 3). Hence, at a stress level of 0.4±0.1, when the depth of failure is close to zero according to previous deliberations, *SFR* = 1 (ranging from 0.5 to 2). No failure and thus no bulking is to be expected and standard support systems will perform well. At a stress level of 0.45 to 0.65, when the depth of failure ranges from about 0 to 0.3a, *SRF* should be increased by one order of magnitude, and when the stress level is higher than 0.65 (d_f > 0.3a), by a second order of magnitude. At the later stage, violent failure in the form of strainbursting is to be anticipated.

Since the depth of failure can be related to the anticipated wall deformation through the bulking factor (Figure 4.7), it follows that the stress reduction factor and the anticipated convergence due to stress-induced bulking can also be related. In other words, the stress reduction factor provides an indirect means to account for bulking. Figure 4.33 illustrates this whereby the

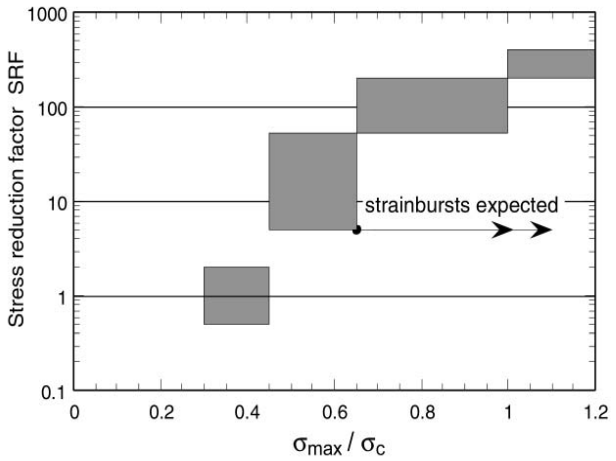

Figure 4.33 : Recommended stress reduction factors (after Kaiser *et al.* (1996); use $0.75\sigma_c$ for strongly anisotropic in situ stresses at $5 \leq \sigma_1/\sigma_3 \leq 1$

previously introduced relationship between depth of failure and bulking is combined with the stress reduction factor chart. For the example introduced in Figure 4.7, a tunnel at low stress would be assigned a *SRF* = 1, a tunnel at the defined in situ stress level a *SRF* = 25 (±10), and the same tunnel experiencing mining-induced stress change a *SFR* of 100 to 300. It can be seen that the mining-induced stress change raises this tunnel into the strainburst-prone region.

This example is also plotted on the stability chart (Figure 4.35) for a tunnel with a span of 5 m. If this tunnel was excavated, e.g., at *Q* = 40, no support would be required at low stress. A modest support with a thin layer of shotcrete (<50 mm) with no or only light,

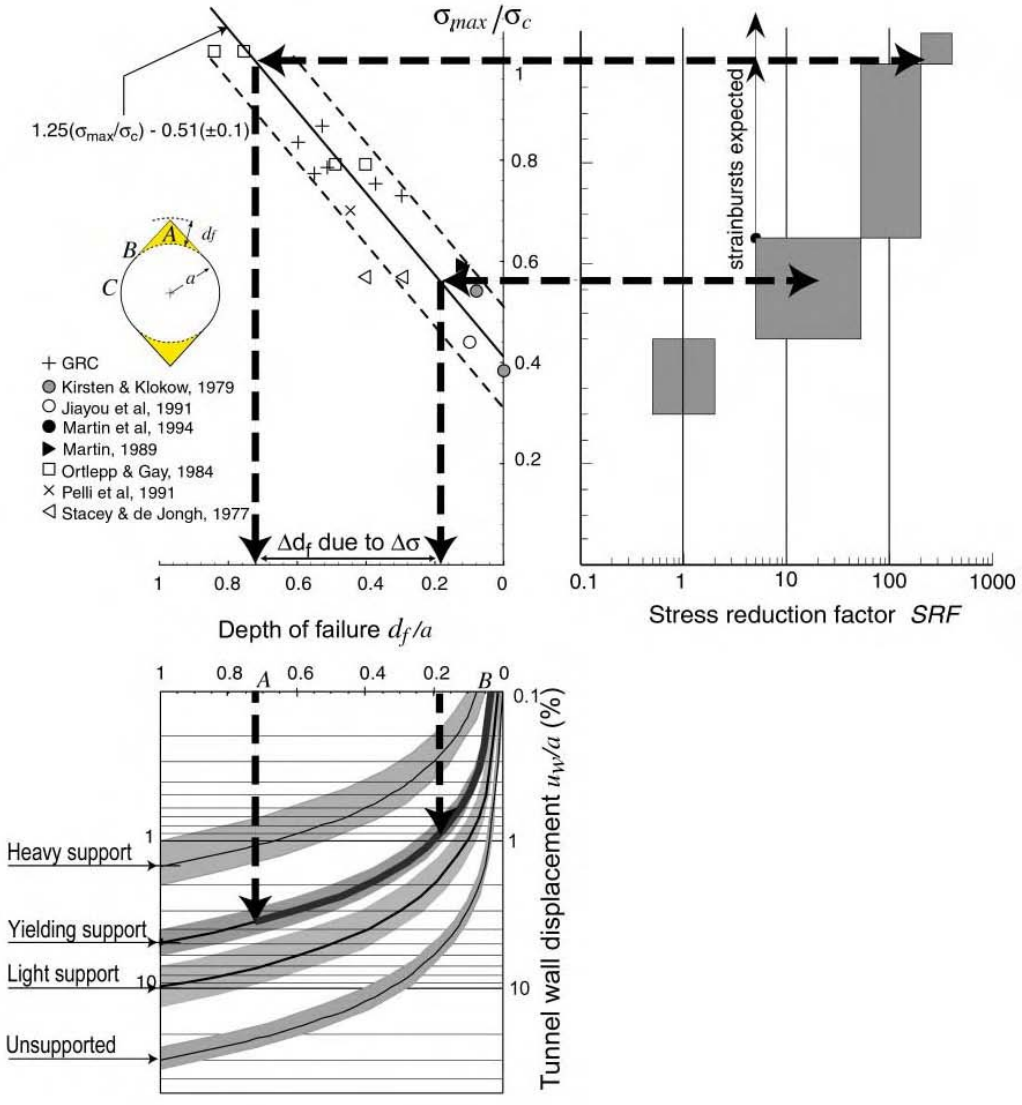

Figure 4.34: Relationship between convergence, depth of failure, stress level and stress reduction factor *SRF*

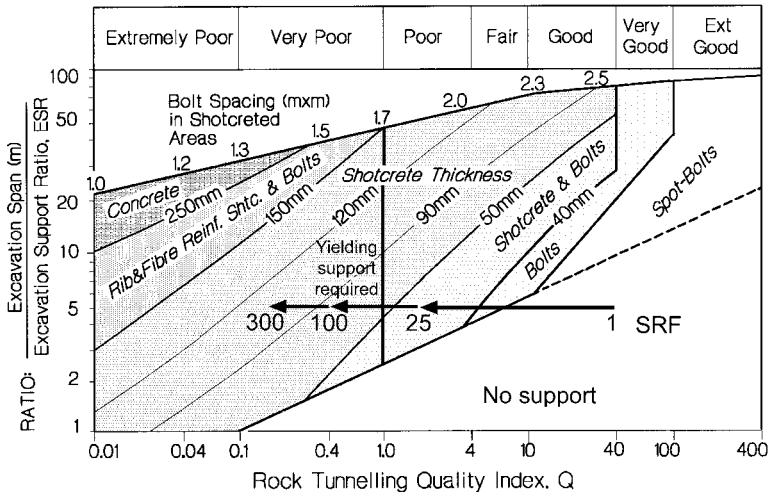

Figure 4.35: Example illustrating increasing support requirements for an excavation experiencing progressively higher stress levels and associated rockburst potential. Starting at *SRF* =1, a 5 m wide excavation in $Q = 40$ does not require support. At *SRF* = 25 for minor burst severity, it can be controlled with standard support. For *SRF* > 50, or for moderate to major rockburst severity, this excavation needs to be supported with a yielding support system.

for burst prone ground as described later.

widely spaced, bolting to control minor slabbing and spalling would suffice for pre-mining conditions (at *SRF* = 25). No excessive deformations would be anticipated and a continuous shotcrete layer would be expected to perform well. Fibre-reinforced shotcrete would be appropriate. However, as mining introduces stress-driven failure (at *SRF* = 100 to 300 or $Q = 0.4$ to 0.1) heavy support with at least 100 mm of shotcrete and bolting would be required. Most importantly, because the tunnel now falls into the zone with $Q < 1$, it must be expected that a standard support system cannot deform sufficiently. Hence, a yielding support system, designed for deformation compatibility, e.g., with yielding slots in shotcrete and yielding, frictional bolts, should be adopted.

This approach for assessing deformation compatibility is particularly useful when selecting support systems

4.5.3 Support for tunnels experiencing strainbursts

It can be seen from that strainbursting is expected when the stress level exceeds about 0.65. In this event, the stress reduction factor should be increased by at least one order of magnitude (Figure 4.33).

The impact of a rockburst beyond that point largely depends on the dynamic stress increment imposed on the excavation and the stress level before the event. A stable excavation will be less damaged than one that is already experiencing instability under static loading. As explained earlier, the effect of a seismic event on the depth of failure can be assessed by considering the dynamic stress increment, which depends on the magnitude of the seismic event, and by choosing an appropriate *SRF* using Figure 4.33. However, because *SRF* quickly increases to more than 100, it follows for most practical situations (except for very small openings) that yielding support will be required when the stress level exceeds about 0.65 to 0.75. At this point, the depth of failure would be on the order of 0.3 to 0.5*a*, which in a 5m wide tunnel would imply failure of about 0.75 to 1.25 m of rock. According to Section 3, this is to be rated as moderate to severe damage potential requiring burst resistant, yielding support to survive relatively large deformations (for details refer to Kaiser *et al.* 1996). At *SRF* = 100, the deformation demand will be relatively limited, particularly if rock reinforcements are used. Fibre-reinforced shotcrete should still perform well, as long as constructive means are implemented to prevent build-up of hoop stresses.

At *SRF* = 300, however, the deformations will likely be large for this example (> 50 mm; see Figure 4.33) and heavy support with mesh-reinforced shotcrete panels, yielding bolts and fully grouted rebar, would be most appropriate. It is interesting to note that even under the most severe burst conditions (Figure 4.35), a shotcrete thickness of only 100 mm is recommended. This is appropriate because the bolting system must control bulking, contribute to the dissipation of the burst energy, and hold the shotcrete panels in place. According to Figure 4.34 the shotcrete panels would be expected to show minor damage after a rockburst, but should maintain their full retention capacity.

Finally, it is worthwhile mentioning, that the conditions described by Figure 4.33 for the tunnel after mining-induced stress change, correspond to conditions that are close to the maximum practical support limit for burst resistant support (Kaiser *et al.* 1996). If more severe conditions are encountered, other means of ground control such as destress blasting must be considered to reduce the demand on the support.

4.6 Summary

Each support component in a support system is intended to perform one of three functions: (1) reinforce the rock mass to strengthen it and to control bulking, (2) retain broken rock to prevent unravelling, and (3) hold rock and retaining elements in place. These functions gain increasing importance as the ground conditions deteriorate, i.e., when rock fails in highly stressed ground or as the rock relaxes. In very poor ground ($Q < 1$), large deformations must be anticipated and support components must retain their functionality over a large displacement range; the support must have superior yielding characteristics.

In brittle rock, the process of stress-induced fracturing near excavations is associated with substantial dilation, called rock mass bulking. This bulking process strongly depends on the support type. In particular, fully grouted rebar has a huge effect on the bulking process. The function of reinforcement is to retain the rock's self-supporting capacity while reducing rock mass bulking. Even if the rock bolts fail due to excessive localized straining inside the zone of failed rock, they are still very beneficial for deformation control.

By combining the stress space with the bi-linear failure envelope cut-off (introduced in Section 2), the depth of failure prediction capability (developed in Section 3), and the interrelationship between rock mass bulking and support, a simple approach for support system selection in overstressed, brittle rock was developed and verified. When used with empirical methods for support design, it is necessary to assess whether excessive deformations, which could damage the support, may be encountered and to determine whether the deformation compatibility limit of a support system may be exceeded. As a general guideline, excavations plotting to the left of $Q = 1$ should be designed in such a manner that the support system is compatible with large deformations. The stress reduction factor provides an indirect means to account for bulking. This approach for assessing deformation compatibility is particularly useful when selecting support systems for burst prone ground.

For the holding function, two detrimental relaxation effects are identified: abutment relaxation leading to an increased demand on the support, and relaxation near cablebolts leading to a loss of holding capacity.

Test results from various retaining elements are compared, and it is shown that strain localization, as often encountered in mining applications, may significantly reduce the retaining capacity of fibre-reinforced shotcrete. It is shown that the effect of only 50 mm of adhering rock almost doubles the capacity of the mesh-reinforced shotcrete. The same effect was not evident when fibre-reinforced shotcrete was tested and this is attributed to strain localization, which reduces the capacity for the fibre-reinforced shotcrete. The high tensile strength of the mesh and spray-on membranes contributed to the superior behaviour of both mesh-reinforced shotcrete and Mineguard™, the spray-on lining tested here. If low strain can be ensured in the fibre-reinforced shotcrete, it provides effective support with high early support reaction stiffness. The selection of an appropriate shotcrete reinforcement strategy largely depends on the anticipated type and amount of deformation.

Mineguard™ applied over mesh produces a very tough support system that is roughly equivalent to 120 mm of mesh-reinforced shotcrete. 8 to 12 mm of Mineguard™ alone produces about double the capacity of 60 mm of fibre-reinforced shotcrete as long as at least 50 mm of rock adheres.

5.0 EXCAVATIONS IN STRUCTURALLY CONTROLLED ROCK MASSES

5.1 Introduction

In this section, a review of current and future trends in permanent civil engineering underground works with a particular focus on structurally controlled stability concerns is presented (for moderately to highly fractured ground; Figure 5.1). Large permanent underground openings or caverns are commonly attributed to their use in the civil engineering sense that cover major applications such as hydropower developments, hydrocarbon storage, transportation structures (large span tunnels, stations and railway crossovers), water treatment and holding tanks, and civil defence openings. Increasingly the use of underground space on a large scale is being considered in conjunction with more demanding applications such as the disposal of nuclear waste and as containment structures for liquids and gases under significant pressure. Lessons learned from such structures are fully applicable to most hard rock tunnelling processes albeit on a reduced cross-sectional scale.

The interaction of the underground excavation space requirements (the geometrical envelope) and the rock mass are critically dependent on a number of factors:

- depth below surface,

- geometrical configuration for intended purpose,
- siting and orientation options,
- available rock mass environments, and
- excavation methodology.

The first three factors are generally purpose dependent and will vary significantly according to the opening function. In some cases, for example urban transportation systems, the underground arrangement will be almost entirely dictated by the system alignment. In other cases, such as bulk fluid storage, there may be almost complete flexibility to optimize the orientation and geometry of the cavern system. Where special linings are introduced for either containment or isolation purposes, these may in turn call for particular geometrical requirements for which the rock mass may need enhanced engineering treatment.

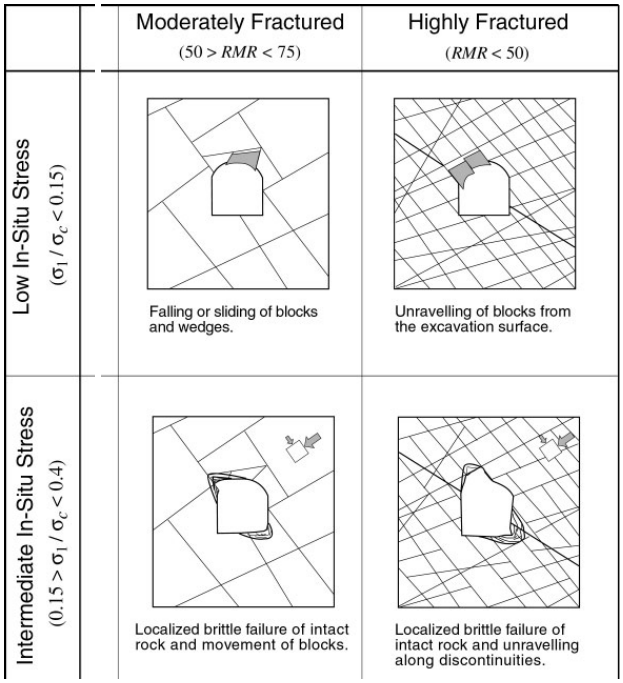

Figure 5.1 Situations dominated by structurally controlled instability (see Figure 1.1)

The aim of this survey is to examine the use of rock engineering technology to develop efficient permanent excavations. Modern practice tends to place maximum reliance on the rock mass intrinsic stability state by the appropriate selection of geological factors, hence, seeking to minimize the degree of engineered support required. The survey concentrated on larger scale openings (generally termed caverns) since these provide the most challenging requirements in terms of excavation design. It is also the case that many tunnels used for civil engineering purposes are concrete lined for safety, hydraulics or ventilation and, hence, often do not represent the cutting edge of underground rock engineering.

The principal requirement of such a system is usually the identification of appropriate geometrical forms that incorporate the governing influence of rock mass structure and the associated induced stress state to provide a cost efficient excavation shape. Whilst this approach has long been recognized in the underground mining industry, its application in civil engineering has been relatively limited.

A key problem with the civil field has been the adoption of a relatively traditional approach to excavation stabilization, which incorporates a formed concrete lining. Based on the design approach for such linings, an arched excavation form is almost always implied which limits optimum consideration of the rock mass properties. In certain cases in well-defined structured rock masses, this blinkered approach has led to actual or near instabilities following excavation and prior to the placement of the so-called final lining. The Portage Mountain Powerhouse excavation, Canada, and the more recent Hanover Würzburg high-speed railway tunnels, Germany, are examples, among many, of such problems. In other cases, perhaps best typified by the NATM approach, the concentration of engineering design on the arch form has been based on a theoretically beneficial induced stress state and lining system. A typical example of this situation is the Waldeck II power station in Germany and more recent major tunnel developments including the UK Channel Tunnel Crossover. The NATM approach and its over reliance on observed behaviour has sometimes led to an inadequate design understanding of the rock mass surround response and, as a result, instability problems or excessive engineering measures have resulted.

From an assessment of past experience, the need to fully understand the likely ground response and its potential behaviour as the primary structure (base component) in the cavern system is becoming increasingly recognized. In some cases, the potential use of the rock mass as the primary component of the system will reveal its inadequacy to provide the necessary support even with heavy reinforcement. Under such conditions the use of rock replacement technology, particularly in weaker rocks, may be appropriate. Using this approach, the rock surround is replaced in zones of critical overstress or instability using concrete placed within limited sized drifts. These can be developed to form a complete structural surround if required. The French Channel Tunnel Crossover was perhaps the most significant application of this technique in rock engineering so far.

A further significant development is the use of pre-reinforcement for critical zones of the excavation profile using pre-placed fully bonded reinforcement from initial access galleries (e.g. Mingtan, Taiwan, (Moy and Hoek 1989)). Such a system can be effectively combined with rock replacement technology.

The excavation system, notably for tunnels, will inevitably influence the cross-sectional profile. In particular, full face mechanized excavation using tunnel-boring machines (TBMs), dictates a circular profile in hard rock conditions. This profile leads to particular support and lining systems that often involve pre-cast segmental linings placed concurrently with the excavation advance. The options for rock reinforcement and shotcrete usage are directly limited by the machine configuration. For more difficult excavation - support applications, open or short single shield machines are preferred (Sharp *et al.* 1996). This specialist excavation approach is of great interest in tunnel development but is beyond the scope of this paper.

In the following survey of design methodology, the primary use of drill and blast or roadheader excavation systems has been assumed together with rock reinforcement as the primary stabilization element for structurally controlled rock masses.

5.2 Geological models of rock masses in relation to discontinuity characteristics

5.2.1 General considerations

It is well recognized that the geological characteristics of a rock mass can be fundamental in the optional siting and detailed design of cavern structures. Where other constraints dictate the location and orientation of the opening, the engineering must take into account the range of geological conditions envisaged. In general, however, for all projects there must be an early and adequate appreciation of the principal geological constraints and consequences on the design and construction. Such factors thus need to be given a representative weighting for meaningful siting and alignment assessments.

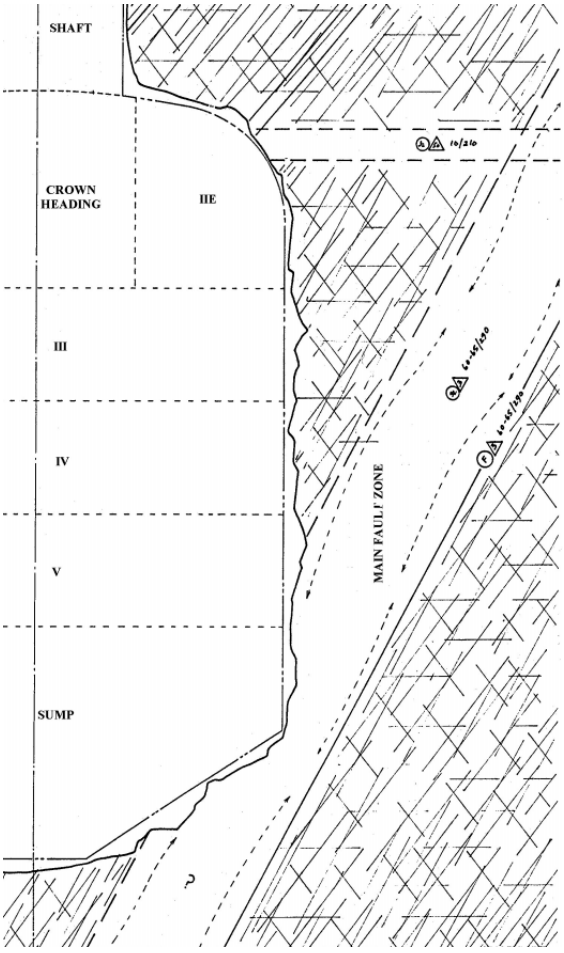

Figure 5.2: Geological section model - typical example (Simon Allen 1995)

Engineering geological assessment typically comprises the development of siting models that are key references in the scheme layout (Fookes 1997). The development of sectional models of the rock mass that facilitate the comparison and evaluation of rock masses for their suitability, and allow the development and subsequent optimization of designs specific to geological environments are often overlooked in design studies. Geological sectional models (Figure 5.2) developed for a host rock mass provide a framework from which stability models can be developed, parameters assigned, and the principal controls of rock mass response identified. The models should take into account the risks and hazards identified which may include items that have not been specifically identified in the site area but are known to be typical of the lithology and therefore features that could be encountered during excavation.

Accurate appreciation of the rock mass response will significantly influence the selection of excavation geometry, methods and support procedures that may not otherwise be evident from general geological data. This becomes particularly apparent in heterogeneous or layered materials, which cannot be represented by single measures of rock quality. The limitations of rock mass characterizations have been summarized in a number of papers including in particular Cripps *et al.* (1993). As Prof. Hudson concluded, “each engineering project could have some unique feature that causes the problem”, which implies the need for a review of the fundamental geology and associated weaknesses prior to attempting

any kind of rock mass classification. Finally, the level of detail incorporated into engineering geological siting studies needs to be commensurate with the particular design stage, from initial feasibility or option evaluation, through to detailed design.

It is unfortunate that often little emphasis is given to the meaningful definition of the physical excavation characteristics with emphasis on the rational treatment of geology, particularly structural. Although being a requisite of many design texts and approaches (e.g., Goodman and Shi 1985), it is not uncommon that the form of analysis (and generally its limitations) will dictate the definition of input criteria thus denying a proper and fundamental account of the controlling physical processes. Important in this context is the example set by Barton and Choubey (1977) and Bandis *et al.* (1983) in the physical description of discontinuity characteristics.

The approach advocated in this section, dealing with structurally controlled excavation design, emphasizes the importance of the fundamental geological model at all stages of design and the related, representative descriptions of the rock mass behaviour. The understanding of the in situ stress and groundwater states and their potential variations needs also to be emphasized.

For the purposes of this general survey the principal influences of rock mass characteristics are reviewed and two contrasting summary generic rock masses developed. For preferred civil underground excavation host environments, the key geological attributes are:

- moderate to high rock material strength,
- good rock mass quality,
- high geomechanical uniformity (homogeneity), and
- absence or low frequency of major geological deformation structures (incl. joints, shears, faults, etc.)

The broad relationships of these attributes to underground excavation design are described next.

5.3 Key geomechanical considerations

In general, cavern developments must address both the geometrical requirements to suit the operational purpose and the optimum arrangement in terms of geological controls. The latter usually relates to structural geological features (principal discontinuity systems) except at depth where induced stresses relative to rock material strength may dominate (see Sections 2 to 4).

In most cases of cavern design and siting, it will be possible to optimize the orientation to avoid the cavern axis running sub-parallel to principal discontinuity sets that are steeply dipping. Such features could adversely impact either crown or sidewall stability (particularly the latter) as indicated by Figure 5.3.

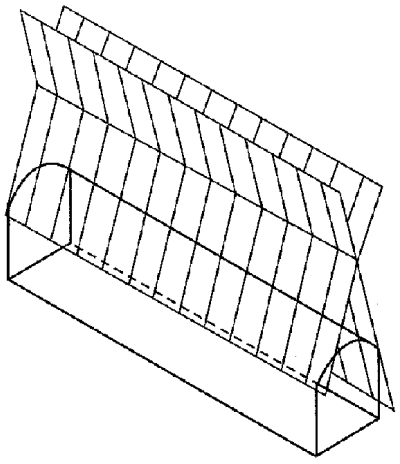

Figure 5.3: Impact of structure on cavern crown stability (after Hudson and Harrison 1997)

5.3.1 Rock material strength

Adequate strength, as defined by the unconfined compressive strength of the rock, is a fundamental index parameter of the rock mass quality, which controls the response of the rock mass to imposed stress and the potential generation of induced fractures (including natural fracture extensions). Detailed designs may also consider the effects of tensile strength, although this is usually of secondary importance for civil engineering structures in fractured rock masses.

5.3.2 Rock mass structure

Geological structures (and their geomechanical properties) control the response of the rock mass to stress, and together with material strength define the overall rock mass quality, strength and elastic constants. Geological structure includes discontinuities in the form of regular jointing patterns in all rock types particularly igneous rocks, bedding in sedimentary rocks and foliation (incl. cleavage and schistosity) in metamorphic rocks.

A degree of structure within a rock mass may, under more elevated stress conditions, be favourable to assist in the redistribution of stress around the cavern opening and the reduction of the risk of material shear failure. However, adversely orientated structure comprising planes of significant weakness is detrimental to cavern stability, both in terms of stress redistribution and local block or wedge instability. A minimum value for rock mass quality *Q* (Barton *et al.* 1974) (which is sensitive to structural variations) as defined for openings of a given span or geometry versus depth, based on precedent, can provide a useful first indicator for underground excavation host stratigraphy pre-selection. A summary interpretation is shown on Figure 5.4 which is a composite plot of *Q*-class (A - G) against depth and span expressed as a limiting envelope from interpretation of precedent cavern data.

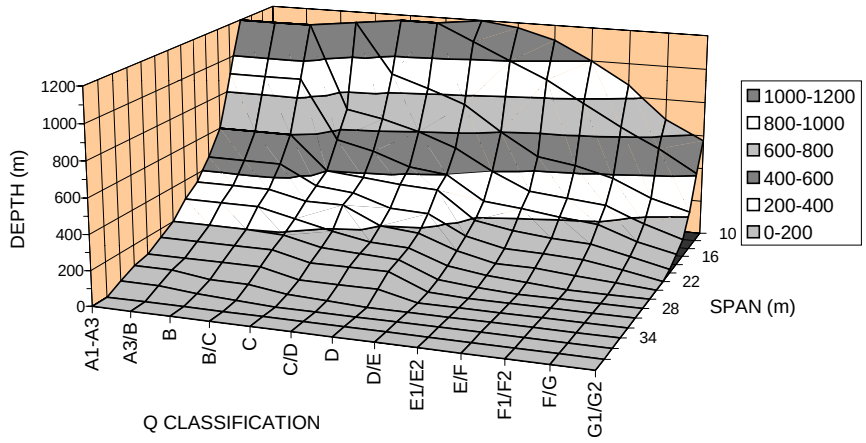

Figure 5.4: Precedent limits of cavern span for various depths for different Rock Mass Quality Indices *Q*

An additional and important aspect of geological structure is its contribution to the primary hydraulic conductivity of most rock masses. This conductivity or connectivity property is of importance in the inflow – outflow characteristics of the opening and is critical in most containment situations involving pressurized fluids or gases.

5.3.3 Homogeneity

Geomechanical uniformity is a key consideration controlling the scale of variation within the rock mass, which is significant in relation to excavation size and zone of stress influence upon excavation. A target lithological unit, potentially situated within an otherwise variable stratigraphy, of greater thickness than 3 to 5 times the proposed excavation height (or span) is suggested for optimum siting and design. This leads to a requirement for a rock mass, which can be considered geomechanically uniform over the target thickness of greater than 30 to 100 m for a typical civil engineering opening. This in turn may imply the need for a relatively detailed appreciation of site stratigraphy particularly for deeper cavern sitings in variable rock masses.

5.3.4 Occurrence of major geological structures

Major geological structures comprising faults, shear zones, zones of alteration (typically hydrothermal) and mineralization or high concentrations of major (master) through-going joints will generally be detrimental or a risk to the intrinsic stability of the cavern excavation. Rock masses where these features are absent or have a low frequency in order that they may be avoided are clearly beneficial in terms of siting. Appropriate, targeted, site investigation can assist with the site development process where such features are to be avoided. Minor rock types as encountered in igneous complexes that have significantly different characteristics from the parent rock should also be assessed in terms of orientation frequency, characteristics and potential behavioural response.

5.3.5 In situ stress regime

The in situ stress state is a fundamental input in the control of underground excavation stability and needs to be carefully established from reference data and in situ measurements. Of particular importance to both the geometrical form of openings and the subsequent intrinsic stability is the stress ratio K_o between the maximum and minimum principal stresses. A three-dimensional appreciation of the stress field is important for the rational siting and orientation of cavern structures as well as in the subsequent analysis of two dimensional excavation cross-sections.

For excavation design knowledge of the overall stress field should be gained from a two-fold approach of geological stress history (especially the geomorphologic and tectonic processes) and in situ measurements

using multiple borehole measurements with a triaxial strain cell device (see Section 2 and Hudson and Harrison 1997). The need for multiple measurements throughout the cavern domain is to allow the overall in situ stress field, pertinent to excavation design, to be reliably inferred.

5.3.6 Additional factors

Host stratigraphy judged to be suitable in terms of geomechanical properties need also to be assessed for their occurrence and geometry, in particular the location and thickness. Other issues that may warrant consideration include the geothermal gradient and tectonic activity. Hydrogeology may also be a concern and may require particular input to alignment models in terms of regional hydro-geological setting, and rock mass hydro-geological containment criteria.

5.4 Categorization of potential host rock masses for cavern siting

In some countries and regions, e.g., Norway, Sweden and Hong Kong, it has been possible to locate most large underground openings entirely within competent crystalline rock masses. Siting within sedimentary and volcano sedimentary sequences is however, becoming increasingly common and, in terms of the large world sedimentary basins, inevitable. The evaluation process can be assisted by categorization of the range of available sedimentary rock masses in terms of concept models for engineering assessment.

For sedimentary rocks, the environment of deposition is the primary control on the observed variation in both lithological composition and homogeneity of the sedimentary stratigraphical units. The range of depositional environments and associated facies thus forms the framework for classification of engineering rock mass concept models. Many other influences including burial depth, diagenesis and structural history will also be significant but are usually subordinate controls.

Engineering geological concept models can thus be defined to constrain the complex variety of lithologies and stratigraphies present. The concept models permit a broad, initial evaluation of the candidate host rock masses in terms of cavern geometry, stabilization and containment potential. For illustration purposes, five summary rock types have been selected from the full range that are likely to represent the most suitable host rock masses. Other rock masses, for example higher-grade metamorphic sequences, may require particular attention due to their complex nature if siting constraints dictate their consideration.

Candidate siting models listed below can be summarized into two groups according to the principal geological structural controls. The principal structure has a significant control over the design of the cavern geometry and the cavern engineering in general. Caverns engineered in Group 1 rock masses will therefore contrast markedly with those in Group 2.

Group 1 - IGNEOUS AND VOLCANIC ROCKS
Principal structural control: Jointing (sub-vertical) :
- Intrusives (Granites)
- Extrusives (may be banded)

Group 2 - SEDIMENTARY ROCKS
Principal structural control: Bedding (shallow dipping) :
- Aeolian sandstones
- Reef limestones
- Alluvial - Shelf sequences (sandstones - siltstones - claystones)

Summaries of the attributes of the two groups are included in Table 5.1.

Table 5.1: Concept summary models – cavern siting and design

Concept Model	Typical strength (MPa)	Typical RMR	Typical Q	Primary discontinuities	Cavern design issues – risks
Group 1	150-250	>60	>20	Sub-vertical jointing	The presence of major structures in the form of shear zones (and major jointing) with associated hydrothermal alteration. Shear overstress developed on the steeply dipping structure in the haunch areas. Block instability caused by adverse dipping joints.
Group 2	50-100	35-70	7-20	Bedding, generally sub-horizontal	Bedding can form significant persistent planes of weakness particularly where interbeds of weaker (argillaceous) material is present. Interbeds tend to be sheared. Shear overstress on such features is likely to be prevalent. Strength is potentially marginal in relation to squeezing rock problems. Will depend on bedding spacing and frequency of other jointing. Solution features and enlargement of joint surfaces of limestones can also be problematical for containment.

Notes:

- *Q* is an assessment of rock mass quality determined in accordance with Barton *et al*. (1974)
- Rock Mass Rating *RMR* is an assessment of rock mass quality determined in accordance with Bieniawski (1974)
- The assessments of rock mass quality is made on the basis of the concept models and knowledge of the rock masses they represent. The values quoted are indicative only and are a measure of the typical rock mass conditions where unaffected by major structure and significant weathering.

5.5 Geometrical forms for cavern developments

Geometrical cross-sectional form of the cavern is the most representative comparative feature of which span and height are the key summary parameters. As noted previously, it is usually possible to optimize the orientation to avoid significant impacts from steeply dipping structure (see Figure 5.3). From this observation, it follows that the exception in terms of cavern arrangement and stability influence optimization is the effect of sub-horizontal bedding and its particular influence on cavern crown (roof) stability. It can however be noted that under such conditions the adoption of a silo (i.e. high aspect ratio vertical opening) may be relevant, particularly for storage facilities to avoid major stability problems.

In general terms, it can be stated that cavern designs normally focus on a single cavern system even if it is subsequently developed as a complex (multiple, usually parallel caverns separated by adequately sized pillars). In addition it can be generally, although not always, identified that the upper cavern cross-section (crown) is of principal importance in terms of geometry owing to its relatively critical stability state and the potentially high unit cost of cross-sectional development compared with lower stages.

In terms of geometrical constraints (including both location and shape) caverns can be broadly classified in terms of degree as shown in Table 5.2.

Table 5.2: Underground caverns – geometrical considerations and constraints

Principal cavern types	Location constraints (degree)	Orientation constraints (degree)	Geometrical constraints (other than geology)
HYDROPOWER	MODERATE	LIMITED	Plant dependent; can use multiple caverns to reduce spans
TRANSPORT			
- stations	HIGH	HIGH	Track / platform layout
- crossovers	MODERATE	MODERATE (Alignment dictated)	Track separation
OIL STORAGE and WATER (fresh, storm or waste) STORAGE	LOW (Proximity to water or pipelines)	NEGLIGIBLE	Minimal; Unless specific lining system (form) employed for containment
GAS STORAGE	MODERATE (Usually stress and/or groundwater requirements for pressure containment)	NEGLIGIBLE	Moderate; pressure response design in terms of stress - containment factors
OTHER BULK STORAGE (Coal, Domestic Waste Archives, Cars)	MODERATE (Possibly high in urban locations)	NEGLIGIBLE (Possibly moderate in urban locations)	Minimal; access for placement and retrieval of product may be important

From the above table, it can be seen that cavern geometry is often not closely constrained by the cavern usage. This is particularly true for most storage uses. Under such conditions therefore, cavern volume unit cost often becomes the guiding parameter for design optimization.

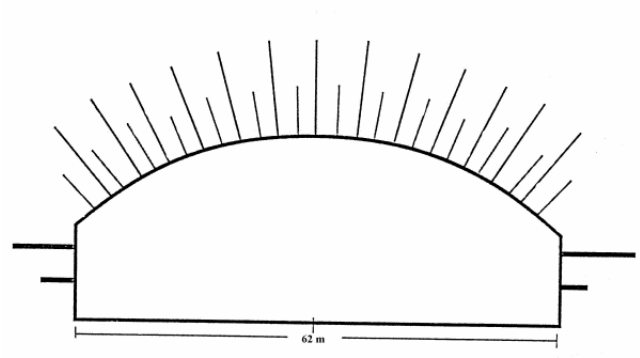

Figure 5.5: Cross-section of the Gjovik ice hockey cavern, Norway

In certain cases such as hydropower with low to moderate head and high capacity units, span may become a critical requirement. In a few cases such as the Gjovik ice hockey cavern (Barton *et al.* 1991*)*, minimum size (in terms of span and plan area) is completely dictated by its end use (Figure 5.5).

5.5.1 Geometry and geology - key principles

The other constraint to geometry, which is the subject of this section, is the structural geology of the rock mass. The recognition of this factor and its incorporation in the fundamental excavation design and layout, along with in situ stress considerations, is still an area for the rock engineering development of underground civil structures.

Hard intrusive or extrusive rock masses

In hard, discontinuous rock masses of these classes, the overall cavern designs will be primarily related to the principal discontinuity sets. The excavation cross-section will usually be formed of two key components, namely: a large radius crown or roof arch, and vertical sidewalls.

Such excavations are typified by large underground excavations for oil storage and hydropower as developed in Scandinavia (Finland, Norway and Sweden), utilising the principles of least cost, unit volume space, as illustrated by Figure 5.6.

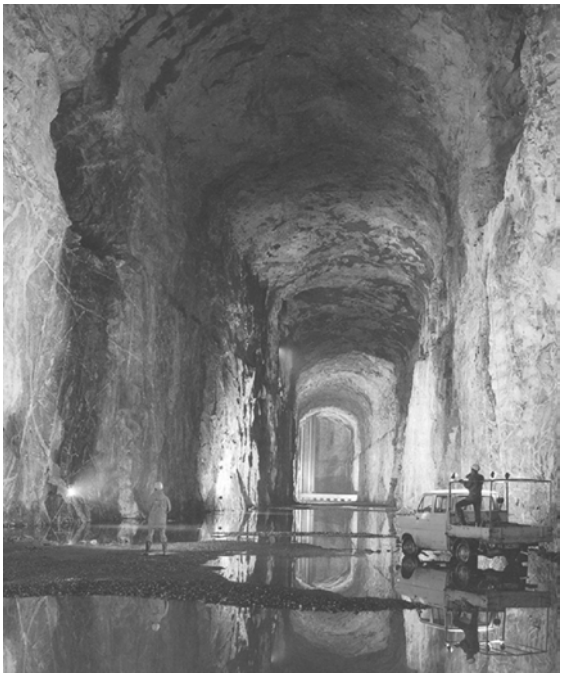

Figure 5.6: Major storage cavern - Sweden (after Franzen and Hultin 1988)

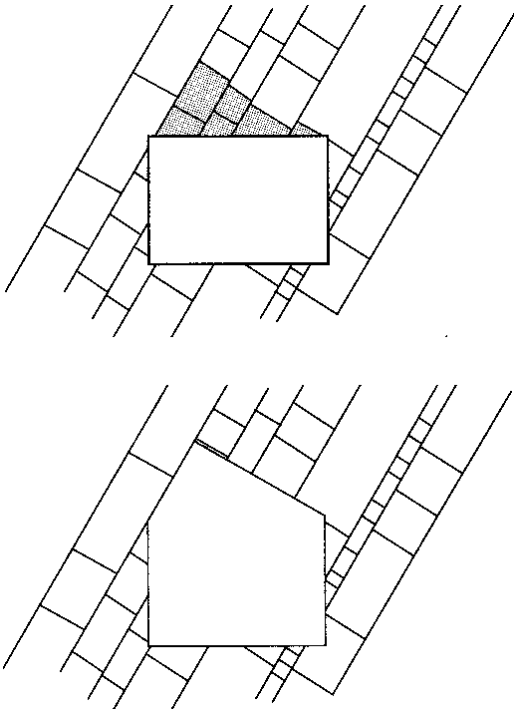

Figure 5.7: Cavern geometry - design with the rock (after Hudson and Harrison (1997)

process is simply explained by the so-called shear overstress; a theory originally applied by Endersbee (1975), and more rigorously presented by Goodman (1989). The inability to assess or reinforce such profiles adequately has led to significant delamination of major spans typified by the incidents at Portage Mountain,

The cavern crown radius can be modified if sub-horizontal discontinuity sets are prevalent to a radius of the order of 5-times the span or greater to avoid excessive haunch instability. Radiused corners (e.g., 0.2-times the span) will assist in the placement of rock reinforcement, the primary support type envisaged for such environments in conjunction with shotcrete linings.

Shallow dipping sedimentary environments

These environments, making up a very significant part of the earth's crust, have historically been exploited for their relative ease of excavation and are structurally defined by bedding. In many cases, significant anisotropy may be present due to variations in the interbedded nature of the rock types. Particular stress conditions (typified by high horizontal stresses) are commonly a feature of such environments.

The relationship between geometry and structure is extremely important in this class of rocks, and whilst the fundamentals of appropriate design have been established for well over a century in mining (particularly in coal mining), the application to large-scale permanent underground openings has been limited. Both experience and theory have shown that in 'flat' (bedded) or 'square' (bedded and jointed) geological structure, opening geometry for large discrete openings should be compatible (i.e. rectangular not circular). Whenever possible design with the rock (see Figure 5.7).

A special issue in this respect is the recognition of a flat roof span (conformable to bedding) that can be reinforced as required based on beam lamination principles. Whilst the system is best known for its application in horizontally bedded rocks (Lang and Bischoff 1984; Coffey 1995), it can also be applied to dipping strata. The alternative use of arched profiles in such rock masses is intrinsically unsound in terms of loosening and hence, destabilization by shear overstress of the critical haunch zones (see Figure 5.8). The

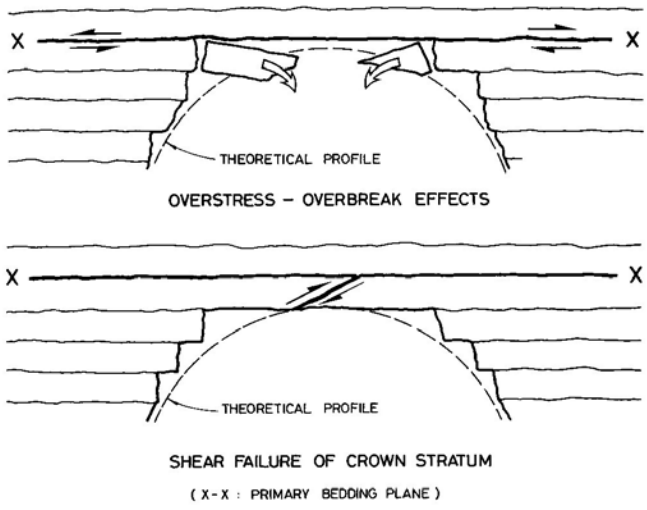

Figure 5.8: Behaviour of arched profiles in bedded rock

Canada in 1968 (130 mm crown deformation on a 26.5 m arch span; Imri and Jory 1979) and more recently at the UK Channel Tunnel Crossover (40 mm sudden crown deflection on a 20 m span).

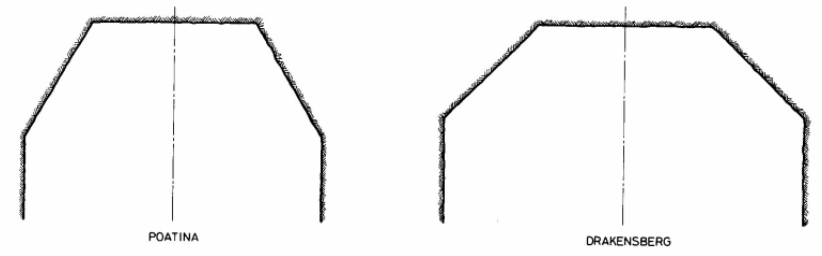

Figure 5.9: Haunch arrangements for caverns to limit flat span extent

The generation of wide, flat spans, using beam lamination techniques, requires special consideration in terms of design approach and methodology. In particular the system relies almost entirely on a composite of rock and rock reinforcement for stability. For this reason, the design needs to be based on a reliable set of geo-mechanical parameters, including in situ stress conditions. Full account must be taken of all uncertainties. In weaker, bedded rock masses, the span may need to be limited by haunches to give a trapezoidal excavation form, as shown on Figure 5.9 (Sharp *et al.* 1984). The use of rock reinforcement, fully integrated with reinforced shotcrete linings, forms a composite reinforcement / lining system in such weak rocks (Sharp and Lawrence 1982; Sharp 1990). The sidewalls of excavations in horizontally bedded rock, even with weak bedding partings and elevated stress conditions, have been shown from well-documented case studies to be inherently stable. They can however be subject to moderate - high lateral deformations and under elevated stress states, time-dependent response (Sharp and Mellors 1982).

5.6 Precedent experience of cavern design – established limits and criteria – Year 2000

5.6.1 General survey scope

In a recent comprehensive study of cavern usage (Geo-Engineering 1996), caverns were indexed into the following key types that are related primarily to end usage. Large cross-section tunnels were also included.

Cavern or opening type	Usage class
I	Power Caverns (Hydro Electric Developments)
II	Storage Caverns
III	Other Major Caverns (including transport related openings)
IV	Large Tunnels (various - mainly transportation and water)
V	Permanent Mine Openings and Chambers (Pump Stations, Hoist Chambers)

The study was based on a wide-ranging global survey and was developed and augmented by a more detailed assessment of related projects that included sufficient data to permit an interpretation of rock mass quality *Q*.

5.6.2 Geological indexing strategy

Geological classification of the projects was used to define a broad basis for comparison between different rock types that was considered to have a material influence on the intrinsic stability characteristics.
The overall strategy described in Table 5.3 was used to define the related geological environment.

5.6.3 Basic cavern geometrical characteristics - type - span - depth

Power caverns (Type I)

Precedent construction in this field is dominated by caverns associated with hydroelectric developments that are generally at a shallow to moderate depth. Depth is controlled both by waterway pressures and access requirements. All classes of geological conditions are found in such examples although there is always a tendency to exploit more competent sites where available. For power caverns, the cavern construction is usually only a single part of a multi-component scheme and hence is not necessarily optimised in terms of minimizing rock support through preferential orientation. The cavern sizing will be dictated by the internal hydro-mechanical plant requirements and will not necessarily involve the development of limiting economic

Table 5.3: Categorization of principal rock mass types for cavern developments

A	Competent Intrusive Rocks	Granite, gneiss, granite schists (including more competent mica schists), massive conglomerates, greenstone	Generally good quality intrinsic rocks (often granitic) with moderately developed jointing. May be partly metamorphosed but not displaying ubiquitous weak fabric. Rock material generally strong. Extended to incorporate more massive rocks not classified elsewhere. If tectonized to any significant degree classified as faulted (F).
B	Competent Extrusive Rocks	Andesite, basalt, rhyolite, ignimbrites, tuffs	Generally good quality extrusive rocks with moderately developed jointing. Tuffs may be weak in some cases. If tectonized to any significant degree classified as faulted (F).
C	Foliated, Metamorphosed Rocks	Slates, phyllites, amphibolites, schists	Rocks with well developed fabric due to metamorphism. Generally strong contrast between discontinuity and material strength. Anisotropic behaviour.
D	Sedimentary Rocks - Non-Calcareous	Sandstones, siltstones, claystones	Generally rocks of varying competence (depending on clay content) and with well developed stratification. May be complex "en masse" as a result of interbedded strong and weak units. Weaker clay-rich units often moisture sensitive.
E	Sedimentary Rocks - Calcareous	Limestones, marble, chalks, marls	Category reserved for calcareous rock classes that may vary from competent, massive limestones to weak chalks, often with stratigraphic characterization. Marls often contain moisture sensitive clay components.
F	Faulted Rocks	Unclassified	

spans except in less competent rock masses. In such cases, the use of multiple cavern complexes is made to limit the maximum span.

Storage caverns (Type II)

The field of storage cavern development is generally dictated by the need to create maximum underground volume at minimum unit cost. Such cavern developments thus represent a particular type class that has usually been optimised to this end. This includes significant geometric factors such as cavern shape, height and span. For bulk storage of fluids, shape is often unimportant but for mechanically handled storage a regular cross-section geometry is usually aimed for. Commonly, storage caverns are located at shallow depth except where particular constraints for pressurized storage are called for.

Other major caverns (Type III)

Major caverns other than power or storage caverns are associated with a variety of end uses, the most notable being transportation. Caverns in this class encompass a range of different geometries, some of which can be very significant in span (most notably the Gjovik ice hockey stadium in Norway, with a span of 62 m). For constructional as well as operational access reasons, such caverns are usually located at a shallow depth.

Permanent mine openings (Type IV)

Permanent mine openings and chambers such as used for plant installation form a special class of cavern, since they are invariably constructed at a significant depth below surface. Unfortunately, they are often poorly documented in terms of geology and rock support and they tend to be located in more favourable rock conditions to minimize support problems and cost.

5.6.4 *Precedent findings - general*

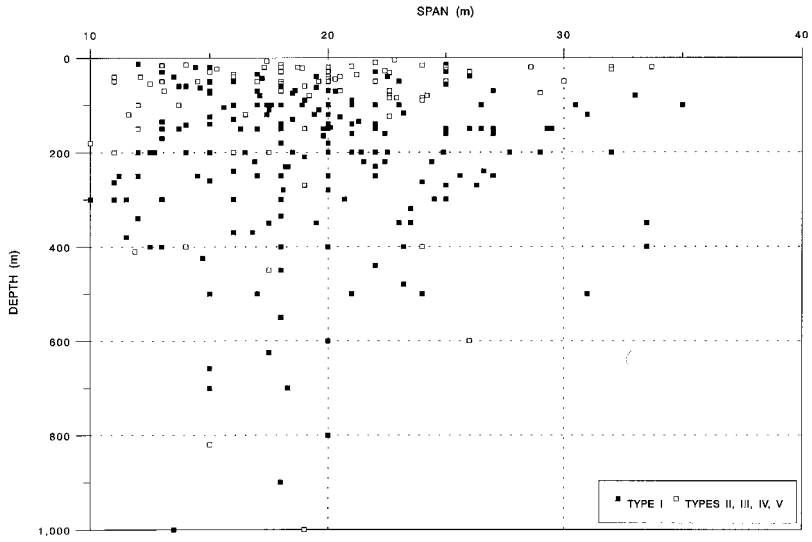

Figure 5.10: Permanent cavern data: span - depth (cover) characteristics

The cavern geometric data have been plotted to show the basic relationship and experience between span and depth. This data according to cavern type are shown on Figure 5.10. (The different cavern types are shown by symbolic presentation.) The data used were drawn in part from the US Corps of Engineers report (1980) with significant updates from other sources, e.g. Sharp (1989) and Geo-Engineering (1996).

From this initial general survey of constructed experience, it is evident that for caverns with a depth of cover up to 200 m, spans up to 35 m are common. Between 200 m and 500 m depth, maximum typical cavern spans generally diminish from 30 m to the order of 20 m.

At depths on the order of 1000 m, the degree of precedent is restricted due to lack of data. Typically cavern spans are always less than 20 m and generally of the order of 15 m.[10]

The prominence of Geology Class (domain) A over all other types is noteworthy as is the paucity of relevant data in Class B, the extrusive rocks class.

5.6.5 *Specific cavern geometrical characteristics*

Span - depth characteristics - rock reinforcement supported caverns

A selected database for caverns principally supported by permanent rock reinforcement, often used in conjunction with shotcrete linings was derived and is shown in Figure 5.11. The database is significant in relation to the total database indicating the generally accepted use of this permanent support system (rock reinforcement) for large cavern excavations.

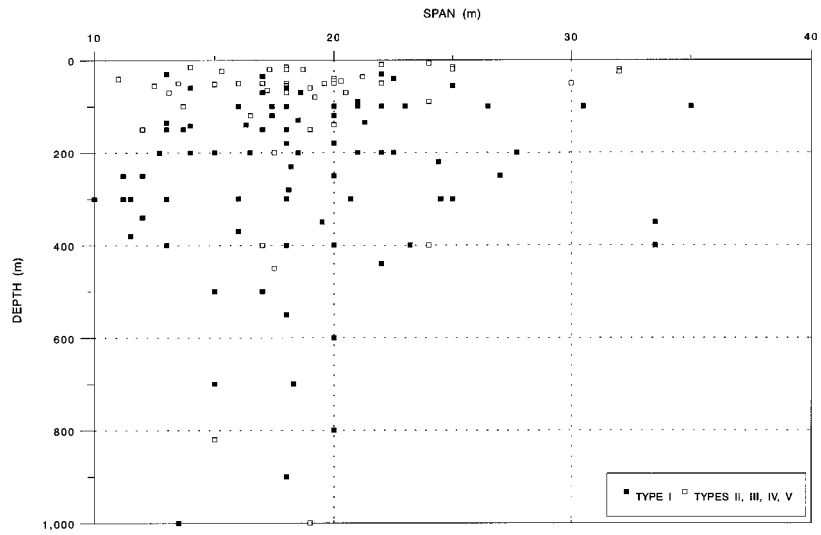

Figure 5.11: Permanent rock reinforcement supported caverns: span - depth (cover) characteristics

Span - height characteristics

The cavern span - cavern height characteristics are of interest in that they indicate the range of precedent for different cavern geometries. The span - height characteristics for all data, in the span range 10 to 40 m, are shown on Figure 5.12.

The trend, ignoring depth, clearly shows a typical upper bound for cavern heights equivalent to twice the cavern span. These data forming

[10] The Solar Neutrino Observatory in Sudbury with a span of 22.9 m at a depth of 2072 m constitutes and exception (Oliver 1992).

this upper bound limit are generally derived from hydro-electric and storage cavern types.

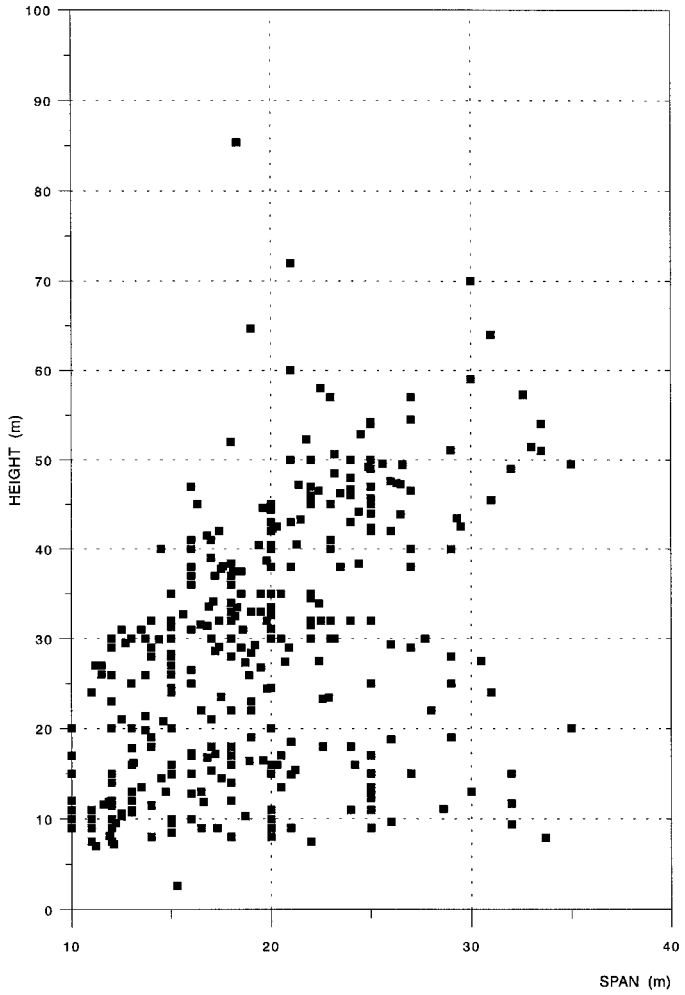

Figure 5.12: Permanent cavern data: span – height characteristics

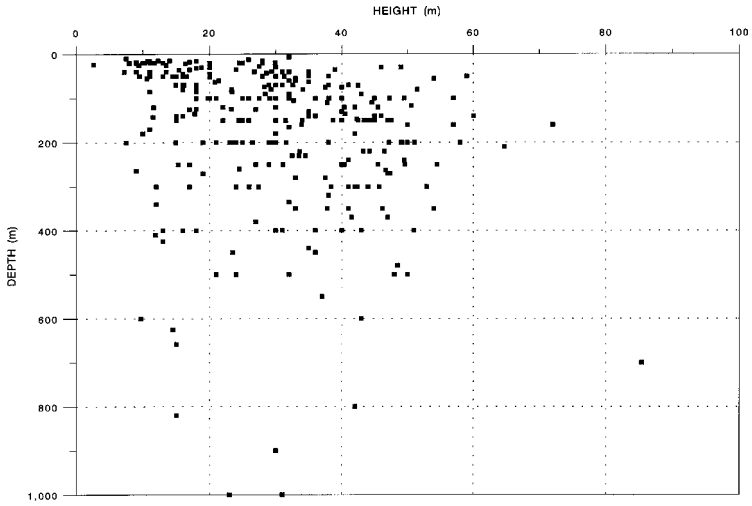

Figure 5.13: Permanent cavern data: height depth (cover) characteristics

Cavern height – depth characteristics

The cavern height, as with the cavern span would be expected to diminish with depth primarily as dictated by increasing support requirements to counter elevated stresses. The cavern height – depth of cover characteristic is shown on Figure 5.13 for depths up to 1000 m.

Up to a depth of about 1000 m, cavern heights of up to 30 m are not uncommon. Below a depth of some 1200 m, cavern heights rarely exceed 20 m. Again, the Solar Neutrino Observatory at more than 2000 m depth is a notable exception.

Span / height ratio – depth characteristics

The span/height ratio is a useful indication of precedent cavern geometry vs. depth and is plotted in Figure 5.14. Of note is that a minimum cavern span / height ratio as low as 0.4 has been commonly utilized at depths up to 600 m where stresses can be considered as significant (height up to 2.5-times the span). Further data to support such low ratios are also available in the depth range 1000 to 1400 m. The comparative figure for the maximum ratio of cavern span / height beyond 200m is on the order of 1.2.

5.6.6 Excavation – support characteristics

Of interest in the application of support systems are the following key factors:

- type of rock reinforcement,
- crown rock reinforcement length – span characteristics,
- sidewall rock reinforcement length – cavern height characteristics,
- crown rock reinforcement support pressure – span characteristics, and
- sidewall rock reinforcement support pressure – cavern height characteristics.

Rock reinforcement

The types of rock reinforcement commonly used for cavern support and as defined in this study are:

- Rock anchors - generally longer length, tensioned, permanent reinforcement units; usually

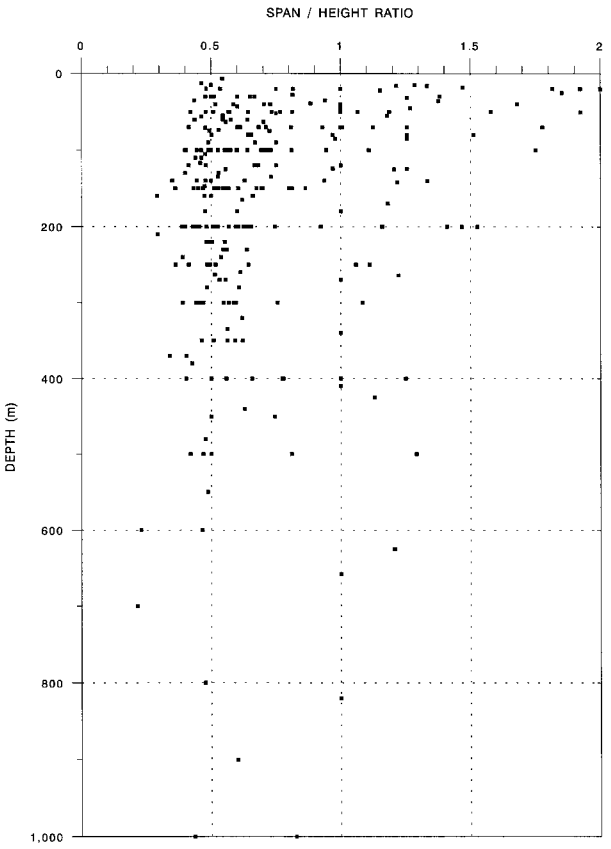

Figure 5.14: Permanent cavern data:
span / height – depth (cover) characteristics

monobars but may be strand type also.

- Cablebolts - generally longer length, grouted cables installed often as pre-support; usually untensioned. Rather specific applications.
- Rock bolts - Shorter length, often termed secondary reinforcement units (to distinguish from rock anchors). Fabricated from monobars; usually tensioned but can be untensioned and commonly then referred to as dowels.

Many cavern support systems comprise different length units that often are split into primary and secondary support functions. This may involve the utilization of a hierarchy of types such as longer rock anchors for primary units combined with shorter rock bolts or dowels for secondary support.

The use of untensioned rock bolts (dowels) is not significant in terms of overall support of major caverns. However, within the scope of the New Austrian Tunnelling Method (NATM), there is sometimes a strong bias towards the use of untensioned fully bonded units partially to allow mobilization of rock mass strength through initial deformations. Whilst this practice originates from experience in deep alpine tunnels in weaker (sheared) rock masses (and sometimes the limited functional importance placed on rock reinforcement), it may have application elsewhere. The philosophy adopted for cablebolt design, originally developed for the mining industry, follows similar lines in assuming the need to accommodate significant deformations.

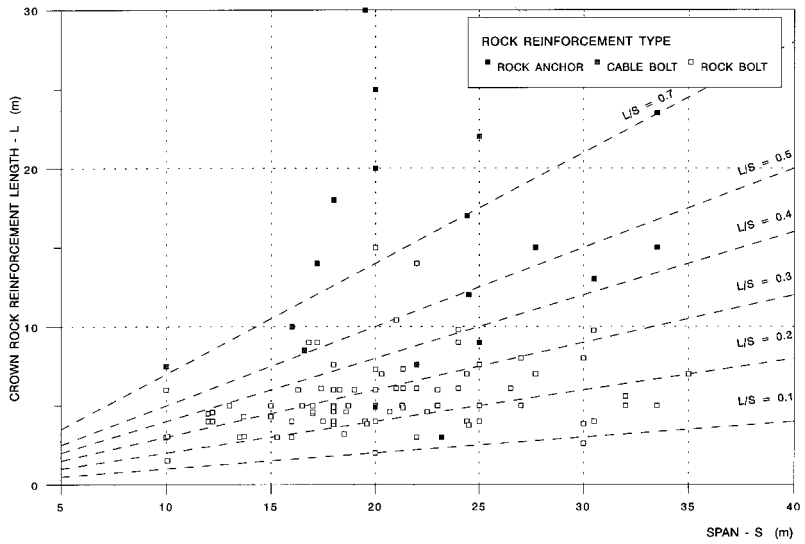

Figure 5.15: Permanent rock reinforcement:
crown rock reinforcement length - span characteristics

For hard, competent rock masses, the use of tensioned reinforcement is generally preferred in order to optimise the effect and benefit of the reinforcement system (see Section 4 and Sharp *et al.* 1979). Results from a comparative study on cavern support are also available from Cai *et al.* (2000).

Shotcrete linings

As noted previously shotcrete linings are commonly utilized with rock reinforcement. Precedent information on lining details is quite limited and therefore not readily amenable to comparative assessment.

Because of the cavern dimensions involved, it is reasonable to infer that for the majority of cases the shotcrete lining performs a secondary function to the rock reinforcement and may in many instances be primarily there for safety protection against minor rockfalls rather than an overall stabilization component.

As the rock mass conditions, in which caverns are constructed, become weaker then the relative significance of the lining increases. For the weaker rock types in Geological Classes C, D, E, F (see Table 5.3), shotcrete

linings may form a key component. Sometimes, however, this is only temporary on the basis that final concrete linings for such rock types are often employed.

Crown rock reinforcement length - span characteristics

Currently available data on rock reinforcement lengths are given in Figure 5.15 for span ranges up to 40 m. The data given are generally the maximum reinforcement lengths for the particular cavern application and hence, indicate the characteristics of the primary system. As might be expected, the use of rock anchors is generally reserved for longer length applications (although not always). Representative data on cablebolt applications for civil engineering applications are quite limited.

It is evident that a minimum (primary) reinforcement length of some 3 m is utilized for caverns up to spans on the order of 20 m. For larger spans, minimum lengths progressively increase from 3 m to 5 m for spans greater than 30 m. Such minimum lengths clearly apply to more competent rock conditions.

The data on maximum reinforcement length are difficult to rationalize, as lengths in excess of 10 m cannot always be justified in terms of the design considerations actually used. It is evident however that a significant number of caverns utilize maximum rock reinforcement lengths on the order of 6 to 7 m for spans up to 20 m with an increase to about 10 m for spans of 30 m.

Sidewall rock reinforcement length - height characteristics

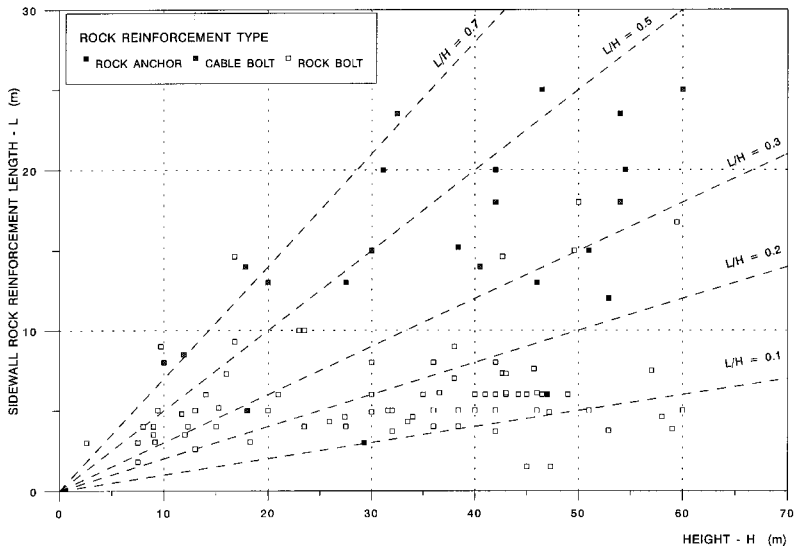

Figure 5.16: Permanent rock reinforcement: ics

The currently available data that could be verified are given in Figure 5.16. In general, the data presentation indicates the use of relatively long rock reinforcement, often in excess of 10 m. When assessing this plot however, it should be recognized that unlike the crown reinforcement *database*, there are many cavern sidewalls up to 20 m in height that are not systematically supported.

Although it is not uncommon for sidewalls to be influenced by particular stability problems involving unfavourably dipping major structures (faults) that may incur longer and higher capacity sidewall reinforcement in specific zones.

From the data field on minimum length, the use of 5 to 6 m long units (usually rock bolts) is common up to cavern heights of 30 m. With increasing heights up to 60 m, the unit length progressively increases to a range of some 10 to 15 m. In terms of maximum representative lengths, typical values range from 10 to 20 m for a corresponding height range of 10 to 50 m.

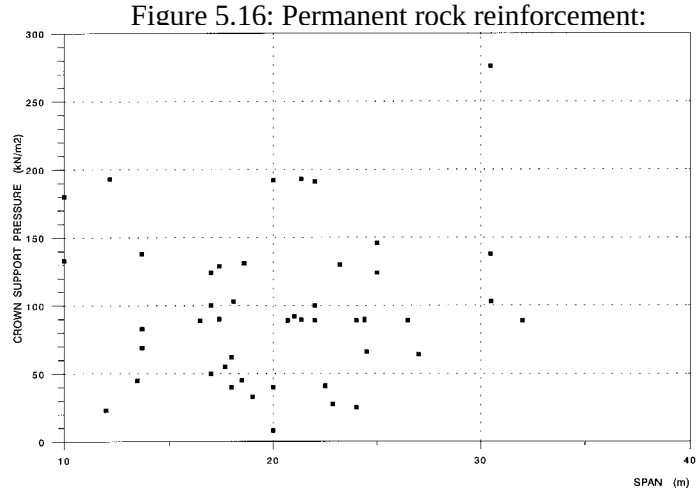

Figure 5.17: Permanent rock reinforcement: crown support pressure - span characteristics

Crown support pressure - span characteristics

The available data, as shown on Figure 5.17, are limited owing to the lack of clear published information on rock reinforcement layouts. In addition it is considered that different national design approaches also influence the consistency of the data.

The support pressure (working capacity)

used varies significantly from 25 up to 200 kN/m^2 (2.5 up to 20 ton/m^2) with little or no support pressure - span trend being evident.

Sidewall support pressure - height characteristics

The available data, presented in Figure 5.18, show a similar degree of scatter to the crown support pressure data reflecting again a wide range of design approaches in practice.

5.7 Design approaches for discontinuous rock masses

5.7.1 Principles

The design of underground openings, as well illustrated by Hudson and Harrison (1997), is in principle a two stage process involving:

- identification of plausible failure mechanisms, and
- design solutions to mitigate against such mechanisms through the application of engineering principles, usually, but not always, utilising rock reinforcement.

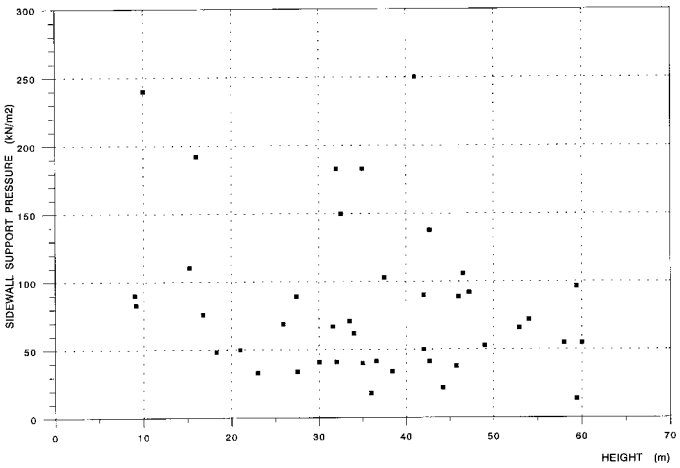

Figure 5.18: Permanent rock reinforcement: sidewall support pressure - height characteristics

The correct identification of plausible failure mechanisms is entirely reliant on appropriate geological and geomechanical evaluations as previously outlined. If these are trivial in nature, uncertain, or incomplete, the design will be likewise and unreliable.

The use of design solutions will involve both the use of appropriate geometrical forms to utilize as far as possible the intrinsic stability of the rock mass (orientation, shape, etc), as well as the introduction of reinforcement and lining elements. In the application of such solutions the key issues to be addressed will be as follows:

- Can the design demonstrate a valid margin of safety for the completed structure bearing in mind geological and geomechanical uncertainties and variability, and modelling (analysis) limitations?
- If not, can the design be validated or accordingly modified by representative (reliable) construction monitoring including geological evaluation and performance assessment?

The issue of construction technology (see Kaiser 1986) is also of key importance in the design of cavern structures.

For all designs that involve novel or extended applications, validation of the design through performance monitoring should be considered as essential. The incorporation of such measures and their validity needs to be addressed as a fundamental part of the construction process and not left as an ad-hoc, 'maybe' pseudo-academic exercise to be defined (or disputed) during construction (Sharp *et al.* 1977; Dunnicliff 1988).

5.7.2 Design methods - general

The identification of underground instability mechanisms and appropriate stabilization designs for discontinuous rock masses have been well covered in texts by Hoek and Brown (1980), Goodman and Shi (1985), Hoek *et al.* (1995), Hudson and Harrison (1997) amongst others. The mechanisms cover the following structurally controlled cases in detail and will not be discussed further here:

- overhead block falls (usually tetrahedral in nature)
- sidewall wedges (usually bounded by a major dipping discontinuity)

Other structurally controlled failures that generally lie outside such texts in terms of both mechanism definition and design (reinforcement) solutions are as follows:

- Shear overstress of rock masses commonly generated by the unfavourable orientation of principal stresses to bedding or cleavage planes (particularly prevalent in the crown and invert of openings in horizontally stratified rock masses).
- Interactive stress - structure effects generating wedges or blocks bounded by discrete discontinuities.
- Slabbing or separation of steeply inclined, often tabular rock blocks in cavern sidewall situations.
- Discrete shear movements on faults or shears critically located in the cavern surround and subject to an unfavourable induced stress state.
- Interactive failures involving water pressure (particularly important in sub-aqueous situations as occur in the UK Channel Tunnel Crossover and the design of the CERN - LHC caverns).
- Stress-induced failures of intact or moderately jointed rock masses.

The principles of the last topic are well covered in Sections 2 to 4 and will not be discussed further here except to note that the degree of measures used in the civil engineering field needs to address the permanent or semi-permanent nature of the excavations.

Rock mass failures, which are complex, require a specific simulation of the particular conditions in order to firstly define the mechanism and secondly to analyse and design the remedial engineered solution. The degree of interaction between the rock material, rock discontinuities, in situ stress field and the water pressure regime prohibits the use of simplified algorithmic solutions and hence, it is necessary to employ a simulation method that can incorporate all such features which, as noted before, must be sufficiently rigorously defined to permit a degree of confidence in the analytical output. This methodology created and developed by Cundall (1980) and implemented in the code UDEC™ [11] (discrete element) allows important explicit modelling of the discontinuity state subject to representative constitutive behaviour as developed by Bandis *et al.* (1983).

For all such assessments, it is valuable to consider in a formal manner the intrinsic state of stability with respect to an unsupported or unreinforced excavation. The intrinsic stability characteristics of the cavern system, particularly at depth, is a key factor in assessing the basic cavern operating response and in the determination of engineering stabilization and lining measures. In general, it is considered important to achieve a cavern configuration that is as stable as possible under the prevailing environment. Given the depth (stress) and precedent response from other caverns, this implies the adoption of a competent geological environment along the lines discussed in Section 5.4 for all cavern developments at depth.

This approach allows proper recognition and consideration of the failure processes and their associated uncertainties. Wherever possible modification of the layout and shape to minimize such failures should be considered. Only after the completion of this stage should stabilization systems be considered.

5.7.3 Discontinuous rock mass assessment for numerical modelling

From initial concept models, targeted site investigation can be designed to provide data to facilitate development of the rock mass characteristics and to derive input parameters for suitable modelling. Where complex, difficult or unprecedented rock mass conditions are involved, very careful consideration should be given to full-scale access to the rock mass using exploratory tunnels and shafts. These will provide not only the opportunity for a direct structural evaluation, but can be used for design property evaluation of in situ stress conditions, groundwater state, etc. The use of trial excavations to observe full-scale performance for subsequent model simulation can also be considered in more extreme environments (Sharp *et al.* 1979; Barla *et al*. 1991).

The pragmatic simulation of the geological structure geometry is obviously very critical in the development of a geological model for use in discontinuum modelling. A key step is to delineate the scales of structure that are most likely to control the deformational responses of the rock mass both in terms of mode and magnitude. Outcrop and tunnel inspection can be invaluable in assessing key characteristics that are less evident from drillhole data, even if the outcrop location is somewhat remote from the site.

An associated concept of importance is that of the effective block size. In discontinuum mechanics, the "effective" block size is considered as an elemental discrete unit, beyond which scale effects in the shear behaviour along the block contacts (viz. bounding discontinuities) will probably diminish. The concept evolved from identified interactions between cross joint spacing, rock mass stiffness, degrees of freedom for independent block movement, modes of deformation (predominately translational vs. rotational shear) and

[11] Available from Itasca Consulting Group, Inc.708 South Third Street, Suite 310 Minneapolis, MN 55415, USA, http://www.itascacg.com

scale effects associated with the shear behaviour of individual discontinuities and is recognized as a key feature of reliable model simulations.

The effective block size is not necessarily the average 'intact' block as defined by the frequency of jointing. The presence of persistent joints enclosing subordinate (in terms of continuity) fractures within a set of joints may increase the minimum 'hinge' length associated with independent block movement in the rock mass. Hence, the rock mass response may be controlled by blocks exceeding in size the so-called natural block size. In addition, considerable differences in shear behaviour may arise when the continuity of the controlling structure is interrupted by cross cutting structure due to joint length associated potential influences on the following components of shear behaviour: peak shear displacement; peak dilation angle; peak shear strength; and peak shear stiffness.

The following geometrical qualities that can be implemented in UDEC™, can be considered as the principal controlling discontinuity functions: fracture spacing; angle of dip; continuity of individual discontinuities; distance (gap) between individual fractures.

5.7.4 Modelling studies for large caverns in discontinuous rock masses

The applied design of caverns requires a systematic input of the geological and rock mass characteristics (including appropriate variability) to a composite design model which will also incorporate any engineered features such as cavern support. As noted above, the design approach needs to utilize a computer simulation model of the rock mass which will include both material and discontinuity properties and the effects of engineered stabilisation systems. Currently it is common for only two-dimensional cross-sectional simulations to be employed. These simulations appropriately model the principal controlling elements in terms of both structure and stress states. (It can often be reasonably assumed that the cavern longitudinal axis will be subnormal to the primary structural trend in terms of sub-vertical or steeply dipping joint sets.) As such modelling assumptions need to be carefully reviewed and finally developed once the main structural trends and the in situ stress state have been identified.

Computer programs such as UDEC are an accepted and valuable method for determining stresses and deformations around openings under varying conditions and in turn relating these to material or discontinuity strength parameters. Different cavern geometries may be evaluated in a theoretical rock mass and rock property assumptions varied together with the magnitude and direction of the in situ stress field. Critical stresses in terms of potential strength exceedance may be evaluated at each sequence of the excavation.

From studies of the interaction of engineered support and the stress state in the rock surround, it is feasible to optimize the support requirements in terms of degree and extent usually in relation to the shear overstress state. Where significant weak features are present in the rock mass, the particular design of the support system can be studied and compared with simpler gravitational wedge solutions.

A further key output from modelling studies is the prediction of cavern opening and rock mass deformations at various stages of the excavation development. These can be extremely valuable in the development of an excavation response model for construction control and design validation purposes during operation.

5.8 Current state of the art – case examples

Several projects from the late 1900's deserve mention as key case reference studies for the 2000's. The list is a mixture of recent developments selected for a particular aspect of rock engineering application for large-scale permanent underground openings. In all cases they embody innovations that are highly relevant to future applications. The choice also, to a degree, reflects the authors' involvement on a number of projects:

Dinorwig Pumped Storage Scheme, Wales (UK) - 1980's

A major cavern complex in slate with large spans (25 m) and major intersections carried out in a well defined, but anisotropic rock mass. The largest cavern complex of its kind in Europe, it pioneered a number of rock engineering systems including a complete dependency on rock reinforcement (Douglas *et al.* 1979).

Drakensberg Pumped Storage Scheme, South Africa - 1980's

A major underground development in weak, horizontally bedded rock that utilized separate caverns to limit spans and machine pits to limit cavern height. The rock engineering was an extension of the Poatina project in Tasmania with rectangular or trapezoidal cavern profiles. The caverns incorporated permanent

shotcrete linings fully integrated with rock reinforcement to protect the siltstones and claystones that deteriorated on exposure (Sharp *et al.* 1984; Endersbee and Hofto 1969).

Givat Shemen Oil Storage Project, Israel - 1990's

A significant cavern complex in weak, fractured chalk that involved long, circular profile caverns excavated by roadheader. Extensive in situ and laboratory studies to define rock mass characteristics were executed. Support was optimized by means of monitored trial enlargements and comprised a rock reinforcement - shotcrete system (Barla *et al*. 1991).

Gjovik Ice Hockey Stadium, Norway - 1990's

With a span of 62 m, this was one of the most innovative cavern developments of the last century. Excavated in hard but fractured rock, it represents the essence of Norwegian technology in underground rock engineering (Barton *et al*. 1991).

Channel Tunnel Crossovers, France, UK - 1990's

There were two significant undersea caverns on the Channel Tunnel Project in weak, bedded chalk marl that was subject to significant hydrostatic pressures. Contrasting excavation - support systems were used involving NATM staged excavation - support system on the UK side and stacked multiple drifts (rock replacement technology) on the French side.

Complex Transportation Tunnels, Hong Kong - 1990's

Major tunnel and portal complex in close proximity for the Airport railway system. Excavated in hard jointed rock below sensitive buildings and adjacent to an operating railway, the excavations are a good example of complex interactive design and construction in rock engineering.

Storm Water Cavern, Jersey - 1990's

An example of modern cavern engineering in very close proximity to an urban environment using a progressive excavation - reinforcement system and integrated shotcrete linings. The linings were finished to a smooth surface to facilitate washdown. Integrated and pressure relieved main tank linings were also a novel aspect of the scheme.

Eastern Distributor Project, Sydney, Australia - 1990's

A major road tunnel system utilising significant flat spans in the horizontally bedded, moderate strength Hawkesbury Sandstone. Major and significant application of rock reinforcement applied to flat spans with shotcrete linings. Intersections involve up to 5 lanes of traffic with a 3 lane double decked tunnel forming the major element. (A development of techniques used previously at the Sydney Harbour Opera House)(Justice 2000)

CERN LHC Project, Geneva - 1990's and 2000's

Major cavern complexes in sedimentary rock below saturated gravels including a twin cavern with a span of 26.5 m + 18 m. Very large cavern cross-sections (1400m^2) and caverns in close proximity. Major shaft and cavern intersections.

5.9 Future trends and challenges

The development of civil engineering related permanent underground openings faces challenges in a number of fields some of the more notable being:

- Discrete excavations at depth for fluid / gas / waste containment purposes.
- Large scale excavation complexes at depth to form underground pumped storage reservoirs.
- Tunnels and associated caverns under high mountains for transportation use (see Section 6).

The application of a widespread spectrum of cavern development has been particularly pioneered by the Swedish rock engineering community (Franzen and Hultin 1988).

In general, as can be seen from the precedent data, the development of caverns at significant depth is currently restricted to those with spans not exceeding about 15 m. The potential to increase this size whilst at

the same time retaining reasonable levels of rock reinforcement and associated lining systems is an obvious area for development.

For the development of large scale discrete openings, there will be a tendency to identify selected rock environments that afford reasonable levels of intrinsic stability as identified previously as Group 1 and 2 rock types. The development of potential future designs in relation to these two environments is considered further below.

5.9.1 Excavation - support requirements

The selected rock mass type groups, namely igneous and competent sedimentary rocks, need to be considered separately in terms of schematic design due to the implied difference in intrinsic response caused by different discontinuity systems.

Igneous rock environments - cavern excavation arrangement

The igneous rock environment is likely to be characterized by a hard, competent crystalline rock material. The rock mass will be characterized by geological structure that is steeply dipping and of a tectonic origin. In some rock types additional discontinuities resulting from cooling could occur.

In such rocks, which will typically be fresh to slightly weathered in nature, the jointing is expected to be limited in development with high degrees of interlock between surfaces and hence strength. Occasional major joints may be encountered that will require enhanced localized stabilization.

An inferred optimum geometry for a cavern in such a rock mass at depth is shown on Figure 5.19 The shape is aimed at minimizing rock reinforcement requirements whilst offering a readily constructable and volume efficient profile. A relatively flat arch crown is utilized with straight upper sidewalls and slanted lower sidewall sections.

Sedimentary rock environments - cavern excavation arrangement

The selected sedimentary rock environment is likely to be characterized by well-cemented sand or silt sized particles giving a competent rock material. The rock mass will be characterized by geological structure that is primarily sub-horizontal in nature (bedding).

The cavern vertical interval would typically be selected to lie within a consistent massive unit of sandstone, siltstone or limestone devoid of major bedding partings due to finer grained sedimentary interbeds or carbonaceous horizons. Other jointing, likely to be sub-vertical, would typically be subordinate in nature relative to the bedding.

The inferred optimum shape for a cavern in such a rock mass at depth is shown on Figure 5.20. A flat crown section is employed with haunches, straight upper sidewalls and slanted lower sidewall sections.

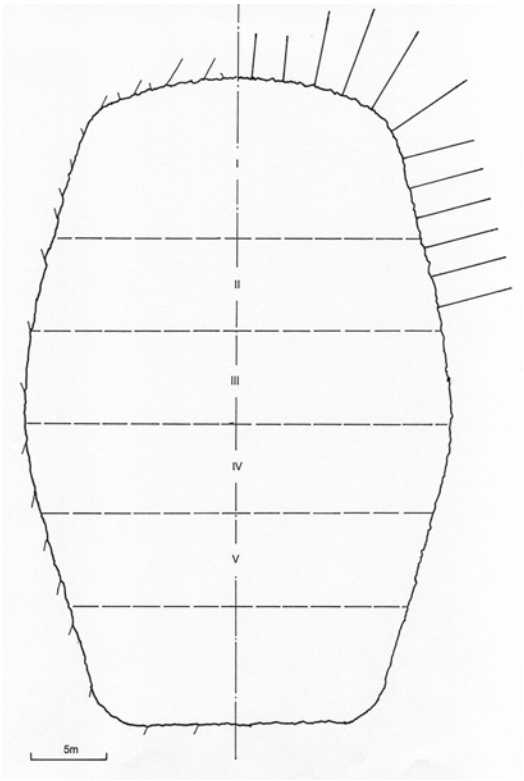

Figure 5.19: Cavern cross-section in granitic rocks - target cross-sectional arrangement and support

excavated rock mass profile is left in as sound a condition as possible.

The excavation standard can be measured using an assessment of the percentage of perimeter blastholes visible. For the storage cavern application a figure of the order of 50 - 75% would be a good target for the favourable rock conditions.

5.9.3 Cavern stabilisation systems

Based on the site selection criteria adopted, the cavern excavation is expected to be stable in an overall sense and hence, will not be subjected to large-scale failures involving deep seated structures and movements.

The cavern stabilization system will primarily satisfy two functions:

- Provision of a general level of cavern profile support as required.
- Reinforcement of specific major structure in the vicinity of the cavern.

Both functions would be achieved by means of a rock reinforcement (rock bolting) methodology using a corrosion protected system to ensure long term performance. In addition to the rock reinforcement, reinforced shotcrete would be used over certain parts of the cavern to provide addi-

5.9.2 Cavern excavation methodology

The cavern excavations, because of scale, will almost certainly be excavated using a drill and blast technique based on the nature of the rock mass as well as the cavern layout. It is however possible that other techniques, such as a full face tunnel boring machine, could be considered particularly for the crown section in future design developments.

In order to achieve a good degree of intrinsic containment from the cavern rock mass surround, a high standard of excavation will be needed in order to minimize any disturbance beyond the excavations profile. The development of a controlled profile will always be cost efficient in comparison to executing remedial works on poorly blasted, damaged surfaces.

A controlled blasting process incorporating a high specification, accurate drilling system, backed up by a comprehensive blast design programme should be utilized. Key features of this programme are the design of the cavern perimeter or profile blasting element using specialized techniques such as pre-split or smooth blasting systems. This in turn needs to be fully integrated with the bulk blasting programme to ensure that the

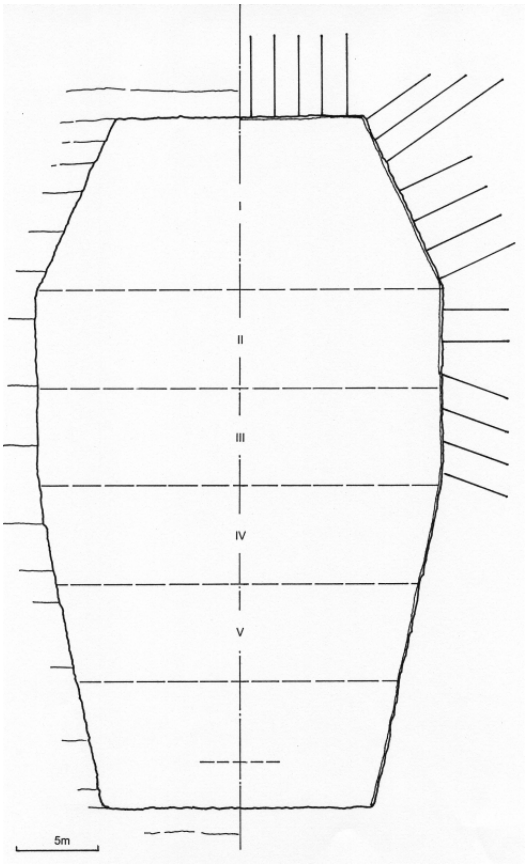

Figure 5.20: Cavern cross-section in sedimentary rocks - target cross-sectional arrangement and support

tional support to localized zones which exhibit profile stability problems (possible as a function of stress related spalling). The shotcrete could also be used to provide a partial containment lining system.

5.9.4 Cavern profile support - general

The reinforcement would be installed as a pattern in line with each excavation stage, primarily to control discontinuity overstress and to prevent spalling of the profile under the inferred induced stress state. The bolt lengths for such processes would be relatively short as indicated. The bolt types would be designed to allow for some controlled rock deformation / strain release to occur principally during the cavern excavation stage.

The reinforcement system would utilize an end anchored bolt arrangement, tensioned deformed bar and faceplate. Following further excavation of the cavern and after due allowance for deformation response, the system would be fully bonded (encapsulated) to allow for both corrosion protection and a long term composite reinforcement response.

The bolting of the cavern systems as shown is obviously only indicative. Final layouts would be based on a detailed design study based on representative rock mass property assessments. It is also likely, considering the nature of the cavern development at significant depth, that in situ trials involving a monitored cavern response would be required.

6.0 (SOME) CHALLENGES OF DEEP CIVIL TUNNELLING

Civil tunnelling is experiencing a new boom, particularly in Europe and Japan. Many new developments have occurred over the last several decades. Mechanical tunnel excavation has become more widespread and new exploratory tools are available. In Switzerland, for example, the 19.1 km long Vereina Tunnel, under construction since 1991, was just put into service in 1999. The construction of deep alpine base tunnels has started with the 34 km Lötschberg Tunnel, and will be followed by the 57 km long Gotthard Base Tunnel. Many important lessons have been learned and new developments together with historic precedents are illustrated here from this recent experience.

6.1 Site characterization for tunnelling – an ongoing challenge

The first deep tunnels were built for the railways, 120 to 140 years ago, to cross below the main ranges of the Alps. These tunnels are located at the mid-level of the mountain ranges at elevations ranging from 1000 to 1200 m above sea level, resulting in 10 to 15 km long tunnels. A century ago, it was just not feasible to drill deep exploratory holes of more than a few meters length, a fact that lead to many undesired problems and several disasters. Site characterization had to rely heavily on surface mapping and projection of these surface structures to the depth of the tunnel. For example, difficulty in drilling deep exploratory boreholes led to the disaster at the Lötschberg Rail Tunnel, built between 1906 and 1913. The pilot tunnel ran into an over-deepened valley filled with saturated gravel. Nearly one kilometer of the pilot tunnel was inundated with gravel and soil, killing and permanently burying the entire shift of thirty men. The initial straight alignment was changed and the deep buried valley by-passed. The Gotthard Railway Tunnel (1874-1882) barely avoided a similar incident. It was discovered later, during the exploration for a possible hydroelectric plant in the 1940's, that the rock cover above the tunnel was only 30 m, the remaining 300 m to the ground surface consisted of water-filled sands and silts.

For the Gotthard Road Tunnel (1965-1976), the alignment was no longer straight, because it had to follow the surface track of the Gotthard Pass in order to accommodate short ventilation shafts required for a road tunnel. Fortunately, this alignment moved the tunnel away from the deep buried valley, but the tunnel remained in poor rock. More extensive exploratory drillings were carried out, yet the extrapolation of the rock behaviour to the tunnel, particularly in the poorer rock zones, remained rather difficult. The actual behaviour of the poor rock was worse than anticipated. A safety tunnel, that served also as a pilot tunnel, was driven ahead of the main tunnel. A distinct size effect was noted between the pilot tunnel (approx. 4 m wide) and the main tunnel (11 m wide).

At present, construction has commenced on the Swiss Alptransit project with the 34 km long Lötschberg Base Tunnel (Steiner 1999) to be followed by the 57 km long Gotthard Base Tunnel. The 800 m deep intermediate shaft at Sedrun has been sunk (1998-2000). The alignment of the Lötschberg tunnel was chosen to bypass the over-deepened Kander valley to the west. Geophysical methods were used in combination with deep drilling, however there were some discrepancies between the two methods. In the northern section, the

tunnel crosses the complex metamorphic formation of the Wildhorn Nappe covering Flysch sediments. With the sub-horizontal layering of the metamorphic nappes and the Flysch, a prediction of the position was nearly impossible. In addition, the behaviour of these soft rocks of the Flysch formation is difficult if not impossible to obtain from surface or from borings. Flysch, a term used worldwide, has its origin in this geographic area and is translated from an expression of a local dialect for "flowing rock". This expression is used now for deposits along a continental margin of an ocean. A 9.5 km long exploratory tunnel, which served first as a drainage tunnel during excavation of the main tunnel and then as a safety tunnel during operation, was excavated. The water inflow encountered (Kellerhals and Isler 1998) was only a third of the initially predicted volume and the rock conditions were in general much better than anticipated, i.e., the swelling and squeezing potential was substantially less.

6.1.1 Challenges of deep exploration - pilot tunnelling and deep borings

For the exploration of the Lötschberg Base Tunnel about fifteen, several hundred meters deep exploratory borings were drilled for various purposes, mainly focusing on possible weakness zones and on locating the over-deepened Kander Valley in the north. The borings in the northern section were 400 to 600 m deep, vertical or inclined. In the southern section, directional drilling with inclined borings was used to verify the position of a sedimentary wedge (Jungfrau-wedge) within the intrusive rocks. The sedimentary rock is the same formation that hosts the thermal springs of Leukerbad some ten kilometers to the west. One 1.3 km long, inclined (49 to 60°) boring encountered a sedimentary zone, less than 10 m thick of which 6 m were marble with a 1 to 2 m wide water-bearing zone of crushed rock.

For the Gotthard Base Tunnel (Schneider 1999), two major domains for site characterization are of interest: the Piora Trough, and the Tavetsch sediment zone between two intrusive rock bodies. The Tavetsch zone has been investigated by several directional borings with a length of up to 1750 m (Schneider 1999; Steiner 1999) and is not further described here. At the surface, some 1700 m above the tunnel alignment, the Piora zone consists of crushed rocks, so-called sugary Dolomite, and other tectonized sedimentary rocks are also encountered (Figure 6.1). The exploratory system for the Piora Trough consisted of a 5.5 km long, 5 m diameter tunnel, 360 m above the alignment of the base tunnel, driven with a TBM from a step in the main valley. A climbing heading was chosen to avoid possible drainage problems in case of water inflow. At the end of the tunnel, directional drilling was foreseen across the Piora zone (Fellner 1999) at the level of the base tunnel. A 360 m deep vertical shaft was considered (but never constructed) to pre-treat and cross this zone before the main tunnel excavation would arrive.

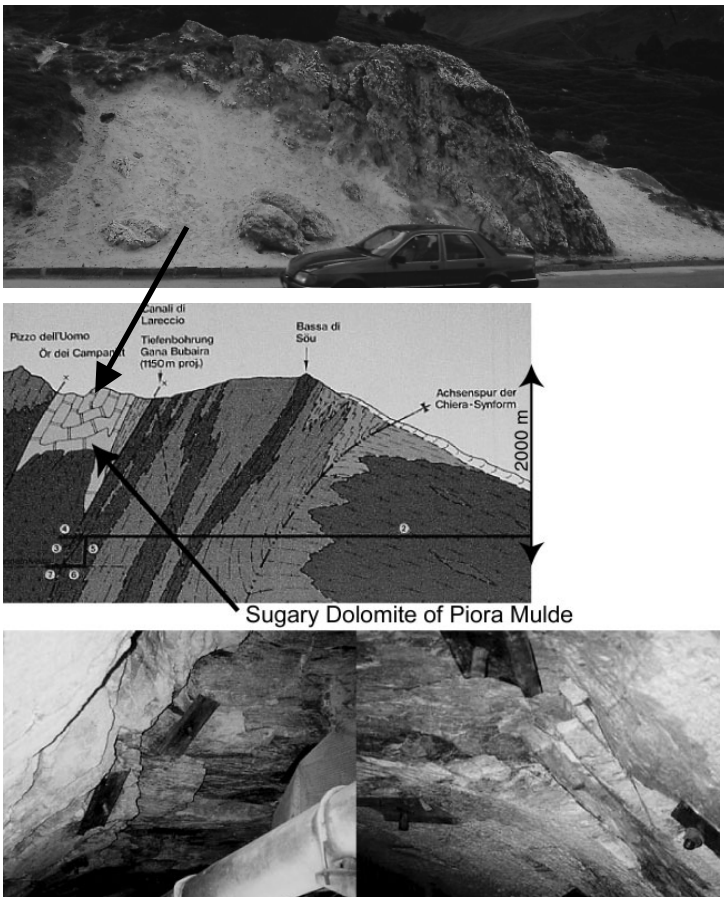

Figure 6.1: Cross-section showing location of sugary Dolomite and exploration tunnel. Close-up of stress-driven break-out above TBM in exploration tunnel.

Experience during construction of the Piora pilot tunnel at an overburden depth of 1400 m showed the presence of stress-driven instabilities in the crown and invert, similar to those described in Section 3, particularly in zones where the rock mass was structured and probably non-uniformly stressed (Figure 6.1). This suggests that the horizontal stress at the level of the exploration tunnel is higher than the overburden stress.

In order to detect possible flowing ground ahead of the TBM, systematic exploratory drilling was carried out. The Piora zone was intersected at the location projected from the surface at the level of the exploratory tunnel, some 360 m above the base tunnel. However, an incident occurred when the blow-out preventer was not properly mounted and operated. The crushed rock with a water pressure of 1000 m washed through the 96-mm drill-pipe. The TBM was buried in washed-out sand and the sand flowed through the drainage channel (cross section approx. 0.5 m^2) to the portal of the exploratory tunnel. Several thousand cubic meters of sand were washed into the tunnel. This incident justified the selection of the climbing heading. The drilling at the level of the exploratory tunnel revealed a 235 m wide zone consisting of an alternating sequence of crushed rock (sugary Dolomite), and intact limestone and Dolomite with Karst features. Most interestingly, during the tunnel advance the rock temperature dropped as the tunnel approached the crushed zone. This was related to the presence of flowing groundwater in the zone of crushed rock (Busslinger and Rybach 1997). A boring was drilled to the projected intersection of the contact zone with the base tunnel, where the rock temperature was found to be much higher and no sedimentary rock was present. A directional boring carried out on mid-level between the exploratory and main tunnel encountered relatively competent rocks. The unconfined compressive strength of the weaker rocks (Dolomite and Anhydrite) range from 30 to 50 MPa.

6.1.2 Overcoming the challenge with pilot and deep drilling

For shallow tunnels it is easiest to carry out exploration with borings. For deep tunnels, the construction of a pilot tunnel may often be a valuable alternative, particularly if it can be integrated in the final tunnelling scheme as a drainage or safety tunnel. With an exploratory tunnel the behaviour of the rock mass can be evaluated much more extensively. Little extrapolation is required and size effects are almost eliminated compared to deep borings. Furthermore, supplementary investigations can be easily carried out. A feasible combination is illustrated by the Piora system for the Gotthard Base Tunnel.

6.1.3 Challenges with stress, permeability and deformation measurements

Stress measurements are primarily carried out in good competent rock. For example, in the Lötschberg Base Tunnel, stress measurements were carried out in the lateral adit "Mitholz" (σ_v = 24 MPa at 900 m depth) in the siliceous limestone (Kieselkalk; σ_c > 250 MPa) of the Wildhorn Nappe (Kister *et al.* 2000). For tunnel design, deformation and strength properties of the rock formations also have to be known. Borehole dilatometer tests, stress measurements with the borehole slotter and hydraulic fracture tests were carried out in three borings of 25 m length. In addition, stresses were measured with flat jacks in the tunnel wall. The measured principal stress trending north-south corresponds to the overburden stress and the east-west stress, oriented parallel to the main chain of the Alps, is half the magnitude of the overburden stress.

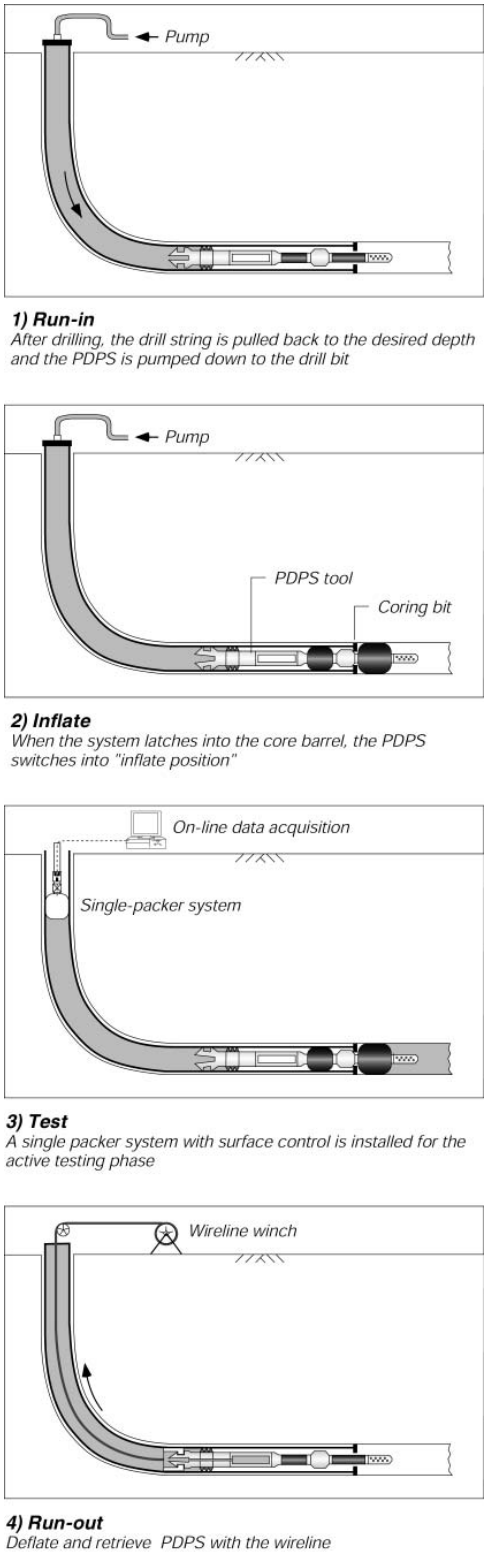

Figure 6.2: Pump-Down Packer System *PDPS* (Bühler 2000)

For the transalpine tunnels, the dilatometer test has been further developed making it feasible to a depth of 1400 m. The determination of the deformability with in situ tests is a very important issue; in particular in softer rock (Steiner 1998). Compared to in situ, tests on core samples may indicate much higher deformability due to induced micro-cracks (core damage as discussed in Section 2). Furthermore, permeability (packer) tests can now be carried out at such depth. These advanced techniques also allow for the determination of the stationary pressure level (Bühler and Thut 1999).
Recently, during the exploration program of the Alpetunnel (Brulard *et al.* 1999), the base tunnel between Lyon (France) and Torino (Italy), long (2.8 km) and deep directional drillings were utilized and packer tests were carried out with a new system (Bühler 2000). The pump-down-packer-system *PDPS* illustrated in

Figure 6.2 is combined with a wire-line coring system. During the drilling operation, the drill string is pulled pack such that the desired length of rock is exposed. The PDPS is pumped down the drill string to the drill bit where it latches on like a standard core barrel. Close to the surface a single packer is installed to apply pressure. The pumping pressure is then increased in the two packers of the PDPS, which separate the test interval in the formation, and the third packer in the interior of the drill string. Once a predetermined value has been reached, the inflation of the packers is terminated. Integrated memory gauges register the down-hole pressure during the entire test sequence. With the surface packer system a hydraulic testing program can be run. After completion of testing, the PDPS packers are deflated by pulling back the drill string. Finally, the PDPS is retrieved by wireline. This novel tool reduces standby time for drilling and testing costs significantly.

6.2 Design challenges

In civil works the underground opening has to be kept open for an extended period of time and the requirements on the lining are much more stringent than in mining. For hydro-electric power generation the water conveyance tunnels have requirements on smoothness, i.e. hydraulic resistance, and water loss from or water ingress into the tunnel when no water is conveyed. Railway and road tunnels have different requirements for protection of the rail bed and catenary traffic space as well as for provision of ventilation channels in road tunnels.

6.2.1 Requirements for hydraulic tunnels

In the Alps and similar mountain ranges with rather variable rock conditions, most water conveyance tunnels are lined with concrete if in- and outside water pressure conditions permit. With a concrete liner consolidation and contact grouting is mandatory. A steel liner may be necessary for extreme pressure conditions. For free-flowing tunnels of low capacity, it may be more economical to use a larger cross section with rough surface (shotcrete lining) than a smooth concrete lining. Many tunnels in the younger mountain ranges (Alps, Andes) also require grouting to consolidate the rock and reduce its permeability. The rock conditions in Scandinavia, in the Scandian-Baltic shield, are much better and unlined tunnels, not requiring grouting, are feasible.

6.2.2 Requirements for road tunnels

Long road tunnels require ventilation channels separated from the traffic. Water flowing into the tunnel, either into traffic space or ventilation channels, is not desirable. A water proofing membrane is required which serves as an umbrella and water is then drained into a drainage system. The most recent tunnels foresee the use of a dual drainage system for environmental protection, one that drains the mountain water and the other the water from the tunnel interior. With a cast-in-place concrete the water proofing membrane system is protected. Waterproofing is also necessary inside the rock, since cold ventilation air may lead to the freezing of water and to associated expansion pressures (Steiner and Bargähr 1997; Dysli 1993; Crory *et al.* 1984). Most interior liners for Alpine tunnels in Switzerland and Austria are made from unreinforced concrete. For maintenance and lighting, a smooth, lightly colored tunnel wall is required that can be easily cleaned. Most road tunnels are thus lined by cast-in-place concrete. Payment provisions for the concrete liner are such that the contractor has the incentive to use drilling and blasting procedures to limit the overbreak from long rounds.

Pre-fabricated elements for the interior lining of road tunnels were introduced some thirty years ago in Switzerland; however, the experience was not satisfactory. Maintenance and safety problems developed, as the suspension systems of the pre-fabricated elements corroded, partly failed and had to be exchanged. Traffic accidents in tunnels often lead to collision with the tunnel wall and to a subsequent collapse of the interior lining system. This system has been substituted with a cast-in-place liner and is no longer in use for new tunnels.

The non-reinforced concrete also has the purpose of protecting the waterproofing membrane, the drainage systems and steel tunnel support against damage from fires that may develop during road accidents. The inner cast-in-place liner is rather resistant to heat.

6.2.3 Requirement for deep railway tunnels

Railway tunnels do not have the same stringent requirements on cleanliness, color and waterproofing than road tunnels. Single shell linings with shotcrete are thus feasible. However, localized zones of water inflow have to be drained. Often half pipes are placed and covered with shotcrete. The surface of the resulting tunnel wall is irregular. The 15.3 km long Furka tunnel and the 19.1 km long Vereina tunnel are mostly lined with single shell shotcrete liner. The trains circulate in these tunnels at a speed of 100 km/h. The new base tunnels for Alptransit are used by trains running at 200 km/h or more. For such high speeds aerodynamics require a smooth surface of the tunnel wall. For this reason these tunnels will most likely be lined by cast-in-place concrete. Nevertheless, developments of new sprayed waterproofing membranes without solvents (Melbye 2000) will open new opportunities for more economic tunnel lining systems.

6.3 Construction issues

6.3.1 Conventional excavation versus TBM excavation

Tunnel costs are composed of the cost for excavation and for placing the various parts of the support system: rock bolts, shotcrete, wire fabric, lattice girders and/or steel sets for conventional excavation, or segmental liner if a TBM with shield is used. The cost of hindrance has to be included and is different in each case. For an economic comparison, the length of a tunnel is a deciding factor, since a TBM depreciation depends on the length of the tunnel among other factors.

6.3.2 Open TBM versus shielded TBM

In Switzerland for tunnels longer than 3 km in soft sedimentary rock (average UCS < 50 MPa, maximum UCS < 80 MPa) of the tertiary bedrock (Molasse) and similar formations, the use of a shielded TBMs with segmental lining has proven economical (Steiner 2000a). Put into historical perspective and combined with recently developed knowledge on stress driven instabilities, the problems associated with instabilities in the Heitersberg tunnel, which led to the development of a shielded TBM with segmental lining, can be attributed to the development of stress-driven failure immediately at the face. In this case, failure occurred above the cutter head in the soft rock at relatively low stresses with only 100 to 200 m overburden.

Typical costs per lineal meter *m'* of different ground classes (Table 6.1), based on reference costs for tunnel construction published by the Swiss General Contractors Association (1999), are shown in Figure 6.3 for a dual lane road or a double track railway tunnel approximately 6 km long. For conventional drill and blast excavation the lowest three ground classes are less expensive to construct with a horseshoe cross section, despite the fact that excavation alone is more expensive. The cost situation changes for the higher three ground classes. The cost for a TBM tunnel remains more or less constant for all classes. For a particular tunnel the preference between a shielded TBM and conventional drill-and-blast construction depends on the distribution of these ground classes. For soft rock tunnels in the tertiary bedrock in Switzerland longer than about 3 km TBM, the total cost is not influenced by the distribution of ground classes. The effect of changing ground classes, from prediction to construction, has been shown (Steiner 2000a) to result in increased costs for drill-and-blast excavation.

For harder rock (σ_c > 150 MPa), the cost of excavation increases (Figure 6.3) due to the increased wear of the disc cutters, the slower penetration of the TBM, and the resulting smaller advance rate (Gmür 2000). The cost of the segmental lining remains high. For harder rock, lower classes may be more economical to be constructed with drill-and-blast excavation, since the distribution of rock classes may shift to the lower classes. In hard rock, an open TBM is often used with a short shield. Support is then placed as close to the face as possible, however, the mechanics of the TBM are present in this area and the application of shotcrete is not de-

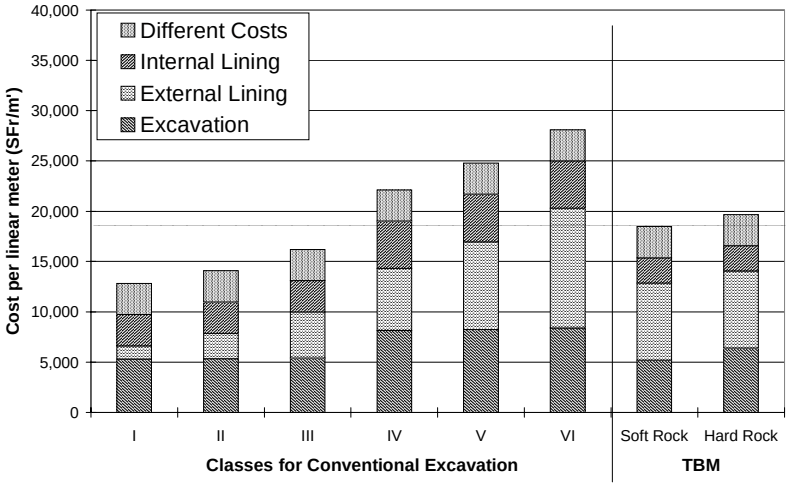

Figure 6.3: Typical costs (1SFr = 1.65 $US-2000) of tunnels per class for conventional excavation and TBM excavation in soft and hard rock (for 4 to 6 km long tunnels); "Different Costs" include costs of auxiliary measures and drainage, waterproofing membrane, interior finish, etc.

Table 6.1: Description of ground classes utilized to produce Figure 6.3

Excavation				External Lining						
Rock Class	Invert Arch	Heading	Invert	Shotcrete		Bolts		Wirefabric	Steelsets	
		(m3/m')	(m3/m')	Nominal thickness (mm)	Applied volume incl. rebound (m3/m')	Average length of single bolt (m)	(Bolts/m')	(kg/m')	(m steel per m')	Weight (kg/m')
I	No	82	-	50	1.2	1	3.3	21	-	-
II	No	82	-	70	3.4	3	2.6	21	-	-
III	No	83	-	110	4.9	4	6.3	76	-	-
IV	Yes	84	7.2	150	6.7	5	8.3	77	-	-
V	Yes	85	7.5	190	8.2	6	10.4	77	20	500
VI	Yes	86	8.0	230	9.2	7	17.0	77	25	810

sired, since it may damage the mechanical gear and hydraulic system of the TBM. Rock bolts and steel straps are therefore typically applied in the crown, and steel sets with wire mesh are placed in poorer ground. Nevertheless, for stress driven instabilities around the circumference (in civil engineering often called "loosening") broken rock pieces accumulate behind the wire mesh. Before shotcrete can be applied, this loosened rock has to be removed in an expensive operation. This may render TBM tunnelling more expensive than drill-and-blast excavation.

New, short and compact tunnel boring machines have been developed and are operating (Hentschel 2000) that allow the placement of support as close as possible to the face. Rock bolts, steel sets and shotcrete can be placed within 4 to 6 m of the face. The cutter head is protected in the crown by a short shield. A 9.5 m diameter and 23.5 m long TBM is currently excavating a 2325 m long tunnel in a cement quarry at Reuchenette in the Jura mountains of Switzerland. For optimal placement of the support, the TBM should be as short as possible. Similar open tunnel boring machines have been ordered for the southern sections of the Lötschberg Base Tunnel. In practice the criteria for selecting a particular system is governed by economics.

6.3.3 Single versus double shielded TBM

For small diameter tunnels (< 4 m) the mechanical requirement of the cutter wheel drive and of the hydraulic jacks require substantial space, such that a double shield is the better choice. For larger diameter tunnels (> 6 m) the cutting wheel drive can be easily placed in the first shield. From a mechanical point of view a single shield is possible. In order to limit damage to the rock, ground support should be placed as close to the face as possible, favoring a short single shield with support following immediately behind the shield. This also means that single shields are to be preferred over double shields.

6.3.4 Measures to crossing fault zones

Most problems with TBMs are encountered in fractured and crushed rock zones, particularly in the presence of ground water (Steiner 2000b). Measures to place additional support ahead of the TBM have to be foreseen and planned. Grouting alone is often insufficient. Grouted spiling is useful and often used in combination with localized dewatering of the crushed and fractured rock. Drainage is essential and is often one of the crucial means to stabilize crushed rock. In extreme cases, ground freezing has been used to stabilize crushed rock in faults. The crossing of fault zones has to be planned well ahead and auxiliary means have to be installed on the TBM and kept ready. With such preventive measures, delays can be reduced and cost-overruns prevented.

6.4 Challenge of water inflow

6.4.1 Issues in controlling water inflow

Water inflow is a major issue in tunnel construction and operation. Civil tunnels are arranged to allow free flowing drainage whenever possible. Tunnels built a century ago and road tunnels built until a decade ago were mostly built as free draining tunnels. Water flowing into these tunnels was captured and conveyed through a drainage system to the portal. Tunnels can lead to depletion of springs and water supplies as was experienced years ago at the Hauenstein summit tunnel (1853-58) which crosses the main chain of the Jura Mountains with a unilateral slope to the south. The water supply to the north was drained away. The then newly established Swiss Federal Court ordered the construction of a smaller, second tunnel to bring back the water from Karst caverns to the northern portal. The drainage from a pilot tunnel has caused large damaging settlements in the rock foundation of an arch dam at a hydropower plant (Biedermann 1982). Environmental regulations in Switzerland and in many other European countries require that the water inflow must now be limited for new tunnels. The useable water regime must not be altered. Water pressures up to about 100 to 150 m of head can be resisted by a waterproofed system, consisting of a concrete liner with a waterproofing membrane. In pervious rock with higher pressures, an impervious ring of treated rock has to be created around the tunnel with grouting.

In deep mines, water inflow has to be limited in order to reduce the pumping quantities and thus the costs. Grouting techniques with cement installed under high pressures (200 bar and more) have been developed and applied in deep mines of South Africa.

6.4.2 Requirements for grouting below Scandinavian cities

The scope in near surface tunnelling in hard jointed granite encountered in Scandinavian bedrock is often to limit a drop of pore pressures in the overlying clay to limit or avoid settlements of normally consolidated, soft clays. It is most important to realize that even minor water flow may have a significant effect on pore pressures. For normal grouting to be effective in already impervious bedrock ($k = 10^{-7}$ m/s; equivalent to one Lugeon) with overlying clays ($k < 10^{-9}$ m/s), the grouted rock mass has to be more impervious to avoid reduction of pore pressures in the clay. The procedures are that a fan of 10 to 14 m long borings, spaced 1 to 2 m, is drilled from the circumference of the face. These borings are then grouted by micro-fine cement to a pre-determined quantity per length of drillhole. One criteria used in quality control is the back flow of grout in near-by drillholes. This criterion is only applicable in these low permeability rocks. The narrow fissures are jacked open and the grout penetrates the rock mass and makes it less pervious. In "normal" grouting practice, the adjacent boreholes have to be closed off by packers.

6.4.3 Environmental constraints on civil tunnels

The new alpine base tunnels will transverse the rock mass below or adjacent to existing, mainly concrete arch dams. Furthermore, to prevent drainage of the rock mass the water inflow into the tunnel has to be limited. Hence, stringent limits on water inflow have been imposed on the shafts and tunnels of the Alptransit scheme in Switzerland. The 800 m deep intermediate shaft at Sedrun for the Gotthard Base Tunnel was grouted ahead of the excavation with a systematic fan of 8, 12 or 16 forty-meter long boreholes. These were grouted with micro-fine cement when water inflow was encountered.

For the Lötschberg Base Tunnel, grouting ahead of the face is foreseen when conditions require it to limit water inflow. This is the case in the limestone zones of the northern section (Mitholz) and the Jungfrau Wedge (Jungfrau Keil) in the southern part of the tunnel. Once the tunnel excavation approaches this zone, grouting 20 to 40 m ahead of the excavation will be carried out to prevent seepage into the tunnel. Grouting pressure is applied against the static head only and not against flowing water.

For large aperture discontinuities (width > 1 mm), regular cement is used with low water cement ratios (w/c < 1.0) plus additives. For rocks with small aperture, micro-fine cements are used. With newer grinding techniques for micro fine cements, the material prices have dropped but are still three times the cost of regular cement. Less than ten years ago, the difference in price was ten times or more.

6.5 Utilization of tunnel muck

The new transalpine tunnels will produce large quantities of tunnel muck of which much comes from rocks that can be used to produce aggregate. Substantial quantities of aggregate are required for shotcrete and cast-in-place concrete tunnel linings. For the construction of the old tunnels over a century ago, rock from the tunnel was used to produce quarried stone, if feasible, or to use at least some of the cobbles as backfill between liner and rock surface. Today, the tunnel muck must be crushed to produce the required aggregate. The influence of different excavation techniques and the effect of treatment with different crushers have been studied for the Alptransit project. Tests with variable spacing of disc cutters were carried out in the access tunnel to the Äspö laboratory in southern Sweden (Büchi and Thalmann 1995) in granite with an unconfined strength *UCS* of 250 MPa, a Point Load Index I_{s50} of 7.5 MPa, and a Cerchar Abrasivity Index of 5.3. Some results from this study (Thalmann 1997) are presented in Table 6.2. Tunnel muck from a drill and blast excavation in igneous rocks yields large aggregate and little fine material, and is much more suitable for the re-use as aggregate than material from other excavation techniques. A third to one half of the material produced by a TBM equipped with point bits ranges from 0 to 4 mm. With the normally used spacing of disc cutters (65 to 86 mm), a substantial quantity of sand (0 to 4 mm) is produced. If the spacing is increased to twice the "normal" spacing, namely 172 mm, the fines are reduced to 20% and the percentage above 32 mm increases. Other investigations with regard to the shape of the tunnel muck were carried out in the same study.

Table 6.2: Gradation for tunnel muck with different excavation techniques (Thalmann 1997)

Method of Tunnel Excavation	Spacing of Disc Cutters	Percentage of Tunnel Muck		
		0 – 4 mm	> 32 mm	> 100 mm

Drill and Blast: Igneous rock	N.A	2 – 5	85 –95	75 – 85
Roadheader in soft limestone	N.A.	15 – 40	5 – 35	0 - 5
TBM with point bits	60 –70 mm	30 –50	2 –20	0
TBM with disc cutters: sedimentary and igneous rocks	65 –85 mm	15 – 50	5 – 50	0 - 10
TBM with enlarged disc spacing	86 mm	45	20	0
	129 mm	40	30	5
	172 mm	20	35	15

Excavation with a tunnel boring machine equipped with disc cutters produces a large quantity of rock powder, i.e. silt and clay fraction (< 0.063 mm). Tests indicate that 3 to 10 % of the material is in the silt fraction (Thalmann 1997). For the use as aggregate TBM muck has to be washed and the fines separated.

For the construction of the Lötschberg Base Tunnel a scheme for managing the tunnel muck has been developed to utilize the muck to the greatest extent possible. Three classes of tunnel muck have been defined (Table 6.3; Zermatten 2000). The tunnel muck will be separated in the area of the portal of the intermediate adit into the three categories. Rock of good quality will be recycled for utilization as aggregate for concrete and shotcrete. The poor rock is used as fill in abandoned quarries.

Table 6.3: Classes of tunnel muck for construction of Lötschberg Base Tunnel (Zermatten 2000)

Class	General characteristics	Requirements on separation, treatment and verification	Typical rocks	Use of muck
K 1	Good rock quality, homogenous rock series	Little requirement for treatment and verification of tunnel muck	Limestone, sandstone, igneous rocks with small percentage of schist (<10 %)	Gravel first class; aggregate for concrete and shotcrete
K 2	Medium to good rock quality, heterogeneous lithology	Increased requirement for separation and treatment of tunnel muck	Shale, Dolomite, argillaceous schist, Marls and marly limestone	Gravel second class; if necessary some class K1 material can be extracted from this muck
K 3	Poor quality rock, unsuited as aggregate for concrete	Little requirement for treatment and separation	Fault gauge (Kakirit) Anhydrite, Flysch	For embankments, backfill, terrain modifications, filling of gravel pits and quarries

7.0 REFERENCES

Aglawe, J.P., 1999. Unstable and Violent Failure around Underground Openings in Highly Stressed Ground. Ph.D. Thesis, Department of Mining, Queen's University, 284p.

Amadei, B., and Stephansson, O., 1997. Rock Stress and its Measurement. Chapman and Hall, London, 327-358.

Bandis, S., Lumsden, A., and Barton, N., 1983. Fundamentals of Rock Joint Deformation. *Int. J. Rock Mechanics and Mining Science & Geomechanics Abstracts*, **20**(6): 249-268.

Barla, G., Sharp, J.C., and Rabagliati, U., 1991. Excavation and support optimization for a large underground storage facility in weak jointed chalk. In Proc. 7th Int. Congress Rock Mechanics, Aachen, 1007-1072.

Barrett, S.V.L., and McCreath, D.R., 1995. Shotcrete support design in blocky ground: towards a deterministic approach. *Tunnelling and Underground Space Technology*, **10**(1): 70-89.

Barton, N., 1994. A Q-system case record of cavern design in faulted rock. In Proc. of Tunnelling in Difficult Ground, Torino, Italy, 8p.

Barton, N., Tunbridge, L., Loset, H., Westerdahl, J., Kristiansen, J., Vik, G., and Chryssanthakis, P., 1991. Norwegian olympic ice hockey cavern of 60m span. In Proc. 7th ISRM Congress Rock Mechanics, Aachen, 1073-1081.

Barton, N., Lien, I., and Lunde, J., 1974. Engineering classification of rock masses for the design of tunnel support. *Rock Mechanics*, **6**(4): 186-236.

Barton, N., and Choubey, V., 1977. The shear strength of rock joints in theory and practice. *Rock Mechanics*, **12**: 1-54.

Bawden, W.F., 1993. The use of rock mechanics principles in Canadian hard rock mine design. *Comprehensive Rock Engineering*, Pergamon Press, **5**: 247-290.

Biedermann, R., 1982. Abnormal behaviour of Zeuzier arch dam. Special issue to ICOLD Rio de Janeiro, *Wasser, Energie, Luft*, Baden, Switzerland, **74**(3): 65-112.

Bieniawski, Z.T., 1974. Geomechanics classification of rock masses and its application in tunnelling. In Proc. of 3rd ISRM Congress, Denver, Colorado, Vol. 2A, 27 p.

Bieniawski, Z.T., 1989. Engineering Rock Mass Classifications. Wiley, New York.

Brace, W.F., Paulding, B., and Scholz, C., 1966. Dilatancy in the fracture of crystalline rocks. *J. Geophysical Research*, **71**: 3939-3953.

Brady, B.H.G., and Brown, E.T., 1993. Rock Mechanics for Underground Mining. 2nd Edition, Chapman & Hall, London, 517p.

Brulard, J., Lacombe, P., Robert, J., and Bois, A.P., 1999. Lyon to Turin railway base tunnel: an Alps geology project. *ISRM News J.*, **5**(3): 6-12.

Brune, J.N., 1970. Tectonic stress and the spectra of seismic shear waves from earthquakes. *J. Geophysical Research*, **75**: 4997-5009.

Büchi, E., and Thalmann, C., 1995. Wiederverwertung von TBM-Ausbruchmaterial; Einfluss des Schneidrollenabstandes (Reutilization of TBM muck; Influence of disc cutter spacing). Symp. Atlas-Copco Robbins, TBM know-how for the NEAT Project, Lucerne, Switzerland, March 1995.

Bühler, C., 2000. Description of pump down packer system. *SolNews*, Solexperts, Switzerland.

Bühler, C., and Thut, A., 1999. Hydraulische und felsmechanische Bohrlochversuche. In Proc. Symp. Exploration and Prognosis for the Base Tunnels at Lötschberg and Gotthard (in German), Löw and Wyss eds., A.A. Balkema, Rotterdam, 217 –228.

Busslinger, A., and Rybach, L., 1997. Prognosis of rock temperature and water inflow zones in deep tunnelling: Examples from the NEAT project, Swiss Alps. In Proc. ITA-AITES Congress, Vienna, Austria, Tunnels for people, Golser, Hinkel, and Schubert eds, A.A. Balkema, Rotterdam, 9-14.

Cai, M., Kaiser, P.K., Uno, H., and Tasaka, Y., 2000. Comparative study of rock support system design practice for large-scale underground excavations. In Proc. 4th Northern American Rock Mechanics Symp. (NARMS), Seattle, Washington, 8 p.

Cai, M., Kaiser, P.K., and Martin, C.D., 1998. A tension model for the interpretation of micro-seismic events near underground openings. *Pure and Applied Geophysics J., PAGEOPH*, **153**: 67-92.

Castro, L.A.M., Grabinbsky, M.W., and McCreath, D.R., 1997. Damage imitation through extension fracturing in a moderately jointed brittle rock mass. *Int. J. of Rock Mechanics and Mining Sciences & Geomechanical Abstracts*, **34**(3/4): 557p.

Castro, L., 1996. Analysis of Stress-Induced Damage Initiation around Deep Openings Excavated in a Moderately Jointed Brittle Rock Mass. Ph.D. Thesis, University of Toronto, 455p.

Coates, D.F., Bielenstein, H.U., and Hedley, D.F.G., 1973. A rock mechanics case history of Elliot Lake. *Canadian J. of Earth Science*, **10**(7): 1023-1058.

Coffey Partners, 1995. ACARP - Geotechnical Design of Roof Support and Reinforcement. (Project Report.)

Collins, D.S., and Young, R.P., 2000. Lithological controls on seismicity in granitic rocks. *Bulletin of the Seismological Society of America*, **90**(3): 1-15.

Cripps *et al.* (eds), 1993. Engineering geology special publication No. 8. In Proc. 26th Annual Conf. Engineering Group Geological Society, 1990, Leeds, UK.

Crory, F.E., Issacs, R.M., Penner, E., Sanger, F.J., and Shook, J.F., 1984. Designing for Frost Heave Conditions in Frost Action and its Control. Berg and Wright eds, Technical Council on Cold Regions Engineering Monograph, ASCE, New York, 22-44.

Cundall, P.A., Potyondy, D.O., and Lee, C.A., 1996. Micromechanics-based models for fracture and breakout around the Mine-by tunnel. In Proc. Int. Conf. on Deep Geological Disposal of Radioactive Waste, Winnipeg, Manitoba, Martino and Martin eds. Canadian Nuclear Society, Toronto, 113-122.

Cundall, P.A., 1980. A Generalized Distinct Element Programme for Modelling Jointed Rock. PCAR-1-80, Contract DAJA 37-79-C-0548, European Research Office, U.S. Army.

Detournay, E., and St. John, C.M., 1988. Design charts for a deep circular tunnel under non-uniform loading. *Rock Mechanics and Rock Engineering*, **21**: 119-137.

Diederichs, M.S., Espley, S., Langille, C., and Hutchinson D.J., 2000. A semi-empirical hazard assessment approach to wedge instability in underground mine openings. In Proc. GeoEng2000, Melbourne, Australia, 8p.

Diederichs, M.S., 1999. Instability of Hard Rock Masses: The Role of Tensile Damage and Relaxation. PhD Thesis, University of Waterloo, 566p.

Diederichs, M.S., and Kaiser, P.K., 1999. Tensile strength and abutment relaxation as failure control mechanisms in underground excavations. *Int. J. of Rock Mechanics and Mining Sciences & Geomechanical Abstracts*, **36**: 69-96.

Douglas, T.H., Richards, L.R., and Arthur, L.J., 1979. Dinorwic Power Station - rock support of underground caverns. In Proc. 4th ISRM Congress, Montreux, Switzerland, **1**: 361-370.

Dunnicliff, J., 1988. Geotechnical Instrumentation for Monitoring Field Performance. John Wiley, Chichester, 577p.

Dysli, M., 1993. Le gel et son action sur les roches et fondations, Presses polytechniques romandes, Lausanne.

Endersbee, L.A., 1975. Rock mechanics principles related to case studies. In Proc. Symp. Recent Developments in the Analysis of Soil Behaviour and their Application to Geotechnical Structures, New South Wales.

Endersbee, L.A., and Hofto, E.O., 1969. Civil engineering design and studies in rock mechanics for Poatina Underground Power Station, Tasmania. *J. of the Institution of Engineers*, Australia.

Espley-Boudreau, S. J., 1999. Thin Spray-on Liner Support and Implementation in the Hard rock Mining Industry. M.Sc. thesis, School of Engineering, Laurentian University, 311 p.

Falmagne, V., Kaiser, P.K., and Martin, C.D., 1998. Micro-seismic monitoring and rock mass degradation, *CIM-AGM*, Montreal. Canadian Institute of Mining, Metallurgy and Petroleum publications (CD), 8p.

Feignier, B., and Young, Y.P., 1992. Moment tensor inversion of induced micro-seismic events: Evidence of non-shear failures in the -4<M<-2 moment magnitude range. *Geophysical Research Letters*, **19**(14): 1503-1506.

Fellner, D., 1999. Resultate der geologischen Erkundigung Sondiersystem Piora. In Proc. Symp. Exploration and Prognosis for the Base Tunnels at Lötschberg and Gotthard (in German), Löw and Wyss eds, A.A. Balkema, Rotterdam, 217 –228.

Fookes, P.G., 1997. Geology for Engineers: the Geological Model, Prediction and Performance. *Quarterly J. Engineering Geology*, **30**(4).

Franzén, T., and Hultin, S.A., 1988. Going Underground. Royal Swedish Academy of Engineering Sciences.

Geo-Engineering, 1996. Large Underground Caverns Precedent Experience Study - Nirex UK Project Report.

Gmür, W., 2000. General Cost estimate, Personal communication.

Goodman, R.E., 1989. Introduction to Rock Mechanics. 2nd Edition, John Wiley, Chichester, 52p.

Goodman, R.E., and Shi, G.H., 1985. Block Theory and its Application to Rock Engineering. Prentice-Hall, London, 338p.

Greer, G.J., 1989. Empirical modelling of open stope stability in a vertical crater retreat application at INCO's Thompson Mine. 91st Canadian Institute of Mining AGM, 8p.

Griffith, A.A., 1924. Theory of rupture. 1st Int. Congress Applied Mechanics, Delft, 55-63.

Grimstad, E., and Bhasin, R., 1997. Rock support in hard rock tunnels under high stress. In Proc. Int. Symp. Rock Support - Applied Solutions for Underground Structures, Broch, Myrvang, and Stjern eds. Norwegian Society of Chartered Engineers, Lillehammer, Norway, 504-513.

Gürtunca, R.G., and Haile, A.T., 1999. Lessons learned from deep mining in South Africa. Symp. "Vorerkundung und Prognose der Basistunnels am Gotthard und am Lötschberg", A.A. Balkema, Rotterdam, 349-357.

Hajiabdolmajid, V., Martin, C.D., and Kaiser, P.K., 2000. Modelling brittle failure. In Proc. 4th North American Rock Mechanics Symp., Seattle, Washington. A.A. Balkema, Rotterdam, 8p.

Hedley, D.G.F., Roxburgh, J.W., and Muppalaneni, S.N., 1984. A case history of rockbursts at Elliot Lake. In Proc. 2nd Int. Conf. on Stability in Underground Mining, Lexington. American Institute of Mining, Metallurgical and Petroleum Engineers, Inc., New York, 210-234.

Hedley, D.G.F., and Grant, F., 1972. Stope-and-pillar design for the Elliot Lake Uranium Mines. The Canadian Mining and Metallurgical Bulletin, **65**: 37-44.

Hentschel, H., 2000. TBM with innovative support concept. *Tunnel*, Bertelsmann, Gütersloh, Germany, **2**: 20-28.

Hepworth, N., 1984. The influence of support on rock deformation in a highly stressed tunnel. Rock Mechanics Laboratory, Chamber of Mines, South Africa, 55-65.

Herget, G., 1993. Rock stresses and rock stress monitoring in Canada. In *Comprehensive Rock Engineering - Rock Testing and Site Characterization*, Hudson ed., Pergamon Press, Oxford, **3**(19): 473-496.

Hoek, E., and Brown, E.T., 1998. Practical estimates of rock mass strength. *Int. J. Rock Mechanics and Mining Science*, **34**(8): 1165-1186.

Hoek E., Kaiser, P.K., and Bawden, W.F., 1995. Support of Underground Excavations in Hard Rock. A.A. Balkema, Rotterdam, 215 p.

Hoek, E., and Brown, E.T., 1980. Underground Excavations in Rock. Institution of Mining and Metallurgy, London, 527 p.

Horii, H., and Nemat-Nasser, S., 1986. Brittle failure in compression: splitting, faulting, and brittle ductile transition. *Transactions Royal Society London, Math Physics Sciences*, **319**: 337-374.

Hudson, J.A., and Harrison, J.P., 1997. Engineering Rock Mechanics. An Introduction to the Principles. Imperial College of Science, Technology and Medicine, University of London.

Hudson, J.A., Brown, E.T., and Fairhurst, C., 1972. Shape of the complete stress-strain curve for rock. In Proc. 13th U.S. Rock Mechanics Symp., Urbana, Cording ed., American Society of Civil Engineers, 773-795.

Hutchinson, D.J., and Diederichs, M.S., 1996. Kaiser, P.K., McCreath, D.R., Thompson, A. and Windsor, C. (Contributors). Cablebolting in Underground Mines, Bi-Tech Publishers Ltd., Richmond, Canada, 406 p.

Imri, A.S., and Jory, L.T., 1979. Behaviour of the underground powerhouse arch at W.A.C. Bennet Dam during construction. In Proc. 5th Canadian Rock Mechanics (3rd Edition), Chapman and Hall, London.

Ingraffea, A. R., and Atkinson, B.K., 1987. "Theory crack initiation and propagation in rock" in Fracture Mechanics of Rock, Atkinson ed., Academic Press, New York, 71-110.

Jaeger, J.C., and Cook, N.G.W., 1979. Fundamentals of Rock Mechanics. Chapman & Hall, London, 593 p.

Jaeger, J.C., and Cook, N.G.W., 1969. Fundamentals of Rock Mechanics. Methuen & Co., London, 513 p.

Jiayou, L., Lihui, D., Chengjie, Z., and Zebin, W., 1989. The brittle failure of rock around underground openings. In Proc. Conf. Rock Mechanics and Rock Physics at Great Depth, Pau, France, Maury and Fourmaintraux eds, A.A. Balkema, Rotterdam, **(2)**: 567-574.

Kaiser, P.K., and Tannant, D.D., 2000. The Role of Shotcrete in Hard Rock Mines. Chapter in Mining Handbook, Hustrulid and Pollock eds, SME, 24 Figs., 22p.

Kaiser, P.K., Yazici, S., and Maloney, S., 2000. Mining-induced stress change and consequences of stress path on excavation stability – a case study. *Int. J. of Rock Mechanics and Mining Sciences*, 15 Figs., 23 p.

Kaiser, P.K., and Tannant, D.D., 1999. Lessons learned for deep tunnelling from rockburst experiences in mining. Symp. "Vorerkundung und Prognose der Basistunnels am Gotthard und am Lötschberg", A.A. Balkema, Rotterdam, 325-337.

Kaiser, P.K., Falmagne, V., Suorineni, F.T., Diederichs, M.S., and Tannant, D.D., 1997. Incorporation of rock mass relaxation and degradation into empirical stope design. CIM'97, Vancouver, (CD) 12 p.

Kaiser, P.K., and Tannant, D.D., 1997. Use of shotcrete to control rock mass failure. In Proc. Int. Symp. Rock Support, Lillehammer, Norway, 580-595.

Kaiser, P.K., McCreath, D.R., and Tannant, D.D., 1996. Canadian Rockburst Support Handbook, Geomechanics Research Centre, Laurentian University, Sudbury, Canada, 314 p. Also published as: Kaiser, P.K., McCreath, D.R., and Tannant, D.D., 1997. Rockburst Support. In Canadian Rockburst Research Program 1990-95. (Published by CAMIRO, Sudbury), Vol. 2, 324 p.

Kaiser, P.K., Tannant, D.D., and McCreath, D.R., 1996. Drift support in burst-prone ground. CIM Bulletin, **89**(998): 131-138.

Kaiser, P.K., 1994. Observational modelling approach for design of underground excavations. Keynote address at SANGORM'94 -- The Application of Numerical Modelling in Geotechnical Engineering, South African National Group on Rock Mechanics, Pretoria, 1-7.

Kaiser, P.K., and Maloney, S., 1992. The role of stress change in underground construction. EUROCK '92, 396-401.

Kaiser, P.K., Yazici, S., and Nosé, J., 1992. Effect of stress change on the bond strength of fully grouted cables. *Int. J. of Rock Mechanics and Mining Sciences & Geomechanical Abstracts*, **29**(3): 293-306.

Kaiser, P.K., 1986. Construction methods for large rock caverns - Trends and innovations. General Report, Symp. Large Rock Caverns LRC'86, Helsinki, Finland, **3**:1877-1907.

Kellerhals, P., and Isler, A., 1998. Lötschberg Basis Tunnel: Geologische Voruntersuchungen und Prognose. Landeshydrologie und –Geologie, Geologische Berichte No. 22.

Kemeny, J.M., and Cook, N.G.W., 1987. Crack models for the failure of rocks in compression. Constitutive Laws for Engineering Materials: Theory and Applications, (Desai *et al.* eds), Amsterdam: Elsevier, **2**: 879-887.

Kirsten, H.A.D., and Klokow, J.W., 1979. Control of fracturing in mine rock passes. In Proc. 4th ISRM Congress, Montreux, A. A. Balkema, Rotterdam, **1**: 203-210.

Kister, B., Teuscher, P., and Ziegler, H.J., 2000. Lötschberg Base Tunnel – Results of rock mechanical investigations and stress measurements at the Mitholz gallery. In Proc. EUROCK 2000, Aachen, Glückauf Verlag, Essen, 215-222.

Krauland, N., and Soder, P.E., 1987. Determining pillar strength from pillar failure observations. *Engineering Mining J.*, **8**(8): 34-40.

Lajtai, E.Z., Carter, B.J., and Ayari, M.L., 1990. Criteria for brittle fracture in compression, *Engineering Fracture Mechanics*, **37**(1): 25-49.

Landriault, D., and Oliver, P., 1992. The destress slot concept for bulk mining at depth. Rock Support in Mining and Underground Construction, Kaiser and McCreath eds, A.A. Balkema, Rotterdam, 211-217.

Lang, T.A., and Bischoff, J.A., 1984. Stability of reinforced rock structures. In Proc. ISRM Symp. Design and Performance of Underground Excavation, Cambridge, UK.

Lunder, P.J., and Pakalnis, R., 1997. Determination of the strength of hard rock mine pillars. The Canadian Mining and Metallurgical Bulletin, **90**(1013): 51-55.

Madden, B.J., 1991. A re-assessment of coal pillar design. *J. of the South African Institute of Mining and Metallurgy*, **91**: 27–36.

Maloney, S., Fearon, R., Nosé, J-P., and Kaiser, P.K., 1992. Investigations into the effect of stress change on support capacity. Int. Symp. Rock Support, A.A. Balkema, Rotterdam, 367-376.

Martin, C.D., Yazici, S., Espley, S., and Tan, T., 2000. Using numerical models to quantify stope dilution. Canadian Institute of Mining (AGM), Toronto, (CD) 8p.

Martin, C.D., and Maybee, W.G., 2000. The strength of hard-rock pillars. *Int. J. of Rock Mechanics and Mining Sciences*, 8p.

Martin, C.D., Kaiser, P.K., and McCreath, D.R., 1999. Hoek-Brown parameters for predicting the depth of brittle failure around tunnels. *Canadian Geotechnical J.*, **36**(1): 136-151.

Martin, C.D., 1997. Seventeenth Canadian Geotechnical Colloquium: The effect of cohesion loss and stress path on brittle rock strength. *Canadian Geotechnical J.*, **34**(5): 698-725.

Martin, C.D., and Chandler, N.A., 1994. The progressive fracture of Lac du Bonnet granite. *Int. J. of Rock Mechanics and Mining Sciences & Geomechanical Abstracts*, **31**(6): 643-659.

Martin, C. D., Martino, J. B. and Dzik, E. J., 1994. Comparison of borehole breakouts from laboratory and field tests. In Proc. EUROCK'94, SPE/ISRM Rock Mechanics in Petroleum Engineering, Delft, A.A. Balkema, Rotterdam, 183-190.

Martin, C.D., and Stimpson, B., 1994. The effect of sample disturbance on laboratory properties of Lac du Bonnet granite. *Canadian Geotechnical J.*, **31**(5): 692-702.

Martin, C.D., 1990. Characterizing in situ stress domains at the AECL Underground Research Laboratory. *Canadian Geotechnical J.*, **27**: 631-646.

Martin, C.D., Read, R.S., and Chandler, N. A., 1990. Does scale influence in situ stress measurements?--Some findings at the Underground Research Laboratory. In Proc. First Int. Workshop on Scale Effects in Rock Masses, Loen, Norway, da Cunha ed., A.A. Balkema, Rotterdam, 307-316.

Martin, C.D., 1989. Failure observations and in situ stress domains at the Underground Research Laboratory. In Proc. Conf. Rock Mechanics and Rock Physics at Great Depth, Pau, France, Maury, and Fourmaintraux eds, A. A. Balkema, Rotterdam, **(2)**: 719-726.

Mathews, K.E., Hoek, E., Wyllie, D.C., and Stewart, S.B.V., 1981. Prediction of stable excavations for mining at depth below 1000 metres in hard rock. CANMET Report DSS Serial No. OSQ80-00081, DSS File No. 17SQ.23440-0-9020, Department Energy, Mines and Resources, Ottawa, 39p.

Maybee, W.G., 1999. Pillar Design in Hard Brittle Rocks. Master's Thesis, School of Engineering, Laurentian University, Sudbury, ON, Canada.

McCreath, D.R., and Kaiser, P.K., 1992. Evaluation of current support practices in burst-prone ground and preliminary guidelines for Canadian hard rock mines. In Proc. Int. Symp. Rock Support, A.A. Balkema, Rotterdam, 611-619.

Melbye, T., 2000. Information on Sprayed Waterproofing Membrane. MBT Master Builders Technology, Switzerland

Mogi K., 1966. Pressure dependence of rock strength and transition from brittle fracture to ductile flow. Bulletin Earthquake Research Institute Japan, **44**: 215-232.

Moy, D., and Hoek, E., 1989. Progress with the excavation and support of the Mingtan power cavern roof. In Proc. Conf. Rock Cavern, IMM, Hong Kong.

Nickson, S., Sprott, D., Bawden, W.F., and Coulson, A., 1997. A geomechanical study for a shaft wall rehabilitation program. In Proc. 99th CIM Annual General Meeting, Vancouver, Canadian Institute of Mining, 20p.

Nickson, S.D., 1992. Cable Support Guidelines for Underground Hard Rock Mine Operations. M.A.Sc. Thesis, Department Mining and Mineral Processing, University of British Columbia, 223p.

Obert, L., and Duvall, W.L., 1967. Rock Mechanics and the Design of Structures in Rock. John Wiley and Sons, New York, 650p.

Oliver, P.H., 1992. The Sudbury Neutrino Observatory (SNO) project. In Proc. 16th Canadian Rock Mechanics Symp., Sudbury, Ontario, Kaiser and McCreath eds, 25-34.

Ormonde, R., and Szwedzicki, T., 1993. Monitoring of post failure pillar behaviour. Geotechnical Instrumentation in Open Pit and Underground Mining, Szwedzicki ed.,: A.A. Balkema, Rotterdam.

Ortlepp, W.D., 1997. Rock Fracture and Rockbursts - An Illustrative Study. Monograph Series M9. South African Institute of Mining and Metallurgy, Johannesburg.

Ortlepp, W.D., and Gay, N.C., 1984. Performance of an experimental tunnel subjected to stresses ranging from 50 MPa to 230 MPa. In Proc. ISRM Symp. Design and Performance of Underground Excavations. Brown and Hudson eds, British Geotechnical Society, London, 337-346.

Pelli, F., Kaiser, P.K., and Morgenstern, N.R., 1991. An interpretation of ground movements recorded during construction of Donkin-Morien tunnel. *Canadian Geotechnical J.*, **28**(2): 239-254.

Potvin, Y., Hudyma, M.R., and Miller, H.D.S., 1989. Design guidelines for open stope support. Canadian Mineral Metallurgy Bulletin, **82**(926): 53-62.

Potvin, Y., 1988. Empirical Open Stope Design in Canada. Ph.D. Thesis, Department of Mining and Mineral Processing, University of British Columbia, 343p.

Pritchard, C.J., and Hedley, D.G.F., 1993. Progressive pillar failure and rockbursting at Denison Mine. In Proc. 3rd Int. Symp. Rockbursts and Seismicity in Mines, Kingston, Young ed., A.A. Balkema, Rotterdam, 111–116.

Salamon, M., 1999. Strength of coal pillars from back-calculation. In Proc. 37th US Rock Mechanics Symp., Vail, Amadei, Kranz, Scott, and Smeallie eds, A. A. Balkema, Rotterdam, **1**: 29-36.

Salamon, M.D.G., and Munro, A. H., 1967. A study of the strength of coal pillars. *J. South African Institute Minerals & Metallury*, **68**: 55–67.

Santarelli, F.J., and Dusseault, M.B., 1991. Core quality control in petroleum engineering. In Proc. 32nd U.S. Symp. Rock Mechanics, Norman, Roegiers ed., A.A. Balkema, Rotterdam, 111-120.

Schmertman, J.H., and Osterberg, J.O., 1968. An experimental study of the development of cohesion and friction with axial strain in saturated cohesive soils. In Proc. ASCE Research Conf. on Shear Strength of Cohesive Soils, 643p.

Schneider, T.R., 1999. Gotthard Basis Tunnel: Strategie der geologischen Untersuchungen", In Proc. Symp. Exploration and Prognosis for the Base Tunnels at Lötschberg and Gotthard (in German), Löw and Wyss eds., A.A. Balkema, Rotterdam, 59 –73.

Schofield, A.N., and Wroth, C. P., 1966. Critical State Soil Mechanics. McGraw Hill, Maidenhead.

Sharp, J.C., Warren, C.D., Barton, N.R. and Muir Wood, R., 1996. Fundamental evaluations of the Chalf Marl for the prediction of UK marine tunnel stability and water inflows. Chapter 32, Engineering Geology of the Channel Tunnel, Thomas Telford, London, 472-507.

Sharp, J.C., 1990. Design and application of integrated shotcrete linings for underground openings in weak rock. In Proc. Conf. on Shotcrete for Underground Support V, Uppsala.

Sharp, J.C., 1989. Design of major caverns in granitic rocks based on precedent practice in Hong Kong and elsewhere. In Proc. Conf. Rock Cavern, Hong Kong.

Sharp, J.C., Endersbee, L.A., and Mellors, T.W., 1984. Design and observed performance of permanent cavern excavations in weak bedded strata. In Proc. ISRM Symp. Design and Performance of Underground Excavation, Cambridge, UK.

Sharp, J.C., and Mellors, T.W., 1982. Rock engineering and design studies for the Drakensberg Pumped Storage Scheme. *Trans SAICE*, **24**(8).

Sharp, J.C., and Lawrence, D.L.J., 1982. Final shotcrete linings for an underground power station in argillaceous rocks. In Proc. Conf. on Shotcrete for Underground Support IV, Colombia.

Sharp, J.C., Pine, R.J., Moy, D., and Byrne, R.J., 1979. The use of a trial enlargement for the underground cavern design of the Drakensberg Pumped Storage Scheme. In Proc. 4th Congress of Int. Society Rock Mechanics, Montreux.

Sharp, J.C., Richards, L.R., and Byrne, R.J., 1977. Instrumentation considerations for large underground trial openings in civil engineering. In Proc. Int. Symp. Field Measurements in Rock Mechanics, Zurich.

Sjöberg, J., 1992. Failure modes and pillar behaviour in the Zinkgruvan mine. In Proc. 33rd U.S. Rock Mechanics Symp., Santa Fe, Tillerson and Wawersik eds, A. A. Balkema, Rotterdam, 491–500.

SRK, 1996. Interim report on the procedure and findings of the unreinforced, mesh and fibre-reinforced shotcrete panel tests. Report 208905/1 Steffen, Robertson and Kirsten Inc., 65p.

Stacey, T.R., and Page, C.H., 1986. Practical Handbook for Underground Rock Mechanics. TransTech, Germany, 145p.

Stacey, T.R., and de Jongh, C.L., 1977. Stress fracturing around a deep-level bored tunnel. *J. of the South African Institute of Mining and Metallurgy*, December, 124-133.

Steiner, W., 2000a. TBM tunnelling – geotechnics influencing mechanics, *Felsbau*, Glückauf, Essen, Germany, **18**(2): 28-34.

Steiner, W., 2000b. Mechanized construction of large tunnels in rock. In Proc. EUROCK 2000, Aachen, Glückauf Verlag, Essen, 235-242.

Steiner, W., 1999. Rock Mechanics challenges from deep alpine tunnels in Switzerland. *ISRM News J.*, **5**(3): 13-19.

Steiner, W., 1998. Choice of construction methods for tunnels in hard soil and soft rock: Influence and reliability of site investigations. Panel report – In Proc. Symp. Hard Rock/Soft Rock, Napoli, Picarelli and Evangelista eds, A.A. Balkema, Rotterdam.

Steiner, W., and Bargähr, H., 1997. Long-term behaviour of short tunnels in hard rock in the Alps. In Proc. Int. Symp. Rock Support, Lillehammer, Norway, 476-491.

Suorineni F.T., Tannant, D.D., Kaiser, P.K., and Dusseault, M.B., 2000. Incorporation of a fault factor into the stability graph method: Kidd Mine case studies, submitted to *Int. J. of Mineral Resources Engineering*, 21p.

Swiss General Contractors Association, 1999. Standard Analysen, Untertagbau (Standard Cost Analyses for Underground Construction). Vol. 1 and 2., Schweizerischer Baumeisterverband, Zürich, Switzerland.

Tannant, D.D., Barclay, B., Espley, S.J., and Diederichs, M.S., 1999. Field trials on thin sprayed-on membranes for drift support. In Proc. ISRM Congress, Paris, France, Vouille and Berest eds, A.A. Balkema, Rotterdam, 1471-1474.

Tannant, D.D, Kaiser, P.K., and Maloney, S., 1997. Load-displacement properties of welded-wire, chain-link, and expanded metal mesh. In Proc. Int. Symp. Rock Support, Lillehammer, Norway, 651-659.

Tannant, D.D., Kaiser, P.K., and McCreath, D.R., 1996. Impact tests on shotcrete and implications for design for dynamic loads. NARMS, Montreal, **1**: 367-373.

Tapponnier, P., and Brace, W.F., 1976. Development of stress-induced microcracks in Westerly granite. *Int. J. of Rock Mechanics and Mining Sciences & Geomechanical Abstracts*, **13**: 103-112.

Thalmann, C., 1997. Alptransit-Ausbruchmaterial: Abfall oder potentieller Rohstoff, Tunnel muck: waste or potential resource. In Proc. FGU-SIA, D0143, 63-71.

U.S. Corps of Engineers, 1980. Engineering and Design Rock Reinforcement. Engineer Manual No. 1110-1-2907, Department of the Army, USA.

Vasak, P., and Kaiser, P.K., 1995. Tunnel stability assessment during rockbursts. CAMI '95 3rd Canadian Conf. on Computer Applications in the Mineral Industry, Montreal, Quebec, 238-247.

Von Kimmelmann, M.R., Hyde, B., and Madgwick, R.J., 1984. The use of computer applications at BCL Limited in planning pillar extraction and design of mining layouts. In Proc. ISRM Symp. Design and Performance of Underground Excavations, Brown and Hudson eds, British Geotechnical Society, London, 53-63.

Wagner, H., 1987. Design and support of underground excavations in highly stressed rock. In Proc. 6th ISRM Congress, Montreal, Herget and Vongpaisal eds, A.A. Balkema, Rotterdam, **3**: 1443-1457

Wiles, T., and Kaiser, P.K., 1994. In situ stress determination using the Under-excavation Technique - Part I: Theory and Part II: Application. *Int. J. of Rock Mechanics and Mining Sciences & Geomechanical Abstracts*, **31**(5): 439-446 and 447-456.

Wiles, T.D., and Kaiser, P.K., 1990. A new approach for the statistical treatment of stress tensors. In Proc. Stresses in Underground Structures, Ottawa, Herget, Arjang, Betournay, Gyenge, Vongpaisal and Yu. eds, Canadian Government Publishing Centre, Ottawa, 62-76.

Wiseman, N., 1979. Factors affecting the design and condition of mine tunnels. Research Report 45/79, Chamber of Mines of South Africa, Pretoria, South Africa.

Zermatten, M., 2000. Materialbewirtschaftung auf Lötschberg Südseite. *Schweizer Baublatt*, March, 9-13.